High-precision, high-speed strip feeding in micro-forming

(Volume I)

Akhtar Razul Razali

Glasgow, June 2010

High-precision, high-speed strip feeding in micro-forming

Akhtar Razul Razali

This thesis is submitted to the Department of

Design, Manufacture and Engineering Management,

University of Strathclyde

For the degree of Doctor of Philosophy

Glasgow, June 2010

'This thesis is the result of the author's original research. It has been composed by the author and has not been previously submitted for examination which has led to the award of a degree.'

Signed : 

Date : 1st July 2010

Dedication:

The author wishes to dedicate the thesis to his mother, father, his wife, son and daughter without whose support and sacrifice, the thesis would have not been completed.

Acknowledgement

The work reported herein was carried out at the Department of Design, Manufacture & Engineering Management, University of Strathclyde, through full time study funded by the Government of Malaysia through Ministry of Higher Education (MOHE). Permission to register for a PhD degree and financial support provided by the university is gratefully acknowledged.

The author wishes to express his gratitude to Prof. Dr. Yi Qin for his phenomenal supervision of the research, constant support and meticulous checking of the manuscript.

The author would like to thank the colleagues of High-precision Manufacturing Engineering Research Group for their encouragement and constant support. The advice offered by the colleagues is particularly acknowledged.

The author is grateful to Mr. Robert Hay, Mr. Barrie Hunter and Mr. Duncan Lindsay for their assistance in the laboratories. The production of all tools, electronic circuits and electrical connections in the department workshop was of the highest quality for which the author is grateful.

Abstract of the Thesis

A high-precision and high-speed feeder was designed and developed with a view to establishing the greater-precision and accuracy of a handling device for micro-sheet-forming applications. Two types of popular commercial feeder for thin-sheet were tested to quantify their performance in terms of accuracy and repeatability, namely a micro-servo roll-feeder and a pneumatic gripper-feeder, tested using three different strips: carbon steel of 50 to 100microns thickness; and stainless steel of 50microns thickness. A non-contact approach was used to determine the feeders' performance. Several different combinations of the feeding parameters were explored, such as: the employment of various feed distances and feed frequencies; the effect of lubrication; and motion-profile optimization. FE simulations were used to study the feeding characteristic of the feeders. Based on the findings, both of the feeders were found to be unsuitable for micro-sheet-forming application due to their high rate of inaccuracy and their lesser repeatability-capability dealing with very thin sheet. Both empirical results and FE-simulation results show good agreement with the observed feeder-performance.

The research has identified a servo linear-motor gripper-feeder as being suitable for use in micro-sheet-forming applications. This new feeder-concept enables a significant improvement in handling accuracy and repeatability when dealing with very thin sheet. Supported by the results of FE simulations, both empirical and simulation results show good agreement on the feeder performance. In the initial tests, better repeatability was achieved. The success of the initial tests led to an optimization process being conducted to increase the potential for achieving better accuracy, which was designed to be at 5-15% of the strip thickness. The optimization method consists in determining the actual payload acting on the system, the adjustment of the control feedback and the adjustment of the motion-profile curve. The optimization method proved successful, the designated accuracy and greater repeatability being achieved for all of the strips tested, employing a similar test set-up to that when using a roll feeder.

The research continued to develop a finished-part transporting mechanism to transport the finished parts/products by using a pocketed carrier-tape. This transportation concept has proven to be successful in transporting the finished parts/products away from the micro-sheet-forming machine. Both the new feeder-system and new transportation-system were finally integrated with the micro-sheet-forming machine to enable synchronization of operation.

List of Publish Papers

(1) Razali, A., Qin, Y., Harrison, C. and Brockett, A. (2009) 'Investigation of feeding devices and development of design considerations for a new feeder for micro-sheet-forming', *Int. J. Nanomanufacturing*, Vol. 3, No. 1/2, 40-54. (Part of Chapter 6)

(2) Razali, A., Qin, Y., Harrison, C., Zhou, J. and Brockett, A. (2009) 'Non-optimized performance of newly developed linear motor gripper feeder for micro-sheet-forming application' *International Conference on Manufacturing Research (ICMR 2009),* 24-30. (Part of Chapter 8)

(3) Razali, A., Qin, Y., Harrison, C. and Brockett, A. (2008) 'Investigation of feeding devices and development of design considerations for a new feeder for micro-sheet-forming', *International Conference on Manufacturing Research (ICMR 2008),* Vol. 1, 493-504. (Part of Chapter 6)

(4) Razali, A.R., (2008) 'Review, issues and gap in micro-forming development' *Innovative Production Machines and Systems Proceedings, 4th I*PROMS Virtual International Conference,* 276-282. (Part of Chapter 2)

(5) Razali, A.R., Razak, A., & Zahid, M.N.O., (2008) 'Issues and Gap In Micro-Forming Development' *2nd International Conference of Science & Technology (ICSTIE 2008): Applications in Industry and Education.* (Part of Chapter 2)

(6) Razali, A.R., Razak, A., & Zahid, M.N.O., (2008) 'Fabrication and Integration Issues on Custom-Build and Commercial Ironless Linear Motor Stage' Development' *2nd International Conference of Science & Technology (ICSTIE 2008): Applications in Industry and Education.* (Part of Chapter 6)

(7) Razali, A.R., Razak, A., & Zahid, M.N.O., (2008) 'Review And Issues In High-Precision Material Handling Development For Micro-Forming Application' Development' *2nd International Conference of Science & Technology (ICSTIE 2008): Applications in Industry and Education.* (Part of Chapter 2)

(8) Razali, A.R., Razak, A., & Zahid, M.N.O., (2008) 'The Effect of Motion Profile Changes On Linear Motor Stage Sizing Development' *2nd International Conference of Science & Technology (ICSTIE 2008): Applications in Industry and Education.* (Part of Chapter 6)

(9) Razali, A. & Qin, Y., (2010) 'FE Simulation of Sheet-Metal Feeding in Micro-Forming', CAPE 2010 Edinburgh. **(Full paper accepted)** (Part of Chapter 4 and 7)

(10) Micro-sheet-forming and case studies, Metal Forming 2010 **(Abstract accepted)** (Part of Chapter 8)

Contents

Nomenclature

u = initial velocity (m/s)

v = final velocity (m/s)

s = distance (m)

a = acceleration (m/s^2)

t = time (s)

f_p = payload force (N)

f_a = acceleration force (N)

f_g = gravitational force due to inclined plane (N)

f_f = frictional force (N)

f_e = cable-management force (N)

m = mass (kg)

ρ = density (kg/m^3 or g/cm^3)

V = volume (m^3 or cm^3)

μ = coefficient of friction

τ = torque is in N.m

f = force (N)

r = radius (m or mm)

I = inertia ($kg.m^2$)

α = rotational acceleration (rad/s^2)

ω = rotational velocity (rad/s)

h = height (m)

F_{peak} = total peak-force (N)

F_{rms} = total root-mean-square force (N)

R_T = thermal resistance (W/°C)

M_C = motor constant (N/√W)

T = temperature (°C)

BEMF = back electro-motive force (V/m/s)

Exp = expansion

ΔT = change of temperature (°C)

w_t = total weight (kg or gram)

I(amp) = current (A)

w = width (m or mm)

l = length (m or mm)

Subscripts

brake = denotes brake

rms = denotes root-mean-square

reel = denotes reel

coil = denotes coil

composite = denotes composite

outer = denotes outer dimension

inner = denotes inner dimension

cycle = denotes cycle

min = minimum

thermal = denotes thermal

total = denotes total

motor = denotes the motor

2hz = denotes as 2Hz frequency

brakerms = denotes brake rms value

MEMS – denotes microelectromechanical system

nobf – denotes no brake force

BF – denotes brake force

PZT – denotes piezoelectric transducer

N/S – denotes not specified

N/A – denotes not available

Chapter 1

Introduction

1.1 Research Background

There are significantly increased demands on MEMS, and micro-products/parts in general, with fast growth in applications taking place in communications and telecommunications. For equipment alone, the market was $197.6 billion in 2005 and is anticipated to reach $446.9 billion in 2010. Wide applications are seen in Bio/medical-technology, information technology and automotive engineering. For example, one source of information [Qin, 2006b] showed that typical micro-parts which can be formed with micro-forming technology are connecting pins that are used widely in computers, communication devices and other electronic products. Together with other micro-products, they had a market value of $45 billion in 2003 and enjoy an annual growth-rate of 20%. Increased demands on micro-products also lead to the rapid development of micro-manufacturing technologies for the manufacture of individual parts and systems, which includes the development of new manufacturing processes, tools and machinery. To-date, the manufacture, however, still relies largely on the techniques based on the removal of material, either by chemical, thermal or mechanical means. Tremendous efforts have been made, to-date, to improve the efficiency of miniature/micro-manufacturing technologies [Peng et al., 2009; Lai et al., 2008; Peng et al., 2007; Qin, 2006a; Vollertsen et al., 2006; Qin, 2006c; Byung et al., 2005; Chern et al., 2004; Peng et al., 2004; Engel et al., 2002; Geiger et al., 2001; Messner et al., 1994], but, however, these have not resulted in a radical change in the technologies. Therefore, miniature/micro-manufacture is still seen as an "expensive" and "wasteful" business.

Conversion of miniature-/micro-materials into engineering products by high-rate plastic deformation (Micro-Forming) would address two key issues that are of particular importance for the industry – reduction of manufacturing costs and improvement of product quality. In addition to the need to deal with the complexity of the forming miniature/micro-materials, which requires a good understanding of material- and interface-characteristics at micro-scales, handling miniature/micro-parts at the fast rates and with the high positional accuracy that match the production expectations of mass-micro-forming is a challenge to current research and development in micro-forming.

High- precision handling in micro-forming is concerned with the manipulation of thin sheet metal with high positional accuracy and repeatability. Typical part dimensions are in the range of sub-millimeters up to a few millimeters, and part features may be in the micrometer range. The typical accuracy is in the range of 5-15% of the sheet thickness used. The micro-domain allows for, and sometimes demands, the application of methods and techniques that are different from those that are applied in the meso-domain. For the forming of thin sheet metal, although the thickness is in tenths of microns, when considering the strip width and size the parts still could be treated as volumes of more than $1mm^3$ where gravitational force can still dominate adhesion forces. The result of this effect is that thin sheet metal is vulnerable to the effects of friction and of high displacement velocity and these effects are not easily predictable during the feeding process. This situation would require detailed study to understand the feeding characteristics during the feeding of the thin sheet material over a designated feed distance. The issue becomes even more complicated when good accuracy needs to be maintained where fast production rate needs to be incorporated, which is normal for mass-production, e.g. when using progressive multistage tooling.

To date, micro-forming still relies on the usze of conventional scaled down/miniaturized handling system/feeders. A conventional handler such as servo roll feeder which typically has a positional accuracy of up to 25µm, may not be able to be miniaturized for its positional accuracy proportionally with its size. In micro-manufacutring, the parts being produced are likely to have sub-millimetre range of overall sizes or feature-sizes. Positional accuracy in tenth of micron somehow may be seen to be similar to the size of a micro-product being produced. Hence, a servo-roll feeder may not be good enough to serve for micro-forming applications.

High-precision positioning usually associated with very slow motion. Many researches around the globe have proven that sub-micron positional accuracy may be achieved. Nevertheless, most of the researches did not address the importance of high-precision over high speed motion [Gao et al., 2006; Yamazaki et al., 2006].

Hence, positioning time usually is neglected to achieve the highest possible positional accuracy where sometime it may take several seconds to settle. This however may not be a good practice in mass production. This research is aimed to study and realize high-precision feeder for micro-forming applications which would enable the production of micro-products in a volume scale, e.g. 100 parts per minute..

1.2 Aims/Objectives

The overall objective of the proposed research was to establish a systematic theory and the technical details of part handling for a micro-sheet-forming application, based upon which a prototype system was to be developed, integrated into a micro-forming testing machine developed within the University of Strathclyde, and tested with forming of selected demonstrators. The micro-part intended to be produced is called micro-hat. The demonstrator partners agreed on this part design with the following dimensions: 50-100µm thick sheet metal;, an 300 µm deep embossed micro-hat and a 500µm slot featureed on each side (Fig. 1). For this kind of the component, feeding accuracy is required to be around 5-15% of the material thickness and production rate is expected to be at around 100 parts per minute.

The following measurable objectives were defined:

i. Investigation of the feeding fundamentals to address mass-production requirements, particularly issues related to precision and production rates;
ii. Qualification of the micro-forming process and product characteristics and definition of the specifications required for sheet feeding in micro-sheet-forming;
iii. Qualification of the feeding methods, processes and equipment for the forming of micro-products;
iv. Development of new feeding concepts for micro-sheet-forming applications;
v. Development of a new feeding system for a micro-forming testing machine (including mechanical and electronics elements); and,
vi. Integration of the feeding system into the micro-forming machine.

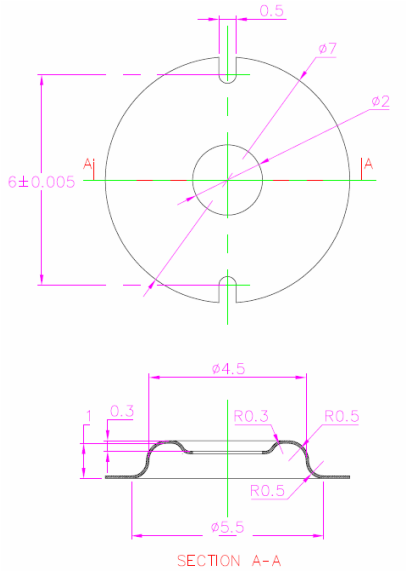

Fig. 1.1: Micro-hat design specification – part that is intended to be produced.

1.3 Approach/Methodology

The proposed study started with examining existing practice and research in micro-forming, particularly of: the micro-sheet-parts that are popularly used in MEMS; of Optical-electronics; and of other sensors/actuators. The part-forms were classified with reference to the handling requirements. Forming experiments will be carried out to study micro-sheet-forming process characteristics, tool-performance, part-tolerances and distortions, etc., as well as their effects on the handling of the thin sheet metal. An investigation into the fundamentals of high-precision thin sheet metal handling (within 5-15% of the thin-sheet thickness) was carried out. Emphasis was given to the high-speed high-precision handling of the thin sheet metal (of the order of a few hundred pieces per minute for micro-sheet-forming) with a great accuracy (within 5-15% of thin sheet metal thickness) which has to match the mass-production characteristics of the micro-forming machine. Based on the qualified fundamentals, existing high-precision handling methods, processes and equipment were examined: these included high-precision handling-system principles, standard systems, piezo-actuation, solenoids, rotary servo-motors, linear-servo motors, supply methods, miniature feeding-systems design (mechanical feeders, vision-based flexible part-feeding, vibration feeding units, conveyance units, finite-element

analysis), clamping principles, micro grippers, etc. The focus was on the gripper-feeder type device, for which the following will be examined: peak and continuous forces, payload, design of the feeder, high-speed high-force clamping device, and feeding characteristic through finite-element analysis. Based on the standard elements (commercially available) a new high-precision thin-sheet-metal handling system was developed which combines motion monitoring and control. Several concepts were generated and these were evaluated with theoretical analysis, experimentation and manufacturing-ability assessment by industry. An optimal concept was selected to develop a detailed design. The system was fabricated, integrated into the micro-sheet-forming testing machine being developed within Strathclyde, and then tested in the forming of several micro-products, for which synchronization of control with other parts of the machine was required.

1.4 The Research Performed

The research was planned and performed in three phases:

Fundamentals studies and analysis were conducted in Year 1 of the study. this being inclusive of the following: Qualification of the micro-sheet-forming process and product-characteristics and the definition of the specifications required for high-precision-handling in micro-sheet-forming, which included the development of a classification methodology for high-precision-handling considerations; investigation of handling fundamentals to address mass-production requirements, particularly issues related to precision and production rates, which involved participation in forming experiments together with other researchers within the micro-manufacturing research group; qualification of thin-sheet-metal handling methods, processes and equipment for the forming of micro-products, which involved communication with other organisations/collaborators, simulation experiments and bench-marking, etc. Based on the foregoing, a methodology for the design of a high-precision handling system for micro-sheet-forming was developed.

In Year 2 of the study, the following were carried out: the development of new high-precision handling methods and system concepts for micro-sheet-forming applications, which included the development of conceptual design models, analysis

methods for assessment, and the, performing of mini-experiments. The concept was optimized and an optimal concept was selected. Detailed design was carried out based on the optimal concept. A prototype of a high-precision thin-sheet-metal handling system for a micro-sheet-forming testing machine (including mechanical and electronics elements) was fabricated, with the collaboration of industrial partners.

In the final year of the study, Year 3, the following work has been done: the prototype of the high-precision thin-sheet-metal-handling system was tested, optimized and enhanced with reference to micro-sheet-forming requirements. The improved system was integrated into the micro-sheet-forming machine being developed within the Centre for Micro-technology, University of Strathclyde. For this purpose, control to enable synchronization of the machine system was performed. The integrated system was tested with the forming of engineering micro-products.

1.5 The Thesis Structure

The thesis consists of eleven chapters:

Chapter 1 – Introduction: This consists of a description and explanation of the background to, the aims/objectives which this research intended to achieve, followed by a detailed discussion of the approach/methodology to be employed to complete the research and the details of the research planning for every phase of the project, and finally a description of the structure of the thesis, for all of the development work carried out.

Chapter 2 – Literature Review: This chapter explains micro-manufacturing, micro-parts/products/features, and micro-forming development work carried out by researchers worldwide, which concerns machine tool development. The review then concentrates on micro-stamping development, including a definition of the micro-stamping process and a description of the micro-stamping machine and tools that have been developed. This chapter is also inclusive of the key issues related to micro-stamping quality, which is elaborated upon in detail. The review then is focused on the handling strategy in micro-sheet-forming, using conventional sheet-feeding machinery as a reference. Two types of feeder for thin sheet metal are

defined – a servo roll-feeder and an air gripper-feeder. Then key issues in the thin-sheet-metal-handling process for micro-sheet-forming applications are addressed. In order to qualify the performance of both of the types of feeder mentioned, several accuracy-measuring concepts are defined, including contact and non-contact methods. Relevant parameters, which are expected to influence the feeding performance, are defined. The chapter ends with a summary of the findings obtained from the review.

Chapter 3 – Fundamental Studies of the Materials Used: This chapter explains all the procedures and types of experiments conducted to determine the mechanical properties of the materials used. The tensile test, surface roughness, and friction measurement/estimation were explained for each material used. Results are described and discussed in detail.

Chapter 4 – FE Analysis of the Roll Feeder: ABAQUS is used as a tool to identify and understand the feeding characteristics of the thin sheet when the roll feeder is used. Some parameters are varied i.e. changes of the motion profile and the application of reel brake-force, etc.

Chapter 5 – Experimental Studies of the Micro-roll Feeder and the Air Feeder: This chapter explains the procedure taken to qualify the performance of the servo roll and air gripper feeder. Tests are divided onto several categories in order to obtain conclusive results and findings about the performance of both of the feeders.

Chapter 6 – Concept Development of a New Feeder: Development work carried out on the new feeder is explained. The works begins with the identification of the high-accuracy and -precision handling strategy used at the present time, followed by comparison studies made on commercial-available linear-motor stages and also analysis to determine the correct size of the linear motor.

Chapter 7 – FE Analysis of the New Feeder Design: FE analysis is conducted on the new feeder design in order to study its feeding characteristics for improvement prior to the fabrication process. Similar to the FE analysis of the servo roll-feeder, two

parameters are chosen to be varied, i.e. changes of the motion-profile curve and the application of brake force. The Results are explained and discussed in depth.

Chapter 8 – Construction of the New Feeder and its Experimental Validation: Details of the fabrication work carried out are explained in this chapter. The determination of a suitable clamping device is also demonstrated and explained. This is followed by the fabrication and assembly work of the new feeder. Design of the machine control and programming language are also conducted and described. Detailed explanation of the integration work between the new feeder and the micro-sheet-forming machine are also addressed in this chapter. A validation experiment is carried out also with a view to validate the performance and usability and the developed feeder.

Chapter 9 – Optimization of the New Feeder: This chapter explains the optimization work carried out on the developed feeder. The optimization approach was categorized into load, motion profile, and feedback-control optimization through P-D compensation. A validation experiment is carried out to qualify the optimized performance of the new feeder. The results obtained are explained and discussed in detail.

Chapter 10 – An Extended Application of the Feeding Design – Part Transport in Micro-sheet-forming: The definition of the purposes of part transport for micro-sheet-forming is explained. Design and motor-sizing analysis are conducted and described in detail in order to determine the appropriate useful forces throughout the system. A validation experiment is described and conducted to validate the developed part-transport system. Results are explained and discussed in detail.

Chapter 11 – Conclusions and Considerations for Future Work: This chapter draws the conclusions from the whole of the development work conducted. Considerations for future work that may assist in further development of the research topic are also given.

Chapter 2

Literature Review

2.1 Micro-Manufacturing in General

The term 'micro-manufacturing concept' in the context of a miniature factory is understood to be a micro-factory and it is a relatively new concept concerning manufacturing systems [Qin, 2006a; Okazaki et al., 2002; Okazaki et al., 2004]. A micro-factory can be defined as a small manufacturing system conceived as a means of achieving higher throughput with less space and reduced consumption of both resources and energy via downsizing of production processes [Claessen et al., 2002]. This means that all of the equipment has necessarily to be reduced to the micro-scale (micro-machines) which could, in-turn, reduce the energy consumptions, preliminary and overhead costs, and material requirements, along with reducing pollutions and creating a more user-friendly production environment. As the scale of the equipment is reduced, the mass of the equipment itself can be reduced dramatically and this will lead to the increasing of tool speed and at the same time will result in improvement of the production rates by the reduction of the manufacturing cycle. In addition to the foregoing advantageous, the force/energy loop and the control loops for small-size equipment are believed by many researchers to be significantly shorter [Qin, 2006b].

In 1990, a research group from the Mechanical Engineering Laboratory (MEL), Tsukuba Japan, studied the effect of miniaturization of production systems. The estimation was made that in the case of a 1/10 size reduction of production machines, the total energy consumption in the factory decreases to approximately 1/100 compared to that of the conventional factory. The most significant advantage of micro-manufacturing is the capability for producing parts which having feature sizes of less than 100μm [Byung et al., 2005; Chern et al., 2004; Chern et al., 2006b; Qin et al., 2008], or little greater than the thickness of a human hair. At this scale, the slightest variation in the manufacturing process caused by material or cutting tool characteristics, thermal variations in the machine, vibration and any number of minute changes, will have a direct impact on the ability to produce features of this type on a production scale [Shanahan, 2006].

2.1.1 Micro-Products/Parts/Components

A meso-part is regarded as a part that is greater in size than a few millimetres (as a reference, the meso-domain is defined as products fitting in a box of 200 x 200 x 200mm^3) [Kolesar et al., 2000]. However, a micro-part is concerned with small parts with typical part-dimensions in the range of sub-millimetres up to a few millimetres, although part-features may be in the micro-meter range. The typical positional precision for such parts is expected to be in the range of 0.1 to 10µm. The micro-domain allows for, and sometimes demands, the application of methods and techniques that cannot be applied in the meso-domain. Fig. 2.1 illustrates the range of part- and feature-size machining capability. Parts with machined features beyond 100µm are known as miniature parts, whereas a maximum size of less than 5mm can usually can be found in MEMS applications.

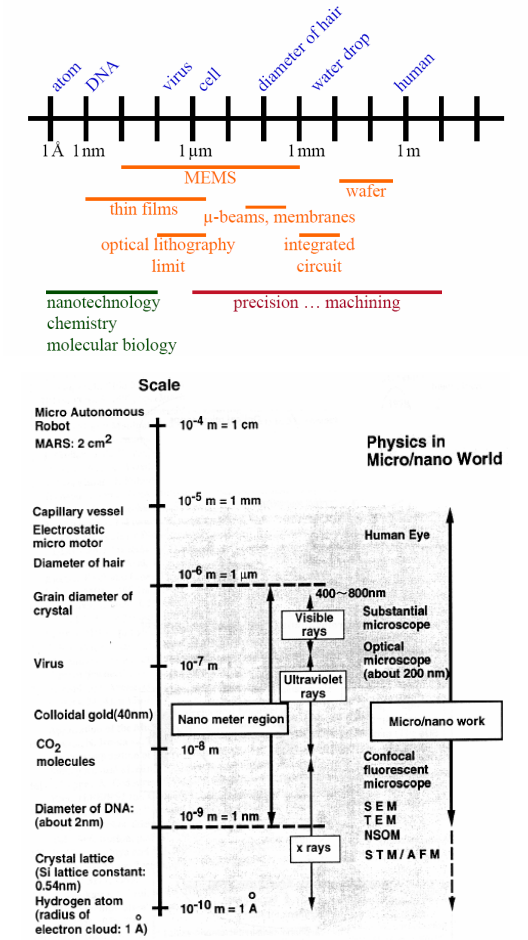

Fig. 2.1: Parts scales and dimensions [Kolesar et al., 2000].

2.1.2 Micro-Manufacturing Methods and Processes

The trend for micro-manufacturing at the present time is more focussed on miniaturizing or down-scaling both conventional and non-conventional methods to produce micro-products. Additionally, there are also emerging methods, such as the hybrid manufacturing method, which combine two or more processes together [Chern et al., 2004]. Manufacturing processes can be categorized according to the type of energy used in the process itself, such as mechanical, chemical, electrochemical, electrical and laser processes. The working principles behind each process include consideration of mechanical forces, thermal effects, ablation, dissolution, solidification, re-composition, polymerisation/lamination, and sintering [Qin, 2009]. According to the way in which components/products are to be made, general manufacturing processes can also be classified into subtractive, additive, forming, joining and hybrid processes. The classification is equally applicable to micro-manufacturing. Typical manufacturing methods against the way of producing components/products are show in Table 2.1.

Table 2.1: Typical methods/processes in micro-manufacturing (as presented by Qin, (2009)).

Subtractive processes	Micro-Mechanical Cutting (milling, turning, grinding, polishing, etc.); Micro-EDM; Micro-ECM; Laser Beam Machining; Electro Beam Machining; Photo-chemical-machining; etc.
Additive processes	Surface coating (CVD, PVD); Direct writing (ink-jet, laser-guided); Micro-casting; Micro-injection moulding; Sintering; Photo-electro-forming; Chemical deposition; Polymer deposition; Stereolithography; etc.
Deforming processes	Micro-forming (stamping, extrusion, forging, bending, deep drawing, incremental forming, superplastic forming, hydro-forming, etc.); Hot-embossing; Micro/Nano-imprinting; etc.
Joining processes	Micro-Mechanical-Assembly; Laser-welding; Resistance, Laser, Vacuum Soldering; Bonding; Gluing; etc.
Hybrid processes	Micro-Laser-ECM; LIGA and LIGA combined with Laser-machining; Micro-EDM and Laser assembly; Shape Deposition and Laser machining; Efab; Laser-assisted-micro-forming; Micro assembly injection moulding; Combined micro-machining and casting; etc.

2.1.3 Micro-Manufacturing Machines/Tools

As to what has been experienced to date, the vast and rapid development of micro-manufacturing technology has covered almost all area in conventional machinery and

processes. In response to this continued development, many researchers and companies have proposed and developed the micro-machine concept.

In the earlier age of micro-manufacturing development, research in micro-manufacturing focused more on assembly and conveyance processes, which research was led by the Japanese researchers and industries [Mishima et al., 2002; Ataka et al., 1999; Suda et al., 2000; Brussel et al., 2000]. This in turn led to the booming of similar development work by European countries, such as Project Miniprod developed by [Gaugel et al., 2001]. Effort was also widened up by the development work of the mini-production system by Klocke Nanotechnik [Klocke et al., 2002; Klocke et al., 2003]. The micro-factory includes a nano-robotics module with a repeatability of 50nm. The plant can be a combination of different modules such as force sensors, wafer probers, manipulators, vacuum-grippers and micro-grippers, etc. All of the development work mentioned involved a gluing process, the transportation of parts and a multi-degree-of-freedom assembly process which was realized by various types of micro-manipulators.

Later, in the year 2000, micro-manufacturing development was focused on the down-scaling of conventional milling and turning processes and once again was led by the Japanese researchers [Okazaki et al., 2004]. For instance, The Mechanical Engineering Laboratory, under the National Institute of Advanced Industrial Science and Technology, renowned as AIST, succeeded in the year 2000 in equipping a micro-lathe with a precision digital-control system. In order to give it real machine-tool functionality as depicted in Fig. 2.2 below, it uses a pair of micro-sliders based on a unique step-feed configuration driven by PZT actuators, and a spindle unit mounted on the orthogonally-stacked micro-sliders. For numerical control, the displacement of each slider is detected using an embedded micro linear-encoder with 62.5nm resolution developed by the Olympus Corporation and fed back to the servo-controller. A single-board custom numerical-controller processes the-part programs and feeds the servo-controller with command pulse trains yielding 0.1μm resolution. The total desktop footprint is about 550 x 450mm.

Fig. 2.2: Micro lathe with numerical control [Okazaki et al., 2004].

The machine has produced good machining results which exceeds the standard of ISO 4287/1E [Davim et al., 2005]. Turning a brass rod, the surface roughness of the cylinder in the base-line direction and the roundness error were measured as 0.5µm R_z or 60nm R_a, and smaller than 0.5µm, respectively. These values are better than those of the original micro-lathe, and are comparable to those from regular-sized machines. NC motion-control enables programmed shape-generation, as shown in Fig. 2.3.

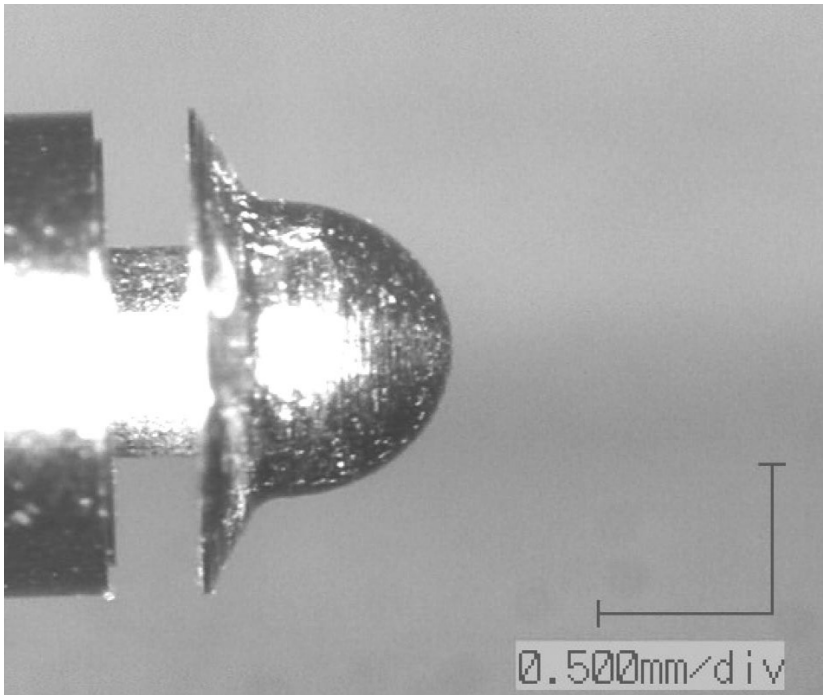

Fig. 2.3: Machined ‘microhat’ by MEL revised microlathe micro-machine [Okazaki et al., 2004].

Another effort made on the development of micro-turning technology was demonstrated by The ‘Desktop Factory Study Group’ of the Nagano Techno Foundation consortium [Sankyoseiki]. The group is composed of members from fourteen local companies and several institutions. They are developing the concept of the micro-factory in order to incorporate it into their manufacturing activities. In 2003 they developed a unique desktop-sized turning centre of which the machine is only about the size of an A3 sheet of paper, as shown in Fig. 2.4. It has three linear axes and two spindles to perform turning and milling operations, and is equipped with an automatic tool changer. Its capability was evaluated by machining tiny metal parts. The development process itself was very intensive, requiring just three months. They also developed an in-line desktop plating system, including pre/post-washing units. Some member companies have incorporated the concept into their dedicated products, including a de-burring machine, micro-drilling/turning/3D-milling/polishing machines, plating machines, washing machines, assembling system, etc.

Fig. 2.4: Desktop turning centre developed by DTF Study Group.

In the middle of year 2000, the maturity of the miniaturization of conventional milling and turning process and its good potential was realized by one of the world's well-known servo- and machinery-manufacturer, Fanuc. In year 2004 Fanuc developed a machine with several combinations of high-precision multi-function machine functions called ROBOnano, as depicted in Fig. 2.5, which can function as a five-axis mill, a lathe, a five-axis grinder, a five-axis shaping machine and a high-speed shaper, this being realized by means of an air-turbine spindle instead of a conventional rotary servo-motor. It uses friction-free servo systems (all linear-slides and -screws include static air-bearings). Shaping is done by using a high-speed shuttle unit capable of producing three grooves per second, and a 3 kHz fast tool servo using a lead zirconate titanate (PZT) actuator. Cutting is nominally accomplished with a single-crystal diamond tool. Control is achieved using a FANUC series 15i control, with error mapping for positional (axial) errors only. The resolution of the linear axes is 1nm and for the rotational axes is 0.00001°. The design of the machine is such that it experiences no backlash and stick-slip motion.

Fig. 2.5: Fanuc ROBOnano versatile micro-machine.

2.1.4 Micro-manufacturing and Key Issues

The design of micro-products for micro-manufacturing needs to address production issues extensively to be able to succeed compared to the situation with prototype-products based on micro-technologies. The high-volume production of micro-components should be the main goal for the design of micro-manufacturing. When these products are designed, not only will functional requirements need to be considered, but also micro-manufacturing-related factors will have to be taken into account. This is because manufacturing these products renders more significant challenges, compared to those for the manufacture of macro-products. Issues related to micro-manufacturing have been addressed intensively by many researchers [Qin, 2009; Alting et al., 2003]. The followings are some typical issues to be addressed at the design stage of micro-manufacturing machinery.

Factors negligible conventionally – There is a limit to how far conventional macro-scale machining can be scaled down for miniaturization. Beyond certain dimensions, factors that can be ignored with conventional machining suddenly play a big part in micro-manufacturing: vibration, tool-offset, temperature, the rigidity of the tools and the structure of the machines, and chip removal, are more important because these factors have a greater influence on micro-products.

Volume production and automation – Another issue occurred in current micro-process technology is in terms of process automation. Stand-alone and manual processes of the developed prototypes have required every aspect on the process to need manual adjustments. Most of the processes such as principal processes; pressing, milling, turning etc, and handling processes; material loading and unloading, tool positioning and aligning; were all manually configured and controlled by separate dedicated controllers to obtain precise and accurate motion and alignment. This time-consuming process has made micro-process suitable only for low yield-rate, and as-yet far removed from the potential of conventional processes. On top of this matter, manual adjustment tends to give greater parallax error compared to that with present automated closed-loop and programmable controllers that have error-compensation features [Fanuc; Kollmorgen; Baldor; Rockwell Automation; Yaskawa; Parker].

Limitation on machinable materials – In parallel with the fairly early stage of micro-machine development, only ductile- and soft-materials with low-strength properties were chosen and studied as the test materials; mainly brass, copper and aluminum [Byung et al., 2005; Chern et al., 2004; Chern et al., 2006a; Okazaki et al., 2004]. The satisfactory machining of soft and ductile materials is easily achievable due to such materials exhibiting low mechanical strength and tending to deform easily under low applied load/force. Only simple micro-features were created successfully by the efforts made, which micro-features were far from being able to be used or applied. Soft materials are very limited in their usage and some manufacturers have found that these materials are not durable enough to meet the

increasing demands of reliability and long life. Therefore, switching to harder and exotic materials is the only option available.

Tooling dimension – Another key-issue in micro-manufacturing development is tooling limitation. At present, 10µm end-mill tools have been realized, these tools being made from carbide (PMT). 25-50micron milling- and-drilling tools currently have been found satisfactory and can be found commercially [Kyocera; Minitools]. Although micro-tooling development started more than a decade ago, there is still limitations existing, which limits the applicability of the tooling [Aronson, 2003; Aronson, 2004]. Only aspect ratios (the ratio of the tool diameter to the drilling depth) of 5 to 10 have been found suitable, and some have aspect ratios of even lower than five. Deeper-plunging and-drilling will result in tooling breakage, hence, makes the tooling unsuitable for the aerospace- and automotive-industries; which require very-high-strength material of low mass. The achievable precision of the drilled holes has not yet been studied extensively and, furthermore, issue regarding the aligning of micro tools of sub-micron precision has not yet been explored extensively because no automatic machine is available at present capable of aligning tools of sub-micron precision [Kibe et al., 2007].

Unwanted external forces – Precise positioning is also a main problem encountered in the handling of micro-parts [Rougeot et al., 2005]. The external forces involved in physical contact, such as the electrostatic, sticking or adhesion effect, and Van Der Waals force, have become key issues and numerous studies have been made to understand the situation and the strategy necessary to eliminate those forces, employing mathematical simulation [Arai et al., 1995; Arai et al., 1997; Feddema et al., 1999; Rollot et al., 2000; Fearing et al., 1985; Bowling et al., 1986; Bowling et al., 1988; Tomas et al., 2007].

Sensor dimension and performance – Moreover, attention has to be paid to sensor's accuracy, since the sensors available at the present time are bulky in size and the achievable precision is basically of the order of tenths of microns. Being excessive large in size makes the sensors difficulty to be placed accurately on a tiny

workspace, while this level of precision is not feasible for micro-parts application, which requires at least sub-micron precision. In addition, most of the calibration-precision capability of current machines is far less than the precision demanded in micro-handling.

2.2 Stamping and Micro-Stamping

2.2.1 Sheet-Metal Forming and Stamping

Sheet-metal components are used extensively in various applications such as vehicles, aircraft, electronic products, medical implants and packaging for consuming goods, typical parts/components including car-panels, aircraft skins, cans for food and drinks, frames for TV/computer screens/monitors/displays, etc. Concerning miniature/micro-products, sheet-metal parts include electrical connectors and lead-frames, micro-meshes for masks and optical devices, micro-springs for micro-switches, micro-cups for electron guns and micro-packaging, micro-laminates for micro-motor and fluidic devices, micro-gears for micro-mechanical devices, casings/housings for micro-device assembly/packaging, micro-knives for surgery, etc. Therefore, sheet-metal parts are closely associated with everyday life [Vollertsen et al., 2006].

Basic process-configurations for the forming of macro-products include shearing, blanking, bending, stamping, deep drawing (including mechanical and hydro-mechanical), hydro-forming, stretching forming, super-plastic forming, age forming, spinning, explosive forming, incremental forming, etc.

One of the popular and highly-in-demand forming processes is stamping. Metal stamping has been defined as a process employed in the manufacturing of metal parts with a specific design from sheet-metal stock and includes a wide variety of operations such as punching, blanking, embossing, bending, flanging and coining [Kalpakjian et al., 2006]. Common examples are sheet-metal machines, automobile parts, metal components used in audio- and video-devices, aerosol spray cans, and even military tanks. A household example is the use of sheets of metal to make pots and pans.

Sheet metal can be deformed into different pre-determined shapes. The metal must be malleable and needs to flow easily in order to be drawn into various shapes. Stamping can be done on metals such as aluminium, zinc, steel, nickel, inconel, titanium, bronze, copper and other alloys. This is a mass-production, economical process with low cycle time. Hence, it is used widely in the manufacturing of large-volume products with semi-skilled labour. The process is also called chipless manufacturing.

Metal-stamping processes use dies and punches to cut the metal into the required shape. The male components are called punches and the female components are called dies. Press machine-tools are used in the stamping process. The die, made of hardened steel, has a contour that matches the shape of the finished part and is mounted on the table of the press. The punch, made of hardened tool-steel or carbide, also matches the contour of the part but is slightly smaller to allow clearance between the die and the punch. It is mounted in the head or the turret, which moves down and punches the metal. The thickness of the sheet metal does not change during this process.

2.2.2 Micro-Stamping Processes

Numerous research investigations have been conducted worldwide covering the micro-forming field and showing that micro-forming is on a promising path towards its application in industrial production [Geiger et al., 2001; Vollertsen et al., 2004; Vollertsen et al., 2006; Qin, 2006a; Qin, 2006b; Qin, 2006c; Geiger et al., 1996]. Moreover, metal forming offers some attractive characteristics that are superior to those of other processes, for example, machining and chemical etching, considering such features as high production-rates, better material integrity, less waste, lower manufacturing costs, etc. Therefore, micro-forming could be a better option for the mass-manufacture of micro-products at a reduced cost, provided that a proper manufacturing facility is developed.

Literally the same as in the conventional stamping process but, instead, macro- and meso-scale products being produced, micro-stamping is intended to produce miniaturized products and components. Micro-stamping is seen useful to produce parts such as wristwatch and micro handheld-device components, medical products etc. [Kalpakjian et al., 2006].

The early stages of micro-stamping development showed a gradual development of the process. Effort had been expended to perform an automatic and hybrid simple punching process on brass strip, as depicted in Fig. 2.6 [Chern et al., 2004; Chern et al., 2006b]. This effort continued with the development of a manually-operated micro-stamping machine (Fig. 2.7) with the capability of employing various punch shapes [Byung et al., 2005].

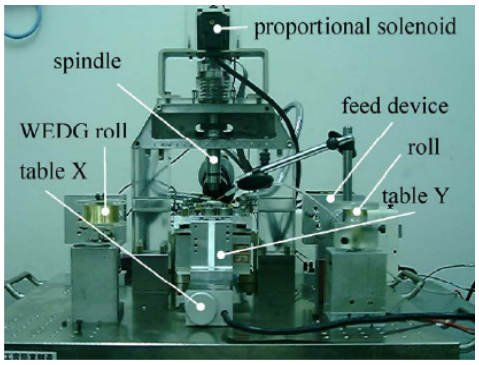

Fig. 2.6: Solenoid driven micro-forming machine [Chern et al., 2006a].

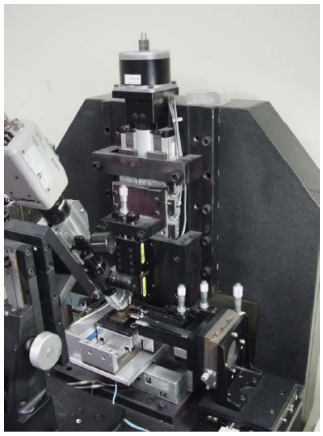

Fig. 2.7: Developed micro-punching press machine [Byung et al., 2005].

The latest efforts in micro-stamping development have demonstrated that multi-stage/progressive die micro-stamping may be used for the micro-sheet-forming process [Qin et al., 2008]. A fully-automatic linear-motor-driven multi-stage/progressive-tool micro-stamping machine has been developed with collaboration between the University of Strathclyde and its European Union partnership (Fig. 2.8).

Fig. 2.8: A bench-top micro-sheet-forming machine, designed by the University of Strathclyde [Qin, 2009].

In the micro-stamping process, not only is the machine itself physically scaled down, but the tools required for the process also have to be capable of producing the required micro-parts through scaling down. Efforts made by Qin et al., (2008) have demonstrated the successful operation of single-stage (Fig. 2.9) and multi-stage tooling (Fig. 2.10) for the micro-sheet-forming process. Various parts with micro-features have been produced successfully, as shown in Fig. 2.11.

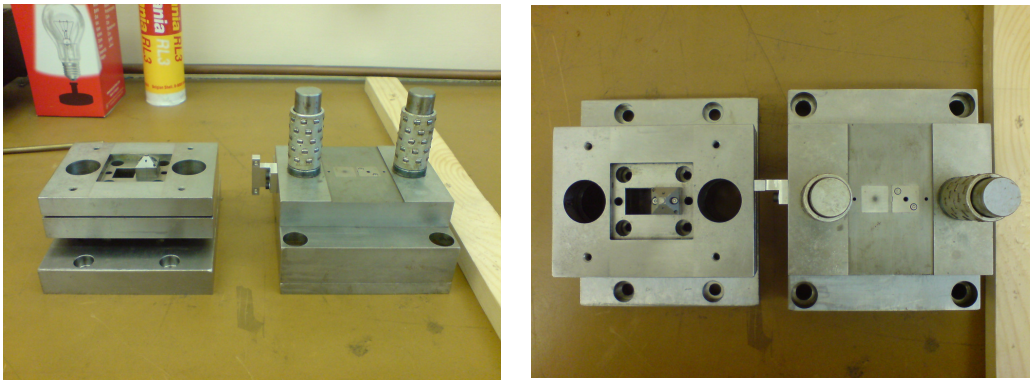

Fig. 2.9: Single-stage tool with a square punch and dies for micro-sheet-forming.

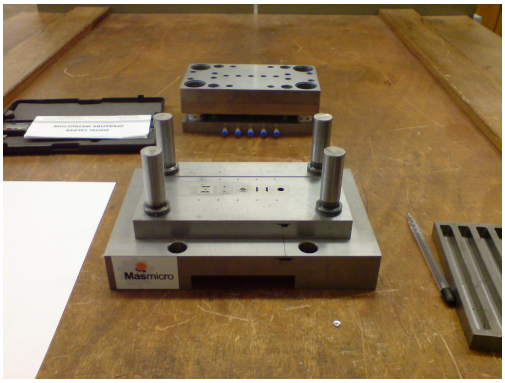

Fig. 2.10: Multi-stage tools with various types of forming/blanking punches and dies.

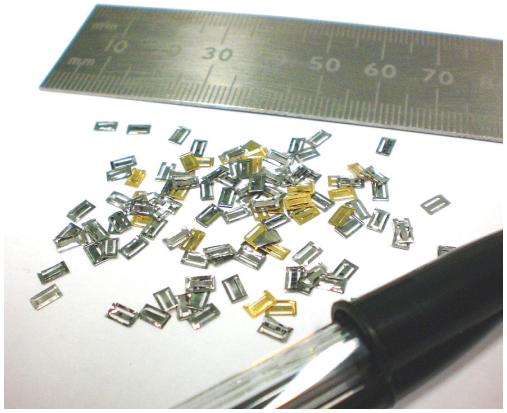

Fig. 2.11: Samples of formed micro components in brass and stainless steel [Qin, 2009].

2.2.3 Micro-Stamping Machines and Tools

The research trend began with fundamental studies of every aspect in micro-forming, covering the work material and the appropriate tooling [Messner et al., 1994; Geiger et al., 1996; Geiger et al., 2001]. Later, in mid 2000, the effort extended to the development of a micro-forming-machine prototype by researchers and joint-venture industries [Qin et al., 2008; Aizawa et al., 2007; Schneider et al., 2004; Vollertsen et al., 2004; Hu et al., 2004].

The initial development of the micro-forming-machine prototype was traditionally based on conventional forming machineries and focused on a diverse range of

forming processes, which included stamping and bulk-forming processes. Effort made by Chern et al., (2004) and Byung et al., (2005) validated the punching of thin sheet-metal by micro-punch. In Chern et al., (2004) the punching process was actuated by a high-force DC solenoid and material feeding was done by an automatic roll-feeder. The results demonstrated a successful punching process, different punch geometries being used. Byung et al., (2005) demonstrated an entirely manually-controlled punching process with a micro-punch.

A new, low-cost, bench-top machine dedicated for micro-sheet-forming was developed at the University of Strathclyde [Qin et al., 2008], with collaboration with its EU MAMSICRO consortium partners [Masmicro]. A linear-motor driving mechanism is used. The maximum frequency of the machine is 1000 strokes per minute (spm), the maximum force is 5.3kN, the vertical-position resolution is 0.1μm, and the load-measurement resolution is 0.1N. The machine enables the micro-stamping/forming of sheet-metal parts (ideally for sheet metals of a thickness of less than 100 μm). The machine has a maximum working space of 400mm x 400mm with a flexible set-up, due to having a modular design, in which the ram-driven form/power is changeable without need of changing other machine set-ups; and four machine-frame columns and supports to the ram guiding bridge can be re-positioned according to the requirements, as well as the sheet-metal feeder, and the part carrier. The bridge for guiding the ram is separated from the main machine frame, and hence it is not affected significantly by the deflection of the main frame and by vibration. Other innovations include monitoring the displacement directly on the tooling (therefore being able to control the punch stroke more accurately), transporting the miniature/micro-parts directly out of the dies by a part carrier, a new vacuum/compression-air chamber design, a new sheet-metal holding design, etc. The machine design was supported by Finite-Element dynamics analysis, which led to the development of a bench-top machine that has very good dynamic performance and machine stability (no connection to the bench is needed, and no significant vibration is felt on the shop-floor). A similar machinery-concept was developed by Schneider et al., (2004) to serve the bulk-forming process a linear motor being used to drive the forming tool: the concept was proven to be successful.

2.2.4 Key Issues Related to Micro-Stamping Quality

Among various micro-metal components, sheet-metal components are used very extensively in MEMS, micro-electronics/optical devices, medical devices/instruments, etc. There has been significant interest in the research into micro-sheet-forming [Qin, 2007; Geiger et al., 1996; Chern et al., 2006a; Mishima et al., 2002; Okazaki et al., 2002; Park et al., 2002; Hess, 2000; Schneider et al., 2004; Qin et al., 2008; Kima et al., 2005; Matsushita, 2003; Jeong et al., 2003; Saotome et al., 2001; Oh et al., 2005]. Nevertheless, most of this research did not address production issues sufficiently, in terms of considering the transfer of the laboratory processes/machines to volume production. One of the key issues relates to the automation of the stamping processes by continuously feeding thin sheet-metals with micron-range precision.

High-precision handling and product quality – Feeding sheet-metals in conventional press-working is no longer a major problem in production [Schuler, 1998]. However, challenges arise when thinner metal-strips are to be used in micro-sheet-forming (e.g. <100 μm) and the parts/features to be formed become smaller (e.g. sub-millimetre ranges). In these cases, the forming a micro-sheet-metal component may require the feeding/positioning of the sheet-metal under the forming tools to be as accurate as within one to a few microns. This is particularly important in multi-stage progressive micro-stamping, in which the neighbouring features of a part may be very close to each other. Therefore, the feeding of the sheet-metal has to be very accurate in order to prevent any inaccurate forming or damage to the neighbouring features and connections of the part/scrap to the strip.

High-precision handling to meet volume production – At the same time, for volume production, feeding the strip (sheet metal) accurately may have to be achieved with a reasonable feed rate, e.g. 120 stroke per minute, for which the stiffness of the thin strip may be a major concern.

Precision feeding for micro-sheet-forming as described above cannot be achieved with conventional, large-scale sheet-metal feeders. Feeding in micro-sheet-forming was addressed only occasionally [Chern et al., 2006a; Schneider et al., 2004] in some studies. Detailed study on the feeding mechanism and performance of the feeders (positional precision) in micro-sheet-forming, considering various process conditions and material parameters has not been undertaken previously.

2.3 Handling for Sheet Forming

2.3.1 Requirements for Feeding in Sheet-Metal Forming

In almost all cases, a conventional sheet-metal forming machine feeder has to meet three main criteria to be successful. Firstly, the feeder must be flexible in terms of set-up. This means that it must allows adjustment to be made easily to cover all set-ups and changes in feed length, material width and gauge, feed- and pilot-releasing-timing and as well as die height. If the feed is for a dedicated system, these variables will be limited to the designated application only.

Secondly, the delivery of the material must be with sufficient precision to meet the precision required by the tool. The feeder must not only move the desired amount of material into the tool, but it must be capable of placing it precisely in the correct alignment with the die; front-to-back, side-to-side, and set square with the tool. Misalignment could result in binding and short feeds due to slippage and strip buckling: short-feeding results in bad parts and broken dies. When properly maintained, the feeder can retain that positional precision for a long time in any application. Nevertheless, the amount of maintenance and the setup time required will vary dramatically from one type of feed to the next, for instance the gripper and the roll-feeder have different maintenance and set-up times.

Feeder installation must be positioned on centre, square to the tool, and rigidly mounted so that no movement can take place between the tool and the feed, as a result ensuring the delivery of material correctly without binding and mis-feeding. In addition to the proper set-up of the feed installation, the tooling must also be placed precisely for each set-up. Some sort of registration device such as positive stops on

the bolster is recommended to be used to insure consistent placement of the tooling [Baeumler, 2001]. Nevertheless, without good-quality material, proper straightening, and precise alignment, there will still be problem a regardless of what feed is selected.

The last criterion is that the feeder must do the feeding at the correct time. The time that a feed actually has to deliver material is the result of the amount of time for one complete press/forming or shear cycle, minus the time that the tooling is engaged, minus the time required to detect a mis-feed and minus the time to stop the press. This means that there is always less time to feed when the die-engagement process takes longer.

On top of these criterion, there are many other important considerations to be take account of, which will ultimately determine how effective the feeder will be during operation: for instance, the amount of time and skill required to work-out the set-up, the cost of energy to operate it and also the time to interface the feeder with the press system as a whole.

2.3.2 Sheet-Metal Feeding Systems in Conventional Manufacturing

High-speed feeding for high production-yield typically refers to the usage of a press-driven feeding system. Thousands of parts may be produced in a minute, if the feeding system is well synchronized and powered by the press itself. Roll feeds (Fig. 2.12) that are driven by the press through mechanical transmission system such as rack-and-pinion or cam feeds, are always synchronized to the rotation of the press. The feeder always begins its motion at some predetermined point in the press cycle and finishes at another predetermined point, regardless of the press speed or die engagement. Although the index speed may be increased or decreased to keep pace with the press motion, the feed can draw as much power as it needs from the press to accomplish this, within the limitations of the mechanical-coupling and -transmission to the press. Press-driven feed always seen to be useful for a specific and dedicated forming process but unsuitable for a process which demands changes in its feeding parameters due to its inflexibility.

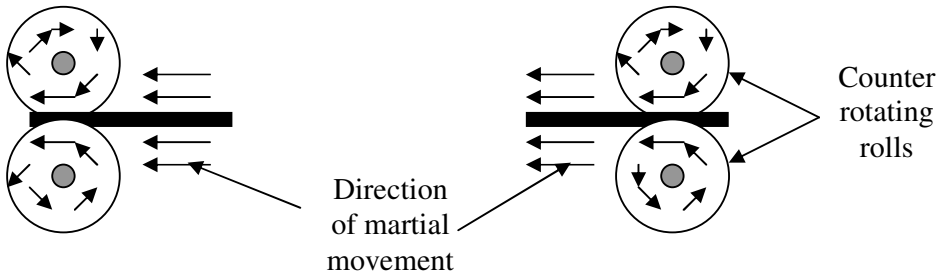

Fig. 2.12: Working principle of the roll feeder.

This differs from a self-powered or stand-alone unit, which begins its motion in response to a signal from the press, but which has a finite, minimum amount of time in which it is capable of indexing, which time is based on the amount of power it can deliver, and the load that it sees. Therefore, the result of this is that the point at which the operation finishes can vary compared to the press speed. The faster the press runs, the later in the stroke of a self-powered unit will the operation finish, or underfeed may result, as opposed to the case with press-driven unit, which always starts and finishes at the same point in the stroke regardless of the press speed.

This synchronization feature allows high-speed indexing on press-driven feeds, the feeding of 'in-die' transfers, or for use with an unloader and for other applications that require the feed motion to be well synchronized with the press rotation in order to avoid collision and tool breakage. Due to the lack of timing adjustment, the feed motion for all dies cannot begin until it reaches a point in the stroke at which the deepest draw-die disengages and hence limits the feed window to the worst-case scenario. On the other hand, air/pneumatic and servo-powered feeds operate independently of the press and allowing adjustment to enable feeding to begin as soon as the die opens.

Inherent to their design, press-driven feeds exhibit a very smooth motion, which is called an 's-curve motion profile', opposed to the 'trapezoidal-movement curve' used by most other feeds. This s-curve motion profile enables the variation of the acceleration rate throughout the index, hence resulting in the elimination of sharp

transitions or changes in velocity, which can cause slippage with other feeds. Most self-powered feeds start their motion from a stationary condition directly into a fixed rate of acceleration which results in a sharp velocity changes or transition called a 'jerk' point. These jerk points typically occur at the beginning, middle, and end of each move in trapezoidal motion. Press-driven feeds make gradual transitions or changes in velocity, with high-acceleration and-deceleration in the interim due to their s-curve-designed cam. This in turn leads to the elimination of these jerk points, while retaining the ability to make high-speed indexes that are within reasonably-good positional precision.

The drawbacks or disadvantages to most press driven feeds are due to their difficulty of adjustment, feed length/distance limitations, lack of inching capability, and the absence of a control interface. Most of the press-driven feeds require gear sets, rollers, or mechanical linkages to be changed to be able to adjust the feed length only. They are also subjected to limitation in their range of feed length/distance adjustment due to their being directly coupled to the press rotation and their lack of ability to jog the strip for threading. In addition, due to lack of electrical controls, mechanical feeds such as press-driven feeds cannot accept a set-up input from, or provide an output feedback to, press-control or automation systems. Servo-driven roll-feed technology has been used in the press-feeding industries for a couple of decades now. The initial apprehension or drawbacks with this developing technology is disappearing as the technology itself matures. Almost every manufacturer of press-feeding equipment has now considered using servo-driven feeds in their feeding arsenal. This servo-driven concept involves the use of a closed-loop positioning drive that usually employs a servo to control the index position of the feed rolls [PA Industries; Chern et al., 2006a; COE Press].

Similarly to press-driven feeds, the advantages of servo-driven roll-feeds include minimal space requirement due their compact size, low maintenance, and high feed-speeds. However, servo feeds have some benefits that press-driven units do not have. Servo feeds utilize a microprocessor-based control that gives them an added capability. Features such as flexibility in changes of feed length/distance,

programmable move patterns, self-diagnostics capability, positional auto correction, and the ability to communicate with an automation system, set them apart from other types of feeds. Servo-drive systems have been used widely for positioning applications in manufacturing processes such as forming for a couple of decades. The technology has matured to the extent that these drives are more reliable, cost-effective and less expensive than they were in the past. The number of domestic and foreign manufacturers also has shown a dramatic increase in the past few years. The increase in reliability, modularity, and self-diagnostic features of servo -systems has eliminated many of the fears that existed earlier [Chern et al., 2006a; COE Press].

Servo-driven roll feeds are also different to press-driven units in the way that they are available in a wide variety of roll-unit configurations, feeder/straighteners and unwinder/feeder/straighteners. Feed-control packages range in sophistication from simple and easy-to-use, single set-up controls with thumbwheels/balls, touchpads or keypads, to systems that allow programming of multi-axis move patterns, controls of auxiliary functions and devices, as well as offering varying levels of servo-drive memory and communications capability [Coilmate-Dickerman; PA Industries]. Most servo feeds manufactured at the present time utilize a trapezoidal move/motion profile with four distinct 'jerk' points that could result in slippage but some are also available with controls that enable the execution of s-curve move profiles to reduce the 'jerking' motion. Servo-drive feed systems that are electronically synchronized to press rotation are also available and require a special controls package and feedback device, either a resolver or an encoder, which is attached to the press crank to track the press rotation, with ±50μm positional precision achievable in slow-speed motion [Coilmate-Dickerman]. Nevertheless, their top speeds are still limited by the available drive-power which differ to the situation with press-driven feeds, which can run as fast as the press and tooling are capable of [COE Press; Grant, 2006; Grant, 2001].

Gripper feeds, as shown in Fig. 2.13, employ a linear motion to move the strip that is differ to the rotary action of roll feeds [Powair] and are available in a wide variety of sizes from very simple mechanisms, compact in shape and low-cost press-mounted

units, to large cabinet-mounted models, which include pull-through straighteners. Gripper feeds utilize a pair of clamps, with the first one, called the retainer, remaining stationary, and the second one moving in the feed and return strokes, called the gripper. The retainer releases the strip during the feed stroke, as the gripper clamps and moves the strip forwards while the tool is open through the top half of the press cycle. On the return stroke, the gripper releases and the retainer holds the strip while the gripper retracts from the press while the tool is closed through the bottom half of the press cycle.

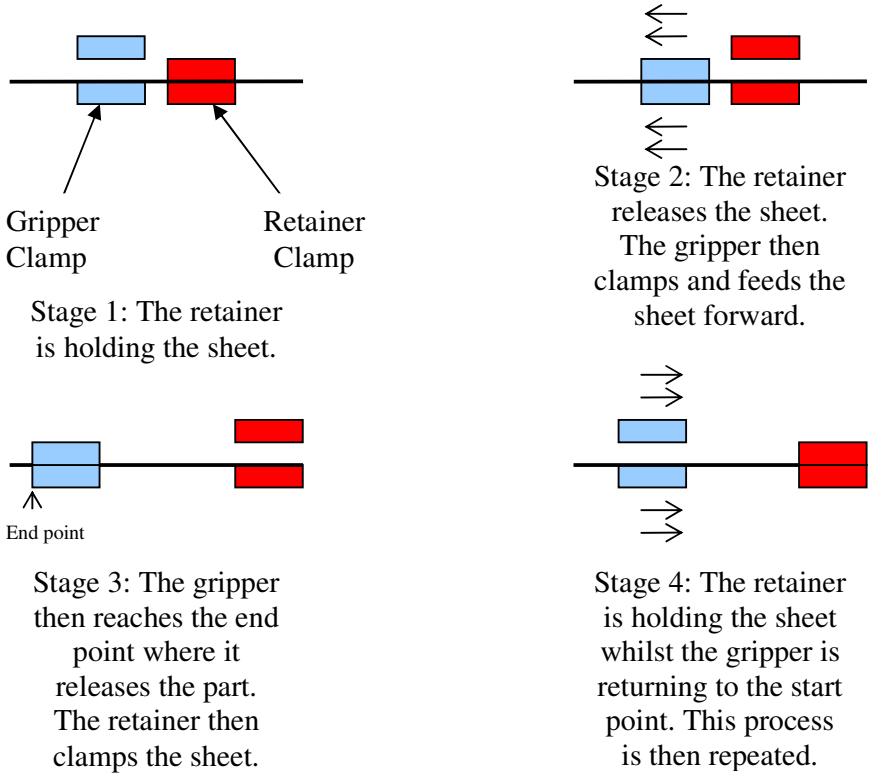

Fig. 2.13: Working principle of gripper feeder.

The gripper- and retainer-clamps can be powered by air or hydraulic cylinders, or can be in the form of one-way roller mechanisms that hold the strip in one direction but allow it to roll freely in the opposite direction. The timing of the clamp and release is critical in cylinder-powered clamps for accurate feeding and can be a limiting factor in terms of speed. The strip can be free at times to fall back due to brake force if the timing is not correct, resulting in short feeds. Solenoid valves or air

logic valves may actuate clamping and the timing can be controlled either electrically or through valve porting.

The thrusting/pulling force for the gripper can be provided in many ways, such as by an air- or hydraulic-cylinder, a hydraulic motor, or by a servo motor. The gripper is usually supported by guideways or rails and is driven by mechanical means, such as cylinder rods, chains-and-sprockets or ball screws. The feed length is set by adjusting a positive stop when air- or hydraulically-powered units are used. The gripper moves until it reaches a stationary stop, some sort of cushion being employs to soften the blow at the end of each stroke. Feed-length adjustment does require the use of tools (i.e. measurement tools) and often involves some trial-and error-attempts, which usually results in longer set-up times.

On the other hand, differently to an air- or a hydraulically-actuated feed system, a servo-powered gripper feed utilizes the advantages of microprocessor closed-loop servo drive and is coupled to a mechanical transmission system, such as a ball screw and nut, to position the gripper, and do not use stops or cushions to arrest the gripper. The feed set-up configuration can be programmed directly into the control unit via an operator interface, or can be serially-downloaded from a control computer. The control unit then send the commands to the servo drive to position the gripper to the designated pre-programmed position. Roll feeds embedded within servo-driven units enjoy many of the advantages of electronic units in terms of programmability and the ability to interface with press-automation systems.

The main drawbacks of gripper feeds is the limitation to a specific maximum feed length/distance based on the model that is selected in anticipation of the longest feed length requirement that must be made at the time of purchase. Each additional increment of length costs extra investment and the longer feed length/distance capability dictates that the machine itself needs to be longer and therefore requires more valuable floor space. The preferred option is to buy the shortest machine that will just satisfy the need and necessity and if there is ever a need to run a longer length than the machine is designed for, multiple cycles on each press stroke are

performed: commonly referred to as "multi-stroking". A more expensive controls package is required to reach the capability and, because of the time required for the return stroke when multi-stroking, the press usually operates in the single-cycle mode.

Air-powered grip feeds for applications requiring low-to-moderate speeds and limited feed lengths usually are inexpensive and are used commonly together with pull-through straighteners to provide a cost-effective alternative to roll feeds with powered straighteners. Greater set-up and maintenance costs and the high cost of energy to operate them will be offset easily in time, due to their low purchase price. Losses due to leaks, pressure drops and contamination have made compressed air often an expensive energy medium. Maintenance costs can be quite high also, because of the many moving parts and the wear of components. In order to sustain good positional precision and performance, these machines require timely scheduled maintenance.

Table 2.2 compares press-driven and stand-alone feeding. In terms of flexibility of changes in process parameters, the stand-alone feeder is the more desirable compared to the press-driven-type feeder. Simple and easy in process parameters had made stand-alone feeders becomes the popular choice for a multiple group-technology forming process. Details of both of these feeders are summarized in Table 2.2.

Table 2.2: Comparative study on press-driven and stand-alone feeder feeding.

Feature	Press Driven	Standalone Feeder
Various feed distance freedom?	Impossible due to feeding distance is subjected to cam profile and gearing mechanism. Fix feed distance is only qualified. To qualify various feed distance, changes in gearing/mechanical transmission must be made.	Flexibility in terms of feed distance. Various feed distance can be qualified by re-programming the intended feed distance.
Process speed	Immediate response. Higher yield rate is qualified. This system works similar to piston and valve concepts but with cam and follower. Both moves and stops at the same time, hence synchronization in high speed operation is qualified. No time delays since no electrical cabling connectivity required to transmit signal.	Time delays in connection (transmit and receive signals usually in milliseconds) limits the motor and control system to serve high speed operation [Trevelyan, 2005]. Synchronization between pressing and feeding is crucial due to feeding is only can take place when dies is opened. This contributes in loss of time.
Achievable accuracy/precision	Good accuracy is achievable as long as the mechanical transmission remains in its working tolerance (BRUDERER).	Good accuracy is qualified by servo tuning. At present, 50µm accuracy is qualified by micro servo roll feed (PA Industries). Sub-micron precision is not achievable with roll feeder.

2.3.3 Feeders for Thin Sheets and Micro-Forming

The two well-known feeders that still serve the metal-forming industries at the present time are the servo-roll feeder and the pneumatic-gripper feeder. As the name implies, the servo-roll feeder uses an electrical servomotor, as described earlier, while the pneumatic-gripper feeder mainly uses pneumatic actuation. In today's technology, giant manufacturers such as PA Industries and POWair have concentrated on a manufacturing feeder for micro-thin sheet metal. PA Industries produce a micro-server roll-feeder with several pulling-force ranges, which uses a high-precision servo motor for better positional precision, while POWair manufacture a pneumatic gripper-feeder with a comparatively high pulling-force of 90N, specifically designed to feed thin sheet metal.

2.3.3.1 Micro-servo roll-Feeder

A micro-servo roll-feeder, depicted in Fig. 2.14(a), was developed by PA Industries for the purpose of micro feeding. It uses a belt-transmission system to transfer rotational motion from the motor to the feeder rollers. Basically, the servo motor is controlled by closed-loop operation, where a rotational incremental encoder is used for positional feedback. The micro-servo roll-feeder is controlled by its own dedicated controller, as shown in Fig. 2.14(b), where various pitch distances can be set directly on the controller. The controller receives an electrical signal-pulse to generate order for the servo-motor motion. Once the pulsed signal is received from the press controller, the servo roll feeder will move the strip by the designated pitch distance as set on its controller. For instance, at 5Hz operation, with 5mm pitch for the process, the press controller will send a 5Hz signal to the servo roll-feeder controller and make the feeder move the strip at 5Hz over the 5mm preset travel distance. If 10Hz and 10mm pitch operation is desired, the pitch distance will be set to 10mm on the servo roll-feeder controller and the press controller will pulse a 10Hz signal ordering the feeder to move. The specification of the feeder is as below.

Maximum Feed Length	= 2500mm
Minimum Programmable Increment	= 0.025mm
Maximum Stock Width	= 50mm
Maximum Stock Thickness	= 1.5mm
Maximum Stock Thickness at Full Width	= 1.0mm
Maximum Material Speed	= 36mpm
Feed Roll Diameter	= 25.4mm
Motor Torque – Continuous	= 0.68Nm
Motor Torque – Peak	= 1.92Nm
Pulling Power, on Strip-Continuous	= 151N
Pulling Power, on Strip-Peak	= 450N
Drive Output Current – Peak	= 5 amps

The time taken to feed the strip over 6.35mm feed distance is around 70ms minimum. This figure shows that basically up to 14 parts can be produce in a second for the designated feed distance, which means 840 parts are produced in a minute. Based on the manufacturer's specification, the minimum feed distance is limited to 25µm. Nevertheless, the degree of positional precision is not mentioned in the feeder's specification.

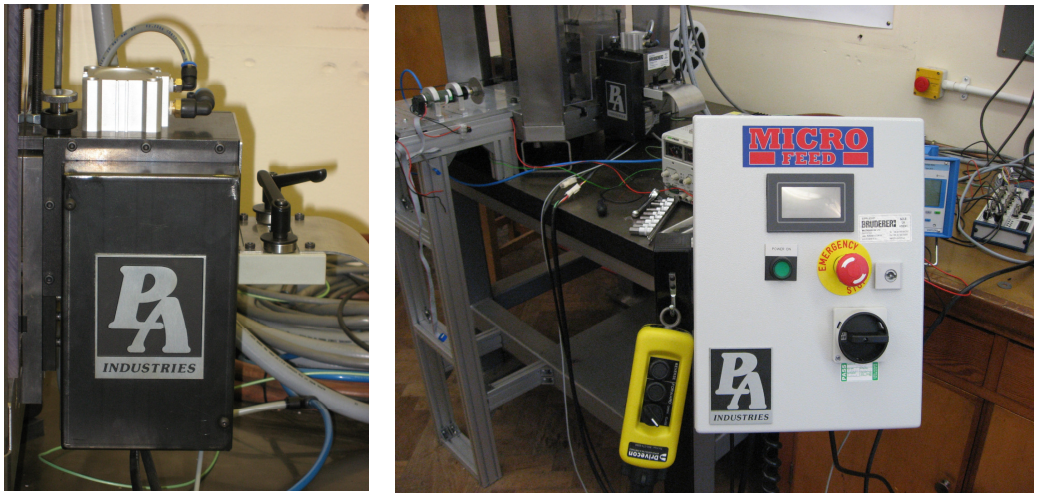

(a) (b)

Fig. 2.14: Showing: (a) a micro-servo roll feeder; and (b) a human interface device and machine controller for micro-servo roll feeder.

2.3.3.2 Thin-sheet Pneumatic Gripper-Feeder

A thin-sheet pneumatic gripper-feeder developed by POWair Industries, as shown in Fig. 2.15(a), is used as an alternative material-handling device, apart from the servo roll-feeder, for the developed micro-sheet-forming machine. The feeder has a comparatively high pulling force of 90N and a soft textile conveyor ensures that the surface of the thin sheet-metal remains unmarked when clamping and retention take place. In order to change the feed distance, manual adjustment has to be made on both the side bolts and the screws to move the fixed stopper, as shown in Fig. 2.15(b). Then the bolts are tightened to prevent the stopper from moving when material feeding is in process.

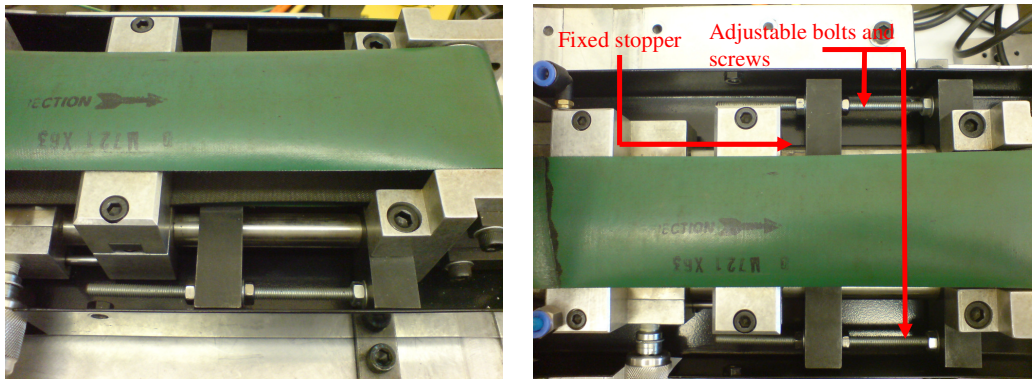

(a) (b)

Fig. 2.15: Showing: (a) a pneumatic gripper feeder; and (b) the location of adjustment screws and bolts to change feed distance.

2.3.4 Other Issues Related to Handling in Micro-Sheet-Forming

A recent review of micro-handling has demonstrated that a vast amount of attention has been paid to various object-geometry handling-devices [Ataka et al., 1999; Suda et al., 2000; Mishima et al., 2002; Engel et al., 2002]. By using an appropriate micro-manipulator, sub-micron precision could be achieved and has been confirmed by many researchers. Nevertheless, the case is not the same when it comes to the handling of thin sheet which has thickness of sub-millimetre for example 100µm thick strip. Although the presence of a conventional feeder in the market had demonstrated a huge success in the forming industry, especially in sheet-metal feeding, the feeder design in the first place was not meant for the feeding of thin sheet. The precision of the conventional feeder, that is obviously good enough for the conventional process, is not adequate in a micro-stamping application, as the precision achieved in conventional stamping is about similar to the thin-sheet thickness used and part features produced in the micro-stamping world. In micro-forming, level of precision required is best demonstrated by the punch- and die-clearance, which is at 5-15% of the sheet thickness [Kibe et al., 2007]. This is beyond the capability of a conventional sheet-feeder.

2.4 Methods and Software for the Analyis of Feeding and Feeders

2.4.1 Fundamental Studies

Fundamental experiments were also conducted to study material properties of the tested strips. The experiment includes surface roughness measurement, uniaxial/tensile testing, electron backscattered diffraction analysis (EBSD) and determination of friction coefficient.

2.4.1.1 Surface Roughness Measurement

The quality of the machined surface is characterized by the precision of its manufacture with respect to the dimensions specified by the designer. Dimension specification is specified and required because every machining operation leaves characteristic evidence (i.e. a pattern) on the machined surface. This evidence may be in the form of finely-spaced micro-irregularities left by the cutting/working tool. Each type of cutting/working tool leaves its own individual pattern, which therefore can be identified. For instance, rolling-process operations impart a specific surface finish of the rollers' surface pattern on the rolled/worked sheets. This pattern is called "surface finish" or "surface roughness" and can be measured using a profilometer. Surface-roughness measurements were conducted because surface roughness is believed to have an influence on a contact-pair's coefficient of friction, as described elsewhere [Sahin et al., 2007].

2.4.1.2 Uniaxial Tensile Testing

A common approach in metal forming is to express the properties of the work-material using stress–strain curves. The mechanical properties of popular engineering materials are often idealised for use in theoretical analyses and could be useful to validate FE works. Several standard test methods may be used to obtain the experimental stress–strain curves: commonly-used methods include tensile, compressive, bending and torsion tests. [Lange, 1985; Kalpakjian et al., 2006]. These tests are usually conducted under prescribed conditions of temperature and strain-rate. Since the stress–strain relationship of a material is dependent on the working conditions, a test may be performed using special facilities to derive accurate descriptions of the behaviour of the work-material under special conditions. While

current efforts are to improve the measurement of the material properties of new materials or those under more complex working conditions, the principal forms of tests remain the same [Lange, 1985; Kalpakjian et al., 2006].

Uniaxial tensile test is the simplest and most convenient method and is used to determine material properties for particular temperature and strain-rate specifications. Tensile tests are mostly used to test the materials that are to be sued in mechanical structures in which the materials deflect elastically or undergo low-levels of plastic deformation. Mechanical-properties analyses on thin sheet-metals has received vast attention worldwide, covering some of the popular engineering materials [Peng et al., 2009; Lai et al., 2008].

2.4.1.3 Electron Backscattered Diffraction (EBSD) Studies

Apart from the determination of mechanical properties through the uniaxial testing that was conducted on each strip, measurement of grain structure is also important because grain size has an influence on the mechanical-properties of the material [Peng et al., 2007; Vollertsen et al., 2004]. Therefore, electron backscattered-diffraction analysis was conducted on each strip with a view to determining grain-orientation, boundaries, shapes and sizes.

2.4.1.4 Friction Coefficient Determination

Estimation of the coefficient of friction was conducted based on published values in the handbooks: for a contact pair of steel and steel this is 0.15 [Roberts, 1978]; for a contact pair of steel and aluminium this is 0.20; for a ; contact pair of aluminium this is 0.30 [Lange, 1985; Kalpakjian et al., 2006]; and for a contact pair of steel and polyurethane rubber this is 0.70 [Rothbart et al., 2006].

2.4.2 Validation Experimental Approaches

There are two measurement-approaches used to observe and qualify the performance of both the micro-servo roll and pneumatic gripper-feeder, as shown in Fig. 2.16. Both of the identified methods involve contact and non-contact measurements.

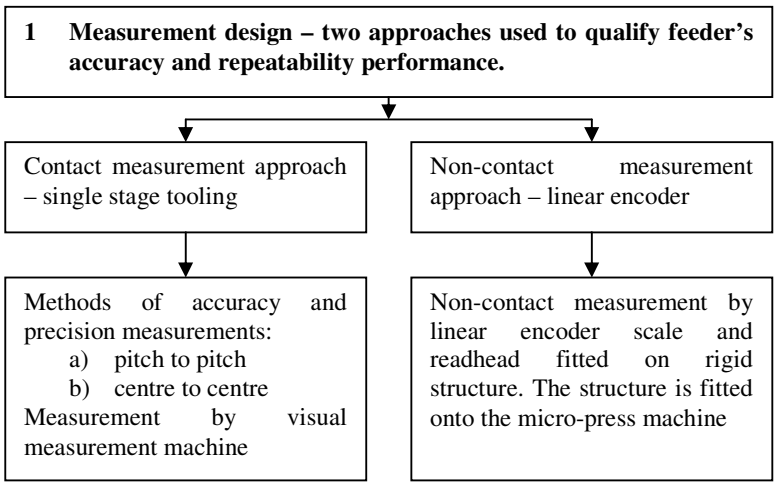

Fig. 2.16: Two approaches used to determine feeder performance: contact and non-contact methods.

2.4.2.1 Contact Measurement

This classical approach has been used effectively for several decades; markings being made on the studied material and the distance between the markings then measured. In the conventional forming-process, feeding-precision measurement is established by measuring the distance between the holes/parts made. There are many methods that may be used to measure the formed distance; the most popular being conventional contact-methods – which use a contact measuring instrument such as a vernier caliper, a scale or a measuring tape. Another technique which has been found to be promising for better measurement-precision is to employ a non-contact vision measuring machine.

Although a vision measuring machine is useful in establishing very accurate measurement, the precision may be depending on the lighting technique used to visualize the subject in the first instance. Different lighting technique could result in different error values being indicated during the measurement process. In addition, inconsistency of the marking/punching process could still cause error in the measurement [Mitutoyo].

In micro-forming, slight error in measurement could lead to catastrophic consequences. Cutting-inconsistency during the forming process somehow becomes a source of measurement error. This may be initiated by a worn tool/die set, which ultimately increases the tool clearance to an unacceptable value.

2.4.2.2 Non-contact Measurement

In order to eliminate the influence of tooling tolerance on the positional precision measurement, hence improving measurement reliability, a new approach to measure positional precision is proposed by the non-contact method. By employing the non-contact method to measure the pitch distance fed by the feeder; accurate measurement can be expected [Castro, 2008; Gao et al., 2007; Gao et al., 2006; Zi-qiang et al., 2006]. Due to there being no influence from the tooling geometry and tolerances, nor from other sources of mechanical inaccuracy, precise measurement can be obtained and recorded.

Gao et al., (2006) used a non-contact measurement system to measure multi-degree-of-freedom error motions of a precision linear-air-bearing stage. They used an autocollimator and a laser interferometer to determine the errors. Both of these non-contact methods gave a greater level of precision, up to nanometer precision, in the measurements, compared to the precision of a linear encoder. Nevertheless, a linear encoder is usable in such applications as do not require nanometer precision, while keeping the cost of measurement lower than that for an autocollimator or a laser interferometer. Normally, linear encoder is used as a positional feedback-mechanism in a closed-loop system. A commercially-available linear-encoder system has sub-micron resolution and a small linear-error over a meter length, which makes it suitable for use as a non-contact micron-range measurement-device.

2.4.2.3 Adjusted Parameters

As the feeder for micro-stamping application is expected to meet a tight design accuracy of 5-15% of the sheet thickness used, various key parameters have to be studied. Several parameters were chose in a view to developing an extensive and conclusive experiment on the performance of a thin sheet-metal feeder. The

flexibility of a servo feeder has allowed changes in the various feeding parameters that suit the demands of varying-operatibility of the forming process to be made more easily. Although a designated forming process requires a designated feed distance, e.g. in a. multistage-stamping process, when it comes to tooling changes, flexibility to cope with different feed distances without major modification is paramount. This creates variation in feeding performance, especially in a micro-stamping application, due to the feeding precision with shorter distance no longer being able to be treated similarly as for a greater feed distances.

In order for a feeder to survive commercially in the market and at the same time maintaining the feeding precision within a designated tolerance, the feeder has to be fast. Therefore, variation of the feed frequency also has to be taken into account, as this will ensure that the feeder speed is within the designated precision tolerance.

A successful feeder design also depends on the capability of the feeder to cope with various sheet thicknesses and materials. Not only restricted to softer material, the feeding of harder and exotic materials is seen to be more useful to the manufacturing industry [Aronson, 2004]. This open flexibility ensures that the feeder can compete and be reliable for any micro-stamping application.

One of the key issues in the forming process is friction during the forming itself. Excessive friction can result in a greater rate of wear and tear of the tooling, hence reducing the tooling life. Although the contribution of friction in material handling is not as critical as the forming process itself, study to examine the effect of lubrication on feed precision may be useful in this development work.

2.4.3 The Finite-Element Method and Software

The finite-element method (FEM) was developed as a technique for the analysis of structures. A number of structural elements may be analysed as an assembly. The feasibility of applying this technique to analyse complex structures was enhanced by the development of digital and fast processing computers. The method was extended subsequently to solve problems relating to the deformation of continuum bodies

which may be subjected to discretisation into a number of small geometrical elements (similar to individual elements). Progress in developing numerical methods for studying and solving finite-element equations for thin sheet-metal strip has been dealt with extensively by [Farzin et al., 2002; Manabe et al., 2007; Messner et al., 1994].

A major advantage of FEM is its capability of obtaining detailed solutions of the mechanics in a deformed body, as well as a body's displacement and behaviour when subjected to external forces, loads, velocities, temperature and pressure. The displaced body and its behaviour can be of such complex geometry as would be very difficult to analyse using classical methods.

2.4.4 ABAQUS/CAE

ABAQUS is an FE analysis system that includes ABAQUS/Standard – a general-purpose finite-element analysis program, ABAQUS/Explicit – an explicit dynamics finite-element analysis program and ABAQUS/CAE – a computer-aided sketching and modelling environment before executing analysis. The system is programmed for application to linear and non-linear analyses of a continuous medium. ABAQUS provide powerful solving-functions that cover static and dynamic-stress/displacement analysis, heat-transfer and thermal-stress analysis, material-fracture analysis, fluid-flow and acoustic analysis. These analyses are supported by comprehensive descriptions of linear and non-linear, isotropic and anisotropic, work-material models. They also provides an efficient means of modelling by including a comprehensive element-library, flexible definition of boundary conditions and node-freedom constraints, efficient pre- and post-processing functions as well as a standard user subroutine interface [Hibbitt et al., 2002a; Hibbitt et al., 2002b; Hibbitt et al., 2002c].

ABAQUS has the following functions that are particularly effective for the simulation of the material-handling process:

- ABAQUS provides large-sliding-contact elements that cover both contact between elastic/plastic and rigid-bodies and contact between two elastic/plastic bodies (deformable bodies) for both 2D and 3D application. These elements enable the simulation of material sliding on tool-surfaces. ABAQUS also retains sufficient numerical-robustness of contact analyses that ensures that the simulation of material-flow on complex tool-surfaces may converge.
- A flexible material-library enables the study of forming with reference to different material-characteristics; the analysis can be further enhanced by using an available material-subroutine interface that allows other material-characteristics than those of ABAQUS standard material-models to be defined by the user.
- The standard friction-formulation and friction user-subroutine interface enable the modelling of friction using a variety of friction models; similar capabilities are provided for thermal surface-interface models. These provide the required flexibility for the simulation of cold-, warm- and hot-deformation processes.
- ABAQUS/Explicit provides an efficient tool for the simulation of dynamic and quasi-static problems. It is particularly useful for the simulation of such as sheet-forming process.
- A flexible job-input-file, written and edited by using a primitive text-reader. This enables complex editing of the model that is unavailable within, or could not be edited within, the ABAQUS environment. The job file also can be executed within the MS-DOS command environment without having to load the program environment.

2.5 Summary of the Findings

Based on the literature study conducted in this chapter, it has been established that micro-manufacturing has received good attention globally in terms of its manufacturing methods/processes (Fig. 2.17). One of the most popular micro-manufacturing processes is micro-forming [Peng et al., 2007; Ocan˜a et al., 2007; Manabe et al., 2007; Chern et al., 2004; Chern et al., 2006a; Byung et al., 2005; Qin et al., 2008]. Many effort has been focused on micro-forming, mainly on the micro-stamping process due to the process itself contributing numerous products, especially in its conventional macro-process. Most every-day products are made by this process. Although there were efforts made to realize micro-stamping for industrial application, the technology itself was seen as being insufficiently mature. Much development work needed to be done, specifically to develop a fully-automated high-volume production micro-stamping machine, which is reliable and at all times ready for operation in terms of it processes, tooling, and material-handling to ensure the successful production of micro-products.

Although effort on the development of a micro-stamping machine has been successful vindicated for high-yield production [Qin et al., 2008] and has confirmed some of the preliminary concepts [Chern et al., 2004], there is still lack of effort to address material handling for the micro-stamping process. Feeding sheet-metals in conventional stamping is no longer a major problem in production [Schuler, 1998]. However, challenges arise when thinner metal-strips are to be used in micro-stamping (e.g. <100 μm) and the parts/features to be formed become smaller (e.g. sub-millimetre ranges). In these cases, the stamping of a micro-sheet-metal component may require the feeding/positioning of the sheet-metal under the forming tools to be as accurate as within one to a few microns. This is particularly important in multi-stage progressive micro-stamping, in which neighbouring features of a part may be very close to each other. Therefore, feeding the sheet-metal has to be very accurate in order to prevent any inaccurate forming or damage to the neighbouring features and connections of the part/scraps to the strip.

In addition to this, another challenge is to meet high-volume production capability. High-precision material handling is somewhat difficult to achieve in conjunction with high-speed motion. Negligible factors such as the machine's stiffness and rigidity, vibration and changes of temperature in the conventional-stamping process can no longer be neglected in micro-stamping material-handling. Therefore, an effort has to be made to realize high-precision material-handling for micro-stamping application by addressing the solution of the two key issues reviewed in this chapter.

Fig. 2.17 illustrates the gap discovered by the present literature-review. Boxes with dotted purple-coloured line show where no effort has ever been embarked upon to develop the system, while the shaded purple-boxes show areas in which this research was intended to embark upon on. The green-dotted boxes represent where no micro-parts have ever been produced by the respective processes.

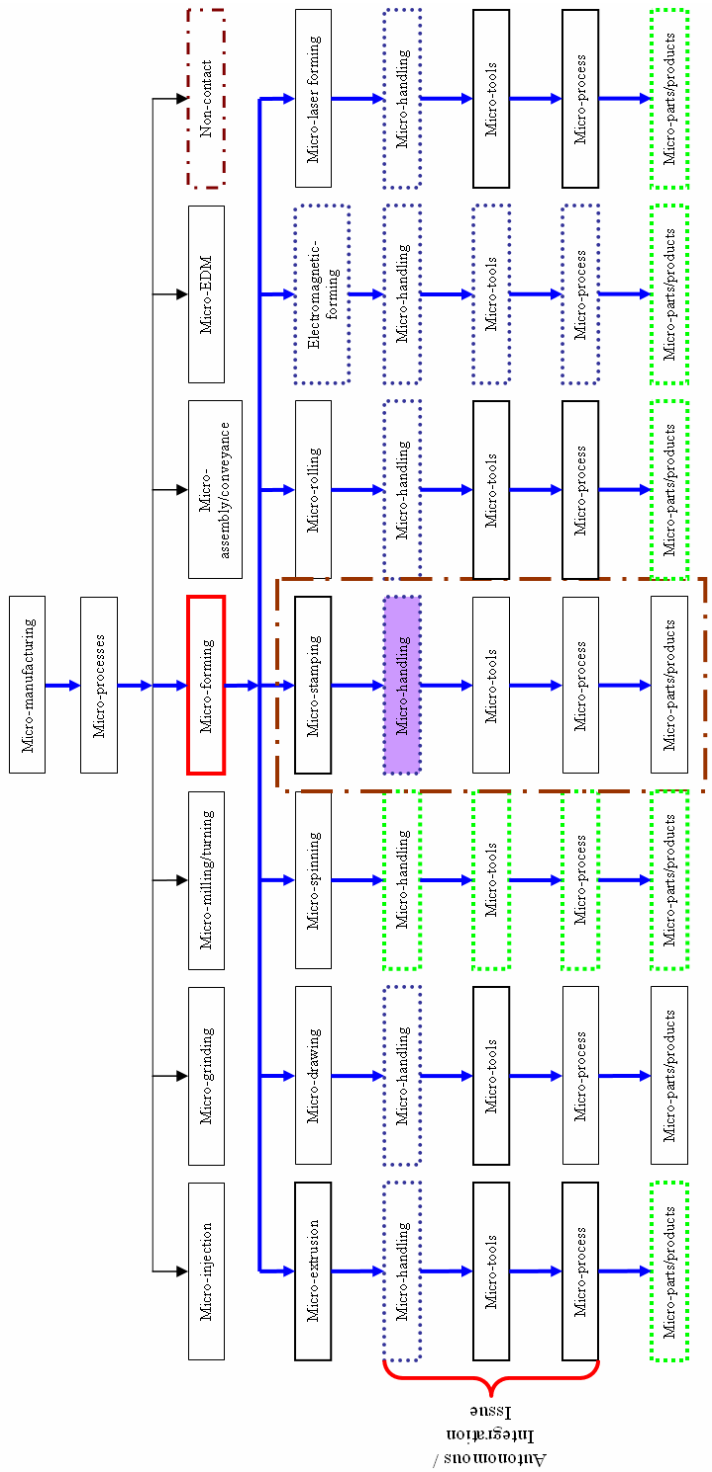

Fig. 2.17: The existing gap in micro-forming development.

Chapter 3

Fundamental Studies of the Materials

3.1 Summary

Usually negligible factors in macro- or miniature size materials such as grain-size effects, may not be neglected in micro-forming processes. Studies had shown that material behaviour varies greatly with the increasing of the scale in the micro-forming world [Lai et al., 2008; Peng et al., 2007]. Therefore, in every micro-forming-related process, especially in micro-stamping, studies and analyses of each material used for the process have to be considered as indispensable in order to be able to understand their behaviour and to be able to correlate their behaviour with the process. Uniaxial tensile-testing experiments have been carried out to determine the strip's properties, behaviour and its correlation with the feeding process in micro-stamping/micro-sheet-forming application. Based on the results of the uniaxial tensile-test experiments conducted, the flow stress was found to decrease with the decrease of the strip thickness and vice versa, due to the size/scale effect. A surface model was used to explain the findings. It is known that surface roughness has some correlation with friction. Therefore, surface-roughness measurements and the coefficient of friction between contact pairs also have been determined in order to study the correlation between the two quantities.

3.2 Introduction

When feature size of a part is reduced to less than 1mm, the so-called size-effect arises, which means that knowledge in terms of empirical and analytical know-how of the conventional forming process cannot be applied directly in the micro-forming world. Numerous research efforts have been made the results of which confirm that material behaviour at micro-scale is different from that at macro-scale [Vollertsen et al., 2006; Engel et al., 2002].

The purpose of this chapter is to describe and understanding the influence of the size effect on material behaviour as well as to determine the correlation between coefficient of friction and surface roughness. Then the material behaviour is discussed with regard to the micro-stamping material-handling process. Finally, correlation between the coefficient of friction and surface roughness is explained.

3.3 Equipment and Materials

3.3.1 Surface Roughness Measurement

The equipment used to measure surface roughness is the profilometer. In this research, the profilometer made by Mitutoyo is used, as shown in Fig. 3.1. This Surftest SV2000 model machine uses maintenance-free ceramic material for the X-axis drive-unit guide, which material is known for its superb anti-abrasive property. Equipped with a high-accuracy stylus for high-accuracy measurement, it is also equipped with various functions such as a 'straightness compensation' function which improves the linear accuracy of the X-axis, a 'circular compensation' function for the vertical movement of the stylus, and a 'stylus-tip diameter compensation' function to take account of the effect of the stylus dimensions on the measurements.

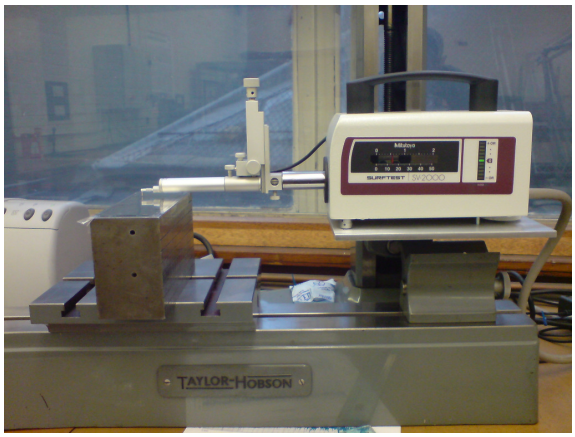

Fig. 3.1: Mitutoyo Surftest SV2000 equipment used to measure surface roughness.

3.3.2 Tensile Testing

A universal testing machine made by Zwick REL Switzerland, Model 2061 (Fig. 3.2), was used to measure the material's mechanical properties. The machine has various ranges of working tensile and compressive load; 0-2.5, 0-5, 0-10, 0-25, 0-50kN, with a resolution of 1N. The maximum actuator stroke is at ±50mm with an actuation speed of up to 5000mm/min. The machine calibration process was done according to the BS EN 150 7500 standard to ensure accurate and reliable results. Data logging was performed using a standard desktop PC with installed dedicated data-logging software. The screw grips are 60mm wide and 55mm deep and can hold material of up to 10mm thickness and as thin as micron-range thickness.

Fig. 3.2: Zwick REL universal testing machine Model 2061 used to determine material mechanical properties.

3.3.3 Electron Backscattered-Diffraction (EBSD) Study

Electron backscatterred diffraction (EBSD), also known as backscattered Kikuchi diffraction (BKD), is a technique used to examine the microstructure-crystallographic orientation of many materials. EBSD can also be used to index and identify a crystal system specifically for the purpose of crystal-orientation mapping, defect studies, grain boundary and morphology studies, phase identification, material discrimination, etc. Differently from the scanning-electron microscope (SEM) which produces an image in the same grey-scale, EBSD enables materials with different compositions to be indexed in different gray-scales (contrast: from brightest to darkest) or colors. EBSD uses similar equipment to that used in the scanning electron microscope (SEM) and is also equipped with a backscatter diffraction camera. The camera consists of a phosphor screen which is inserted in the specimen chamber and mounted at greater than or equal to 90° to the pole piece. It also uses a charge-coupled device or a CCD image-sensor (converts light to electrons for digital-image interpretation) to ensure a sharp, vivid and crisp image. The testing specimen must be a really flat and polished crystalline specimen, which is placed in the normal position in the specimen chamber and highly tilted up, to 70° (measured horizontally), towards the diffraction camera.

An electron beam is projected onto the specimen where, due to the angle of the specimen, diffracted electrons escaped from out of the specimen material. The electrons are then redirected towards, and collide with, the phosphor screen of the diffraction camera, causing it to illuminate/fluoresce. The diffracted electrons produce a diffraction pattern and are detected by the camera's CCD. This pattern is sometimes called an Electron Backscatter Pattern (EBSP).

Recent efforts made elsewhere [Gao et al., 2005] have revealed that the use of EBSD has proven to be an excellent tool for quantitative metallography. Research work has revealed the capability of EBSD analysis, which is not only limited to grain size determination, but also there are a number of important microstructural parameters

that may be determined through the analysis that are not obtainable by conventional light microscopy.

EBSD analysis also may reveal a greater number of grain-counts compared to the use of conventional light-microscopy methods. This in turn leads to a better range of microstructural analysis that covers analysis from the smallest to the biggest grain size. Consequently, this leads to better and more accurate measurement of grain-size, deviation and aspect-ratio. EBSD testing, however, may be considered expensive, as the equipment itself requires a substantial investment. Therefore, only a few companies/institutions may own such a machine, which will be dedicated to microstructural-crystalline studies related to the core business of the company/institution concerned. For the purposes of this research, due to the unavailability of a machine, the experiments were out-sourced to the National Physical Laboratory (NPL), the EBSD system used there being an Oxford Instruments/HKL Nordlys detector.

3.3.4 Materials Used

3.3.4.1 Tensile-Testing Specimen

The tensile tests first require the preparation of a test specimen, typically from a sheet coil, as shown in Fig. 3.3. The specimens were prepared according to ASTM D 638 specification (Fig. 3.4) and cut using an abrasive water-jet (Fig. 3.5). This cold-cutting process is favoured in order to avoid the accidental production of any heat-treated edges, which possibly could happen if laser or electro-discharge-machining processes were chose. Specimens were prepared in both the transverse and rolling directions with gauge lengths in the transverse and rolling directions of 14mm and 13mm respectively. Three types of specimen were used: 50µm and 100µm thick carbon-steel strips; and 50µm stainless-steel strips; and prepared to the same nominal size.

Fig. 3.3: Carbon- and stainless-steel strips used in the research.

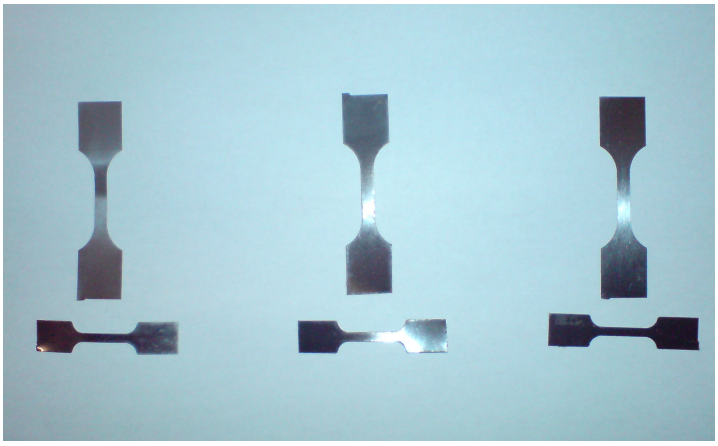

Fig. 3.4: Tensile testing specimens.

Fig. 3.5: Abrasive water-jet cutting used to prepare the specimens.

3.3.4.2 Electron Back-scattered Diffraction (EBSD) Specimens

There were six steps used to prepare each of the strip specimens for EBSD testing, namely, sectioning, mounting, grinding, polishing, chemical etching and the application of a conductive coating [Schwartz et al., 2000]. Sectioning was conducted to remove a representative area from each of the parent specimens. The specimens were cut to 10mm length (in the rolling direction) and 5mm width (in the transverse direction) and mounted (using a short cylindrical mould of 30mm diameter and 16mm in height) in acrylic resin, the cross-sectional area being exposed for examination. Preparation by using bakelite was found unsuitable for thin sheet, as the sheet would not adhere easily to the bakelite. Moreover, the application of compacting pressure along with a relatively high baking temperature could lead to severe deformation of the strip as well as loosening of the bond, allowing the sample to flex. Therefore, acrylic mounting was seen as the best way of preparing the specimens. A similar preparation-technique was employed for all of the strips to ensure that a fair comparison could be made.

These specimens were ground to remove any deformation layer introduced during sectioning and to produce a flat surface for examination. Grinding was done with several grades of sand-paper (SiC), started from 240 grit SiC, continuing to 800 grit SiC and finally finishing with 1200 grit SiC. Water was used as a lubricant during grinding and also to flush away any retaining material, thereby exposing a fresh abrasive surface. Next, polishing was conducted to remove any deformation developed earlier during grinding. An oxide polishing suspension (OPS) and polishing clothes were used to polish the specimens to a surface finish of 0.05μm.

Chemical etching (nital and cupric etchant) was used as an alternative to electro-polishing. Polishing by electro-polishing requires some kind of electrolyte to etch the specimen. In this technique, an optimum configuration of voltage and current are required for each strip: there is also no universal electrolyte available and will work with all material at one time, thus resulting in difficulty in preparing each specimen. Therefore, chemical etching is seen as being more favourable due to the process not

requiring excessive set-up time and too many configurations, as well as experimentation for determining the optimum operating conditions. During the etching process, the specimens are swabbed with an etchant that can dissolve the surface material to remove any remaining surface deformation due to polishing. A specimen at this stage of preparation is shown in Fig. 3.6.

Fig. 3.6: Prepared EBSD specimens.

Due to charging effects, observing non-electrically-conductive material is found to be difficult when using scanning-electron techniques, which also include EBSD. Charging effects degrade the observed microstructural pattern as well as causing the beam to drift. Although the samples used were steel, which is a very conductive material, due to the natural characteristic of the mounting material, acrylic resin, which is non-conductive, it may be possible to obtain a clear mapping of microstructural pattern. To reduce the chance of degraded-image mapping, the specimens were mounted in thermosetting bakelite and then were polished again. Polishing was carried out using diamond polish, beginning with 9µm, followed by 6µm, then down to 1µm. Finally, the specimens were polished using colloidal silica for 30 minutes. A conductive carbon coating of approximately 25angstroms thickness was applied to the specimen to achieve a clear mapping pattern, thereby producing clear index and hence an accurate analysis.

3.4 Procedure

In order to determine the basic mechanical properties of the strips studied, three types of analyses were categorized and designed. First surface roughness testing was conducted on each strip, followed by uniaxial testing and electron backscattered diffraction (EBSD). Five random points were selected on the specimens studied and measured in both the transverse and the rolling direction on both sides, as shown in Fig. 3.7. Six measurement-samples length of 0.8mm each were tested, which complies with the BS 2634 [British Standards Institution, BSI] standard related to the determination of surface roughness. A Gaussian-filtered straightness-compensation measurement was performed to negate the effect of waviness of the strip and the supporting base. Both the measurement and the evaluation conditions are given in Table 1. For uniaxial testing purpose, 15 workable specimens of each strip (50µm- and 100µm-thick carbon-steel and 50µm-thick stainless-steel strips) were tested and the stress–strain curve for each strip was plotted and discussed. The EBSD system used was an Oxford Instruments/HKL Nordlys detector. The polished samples were mounted at 70degrees to the horizontal and were examined using a Zeiss Supra 40 FEGSEM at 20kV with a beam current of about 2nA.

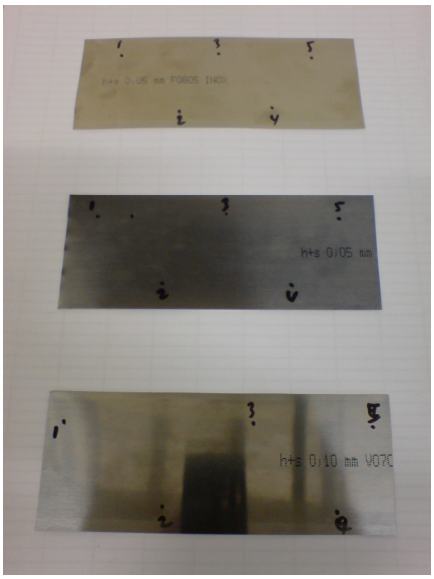

Fig. 3.7: Surface-roughness measuring point on each strip material.

Table 1: Measurement and evaluation condition of surface-roughness testing.

Measurement Condition	
Measurement Length	5.6mm
Speed	0.5mm/s
Over Range	Abort
Number of Points	11200
Range	80.0μm
R-Surface Auto-Measurement	Off
Pitch	0.5μm

Evaluation Condition	
Standard	OLDMIX
Kind of Profile	R (roughness)
Sampling Length	0.8mm
No. of Sampling	6
Lc	0.8mm
Kind of Filter	Gaussian
Evaluation Length	4.8mm
Pre-Travel	0.4mm
Post-Travel	0.4mm
Smooth Connection	Off
Mean Line Compensation	Off

3.5 Results

3.5.1 Surface-Roughness Result

Profilometer measurement on side one (identified with a strip-identification mark for all cases) of 50µm-thick carbon-steel strips in the transverse and rolling directions were recorded as 0.0762µm and 0.1258µm, respectively, as shown in Fig. 3.8. Shown on the same figure, for side two, are the surface-roughnesses for both directions, recorded as about 0.0786µm and 0.119µm, respectively. Based on the recorded-value measured on both sides of the strip, the transverse-direction surface-roughness is lower than that in the rolling direction. Similar and consistent surface-roughness patterns were also observed on 100µm thick carbon-steel strips, where the roughness in the transverse direction was observed to be lower than that in the rolling direction. Nevertheless, the observed surface-roughness values were lower than those for thinner carbon-steel strips. On the side with the manufacturer's marking (side one), both the transverse and the rolling direction roughness were recorded at 0.0480µm and 0.0614µm, while on the non-marking side (side two) they were 0.0632µm and 0.0906µm, respectively. Changing to 50µm thick stainless-steel strips confirmed the roughness trend, where the transverse roughness was recorded as being lower than that for the rolling direction. On the side with the manufacturer's marking (side one), the transverse roughness was observed to be 0.0602µm, while the rolling-direction roughness was 0.0944µm. Almost the same range of surface-roughness values was recorded on the second side of the strip, where the transverse-direction, roughness was 0.0620 and rolling-direction roughness was 0.0958µm. Table 2 summarizes the surface-roughness results for the various tested specimens – strips, feeder-rollers, retainers and gripper parts.

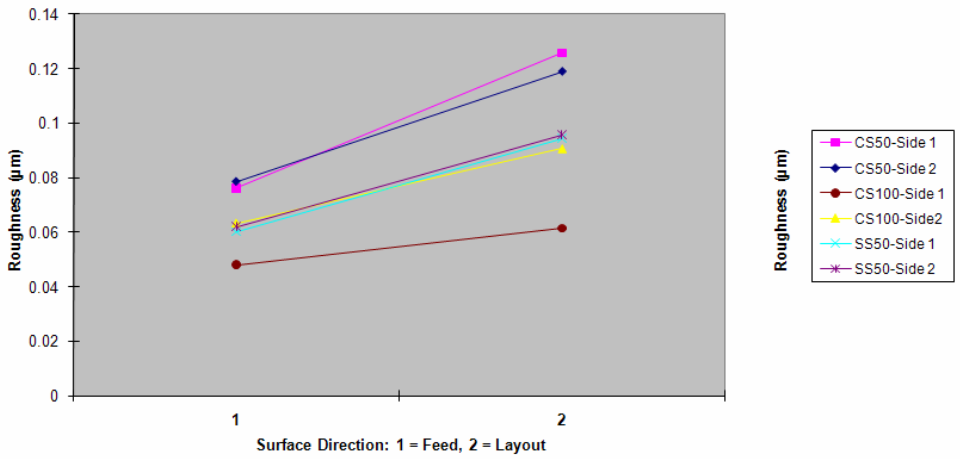

Fig. 3.8: Measured surface-roughness of strip materials.

Table 2: Surface-roughness results.

Specimen/Side	Direction	
	Transverse (µm)	Layout (µm)
50µm carbon steel (CS50) – Side 1 (marked side)	0.0762	0.1258
50µm carbon steel (CS50) – Side 2 (non-marked side)	0.0786	0.1190
100µm carbon steel (CS100) – Side 1 (marked side)	0.0480	0.0614
100µm carbon steel (CS100) – Side 2 (non-marked side)	0.0632	0.0906
50µm carbon steel (SS50) – Side 1 (marked side)	0.0602	0.0944
50µm carbon steel (SS50) – Side 2 (non-marked side)	0.0620	0.0958
Roll feeder		
Steel roller	-	0.0630
Rubber roller	-	1.1974
New feeder		
Retainer 1 – Base	0.2054	0.7924
Retainer 1 – Jaw	0.3404	0.2986
Retainer 2 – Base	0.2244	0.5634
Retainer 2 – Jaw	0.3970	0.2612
Gripper – Base	0.2294	0.4110
Gripper – Jaw	0.3124	0.3678

3.5.2 Tensile-Testing Results

Fig. 3.9 to Fig. 3.14 show experimental tensile-test results for thin carbon-steel and stainless-steel strip. Brittle materials such as 50µm and 100µm thick carbon-steels do not have a yield point, and do not strain-harden. This means that both the ultimate strength and breaking strength of each material are the same. The stress–strain curves for both the thin and thick carbon-steel strips are shown in Fig. 3.9 to Fig. 3.12 in both transverse and rolling directions. Typical brittle materials such as these carbon-steel strips do not show any plastic deformation but fail in the elastic-deformation region. One of the characteristics of the failure of carbon-steel strips failure is that the two broken parts can be reassembled to produce the same shape as the that of the original component, as shown in the previous figure, during specimen preparation. Therefore, linear stress–strain curves for both strips were observed.

From the figures, it was obvious that the flow stress–strain curves vary greatly with the sheet thickness. For carbon-steel strips, with the decrease of the thickness, the corresponding flow-stress in the transverse direction decreases, as depicted in Fig. 3.9 and Fig. 3.11. In the rolling direction however, almost similar stress–strain curves was obtained for CS50 and CS100 strips. The testing also revealed that less deformation was observed where none of the tested carbon-steel strips had significant plasticity deformation, hence no region of obvious plastic deformation was observed. The strips, however, were believed to fracture during elastic deformation, which was indicated by an almost linear stress–strain curve.

Differently to the case for stainless-steel strip (SS50), significant plastic deformation was observed in the given recorded stress–strain curves, as shown in Fig. 3.13 and Fig. 3.14 the strip being seen to be more ductile and possibly plastically-deformed before fracture. However, less force was required to result in fracture and failure. Table 3 shows the calculated modulus of elasticity for all of the strips tested. The modulus of elasticity is one of paramount parameter required for use in the finite-element analysis of feeding characteristics. Due to the modulus of elasticity

representing a material's stiffness, its relationship with feeding characteristic may be usefully observed and studied.

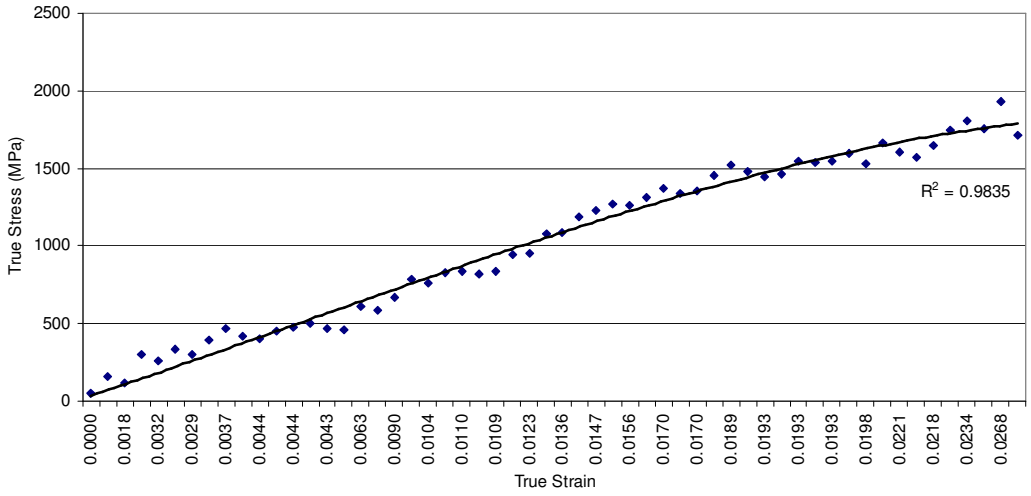

Fig: 3.9: Stress- (long stroke, not hyphen)strain curve for 50µm thick carbon steel strip in transverse direction.

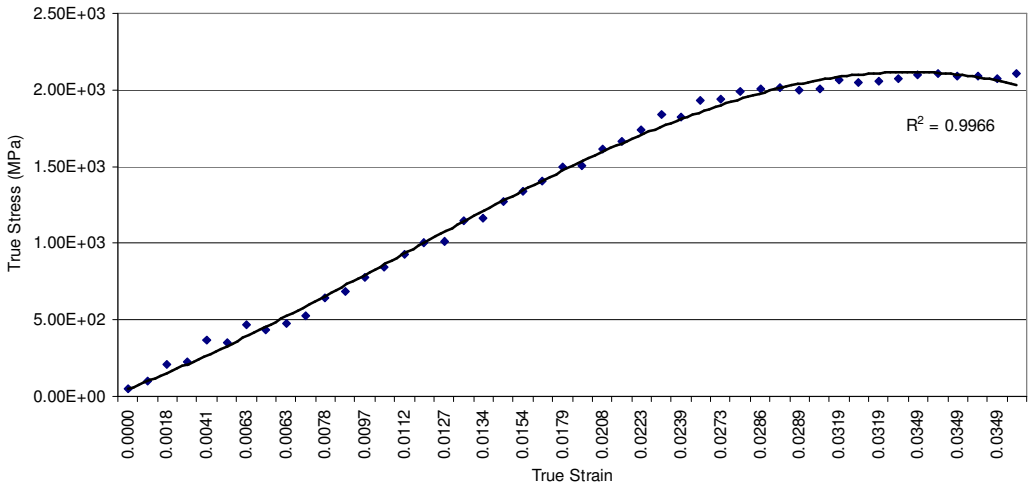

Fig: 3.10: Stress-(long stroke, not hyphen)strain curve for 50µm thick carbon steel strip in layout direction.

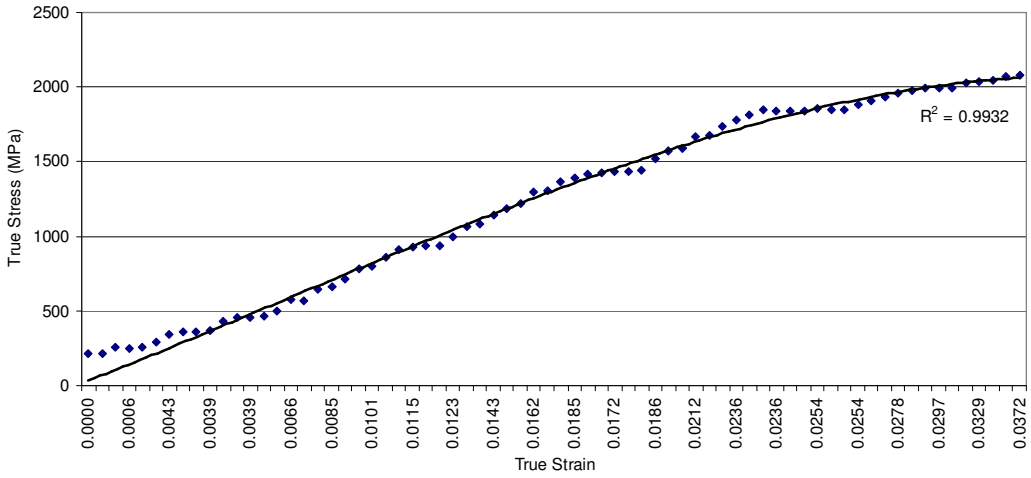

Fig: 3.11: Stress-(long stroke)strain curve for 100µm thick carbon steel strip in transverse direction.

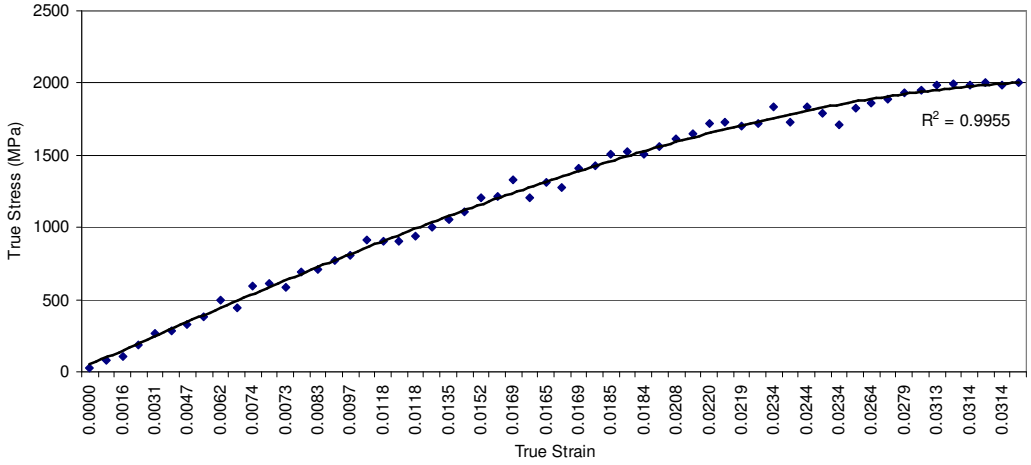

Fig: 3.12: Stress-(long stroke)strain curve for 100µm thick carbon steel strip in layout direction.

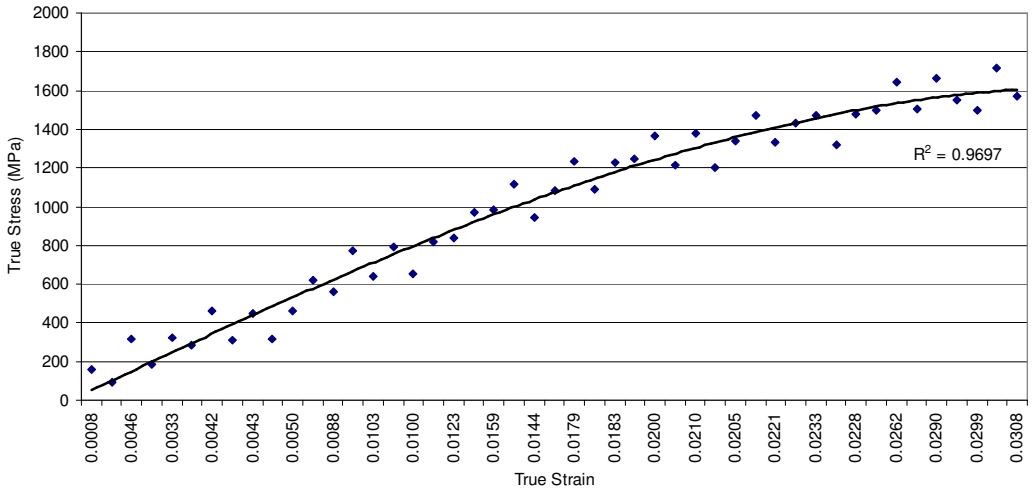

Fig: 3.13: Stress-)long stroke)strain curve for 50µm thick stainless steel strip in transverse direction.

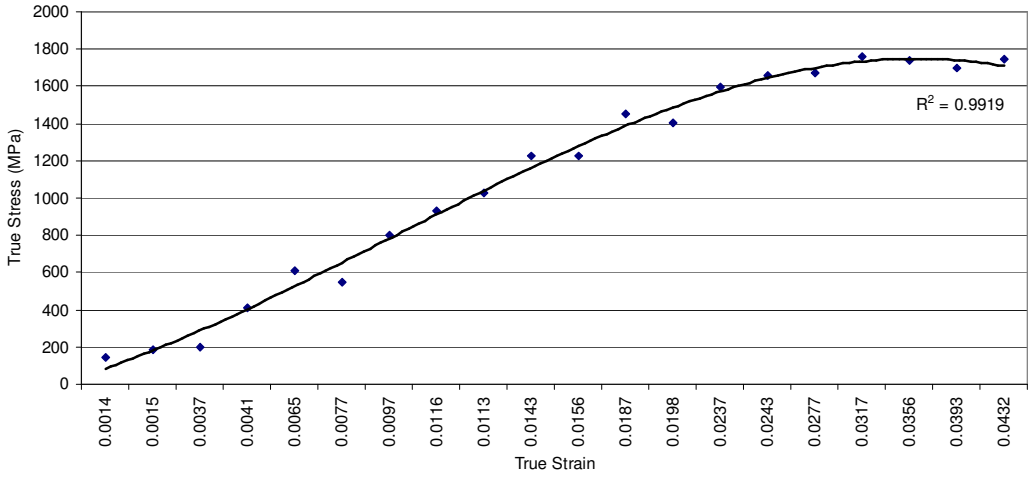

Fig: 3.14: Stress-(long stroke) strain curve for 50µm thick stainless steel strip in layout direction.

Table 3: Modulus of Elasticity

Specimen	E (GPa)
50µm carbon steel	78.3
100µm carbon steel	99.0
50µm stainless steel	75.0

3.5.3 EBSD Study Results

Inspection by conventional light-microscopy at 500x magnification (Fig. 3.15) revealed a bluish martensite region as well as a cementite content in the 50µm carbon-steel strip (CS50) due to the heat-treatment process. Quenching of the strip has resulted in some of the carbon content being formed into iron carbide. Iron carbide, also known as cementite (white spots), usually measures less than 1µm and increases the mechanical properties of the strip. This technique, light-microscopy, however, was found unable to provide grain sizes, orientation and neighbouring grain-patterns, hence the EBSD technique was employed. Fig. 3.16 shows grains coloured by size with the darker/red coloured being the larger grain size for 50µm carbon-steel strip. Although no specific shape may be used to define the grain, the grain was defined as areas enclosed by boundaries. A step-size of 0.05µm was used to create a reasonably clear resolution for accurate indexing of the microstructure. This step-size covers an image-mapping area of 30x35µm. Based on the analysis of the mapped image, there were 3404 counted grains. The smallest and largest measured grains were 0.0564µm and 5.2757µm, with an average of 0.4028µm. The numbers of small grains were seen to be dominating the microstructural pattern and no specific and uniform grain shapes were observed. This suggests that the previous deformed-grain (due to hot-rolling) might be reformed/reshaped due to the tempering process. A large aspect ratio was observed also, where each grain on average has an aspect ratio of 2.2288 and a maximum of 12.2060. A large and slender aspect ratio may cause the microstructure to become weak and less resistant to external forces.

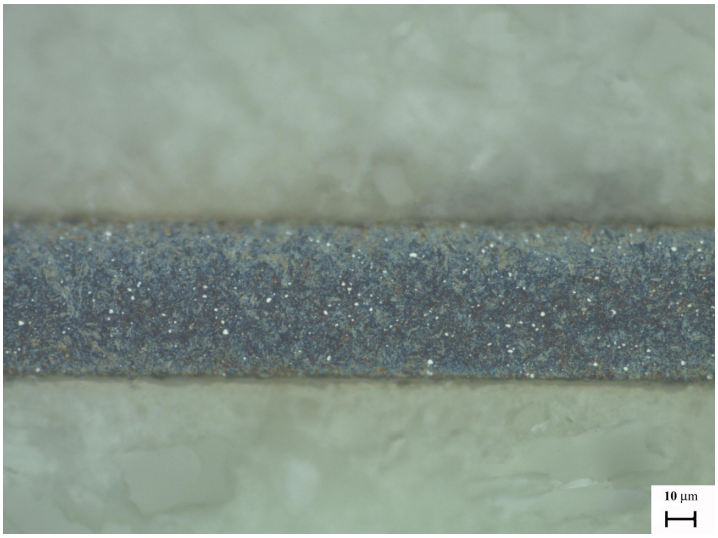

Fig. 3.15: CS50 at 500x magnifications, showing iron carbide/cementite (white colour).

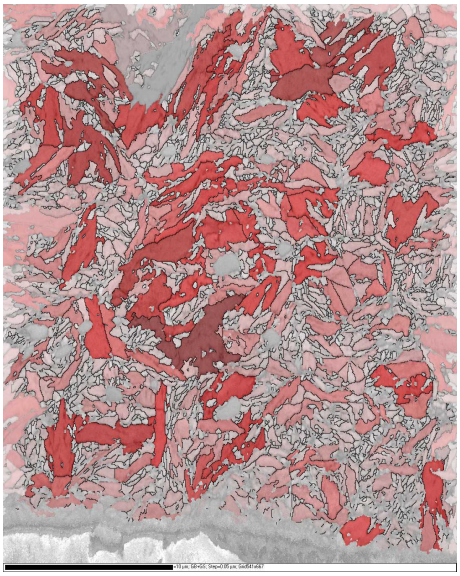

Fig. 3.16: EBSD microstructure mapping image of CS50 strip.

Fig. 3.17 shows an image of a photomicrograph of a 100µm thick carbon-steel strip (CS100) under light microscopy at 500x magnification. This technique may be found useful as a fast way to reveal the type of process that has been undergone by the strip material. Although this technique was unable to reveal greater numbers of grains than EBSD was capable of, the technique has proven able to identify irregularity-content of the strip. White spot on the image was identified as cementite, which may

cause an increase of the strength and brittleness of the strip. The presence of cementite on this strip was observed to be twice as much as for the CS50 strip.

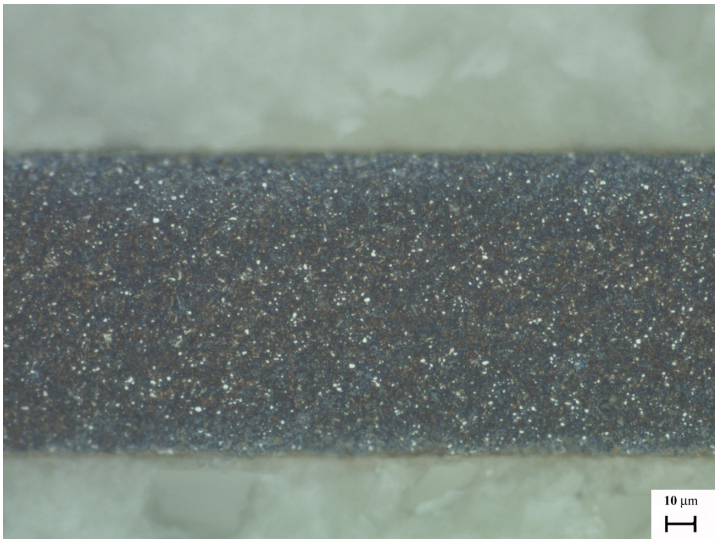

Fig. 3.17: Light-microscopy image of CS100 strip at 500x magnification with cementite shown (white colour).

An EBSD microstructure-mapping image of CS100 strip is shown in Fig. 3.18. A similar scanning-step as that for CS50 was used to observe the microstructure. A similar number of pixels was used to ensure that a broad and wide image would be captured, using the same total mapped area of 30x35µm. 6438 grains was successfully mapped with a grain-size average of 0.2661µm, the smallest and largest grains being 0.0564µm and 3.2762µm, respectively. The number of grains revealed was found to be twice many when compared with the number for CS50. This indicates that the CS100 microstructure was very dense and also consists of many tiny grain-sizes, smaller than those for CS50. This was confirmed by the average grain-size obtained throughout the examination, which revealed that CS100 grains were 34% smaller than CS50grains. An almost similar maximum aspect ratio as that for CS50 was found for CS100, which was a 12.3760. However, the average aspect ratio for CS100 was found to be slightly smaller than for the thinner carbon-steel strip, which was 1.8331. Due to the smaller aspect ratio, the grains might be able to stay close to each other, resulting in a very dense grain pattern.

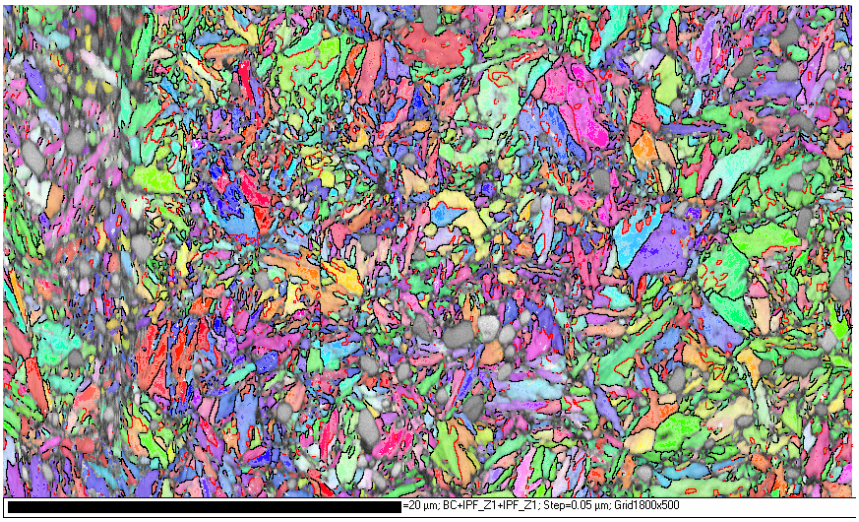

Fig. 3.18: EBSD microstructure-mapping image of CS100 strip.

The mapping of 50µm thick stainless-steel strip (SS50) using conventional light-microscopy at 500x magnifications (Fig. 3.19) shows many grains, which were heavily deformed due to the hot-rolling process. Nevertheless, the image from this technique was seen to be unable to show important microstructural information such as grain boundaries and clear distribution of neighbouring grains. Due to the larger grain size that may be obtained from a stainless-steel specimen, a large scanning step may be used to map and index its microstructure. 5618 grains were successfully mapped and indexed (Fig. 3.20) with an average grain size of 0.7698µm, which was larger than that for the tested carbon-steel strips. The minimum and maximum indexed grain-size were 0.2820µm and 20.2870µm, respectively. Due to the grains being heavily deformed, a large part of the mapped area could not be indexed, hence a large number of blanks were observed on the image. In order to obtain a clear view of grain boundaries and orientation, the mapped image was split into two images. Both of these images represent the indexed grain size, which is <1µm and >1µm, as depicted in Fig. 3.21 and Fig. 3.22, respectively. The analysis also reveals that SS50 has many larger grains compared to carbon-steel and has the greatest grain aspect-ratio of 19.7060. This has resulted in a lesser grain density, which may be affecting its mechanical properties. Table 4 tabulates all of the results obtained.

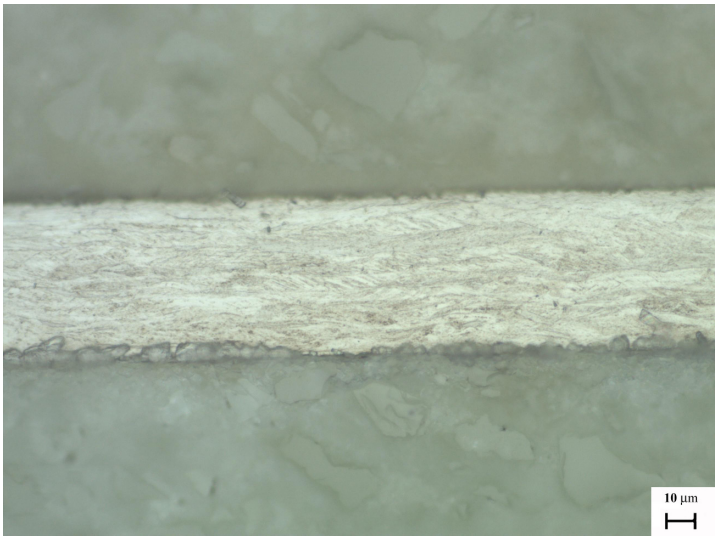

Fig. 3.19: Light-microscopy image of SS50 strip at 500x magnification.

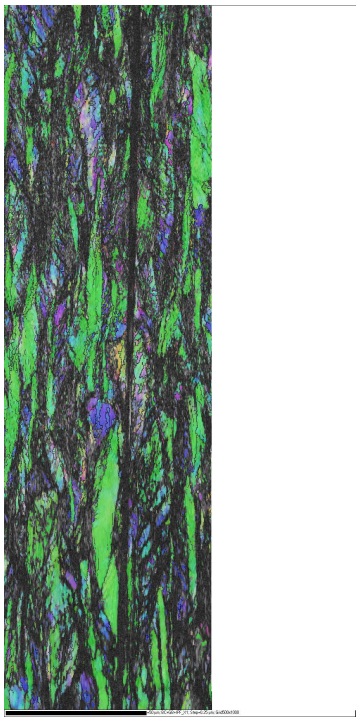

Fig. 3.20: EBSD microstructure-mapping image of SS50.

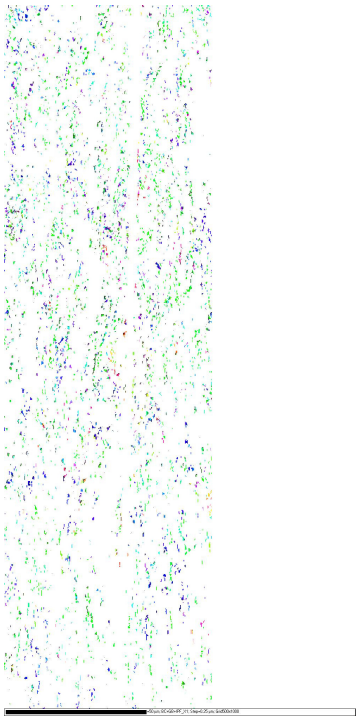

Fig. 3.21: EBSD mapping image of indexed <1µm grain size.

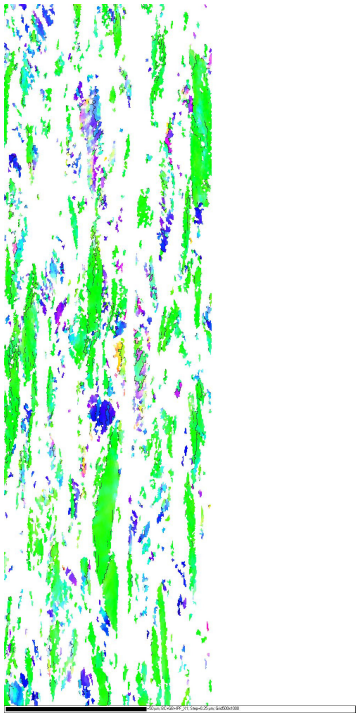

Fig. 3.22: EBSD mapping image of indexed >1µm grain size.

Table 4: EBSD and modulus of elasticity.

	CS50	CS100	SS50
Count grain, N	3404	6438	5618
Mean (µm)	0.4028	0.2661	0.7698
Minimum (µm)	0.0564	0.0564	0.2820
Maximum (µm)	5.2757	3.2762	20.2870
Standard deviation (µm)	0.3980	0.3072	1.0114
Grain aspect ratio			
Mean	2.2288	1.8331	2.0039
Minimum	1.0000	1.0000	1.0000
Maximum	12.2060	12.3760	19.7060
Standard deviation	1.0546	0.8834	1.2024

3.6 Discussion

3.6.1 Surface Roughness and Friction Correlation

A huge difference of surface-roughness value between the two directions suggested that transverse direction had imparted on it the forming roller's surface pattern. There are the obvious irregularities of fine straight-line micro-peaks and a valley surface-structure parallel to the rolling direction, as illustrated in Fig 3.23. Nevertheless, this fine straight-line irregularity is difficult to be traced by stylus if compared to the situation for the other direction. In the other direction, the presence of this fine-irregularity straight-line was traced easily.

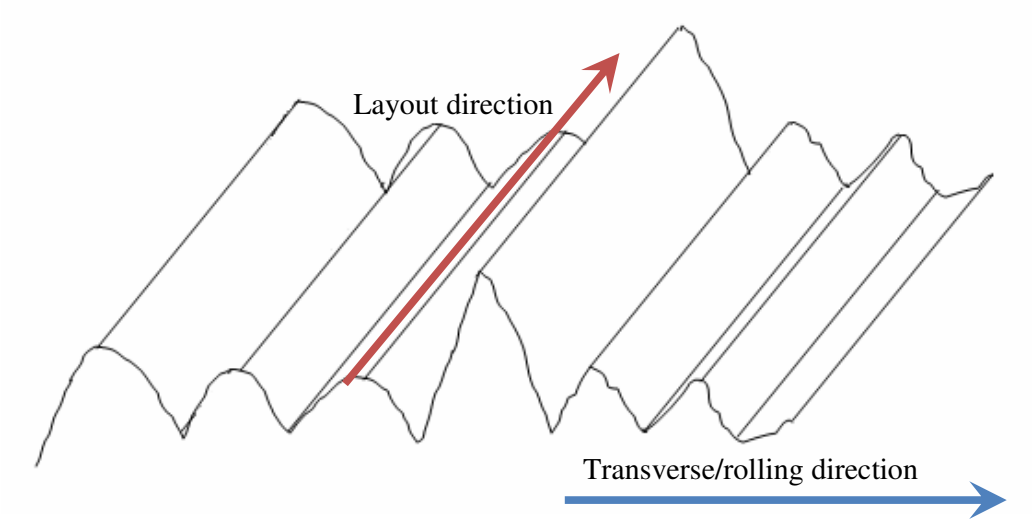

Fig. 3.23: Surface-roughness pattern.

Numerous research works has been carried elsewhere to investigate the correlation of surface roughness and coefficient of friction [Jung et al., 2008; Sahin et al., 2007]. Nevertheless, it is still unclear to discuss on the relation between the two in this case.

3.6.2 Size Effect and Material Stress–Strain Relation

Studies had demonstrated that the flow stress of thin sheet-metal decreases compared to that of its bulk material due to the size effect, and decreases proportionally with miniaturization [Peng et al., 2007; Vollertsen et al, 2006; Engel et al., 2002]. Commonly, there are two categories of the size effect that can be investigated: the grain-size effect and the feature-size effect.

Many investigations have been conducted elsewhere [Vollertsen et al., 2004; Peng et al., 2009] and have shown that sheet metals of different grain sizes show different mechanical properties. The grain-size effect was already known to follow the Hall–Petch equation, which topic has been elaborated upon elsewhere [Mahabunphachai et al., 2008]. This equation simply states that a material with a greater grain size has less strength compared to one which has a smaller grain size. This effect is purely reliant on the average grain-size of the material and is mostly dominant in macro-scale material. Although the tested strips were very thin, due to their relatively large width and length, they can still be considered as macro-scale material. According to the EBSD results conducted on all of the strips, the stainless-steel strip (SS50) were found to have a greater grain size, followed by that of the 50µm-thick carbon-steel strips (CS50), and finally that of the 100µm-thick carbon-steel strips (CS100). Good agreement of the results achieved between those for EBSD and those for tensile testing, have established and confirmed the effect of varying grain size. The least flow-stress was observed with SS50, which in turn has the larger grain size, this being followed by CS50 and finally CS100. This is because when a material of greater grain size is deformed, dislocations are easier to move compared to the situation with a smaller grain size. Less force is required and a lesser number of grains has made a larger grain-size material prone to fail a lot more quickly than would a smaller grain-size material.

Moreover, feature size also has a significant effect on a material's flow stress. The decrease of flow stress with the decrease of sheet thickness may be explained by the so-called surface-model, as depicted in Fig. 3.24 [Lai et al., 2008]. This model was used to describe the correlation between flow stress and miniaturization and has been popularly validated elsewhere [Lai et al., 2008; Peng et al., 2007; Vollertsen et al., 2006; Engel et al., 2002; Geiger et al., 1996]. According to the model, the grains located at the free surface are less restricted than are the internal grains. This in turn leads to the surface grains being subjected to less hardening, and having a lower resistance against deformation, because dislocations move through the grains during deformation and pile-up at grain boundaries, but not at the free surface. With the decrease of strip thickness, the share of surface grains increases, hence lower flow

stress. On the other hand, thicker sheet, in this case 100µm carbon-steel strip, the share of surface grains decreases and this in turns leads to a relatively higher flow stress compared to that for thinner strip.

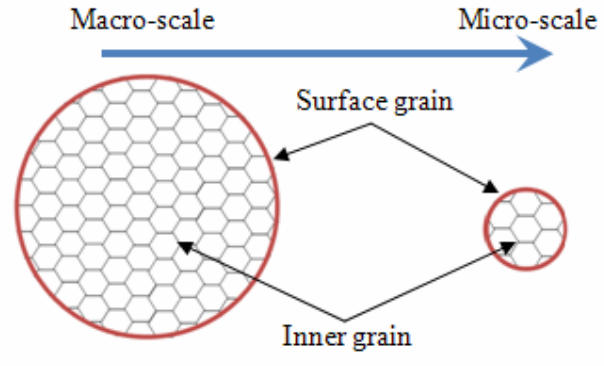

Fig. 3.24: Grain distribution in a material section of different material/feature size.

3.7 Conclusions

Based on the experiments conducted, the following conclusions are drawn:

i. Tested thicker carbon steel strip has the smallest grain size, followed by the tested thinner carbon steel strip and finally stainless steel strip.
ii. The thick carbon-steel strip has the greatest modulus of elasticity (stiffness) followed by the thinner carbon-steel strip and finally the stainless-steel strip.
iii. It may be concluded that thicker carbon steel strip has the stiffer characteristic compared to the thinner carbon and stainless steel strip.

Chapter 4

FE Analysis of the Roll-Feeder

4.1 Summary

The flexibility of a conventional sheet-forming process in respect of changes of feeding parameter may be achieved with the application of a servo roll-feeder to handle the sheet material. Not only high-speed feeding operations can be achieved, simplicity in threading the sheet and effortless changing of the feed distance ensure that the servo roll-feeder is the first choice for such applications. FE simulations were conducted to quantify servo roll-feeder performance with a view to determining the feeding characteristic and level of success when feeding thin-sheet for the micro-sheet-forming process. FE simulations were used to study the strip feed-characteristic by a micro-servo roll-feeder with a view to acquiring a better understanding of the system for micro-sheet-forming applications. Various parameters were tested and simulated to obtain extensive coverage of the feed characteristic when different configurations were employed. Based on the results, longer and higher feed distance and frequency produce greater positional accuracy compared to shorter feed distance and lower feed frequency. It is also revealed that the presence of brake force was able to improve positional repeatability but at the same time producing underfeed positional accuracy pattern. The presence of lubrication on the system did not really contribute towards improving positional accuracy.

4.2 Introduction

Long and thin sheet-metal strip, if not constrained, tends to react to gravitational force, which in turn lead the strip to bend downwards. The strip may be easily vibrated and cause to assume excessive waviness when subjected to unexpected external forces. To reduce the consequence of excessive vibration and waviness therefore, both ends of the strip may need to be constrained. Hence, the greater resistance towards unwanted forces that is provided could enable gravitational force to be neglected. Immunity towards vibration via maintaining good strip-tensioning indirectly promotes better dynamics stability, especially when the strip is in motion, hence less positional error can be expected. The effect of applying external force to maintain strip tension in strip feeding could be an influential parameter in improving positional accuracy. Thus, the effect of this feature can usefully be studied and modelled by FE analysis.

The purpose of this FE analysis is to study the strip behaviour and the characteristic of feeding process. Several key factors having a bearing on feed characteristics have been considered for analysis. The examination of these factors is considered to be relevant in the understanding of strip behaviour during the feeding process. The application of brake force to the system and the uniformity of strip tension throughout the feeding process were considered. Additionally, the contribution of brake force towards the achieving of a settled position also needed to be understood. The next factor considered was the variation of the motion-profile curve. Study had revealed that change of the motion-profile curve does affects the positional stability through the existence of 'jerk', therefore various motion-profile curves were introduced into the analysis with a view to determine their influence on positional accuracy. Change to different strip materials and thicknesses were conducted with a view to studying the influence of the mechanical properties of the strip on the feed performance. The identification of the correlation between the feed distance and the positional accuracy was also explored. Intensive and detailed study and analysis by means of the FE method are seen as vital to a good understanding of the feed characteristics, to enable future improvements to be made to micro-sheet-forming processes.

4.3 Procedure

Accurate, wide and various angles of geometry may be achieved by simulating using a 3D dynamics-explicit model, compared to using a 2D model [Hibbitt et al., 2002a]. Although 3D dynamics explicit analysis is time-consuming (Fig. 4.1), modelling the thin sheet-metal from a shell and inappropriate meshing scheme are seen to produce better approximation of the thin-sheet behaviour and characteristics during the feeding process: this in turn reduces the modelling time-increment and CPU time.

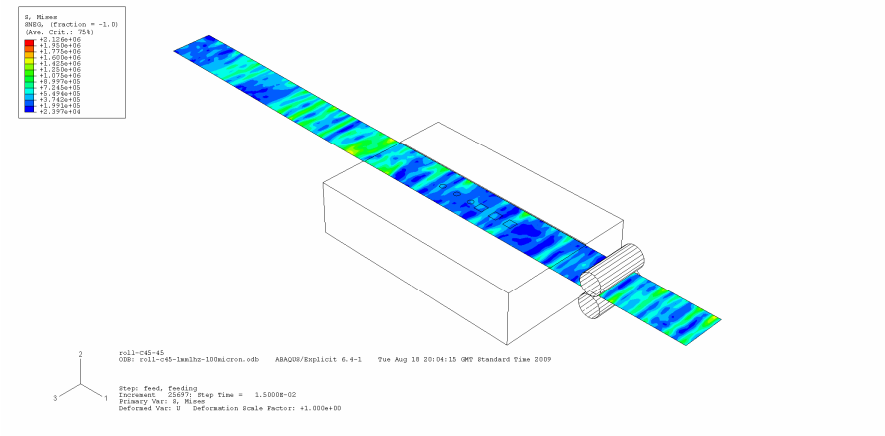

Fig. 4.1: 3D model of a roll feeder.

Several feed key parameters were identified and been considered to establish an intensive FE analysis of the characteristics of the roll-feeder feeding. Analysis was conducted to simulate roll-feeder feeding at 1 and 2Hz feed frequency. An appropriate feed velocity at this frequency was determined by trapezoidal motion-profile analysis, a similar motion-profile curve then being configured for the amplitude of the FE analysis, so as to mimic lifelike feeding conditions. The model of the roll feeder model was constructed by ABAQUS/CAE, and was based on the actual size.

Each contact-pair was defined with a specific coefficient of friction value gathered in the Chapter 3. The friction coefficient between contact pair of an upper roller made from polyurethane rubber and a steel strip was defined as 0.7 [Rothbart et al., 2006]; the coefficient of the friction of the contact pair of a bottom steel-roller and a steel strip was defined as 0.15 [Roberts, 1978]; the contact pair between a steel strip and

the tooling (steel forming-dies) was defined as 0.15 [Roberts, 1978]; and the contact-pair coefficient of friction between the rollers was defined as 0.7 [Rothbart et al., 2006].

The upper synthetic-rubber roller was subjected to 220N clamping force, which was pre-determined from the manual for the servo-roll feeder, while the bottom roller was constrained in all directions. An appropriate brake-force value was applied to one of the free-ends of the strip to represent the brake force generated by the decoiler (which is explained in other chapter). Each bottom- and top-roller was subjected to a designated velocity for each feed distance: 0.9697rad/s and 4.8485rad/s both for 1mm and 5mm feed distances, respectively (at 45-45 motion-profile configuration). The time taken to accelerate was defined by the designated motion-profile curve for each feed distance. Both the 1mm and 5mm feed-distances shared the same acceleration–deceleration phase value. Two type of motion-profile curve to define different acceleration–deceleration phases was used, namely as 45-45 and 50-50. The 45-45 motion-profile curve represents 45% of the total time of 150ms is allowed for acceleration time and another 45% for deceleration time, the remaining 10% of total time being for a constant-velocity phase, as depicted in Fig. 4.2. Similarly as for 45-45, the 50-50 phase was designed for 50% of total time just for acceleration time and the remaining 50% for deceleration time, as depicted in Fig. 4.3, with a radial velocity of 1.0667rad/s and 5.3334rad/s for 1mm and 5mm feed distances, respectively.

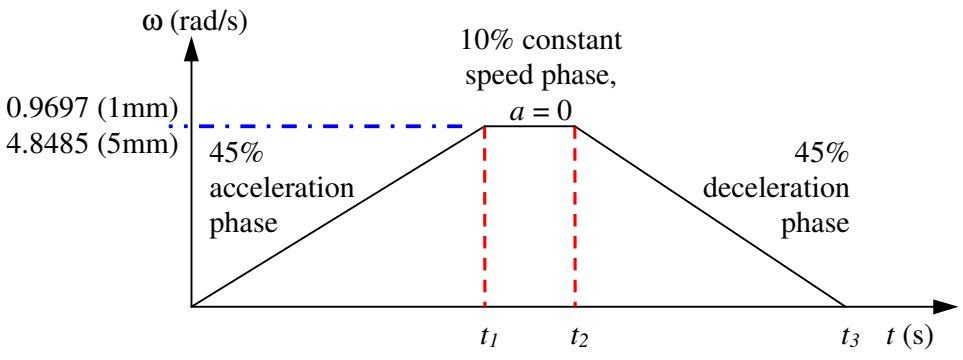

Fig. 4.2: Illustration of the 45-45 motion-profile curve.

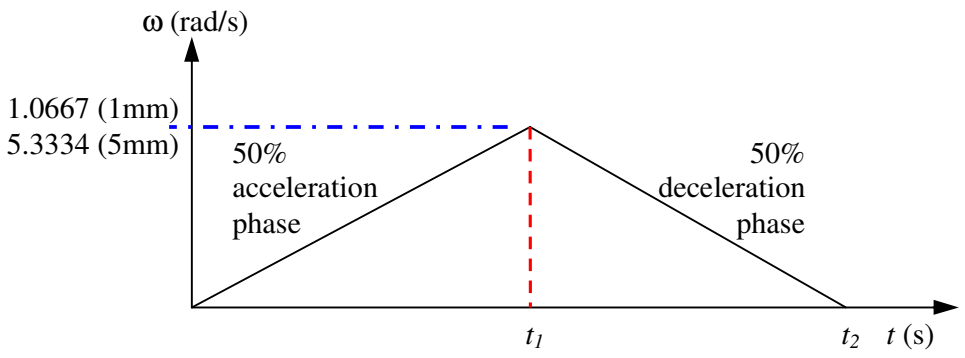

Fig. 4.3: Illustration of the 50-50 motion-profile curve

In the model, both the bottom and top rollers and the tool/die set, were assumed to be rigid and were described by rigid boundary-conditions. The thin sheet-metal was assumed to be deformable. The value of the modulus of elasticity (Young's modulus) of the thin sheet-metal was determined by the uniaxial tensile-test described in the previous chapter. Element types S4R (3D explicit analysis) were used for modelling the thin sheet [Hibbitt et al., 2002b; Hibbitt et al., 2002c]. The simulation was performed using the dynamics-explicit procedure to cope with vast non-linear geometrical displacement. The decision on the final mesh-size was made on a trial basis, where a compromise is usually required between computing-time, computer memory and simulation precision.

Different nodes were selected with a view to establishing the overall behaviour of the thin sheet during feeding, at five points: at both strip-ends, at the middle; and the remaining two at the mid-point between the centre and the ends of the strip. The selection of these five nodes ensures that the positional accuracy at the die position is also taken into account, hence how large the positional inaccuracy could be is determined directly. In order to avoid difficulty and-time consuming 3D modelling, an appropriate fine-mesh was used, which also reduces the error generated due to an excessive aspect-ratio.

4.4 Results

4.4.1 Strip-Feeding Characteristics

a) 1hz Feed Frequency

The tendency of the strip to vibrate and become wavy during the feeding process may be one of the challenges in the high-precision feeding process in micro-sheet-forming. Not only may the positional accuracy be jeopardized, the strip may be deformed accidentally to an unwanted/inappropriate shape during the forming stroke. The strip may be too vulnerable to vibration without brake force being applied to the system, as demonstrated in Fig. 4.4 and Fig. 4.5. Different starting-points prior to the feed step were observed for all of the strips tested at this feed frequency, 1Hz. This pattern continued until the end of the feed process, with a different settled-position for each strip. At shorter feed-distance, a huge fluctuation was also observed with the CS50 strip being caused to fluctuate beyond the designated feed distance. However, SS50 and CS100 strips showed an underfeed settling-pattern, as depicted in Fig. 4.4. The underfeed settling-pattern diminished when a longer feed-distance of 5mm was used, as depicted in Fig. 4.5. CS100 and SS50 settled closer to the designated position, while CS50 was observed to settle far beyond the designated position, thus resulting in deterioration in positional accuracy.

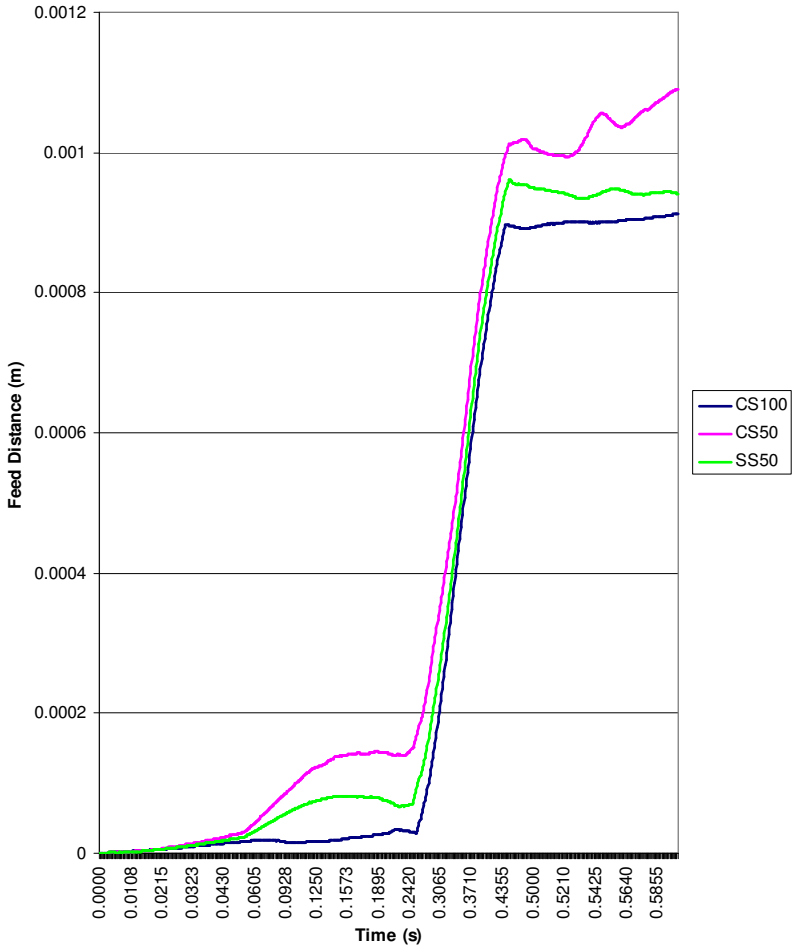

Fig. 4.4: Feeding characteristics for all strips for 1mm feed distance configured at 45-45 motion-profile without brake force at 1Hz feed frequency.

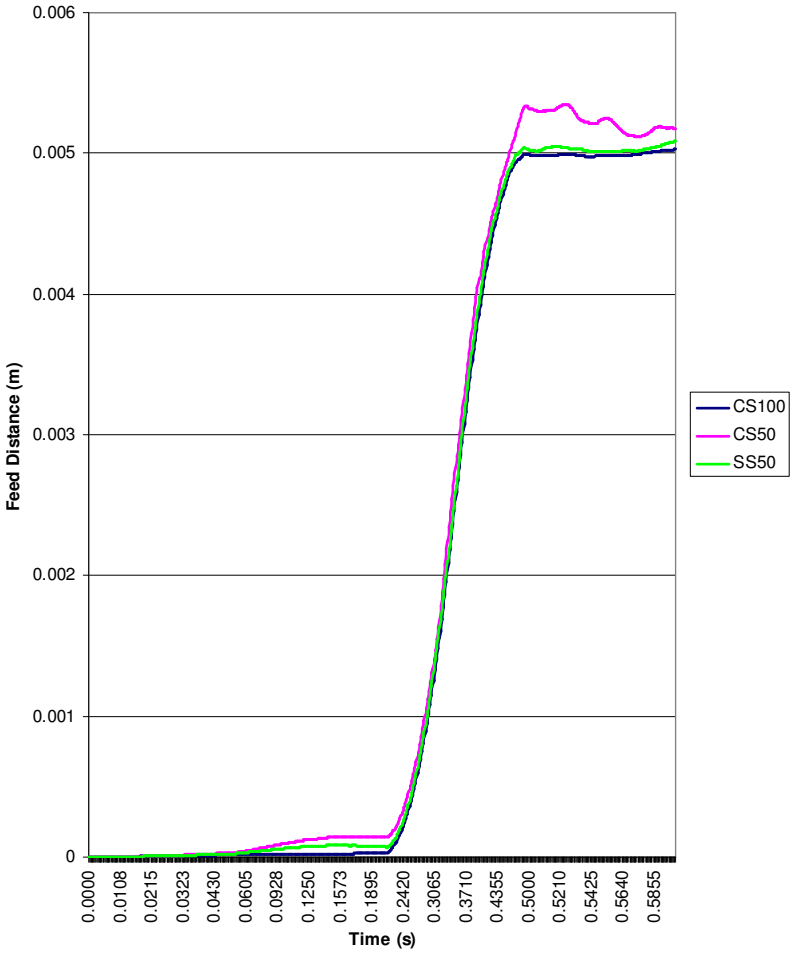

Fig. 4.5: Feeding characteristics for all strips for 5mm feed distance configured at 45-45 motion-profile without brake force at 1Hz feed frequency.

The application of brake force with the 45-45 profile may be seen as a successful way to control different feed-starting-points for each strip. Although the strips tend to vibrated, brake force was seen capable of attenuating and dampening the vibration of the strips vibration and retaining uniform strip-tension prior to the feed process. As shown in Fig. 4.6 and Fig. 4.7, a uniform and consistent starting-point may be expected with the presence of brake force. Although uniform starting point was achieved, although the application of brake force has resulted in a significant underfeed settling-pattern for all of the strips, at shorter 1mm, and longer 5mm, feed-distances.

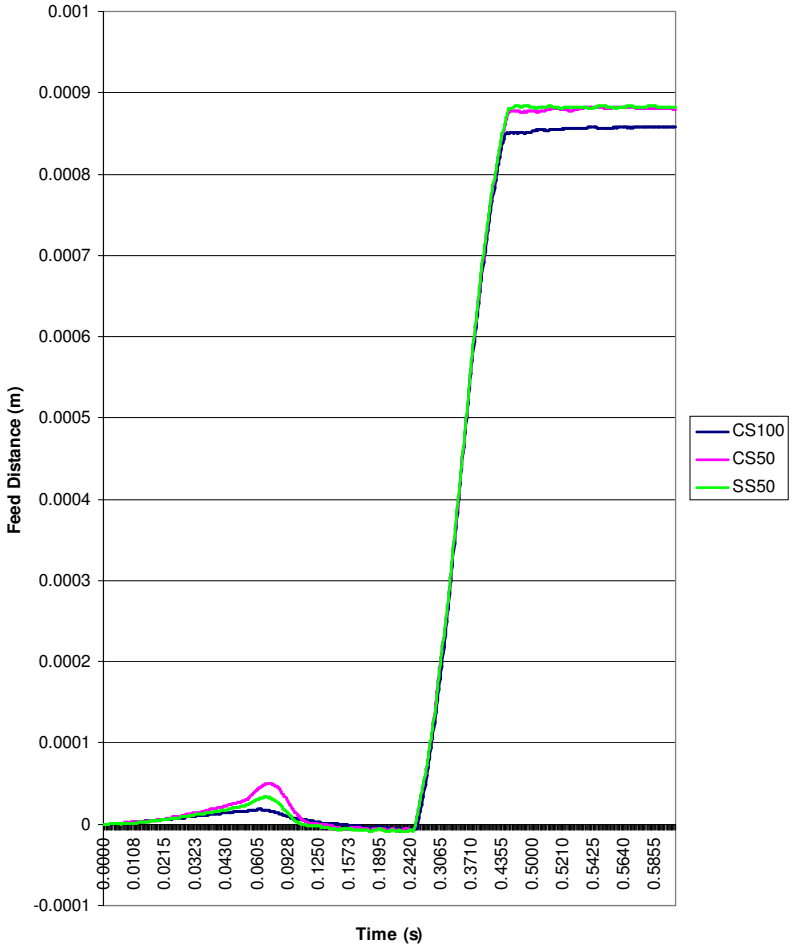

Fig. 4.6: Feeding characteristics for all strips for 1mm feed distance configured at 45-45 motion-profile with brake force at 1Hz feed frequency.

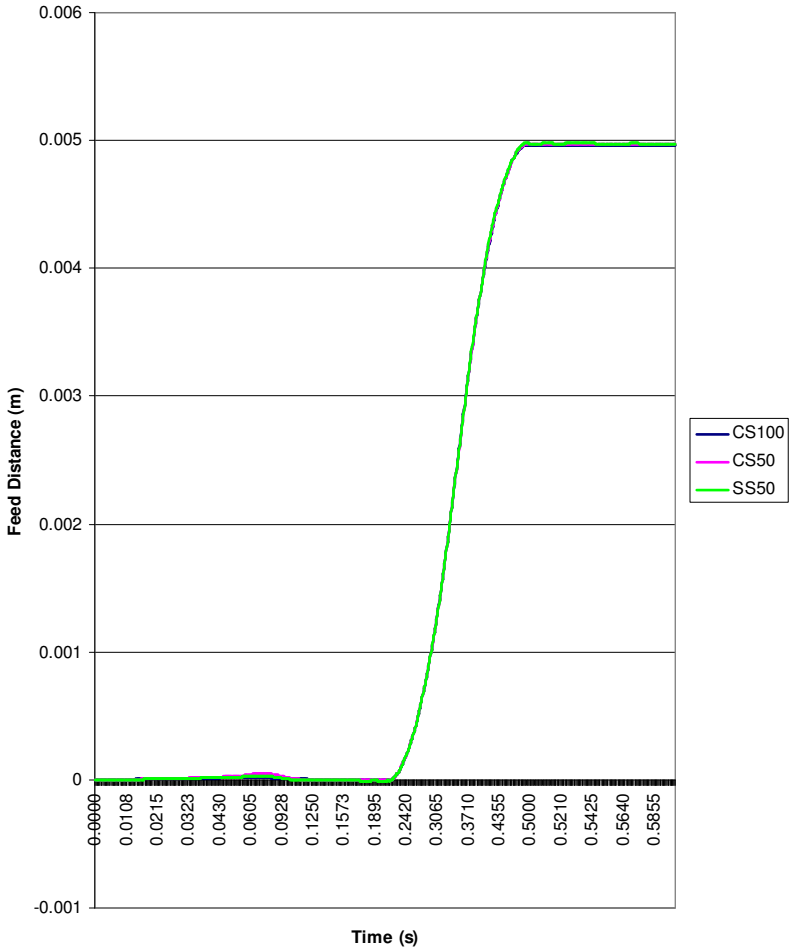

Fig. 4.7: Feeding characteristics for all strips for 5mm feed distance configured at 45-45 motion-profile with brake force at 1Hz feed frequency.

Change to the different motion-profile configuration of 50-50, however, did not improve the settled-positional accuracy for 1mm feed distance. As shown in Fig. 4.8, a similar observation was recorded as in the result presented for the 45-45 motion profile (Fig. 4.6). This suggested that increases in the 'jerk' rate did not promote better settling positional accuracy. Fig. 4.9 confirmed the insignificance effect of the high 'jerk' effect in establishing better positional-accuracy. Good agreement in the findings was observed between Fig. 4.9 and Fig. 4.7, where no significant improvement on positional accuracy can be expected with change to a steeper motion-profile pattern.

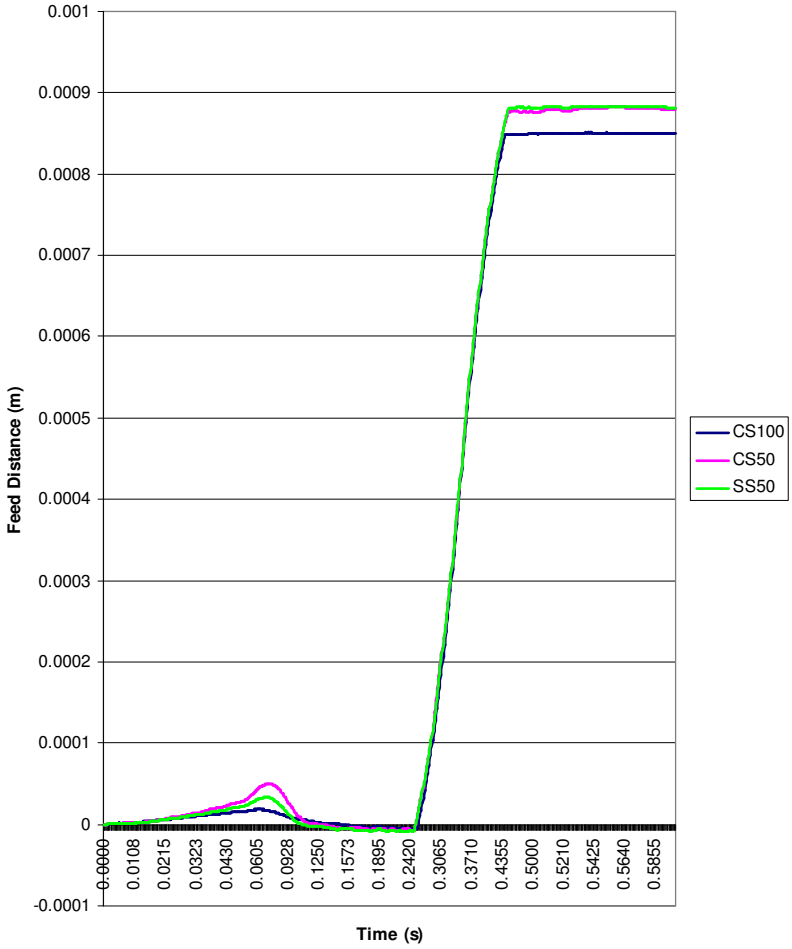

Fig. 4.8: Feeding characteristics for all strips for 1mm feed distance configured at 50-50 motion-profile with brake force at 1Hz feed frequency.

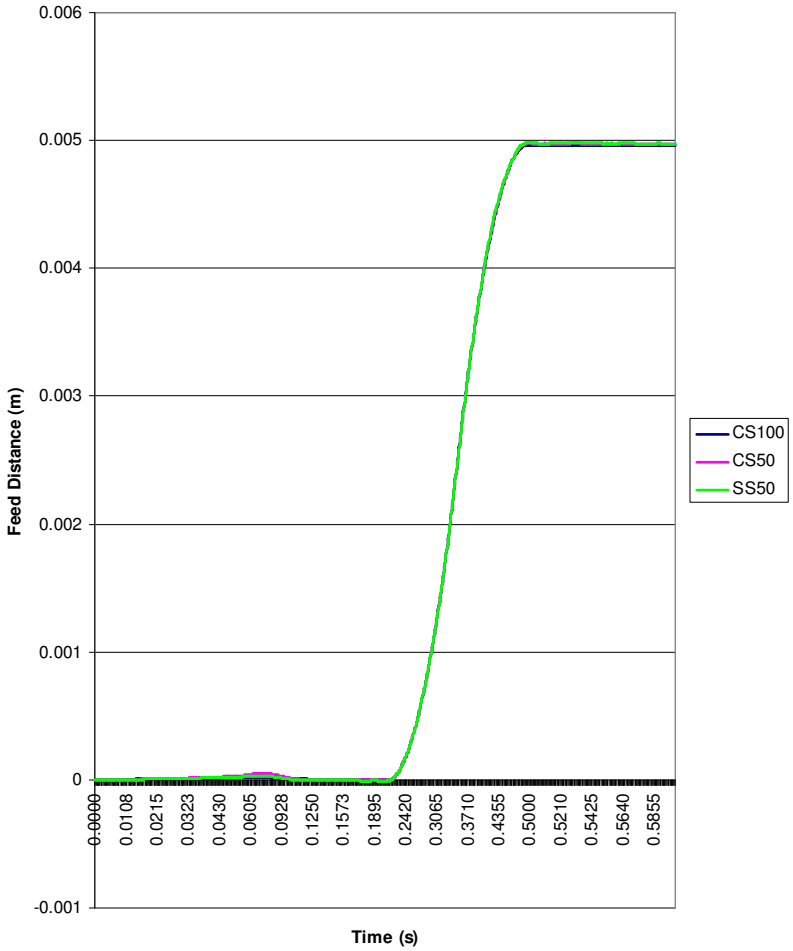

Fig. 4.9: Feeding characteristics for all strips for 5mm feed distance configured at 50-50 motion-profile with brake force at 1Hz feed frequency.

b) 2hz Feed Frequency

At the beginning of the feeding process, feeding without an applied brake-force for the 45-45 motion profile, thin sheets were seen to have an unsettling effect on the desired starting point. As depicted in Fig. 4.10 and Fig. 4.11, less stiff materials such as CS50 and SS50 were wavy far from the feed starting-point for both of the feed distances. Stiffer CS100 was seen to be less disturbed and remaining closer to the feed starting-point. This varied feed-starting-point resulted in a different feed-pattern for each strip, the effect continuing up to the completion of the feeding process, where different settling-points for the strips were observed.

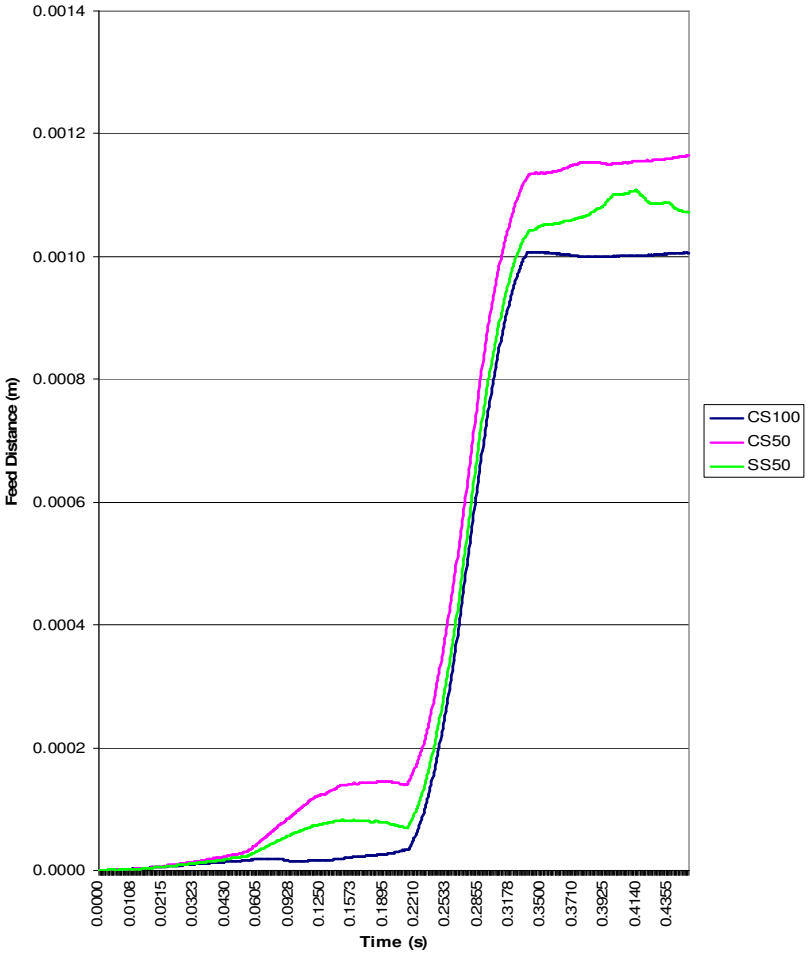

Fig. 4.10: Feeding characteristics for all strips for 1mm feed distance configured at 45-45 motion-profile without brake force at 2Hz feed frequency.

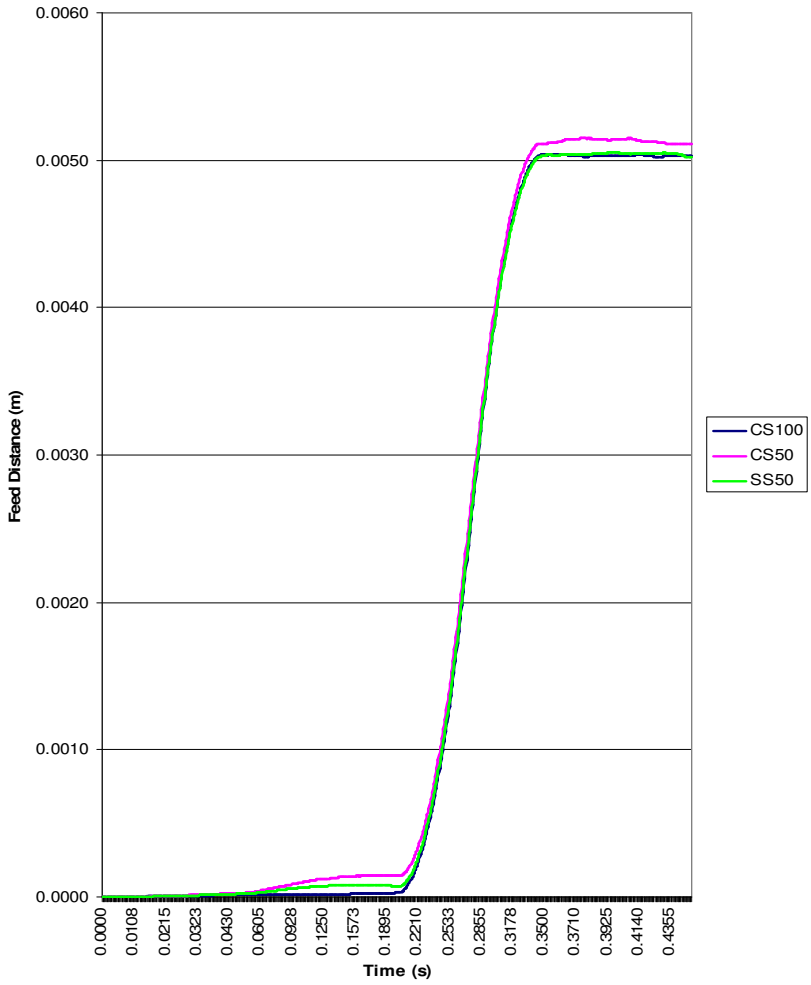

Fig. 4.11: Feeding characteristics for all strips for 5mm feed distance configured at 45-45 motion-profile without brake force at 2Hz feed frequency.

With the same motion-profile set-up, the application of brake force improved the starting point for all strips for both 1mm and 5mm feed distances, as shown in Fig. 4.12 and Fig. 4.13. The initial stage of brake-force actuation showed a gradually-increasing strip tension, hence bringing back the strips closer to the desired feed starting-points. Uniform feed-patterns were also observed when the strip was moved to the designated feed distances and continued until the end of the feed process.

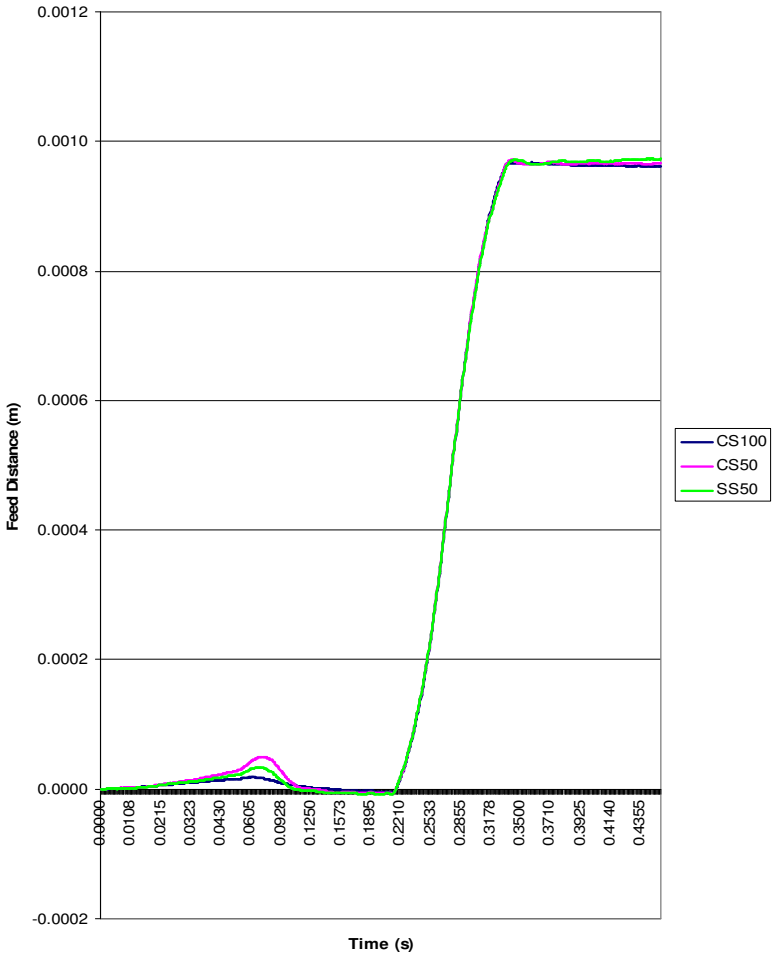

Fig. 4.12: Feeding characteristics for all strips for 1mm feed distance configured at 45-45 motion-profile with brake force at 2Hz feed frequency.

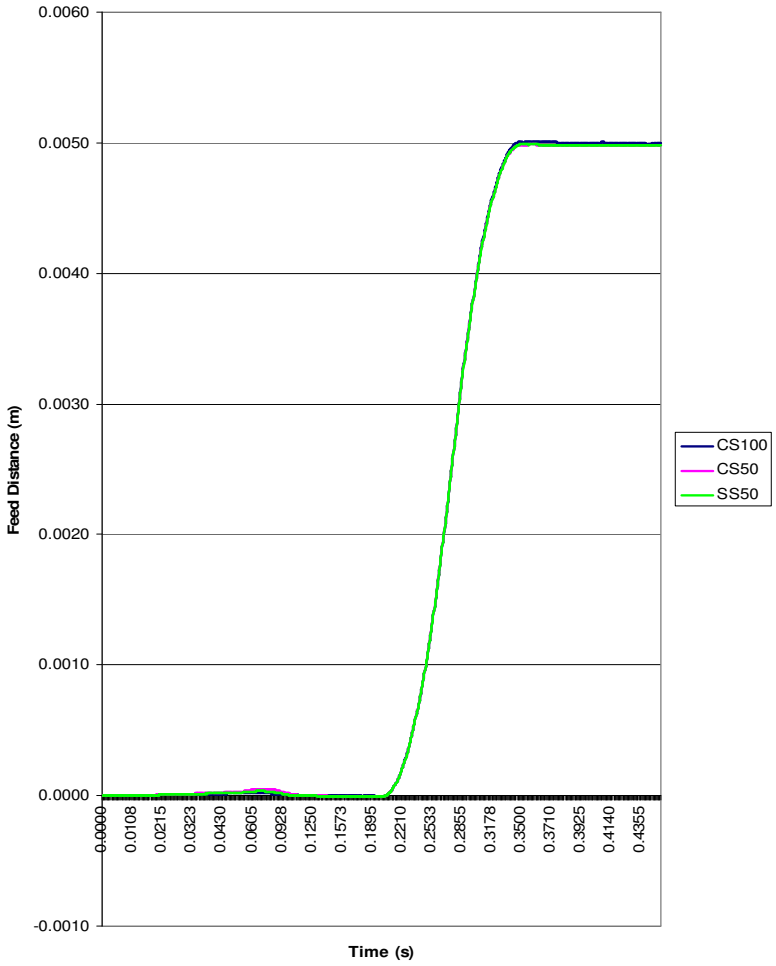

Fig. 4.13: Feeding characteristics for all strips for 5mm feed distance configured at 45-45 motion-profile with brake force at 2Hz feed frequency.

A similar observation was made when the motion-profile was made steeper, to 50-50. Nevertheless, less settling-stability was observed, specifically for less-stiff strip, such as SS50 in Fig. 4.14 and Fig. 4.15. For a greater feed-distance, the settling pattern for the material was unstable, compared to the other settling patterns.

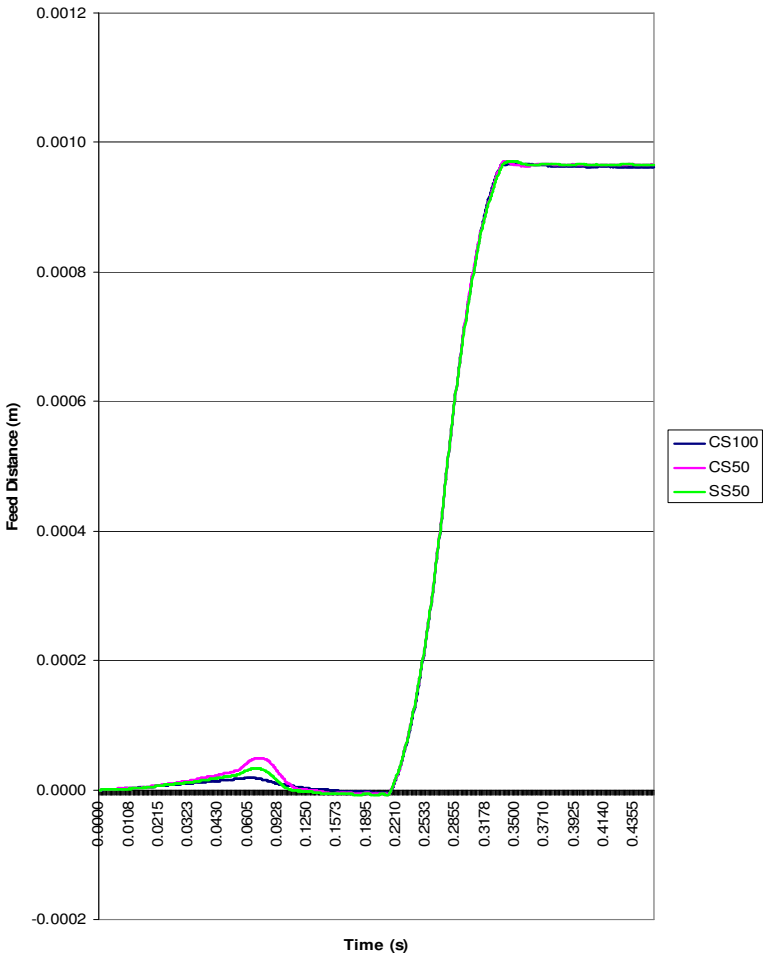

Fig. 4.14: Feeding characteristics for all strips for 1mm feed distance configured at 50-50 motion-profile with brake force at 2Hz feed frequency.

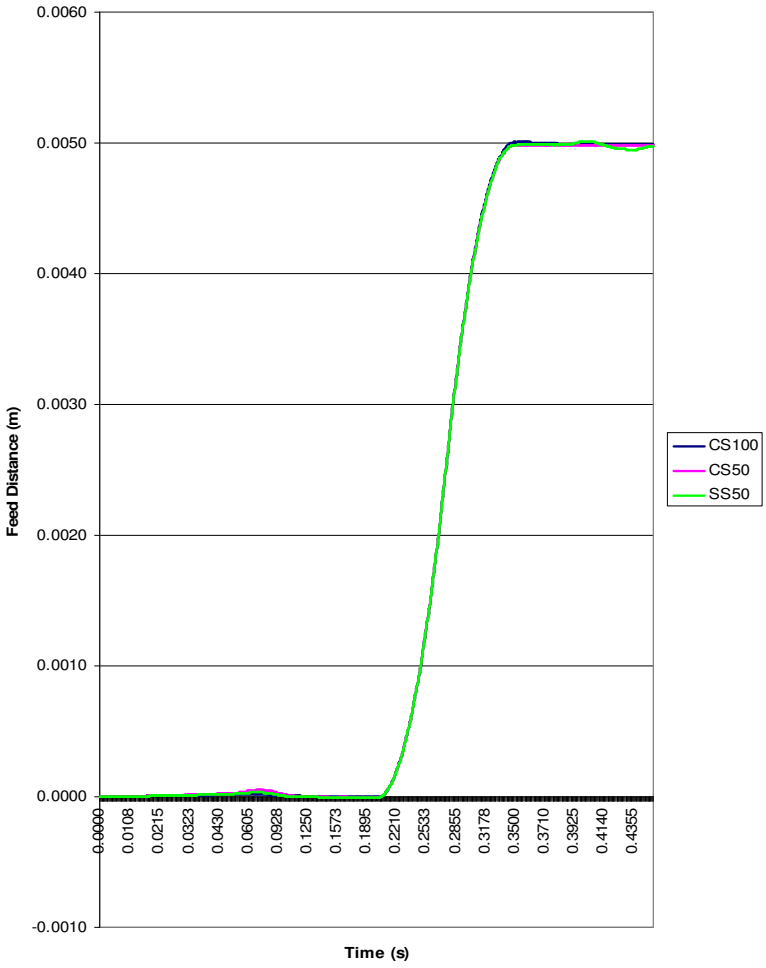

Fig. 4.15: Feeding characteristics for all strips for 5mm feed distance configured at 50-50 motion-profile with brake force at 2Hz feed frequency.

4.4.2 Effect of the Brake Force and the Motion-Profile Curve

a) 1mm feed distance 1hz feed frequency

Fig. 4.16, Fig. 4.17 and Fig. 4.18 show the settled pattern for each strip when subjected to brake force and various motion-profile configurations. Due to the less-stiff property of CS50 (Fig. 4.16), the strip was observed to fluctuate substantially beyond the desired settle-position. A similar observation was found for CS100 and SS50 (Fig. 4.17 and Fig. 4.18) without brake force being applied, a greater deviation being recorded, which means that the strips fluctuated, hence promoting an unstable settling-pattern. For similar motion-profile configurations, the presence of brake

force was observed to successfully dampen strip fluctuation, for all of the materials tested. More stable settling-pattern was observed throughout the feed process. Although a good and maintained strip-tension was achieved, the brake force, however, has resulted in significant deterioration of the positional accuracy, for any motion-profile configurations. A less-gripping contact-surface between the rollers and the strip may be seen as a primary source of further deterioration in positional accuracy due to slippage between the strip and rollers during feeding process.

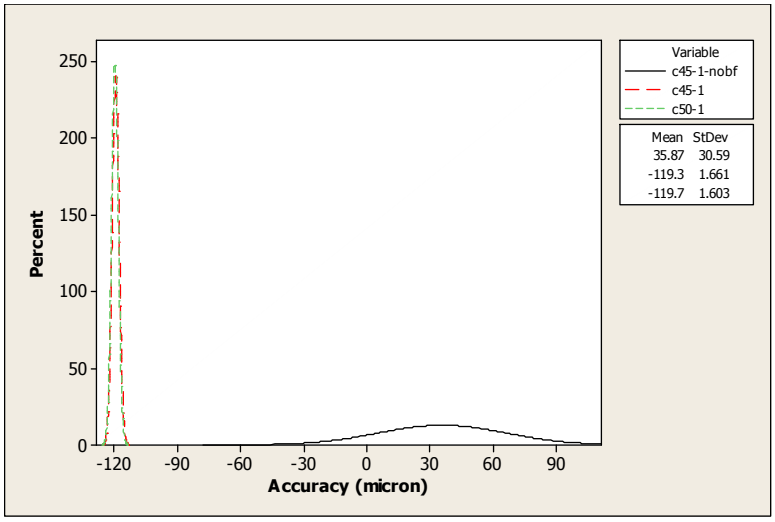

Fig. 4.16: Settled-positional accuracy-pattern for different motion-profile curves and the effect of brake force for CS50 strip at 1mm feed distance and 1Hz feed frequency.

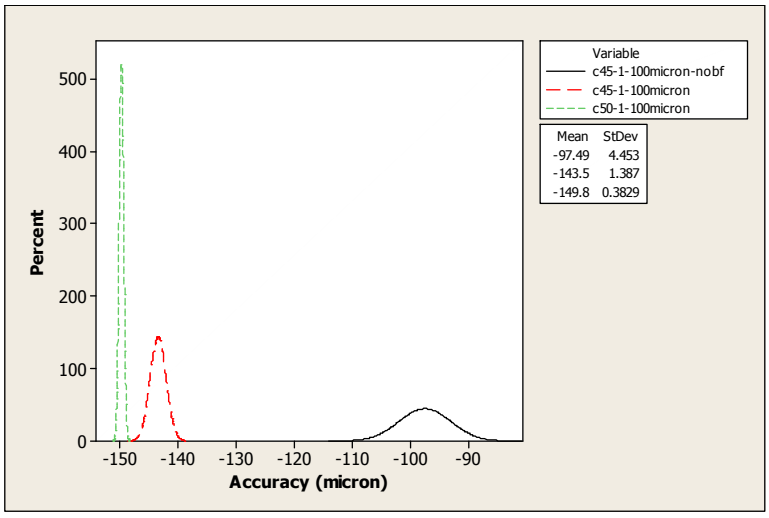

Fig. 4.17: Settled-positional accuracy-pattern for different motion-profiles curve and the effect of brake force for CS100 strip at 1mm feed distance and 1Hz feed frequency.

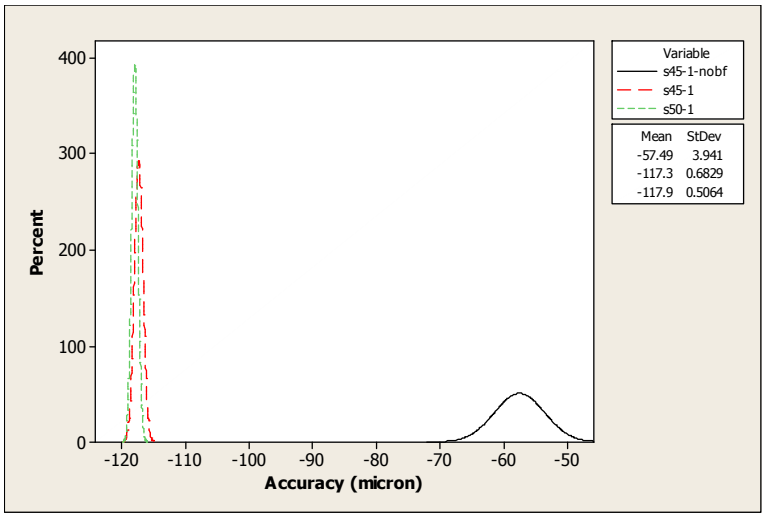

Fig. 4.18: Settled-positional accuracy-pattern for different motion-profile curves and the effect of brake force for SS50 strip at 1mm feed distance and 1Hz feed frequency.

b) 1mm feed distance 2hz feed frequency

Feeding without brake force showed an unstable settling-pattern for all of the material types and thicknesses tested, as depicted in Fig. 4.19, Fig. 4.20 and Fig. 4.21. Huge positional errors were observed throughout the experiments, with CS50 strip recording the worse positional-error. This suggested that higher-strength and stiffer strips, which is in this case are CS100 and CS50, might be positioned with less error compared to the case with less-stiff material (SS50). Although the positional error of stainless steel (SS50) is lower than that of CS50, the feed characteristic for this material demonstrated a lack of positional stability and an inconsistent pattern, compared to the more-stable CS50 feed characteristics.

The application of brake force to the system showed a slight improvement to the underfeed-pattern (a smaller deviation trend), to stabilize the settled-position as shown in each of Fig 4.19, Fig. 4.20 and Fig. 4.21. CS100 was found to have the least positional-error, hence a stable settled-position pattern and lesser error compared to the case with CS50 and SS50. Change of the motion-profile curve resulted in an insignificant effect towards improving the positional pattern for carbon-steel strips. The 45-45 and 50-50 motion-profile curve tends to have a similar pattern with the stiffer carbon-steel strips at this feed distance. However, slight more stability and better positional accuracy was observed for SS50 strip when the 45-45 motion-profile was used, as shown in Fig. 4.21. A large, inconsistent and unstable

settled positional-feed was observed for the 50-50 motion-profile curve for this material at the designated feed distance.

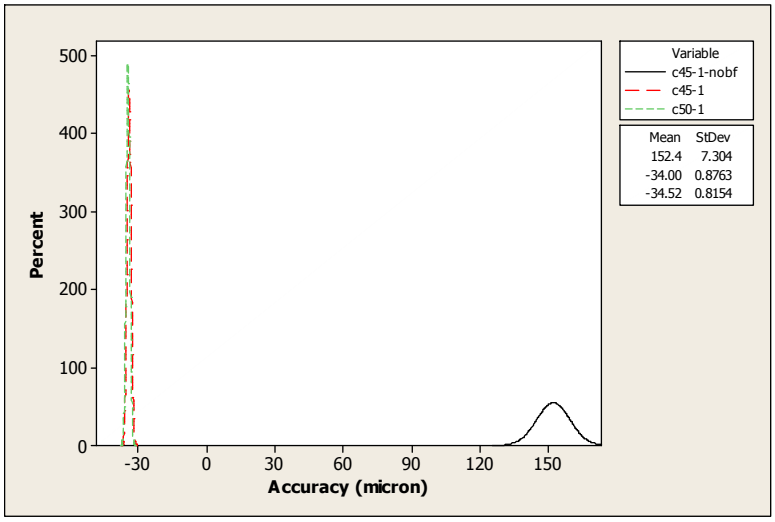

Fig. 4.19: Settled-positional accuracy-pattern for different motion-profile curves and the effect of brake force for CS50 strip at 1mm feed distance and 2Hz feed frequency.

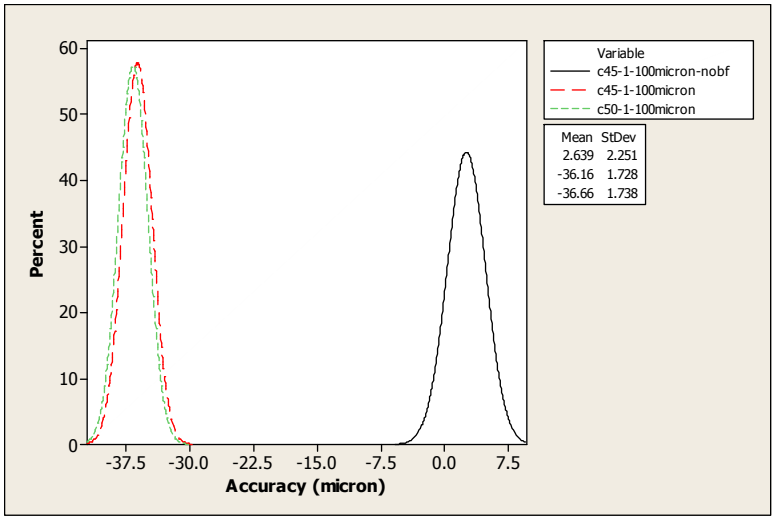

Fig. 4.20: Settled-positional accuracy-pattern for different motion-profile curves and the effect of brake force for CS100 strip at 1mm feed distance and 2Hz feed frequency.

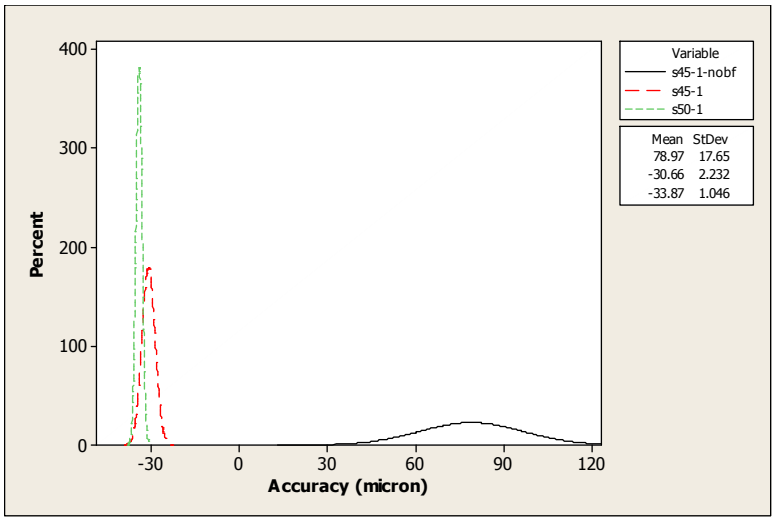

Fig. 4.21: Settled-positional accuracy-pattern for different motion-profile curves and the effect of brake force for SS50 strip at 1mm feed distance and 2Hz feed frequency.

c) 5mm feed distance 1hz feed frequency

At longer feed distance, similar observation was found as Fig. 4.16, where huge strip fluctuation was discovered for CS50 strip when not subjected to brake force (Fig. 4.22). Although fluctuated, CS100 and SS50 fluctuation was observed less than CS50 as depicted in Fig. 4.23 and Fig. 4.24. At this feed distance, settled pattern for all tested strips when subjected to brake force showed significant improvement on positional accuracy, which was closer to designated feed position. Less stiff material such as CS50 and SS50 were observed to have closer settling point to the desired position while CS100 recorded double of positional inaccuracy obtained for both CS50 and SS50. There was no significant different of achieved positional accuracy between 45-45 and 50-50 motion profile as depicted in Fig. 4.22, Fig. 4.23 and Fig. 4.24. This finding has good agreement with result presented in Fig. 4.16, Fig. 4.17 and Fig. 4.18 previously.

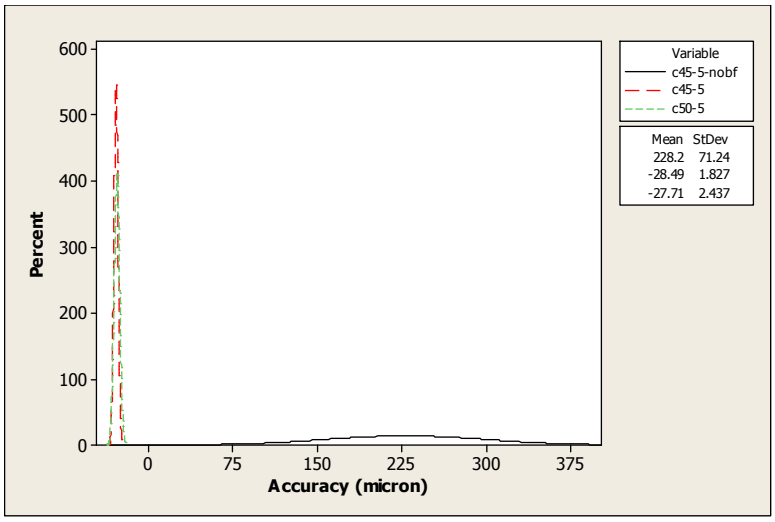

Fig. 4.22: Settled-positional accuracy-pattern for different motion-profile curves and the effect of brake force for CS50 strip at 5mm feed distance and 1Hz feed frequency.

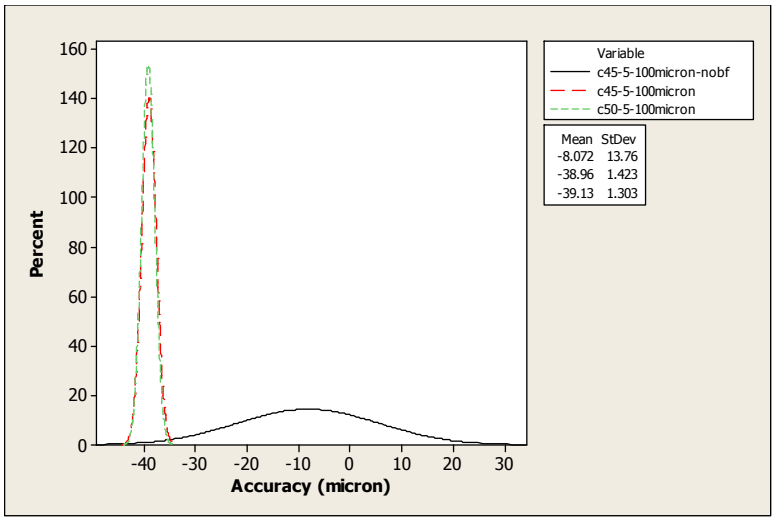

Fig. 4.23: Settled-positional accuracy-pattern for different motion-profile curves and the effect of brake force for CS100 strip at 5mm feed distance and 1Hz feed frequency.

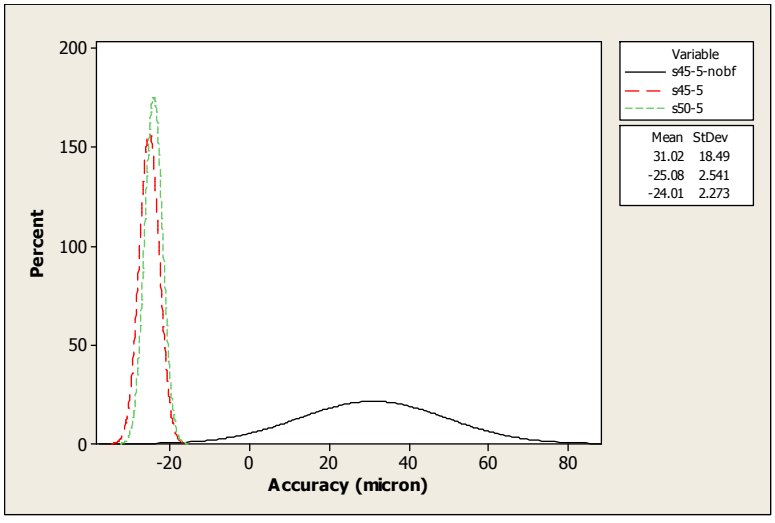

Fig. 4.24: Settled-positional accuracy-pattern for different motion-profile curves and the effect of brake force for SS50 strip at 5mm feed distance and 1Hz feed frequency.

d) 5mm feed distance 2hz feed frequency

At 5mm feed distance, without the presence of brake force, huge positional error and instability pattern was observed on all tested strips as depicted in Fig. 4.25, Fig. 4.26 and Fig. 4.27. At this configuration, CS100 was observed to have the most stable feed pattern followed by SS50 and lastly CS50. This suggested stiffer material may be positioned or being fed better than less stiff material.

The presence of brake force to the system had contributed better and more stable settled position. Smaller deviation has showed that less waviness and more stable feeding was achieved. CS100 was observed to be the most stable material being fed. This in turn leads to less feed positional error. It was also been demonstrated by the Fig. 4.25, Fig. 4.26 and Fig. 4.27 that for all strips tested, stiffer strip may be stably positioned with consistent pattern and relatively low level of error.

Change of motion profile curve from 45-45 to 50-50 had showed consistent yet stable positioning pattern for carbon steel strips as depicted in Fig. 4.25 and Fig. 4.26. Although consistent patterns were observed for both motion profile curve, 45-45 curve was seen the most favourable for all the tested strips due to stable feed characteristic showed and slightly lesser positional error compared to 50-50 motion profile curve. 50-50 motion profile curve had caused instability to feed pattern specifically when less stiff material was used as demonstrated by Fig. 4.27.

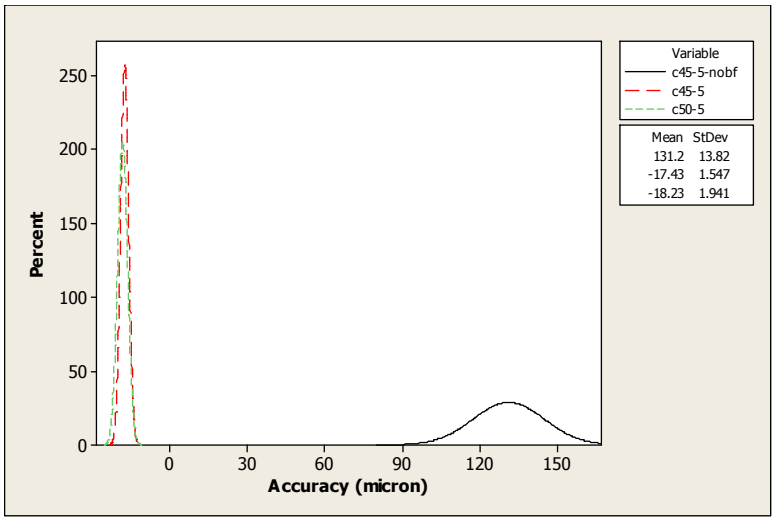

Fig. 4.25: Settled-positional accuracy-pattern for different motion-profile curves and the effect of brake force for CS50 strip at 5mm feed distance and 2Hz feed frequency.

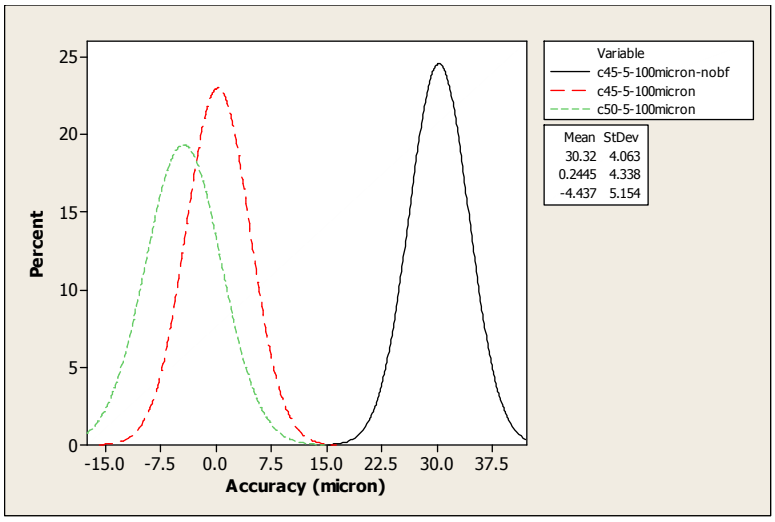

Fig. 4.26: Settled-positional accuracy-pattern for different motion-profile curves and the effect of brake force for CS100 strip at 5mm feed distance and 2Hz feed frequency.

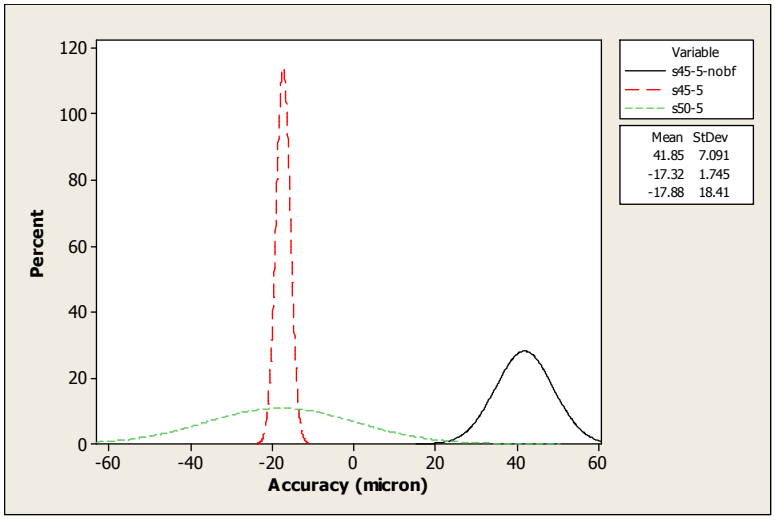

Fig. 4.27: Settled-positional accuracy-pattern for different motion-profile curves and the effect of brake force for SS50 strip at 5mm feed distance and 2Hz feed frequency.

4.5 Discussion

4.5.1 Effect of Brake Force

The application of brake force demonstrated better stability on the settled pattern while keeping the positional error at a low level. The brake force, which was applied to the ends of the strip-edge to represent the decoiler brake-force effect on the feed process, resulted in consistent strip-tension throughout the roll feeder and decoiler, hence reducing error and increasing the stability during positional settling. This was achieved by reduction of the waviness of the strip through proper constraint introduced on one of the strip's end while the other end was kept constrained by the rollers. Reduced waviness of the strip through maintained- and consistent-tension has made the strip less susceptible to a disturbing force during the feeding process. On the other hand, without brake force being applied to the system, the free end of the strip is more vulnerable to disturbance and the strip is easily able to absorb unwanted disturbance forces that lead it to become wavier.

4.5.2 Effect of Change of Motion Profile

Acceleration is defined as change of velocity rate. 'Jerk', on the other hand, is defined as change of acceleration rate. A high 'jerk'-rate is usually associated with high-speed motion. Based on the results presented, a high 'jerk' affects the settled pattern and the positional error of the least-stiff material through increasing the strip waviness. It is suggested that reduction in 'jerk' promotes better settled-stability and lesser positional-error, which suggestion is supported by the 45-45 motion-profile curve. For this configuration, the tendency of a high 'jerk'-rate was eliminated by introducing a constant-velocity phase, hence, reducing any sharp transitions during change of acceleration and deceleration. According to Newton's Law, increases in acceleration rate result in increases in force. A sudden change of this force results in various curvature-formations being introduced into the strip, as explained elsewhere [Uraoka et al., 2009], hence leading to strip waviness. Also, waviness tends to propagate along the body of the strip, gradually disappearing. Nevertheless, in a high-speed process, waviness may not be dampened quickly enough to settle the thin sheet accurately within the specification. Moreover, high 'jerk' motion in turn leads

to a greater sudden change of force that may cause large curvature during feeding. For the 45-45 motion-profile configuration, the minimization of the 'jerk'-rate led to a decrease of acceleration, hence keeping the reaction force low. Additionally, a low acceleration value leads to low strip-inertia, low 'jerk' and consequently a reduction in strip-curvature formation, this in turn reducing the tendency to waviness.

4.5.3 Effect of Change of Feed Distance

A longer feed-distance requires a high velocity and acceleration to accomplish feed process within the same given time as for a shorter feed-distance. This indirectly increases the inertial resistance of the rollers and the driven strip [Ghayesh et al., 2008]. This inertial disturbance was found to be a useful source of compensation for the brake force, and helped the roller to move the driven strip as closely as possible to the desired feed-distance. Another factor which possibly could increase the inertial resistance is the mass of the strip. A thicker strip possesses more mass than does a thinner strip. This in turn leads to increase of the total inertia during the feed process. Added to the inertia resistance from high-speed motion, a greater compensatory effect may be present, to partially offset the brake-force acting on the strip.

A shorter feed, on the other hand, requires lesser velocity and acceleration to accomplish the desired feed-distance. This in turn leads to a lesser inertial value produced during the feeding process to compensate for the acting brake force, so that there may be lesser curvature formation. [Uraoka et al., 2009]. The huge positional error observed with thinner strip could be explained by its mass. A thinner strip has less mass than the thicker CS100, which in turn leads to relatively lesser inertial-resistance than that of thicker strip. Lesser mass-inertia along with lower inertia due to low-speed motion result in lesser force to compensate for the acting brake-force, hence produces slightly huge positional error. However, this condition may be existed up to a certain optimum motion speed where speed beyond the optimum point may cause deterioration on the feeder's positional accuracy.

4.5.4 Limitation of the FE Software

In general FE simulations, the work-material is invariably assumed to be perfectly uniform – geometrical- and metallurgical-defects are assumed not to prevail. In addition, the angular velocity of the rollers, was assumed to be the same as the rotation incurred in reality by the rotary motor in reality, i.e. the mechanical transmission was assumed to be perfect – no backlash, play, wear and tear were modelled.

In the servomechanism, the motion step-response usually tends to exhibit positional overshoot: such positional overshoot can be found more easily, and is more associated with, high-speed motion. This is mainly because of sudden changes of the acceleration-deceleration phases and vice versa. The model was designed based on the S-curve amplitude, where changes of the acceleration-deceleration phase or 'jerk' may be minimized, hence producing better positional accuracy without high positional-overshoot. This is supported by the observation that when the acceleration-deceleration phase changed, no excessive positional overshoot was observed.

4.6 Conclusions

The feeding characteristic of thin sheet by a servo roll-feeder were studied with reference to the changes of feed distances, material thickness and types, motion-profile curves and the application of brake force. From the FE simulation results, it can be concluded that:

i. Servo roll feeder is inappropriate for use in micro-sheet-forming applications.
ii. A stiffer sheet-material was positioned better than less-stiff material, and a better settling positional accuracy was achieved for CS100 compared to that for the thinner CS50 and SS50.
iii. The application of brake force improved the feed-settling pattern, where better settling-stability and positional accuracy may be achieved.
iv. The low-jerk 45-45 motion-profile was the best profile for the feed process due better positional accuracy is achieved.

Chapter 5

Experimental Study of the Micro Roll and Air-Feeder

5.1 Summary

Precise feeding is necessary to ensure that precise micro-parts can be produced in multi-stage micro-stamping, while high-speed feeding is essential for high-throughput production. A series of tests was conducted on a micro-servo roll-feeder and an air-gripper feeder to validate their positional accuracy and precision in a study of the feasibility of these kinds of feeder to serve for high-precision feeding in a micro-forming process. Also, pilot/locating pins were used to improve the positional accuracy of a micro-servo roll-feeder in the default-setting configuration. Then the servo roll-feeder motion-profile curve is changed determine how this affects the feeding performance. Non-contact measurement by an optical linear-encoder was used to acquire the necessary measurements. Several parameters were varied to create a range of test conditions: feed distance, feeding speed/frequency, change on strip thickness and material and finally by introducing lubrication into the system. The results showed that the positional accuracy and repeatability (precision) of the feeding is influenced significantly by the process conditions. The application of pilot/locating pins is seen to be unable to improve the positional accuracy, because thin sheet tends to deform easily rather than to be positioned accurately. It was also revealed that a stiffer material tends to give a better positional accuracy level, compared to a less-stiff material. With the air gripper-feeder, the positional accuracy was observed to be about the same as the servo roll-feeder performance. However, difficultness and inflexibility of this feeder prevented the feed distance from being changed easily. Moreover, the manual adjustment required to set the designated feed-distance has proven to cause a huge positional-error. The results were used as a reference in the development of a new feeder for micro-forming.

5.2 Introduction

Feeding sheet-metals in conventional press-working is no longer a major problem in production. However, challenges arise when thinner metal-strips are to be used in micro-sheet-forming (e.g. <100 μm) and parts/features to be formed become smaller (e.g. sub-millimetre ranges). In these cases, the forming of a micro-sheet-metal component may require to feed/position the sheet-metal under the forming tools as accurately as within one to a few microns. This is particularly important in multi-stage progressive micro-stamping in which neighbouring features of a part may be too close to each other. Therefore, feeding the sheet-metal has to be very accurate in order to prevent any inaccurate forming or damage to the neighbouring features and connections of the part/scrap of the strip. At the same time, for volume production, feeding the strip (sheet metal) accurately may have to be achieved at a reasonable feed rate, e.g. 100 strokes per minute, for which the stiffness of the thin strip may be a major concern.

Precision feeding for micro-sheet-forming, as described above, cannot be achieved with conventional, large-scale sheet-metal feeders. Feeding in micro-sheet-forming has been addressed only occasionally [Chern et al., 2006b; Groche et al., 2004] in some studies. Detailed study of the feeding mechanism and performance of the feeders (positional accuracy and repeatability) in micro-sheet-forming, considering various process conditions and material parameters has not been undertaken previously.

Using a micro-servo roll-feeder in combination with pilot/locating pins, and also an air gripper-feeder, a study of the characteristics and performance of the feeder for micro-sheet-forming was undertaken, which considered various process-conditions and material- and surface-parameters such as feeding speed, feeding distance, materials type and lubrication. The results were used as a reference in forming-error estimation and in optimisation of the feeding-control in micro-sheet-forming.

5.3 Equipment and Materials

Experiment was performed on a micro-forming-machine system developed at the University of Strathclyde [Qin et al., 2008]. Among the possible, commercially available, sheet-metal feeders for sheet-forming, the micro-servo roll-feeder was one that was identified to be generally suitable for micro-sheet-forming applications due to its compact design, easy control-features and high positional accuracy. Another type of feeder which is found to be competent, apart from a servo roll-feeder, is an air gripper-feeder. This feed was therefore chosen to be one of the main feeders to be investigated. Nevertheless, the effects of the process- and material-parameters on the positional accuracy and repeatability in this study are of general significance for the study and may be useful for the development work of other types of feeder.

5.3.1 The Machine-Control Architecture

The control-architecture of the micro-forming-machine used for the testing along with the servo roll-feeder is illustrated in Fig. 5.1. The heart of the machine is a MAYR control box, which receives a signal from a linear-encoder to control and position the linear ram. At certain designated encoder-increments, a 24VDC signal is pulsed from the logic circuit of the MAYR box to the micro-servo roll-feeder controller box. A triggered open-loop signal activates the feeder to feed material by a preset feeding-distance. C++ programming language and a RS232 interface are used to create forming program, and to control the machining parameters and other communication aspects (downloading/uploading). The position of the ram is controlled by a linear encoder embedded inside the linear-motor used for actuation. The encoder also tells the home position, which represents the starting point of the ram before being moved. The motion frequency of the ram is considered as the forming speed and is recorded as the number of strokes per minute (spm). SPM is referred as the number at which the machine to be operated and can be amended through program editing. An amendment to the process speed or to any other command, if required, is done in the communication-terminal software before being downloaded to the servo drive controller via the RS232 communication port. The program is stored in the servo-drive ROM for the operation, which may be run automatically.

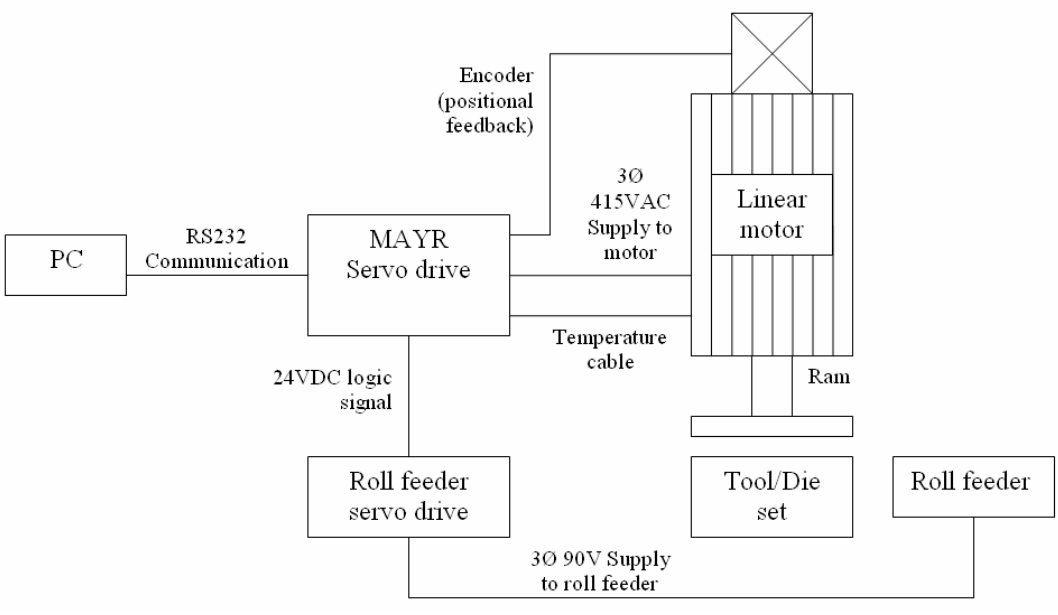

Fig. 5.1: The machine control architecture and the servo roll-feeder.

5.3.2 The Micro-Servo Roll-Feeder

The servo roll-feeder uses a belt-transmission system to transfer rotational-motion from the motor to the feeder rollers. Basically, the servo-motor is controlled by a closed-loop operation, where a rotational incremental-encoder is used for positional feedback. The feed-distance versus time characteristic data gathered from the manufacturer's specification is shown in Fig. 5.2. Strip is pulled into the machine in order to avoid buckles and wrinkles during feeding [Jacques et al., 2007].

From the graph, the time taken to feed strip at 5mm feed distances is about 70ms minimum. This figure shows that basically up to 14 times of feeding may be achieved per second for the designated feed-distance which equates to 840 parts being produced per minute.

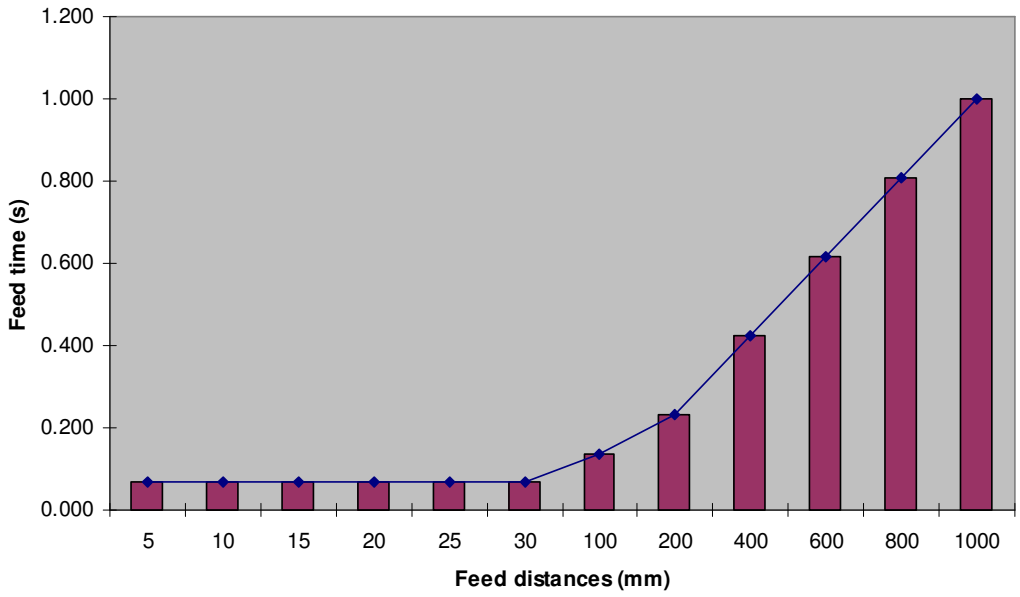

Fig. 5.2: Feeder feeding-performance.

5.3.3 The Air Gripper-Feeder

The gripper-feeder utilizes a pair of clamps; one remaining stationary, called the retainer, and the other moving in the feed and return strokes, called the gripper. During the feed stroke, the retainer releases the strip as the gripper clamps and moves it forwards through the top half of the press cycle while the tool is open. On the return stroke the gripper releases the strip and the retainer holds it while the gripper retracts from the press through the bottom half of the press cycle, while the tool is closed. All actuation processes were realized by a pneumatic system. Linear actuation for the feeding operation was driven by 90N of driving force. The feeder has a belt-type conveyance system, as shown in Fig. 5.3, which allows better grip of the thin sheet while at the same time preserving the surface of the sheet from scratches. A 24VDC solenoid was used to control, divert and relay the air path during the feeding process. The feed-distance travel requires manual adjustment by adjusting bolts that secure a dead-stop block.

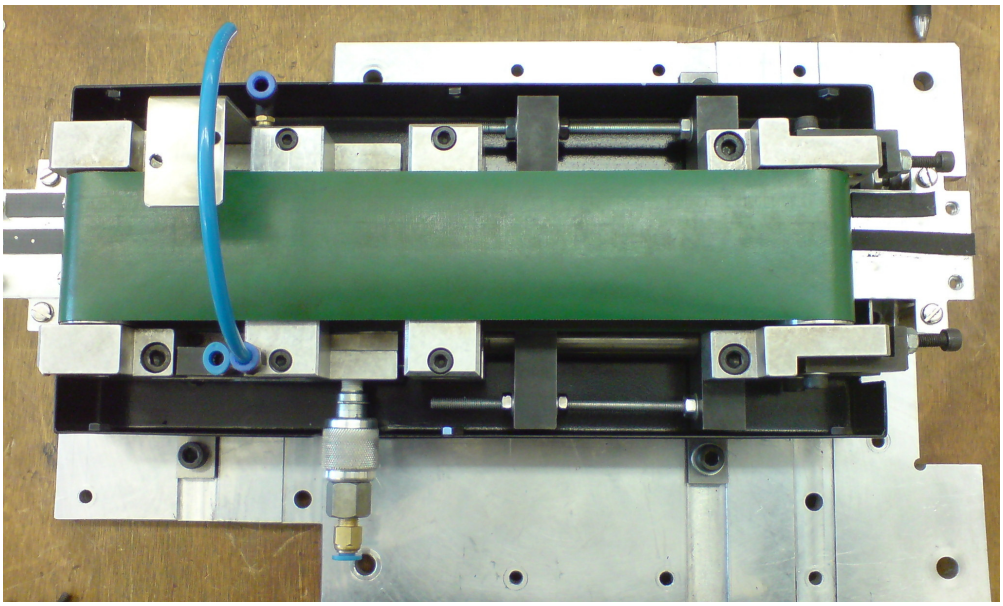

Fig. 5.3: The air gripper-feeder used in the experiments.

5.3.4 The Linear Encoder

In order to eliminate the influence of tooling tolerance on the positional accuracy measurement, a new approach to measure positional accuracy was employed by using a linear encoder. Normally, a linear-encoder is used as a positional-feedback mechanism in a closed-loop system. By employing a non-contact measurement method, such as using a linear-encoder to measure the pitch distance fed by the feeder, accurate measurement may be expected [Gao et al., 2006]. This is due to there being no influence from the tooling geometry and tolerances and other sources of mechanical inaccuracy, so that precise measurement can be obtained.

A similar non-contact measurement-approach was used to measure the multi-degree-of-freedom error-motions of a precision linear-air-bearing stage [Gao et al., 2006], in which an autocollimator and a laser -interferometer were used to determine the errors. Both of these non-contact devices give a higher level of reading of up to nanometer precision in the measurements, compared to what is obtained with a linear-encoder. Nevertheless, a linear-encoder is usable in such applications as do not require nanometer precision while keeping the measurement-cost lower than that when using an autocollimator or a laser-interferometer.

The approach begins with designing a straight long platform to accommodate a 2m-long metal strip to be studied. A linear-encoder was mounted at ¾ of the platform length and 4 V-guide rollers were mounted as a self-aligning mechanism for the metal strip. Fig. 5.4 shows the proposed experiment platform for the measurement of the positional accuracy of feeding when using the servo roll-feeder. The platform is then mounted on the micro-forming-machine so that the positional accuracy-measurement processes exactly mimic the actual feeding-process during micro-forming. A separate 24VDC power-supply unit and a low-frequency function-generator are used to generate 24VDC signal pulses to trigger the motion of the servo-roll and the air-gripper feeder.

The linear-encoder platform is mounted onto the machine and reading-acquisition is done using a National Instrument (NI) controller-interface BNC-2120. The linear-encoder was connected to the NI BNC-2120 terminal interface and all of the measurement were processed using LabView application software (to start and end the measurement, to retrieve the measured data, etc.).

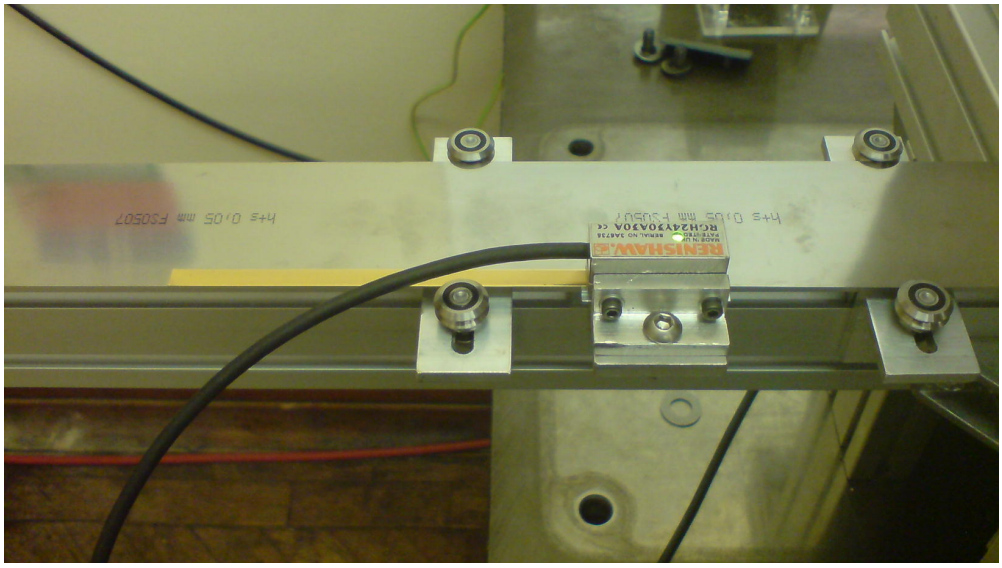

Fig. 5.4: Installation of the linear encoder on the machine structure.

5.3.5 The Materials Tested

Material preparation began with cleaning the strip surface with degreaser detergent at the location where the strip in intended to be adhered. This is to ensure that the surface is free from oil/grease to ensure better adhesion of the linear-encoder strip. Next, adhering of the 150mm linear-scale tape onto the metal strip under study was carried out (in this case carbon-steel strip 50µm and 100µm thick and 50µm thick stainless-steel strip) on the cleaned side/edge parallel to the feeding direction. Fig. 5.5 shows the strip used in the experiments and Fig. 5.6 the placement of the linear-encoder strip.

Each strip was aligned properly in order to obtain consistent readings from the linear-encoder read-head, (indicated by a green light on the read-head: otherwise, a red indicator is shown to indicate that slight adjustment of the strip and platform is required).

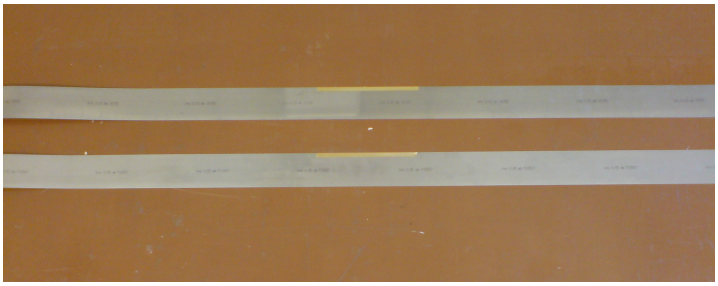

Fig. 5.5: 50µm and 100µm carbon-steel strip used in the experiments.

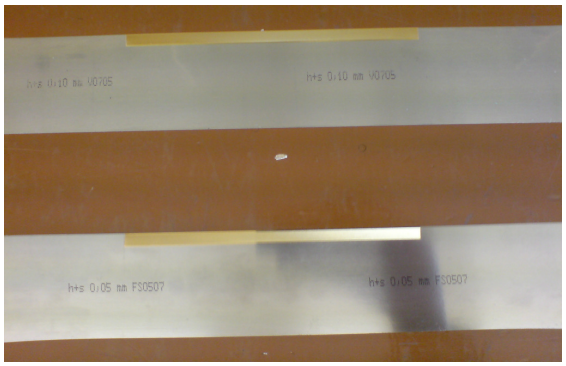

Fig. 5.6: The linear tape-scale fixed onto the strips.

5.4 Procedure

Experiments were divided onto two categories; default and optimized-configuration. The default-configuration represents the initial-setting of the feeder configured by the manufacturer. In this configuration, the velocity and the acceleration time-phases were based on the manufacturer's setting of the respective values, the maximum velocity being 1.04m/s. Then experiments were repeated with pilot/locating pins installed on the progressive-multistage-tooling as a means of improve the positional accuracy. Experiments then were re-configured for the optimized configuration: the latter is aimed mainly at the optimized motion-profile curve, to obtain the best possible positional accuracy of the servo roll-feeder. Both of the configurations shared a similar experiment set-up. Nevertheless, with the optimized configuration, the feed frequency was limited to 2Hz operation, to avoid excessive dynamic-instability and to enable the greatest positional-accuracy to be achieved. The application of brake force was also introduced into the optimized configuration. Details of the brake force calculation of 1.4N used in the experiments is described subsequently. The experimental procedure is summarized in Fig. 5.7.

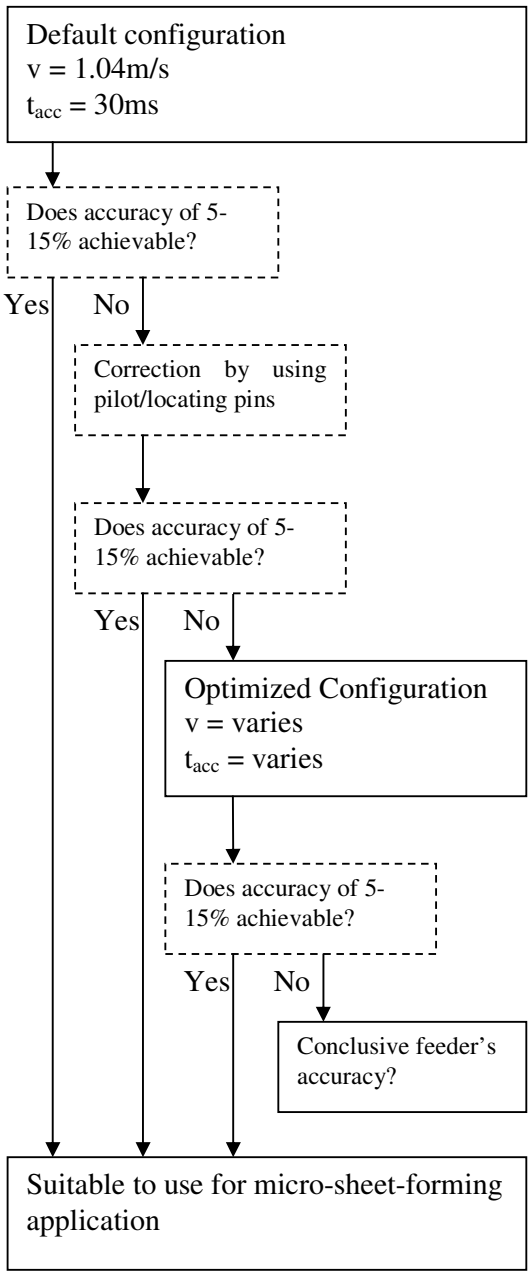

Fig. 5.7: Flowchart of the experiments' procedure.

The overall experimental set-up diagram is shown in Fig. 5.8. Two different feed distances were used (1mm and 5mm) to study the correlation between positional accuracy and the increment of feed distance. The feed frequency, which reflects the parts produced per minute (ppm), was varied between 1-14Hz using a digital function-generator, the latter being used to bypass the micro-forming-machine so that

this experiment can be performed safely in a stand-alone mode within the University's health and safety regulations.

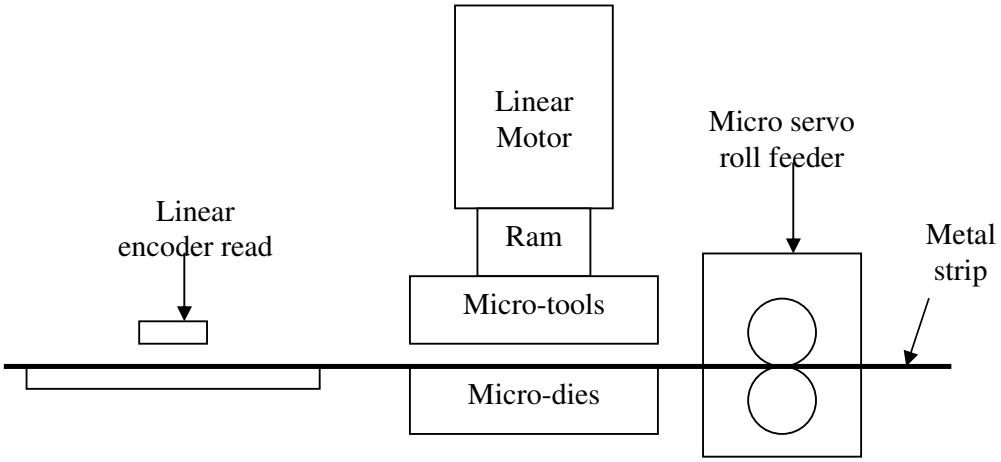

Fig. 5.8: Placement of the linear encoder on the machine and the experimental set-up.

First, 50µm-thick carbon-steel strip was tested with no-lubricant being used on the tooling and on the machine's bridge. Then the experiment was repeated with 100µm-thick carbon–steel, followed by 50µm-thick stainless-steel strip. Finally, 50µm-thick carbon-steel strip was tested in the presence of lubricant. Five parameters were varied to explore the effect on the positional accuracy of the feeder of: feed distance, feeding frequency, strip thickness, strip material and lubrication condition.

The feeding frequency was tested at values of 1, 2, 3, 6, 9, 12 and 14Hz. These feeding frequencies were then divided into three categories, namely low-, intermediate- and high-frequency feeding. Low-frequency feeding consists of 1, 2 and 3Hz frequency; intermediate, 6 and 9Hz; while high-frequency feeding is rated at 12 and 14Hz. Both of the feed distances (1mm and 5mm) were tested at each designated feeding frequency, for all material-types.

All the experiment results were sorted by examining the contribution of each of the parameters towards the feeder's positional accuracy. Firstly, the effect of change of feed-frequency was studied for 50µm-thick carbon-steel strip for both feed distances, under non-lubricated conditions. Secondly, the effect of lubricant presence on the system was compared with the results for non-lubricated conditions. Thirdly, comparison of the positional-accuracy between the use of thicker and thinner carbon-

steel strip was made. Finally, the effect of the achievable positional accuracy when the strip material is changed to stainless-steel is examined.

The experiments were repeated to confirm the observations of the feeder performance during the feeding process, and of the obtained positional accuracy. The positional accuracy was determined by measuring the distance covered from the beginning of the cycle to the point where the settling time cycle ends. The settling time is the time required for the feeder to settle its motion at the designated feed distance. Positional overshoot may occur when high acceleration-deceleration motion is involved during the feeding process, but is gradually corrected as the feeder achieves the desired value. When the desired position is achieved, the feeder settles and waits for the next cycle to begin. The positional accuracy was measured by finding the positional-difference between two consecutive settling times, as shown in Fig. 5.9. Repeatability may be calculated as the difference of two consecutive accuracies.

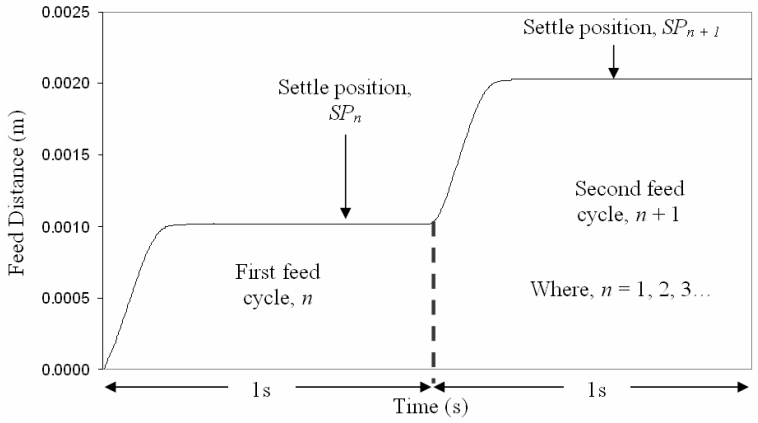

Fig. 5.9: Settling-time curve.

Both positional accuracy and repeatability may be expressed, as below, as mathematical arithmetical progressions. It is supposed that the settled-position of the first feed is denoted as SP_n and the following settled-position is denoted as SP_{n+1}, where a_n and r_n are the positional accuracy and repeatability at the *nth* cycle, where n is an integer. The positional accuracy of the following consecutive feeds (where $n \neq 0$) may be expressed as:

$$n \neq 0$$
$$a_{n+1} = SP_{n+1} - SP_n \quad (1)$$

The positional accuracy for the first feed (where $n = 0$) may be expressed as:

$$n = 0$$
$$a_{n+1} = SP_{n+1} - d \quad (2)$$

where d is the absolute feed-distance.

The positional repeatability then may be expressed as:

$$n \neq 0$$
$$r_n = a_{n+1} - a_n \quad (3)$$

Experiments were repeated with a similar configuration as for the micro-servo roll-feeder, to observe the performance of the air gripper-feeder.

5.5 Results

5.5.1 Effect of Changes of Feed-Frequency and Feed-Distance on Positional Accuracy

Experiments were first conducted on 50µm-thick carbon-steel strip with no lubricant being used. All frequency ranges were tested for both 1mm and 5mm feed-distances.

a) 1mm feed-distance

From the experiment results, in low frequency feeding at 1mm feed distance, the positional accuracy pattern seems to be consistent for all of the frequencies tested, with the achieved positional accuracy being within the range 6.1-6.6µm, as depicted in Fig. 5.10(a) to Fig. 5.10(c). This quite-impressive positional accuracy was achieved due to the feeder having ample time to correct the overshoot feeding position as to be as close as possible to the designated absolute value of 1mm. However, a large deviation was recorded for the whole of the frequencies tested, of ±3.2 to 4.8µm, hence suggesting that inconsistency in repeatability occurred. For an intermediate feed-frequency, the positional accuracy achieved deteriorated to within 7.1 to 7.2µm, with an achieved repeatability of ±4.3 to 4.9µm. At higher feed frequency, the positional accuracy decreased slightly proportionally to the increase of the feed frequencies. An positional accuracy of within 8.5µm was recorded at higher frequency (12 and 14Hz) and the repeatability was determined to be ±4.2 to 4.9µm.

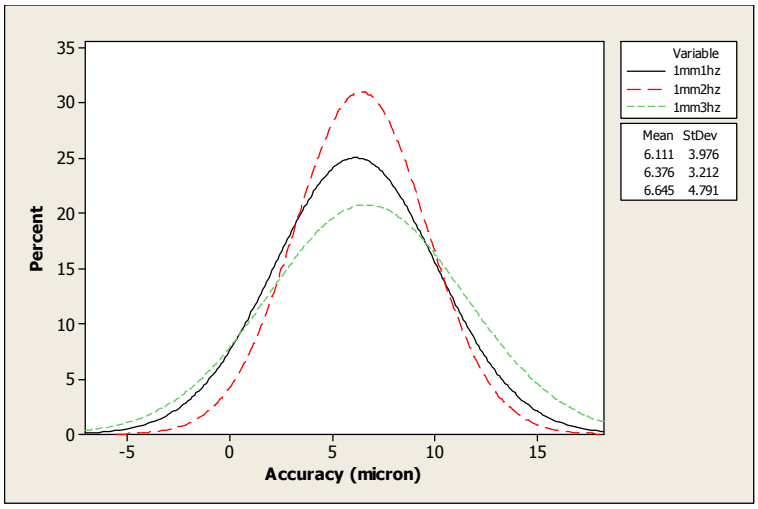

(a)

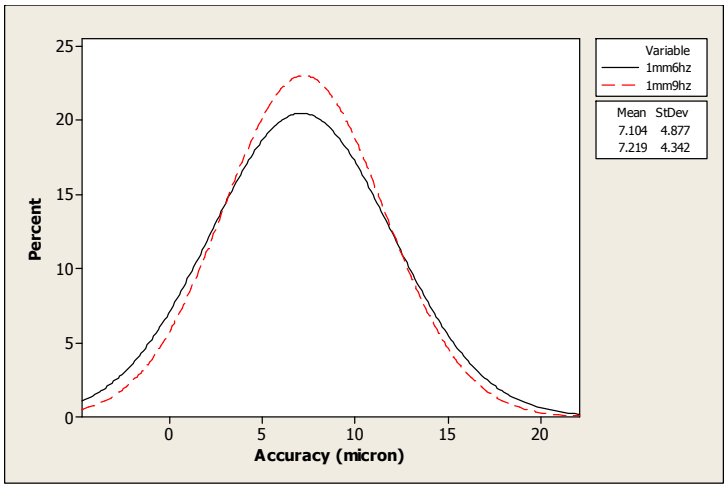

(b)

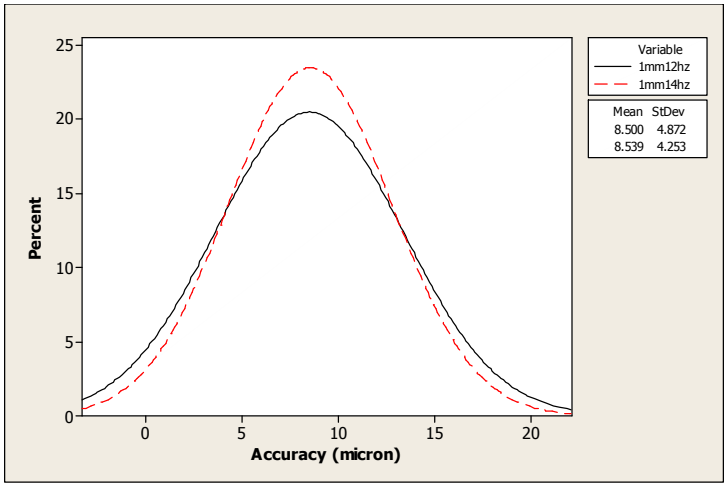

(c)

Fig. 5.10: 3 types of feeding frequency for 1mm feed-distance: (a) low frequency (1, 2 and 3Hz); (b) intermediate frequency (6 and 9Hz); and (c) high frequency (12 and 14Hz).

b) 5mm feed-distance

Change of feed distance to a greater value significantly reduces the positional accuracy and repeatability of the feeder. As depicted in Fig. 5.11(a), Fig. 5.11(b) and Fig. 5.11(c), 5mm feed distance has a mean positional accuracy of within the range 9.1-10.2µm and a huge deviation or repeatability of ±5.7 to 7.0µm for a low feed-frequency, this figure increasing slightly for an intermediate feed-frequency with a mean positional accuracy and a repeatability of 10.4 to 10.6µm and ±7.3 to 8.1µm, respectively. The positional accuracy level reduces dramatically for a high feed-frequency, with a recorded mean-positional accuracy of 12.7 to 15.1µm and a repeatability of within ±38.2 to 38.8µm.

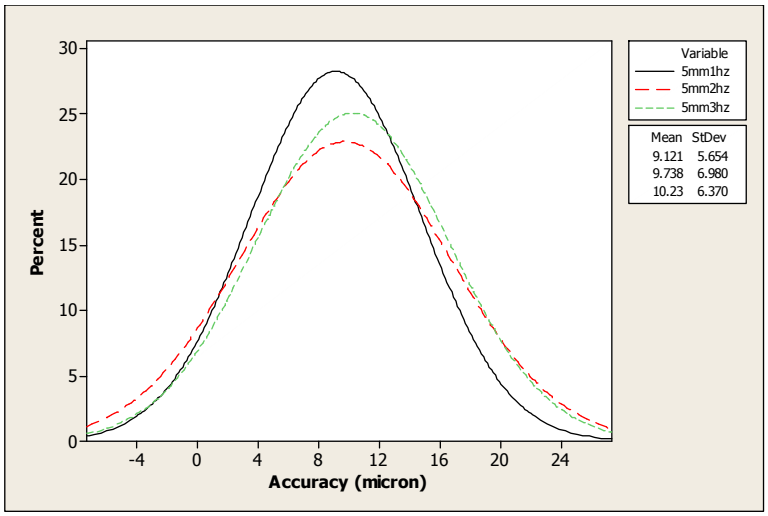

(a)

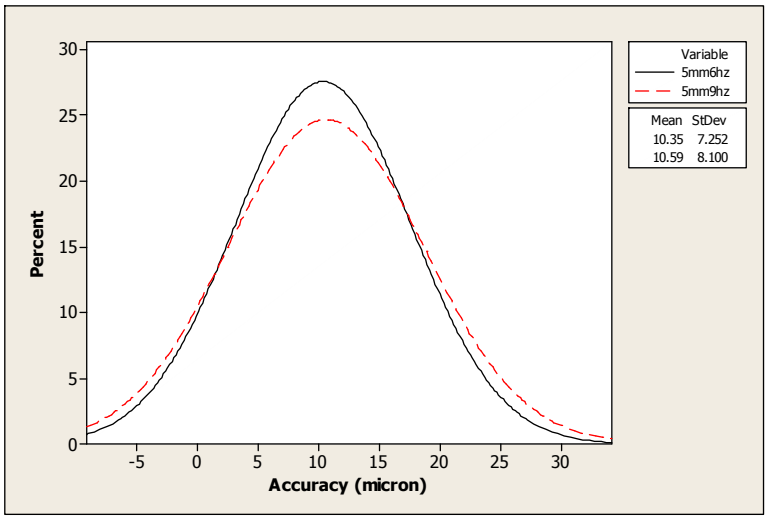

(b)

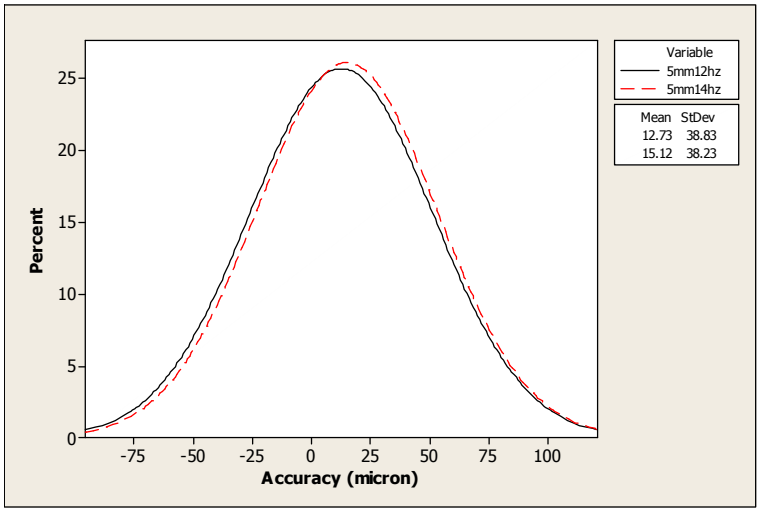

(c)

Fig. 5.11: 3 types of feeding frequencies for 5mm feed-distance: (a) low frequency (1, 2 and 3Hz); (b) intermediate frequency (6 and 9Hz); and (c) high frequency (12 and 14Hz).

c) Comparison of positional accuracy between 1mm and 5mm feed-distances

Fig. 5.12(a) to 5.12(g) show the comparative details of the positional accuracy between 1mm and 5mm feed-distances. From those figures, the mean-positional accuracy for the shorter feed-distance was observed to be 30-32% better than that for the longer feed-distance both at low and intermediate feed-frequencies. At feed-frequencies of 12-14Hz, this figure increased to 33 to 43%, which indicates that a better mean-positional accuracy is achieved with a shorter feed-distance compared to that for a longer feed-distance. A generally-similar deviation was recorded for both shorter and longer feed distances at feed-frequencies of between 1-6Hz. However, at 9-14Hz feed-frequencies, significant reduction of the deviation was observed for the longer-feed distance. This suggests that the feeder could not maintain good repeatability during operation.

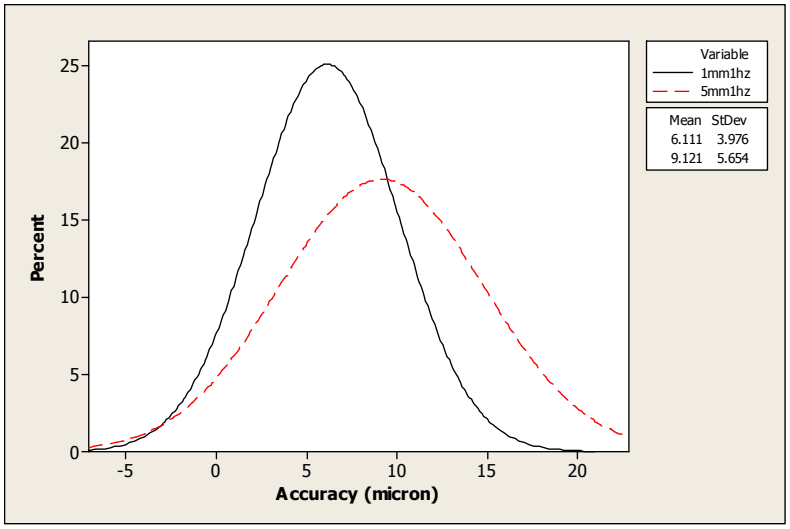

(a)

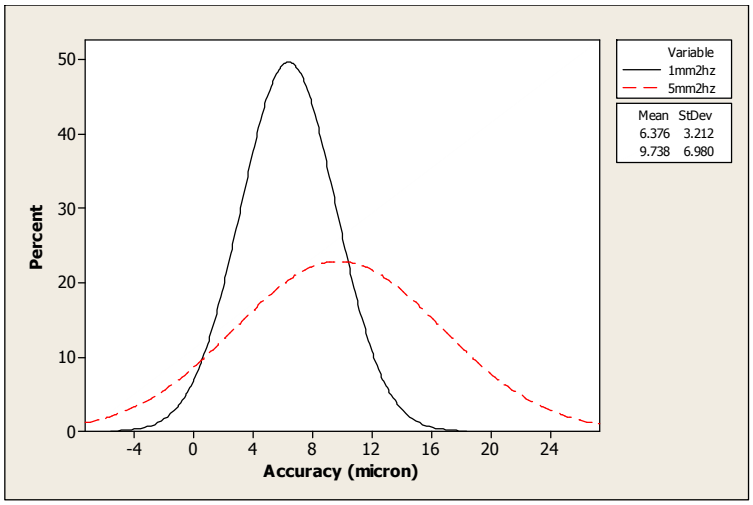
Variable
1mm2hz
5mm2hz
Mean StDev
6.376 3.212
9.738 6.980
Percent
Accuracy (micron)

(b)

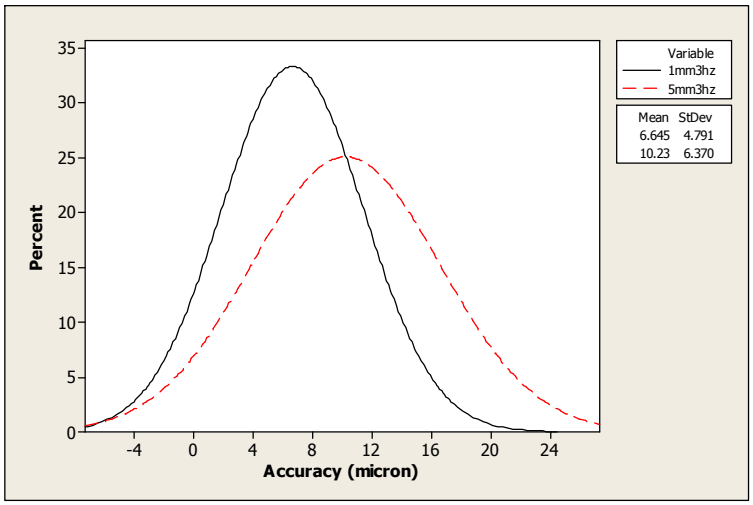
Variable
1mm3hz
5mm3hz
Mean StDev
6.645 4.791
10.23 6.370
Percent
Accuracy (micron)

(c)

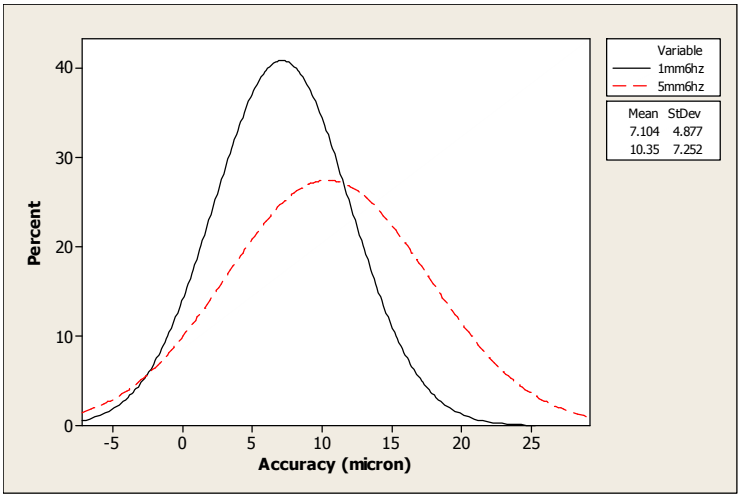
Variable
1mm6hz
5mm6hz
Mean StDev
7.104 4.877
10.35 7.252
Percent
Accuracy (micron)

(d)

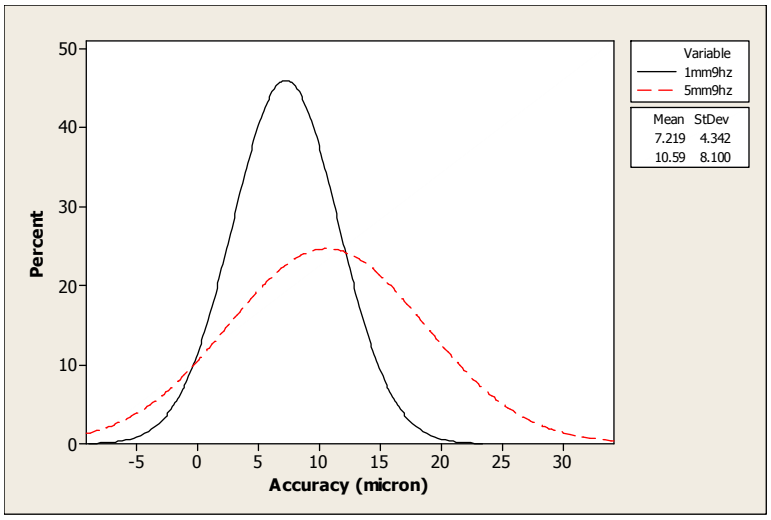

(e)

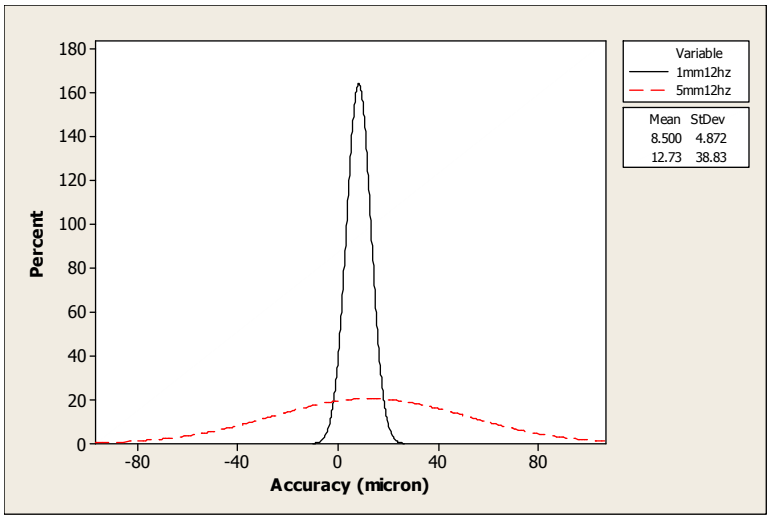

(f)

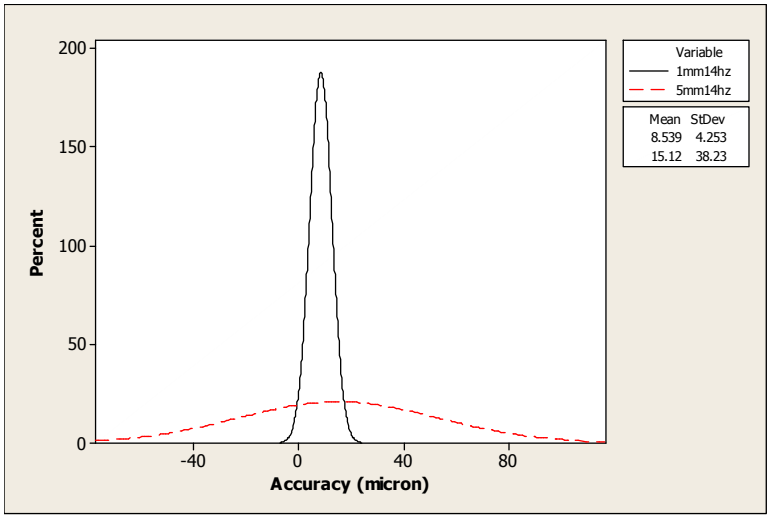

(g)

Fig. 5.12: Comparison of positional accuracy for all feeding frequencies and 1mm and 5mm feed-distance: (a) 1Hz; (b) 2Hz; (c) 3Hz; (d) 6Hz; (e) 9Hz; (f) 12Hz; and (g) 14Hz.

5.5.2 Effect of Lubrication on Positional Accuracy

Lubrication of the tooling has small influence in improving positional accuracy, specifically at both low and high feed-frequency for 1mm feed-distance, as shown in Fig. 5.13. The positional accuracy-trend for the lubricated condition was found to be similar to that for the non-lubricated condition. Nevertheless, excessive lubrication tends to promote slip between the strip and the rollers of the feeder, due to the small contact area between the rollers and the surface area of the strip, thus resulting in reduced positional accuracy. According to Ivaska, 2003 and Rueter, 2002, to prevent corrosion of the strip metal, the manufacturer usually applies a thin film of lubricant on the strip coil, which acts as a lubricant in the forming process to which the strip is subjected ultimately. Therefore, additional lubricant (excessive lubrication) does not have much influence in improving positional accuracy.

a) 1mm feed-distance

At low feed-frequency, although the presence of lubricant was observed to reduce the deviation or increase the repeatability, the mean-positional accuracy was also noted to be slightly better than that for the non-lubricated case. At 1Hz feed-frequency, as depicted in Fig. 5.13(a), a non-lubricated experiment recorded a mean-positional accuracy of 6.1µm, while for the lubricated case the value was 5.1µm. The deviation and repeatability were recorded at ±4.0µm and ±4.1µm, respectively, both for the non-lubricated and lubricated cases. A similar finding was observed for 2Hz feed-frequency, as shown in Fig. 5.13(b), where a mean-positional accuracy and repeatability of 6.4µm and ±3.2µm were recorded for the non-lubricated, and 5.7µm and ±3.3µm with the presence of lubricant. At 3Hz, as in Fig. 5.13(c), the presence of lubricant was observed to slightly improve the mean-positional accuracy from 6.6µm to 5.7µm: however, an almost similar repeatability was recorded for both conditions, at ±4.8µm.

At intermediate and high feed-frequencies, a consistent finding was observed where the presence of lubricant slightly improved the mean positional accuracy, but at the same time reduced the repeatability. Depicted in Fig. 5.13(d) and Fig. 5.13(e), a 20% improvement of the mean-positional accuracy was recorded when lubricant was

used. On the other hand, 8 to 24% deterioration of the repeatability was observed. At higher feed-frequency, as shown in Fig. 5.13(f) and 5.13(g), an improvement of 31% was recorded for the mean-positional accuracy when lubricant was used. However, the repeatability was observed to decrease by 13 to 20%.

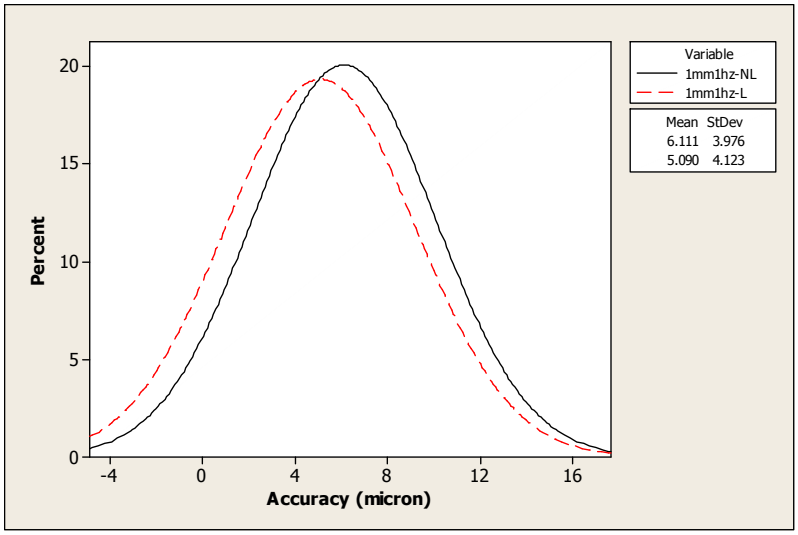

(a)

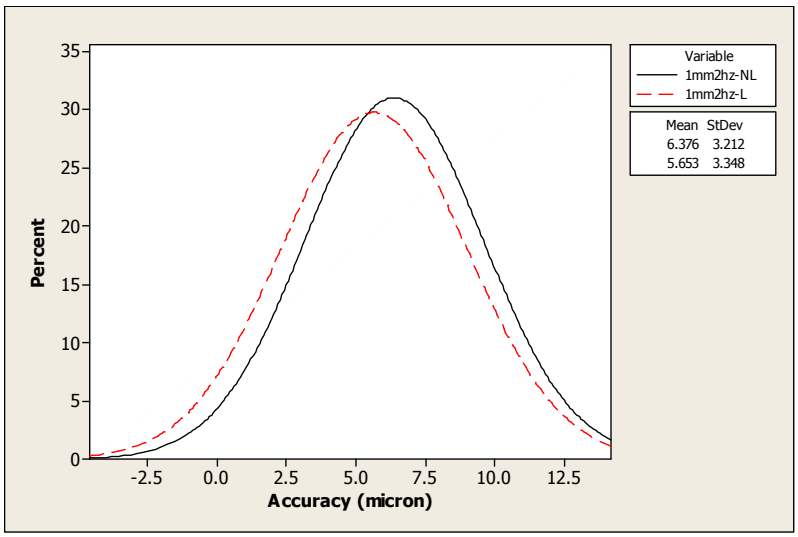

(b)

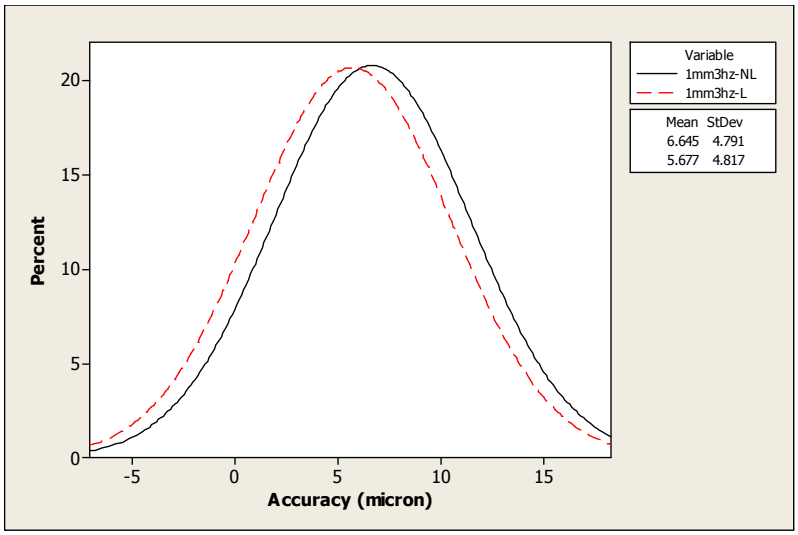
Variable
1mm3hz-NL
1mm3hz-L
Mean StDev
6.645 4.791
5.677 4.817
Percent
Accuracy (micron)

(c)

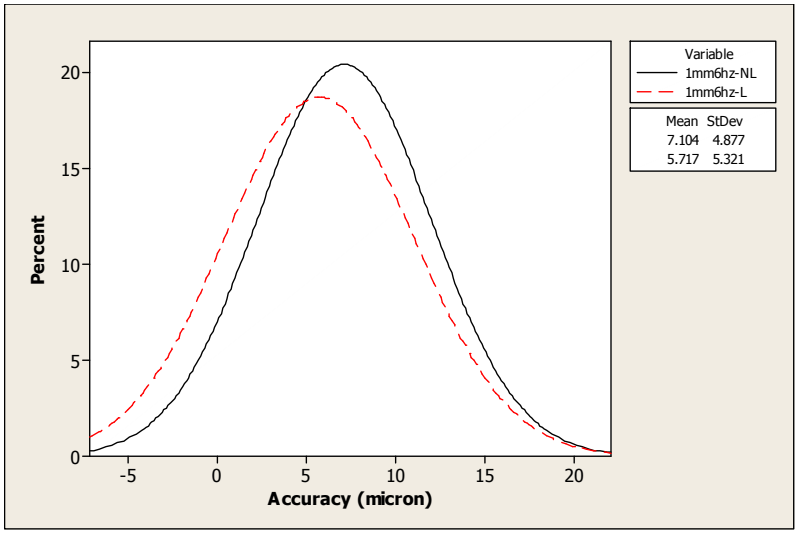
Variable
1mm6hz-NL
1mm6hz-L
Mean StDev
7.104 4.877
5.717 5.321
Percent
Accuracy (micron)

(d)

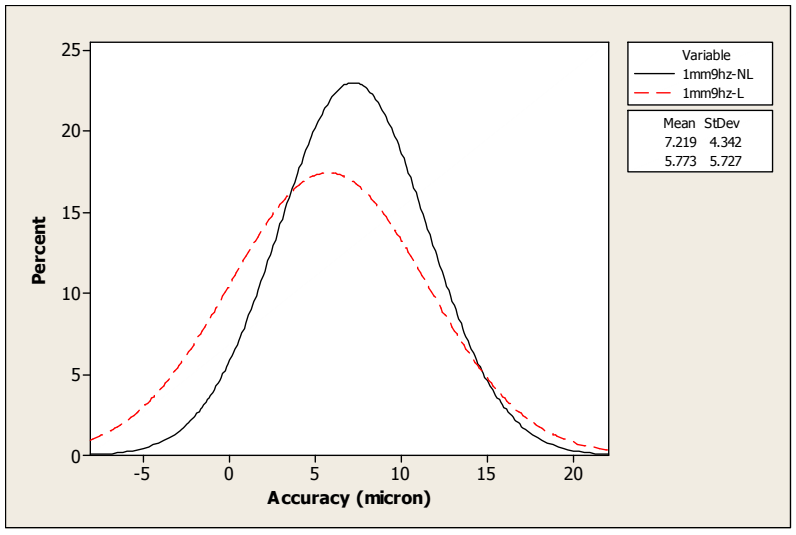
Variable
1mm9hz-NL
1mm9hz-L
Mean StDev
7.219 4.342
5.773 5.727
Percent
Accuracy (micron)

(e)

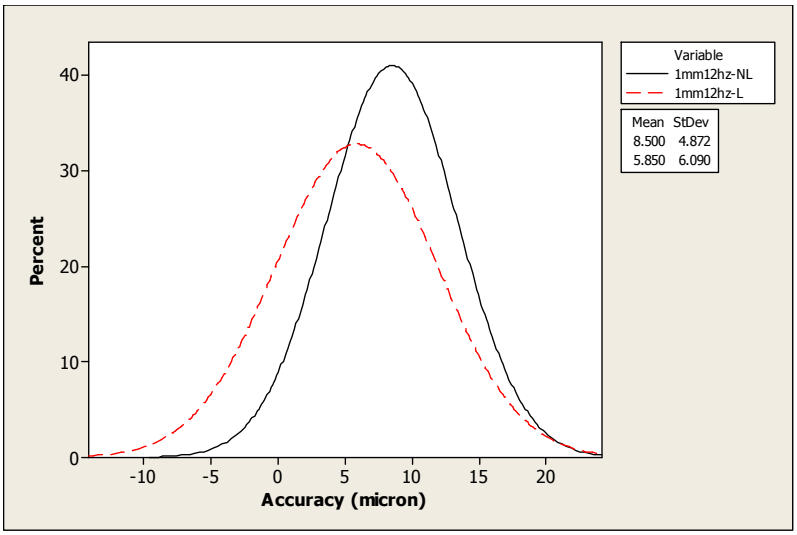

(f)

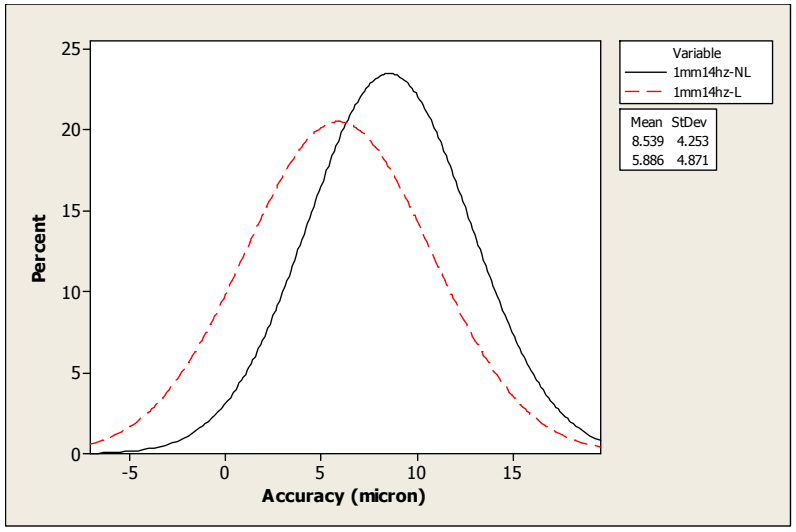

(g)

Fig. 5.13: Recorded positional accuracy for various feed-frequencies at 1mm feed-distance: (a) to (g) represent 1, 2, 3, 6, 9, 12 and 14Hz (representing all frequency-range cases).

b) 5mm feed-distance

For the longer feed-distance, the positional accuracy seems to be improved with the presence of lubricant, specifically at low feed-frequency, as depicted in Fig. 5.14(a), 5.14(b) and 5.14(c). At this feed-frequency, an improvement of the mean-positional accuracy of between 3.0 to 3.2µm was recorded with the presence of lubricant. However, no improvement in repeatability was observed.

At intermediate feed-frequency, as depicted in Fig. 5.14(d), 6Hz operation gave similar findings as the results for low feed-frequency. Although the mean-positional

accuracy was seen to be slightly improved, the repeatability was found to be reduced. At 9Hz feed-frequency, the presence of lubricant was observed to slightly improve the positional accuracy and repeatability, from 10.6µm to 9.8µm, and from ±8.1µm to ±5.2µm, respectively as shown in Fig. 5.14(e).

At high feed-frequency, lubrication slightly improved the overall positional accuracy and repeatability, as shown in Fig. 5.14(f). Slight improvement of the mean positional accuracy was recorded of from 12.7µm to 10.9µm and repeatability was improved from ±38.3µm to ±28.5µm. At 14Hz frequency, as depicted in Fig. 5.14(g), the mean-positional accuracy was observed to improve significantly, from 15.2µm to 11.4µm but the repeatability was improved to a lesser degree, from ±38.2µm to ±37.0µm.

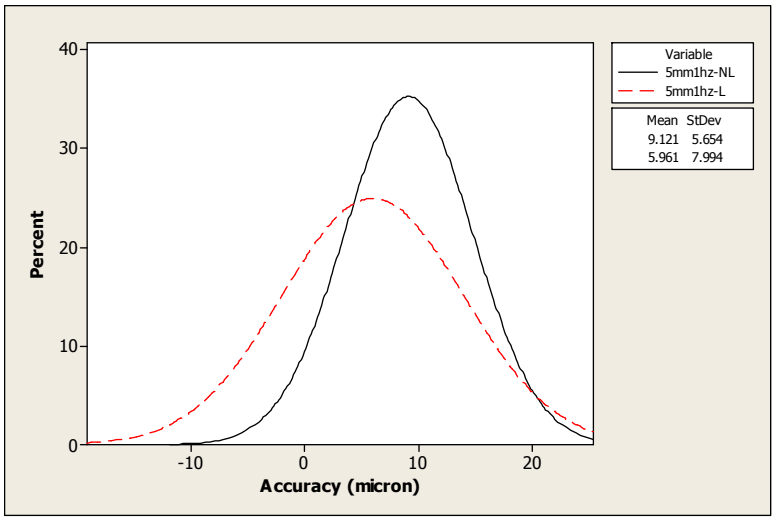

(a)

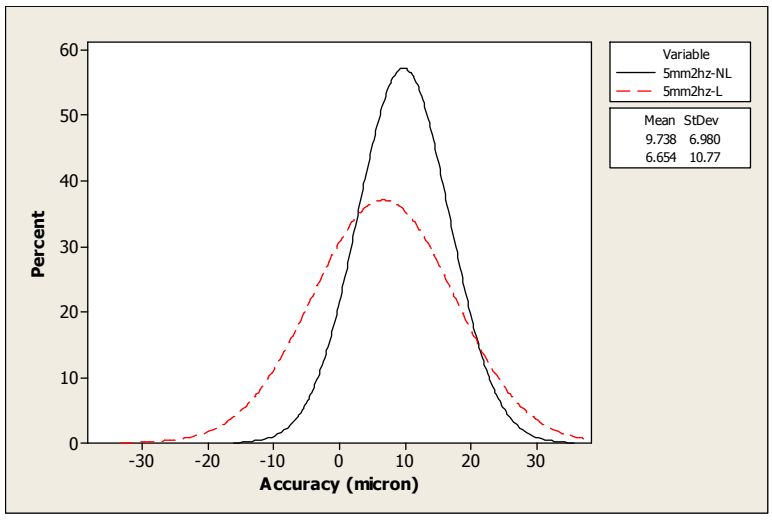

(b)

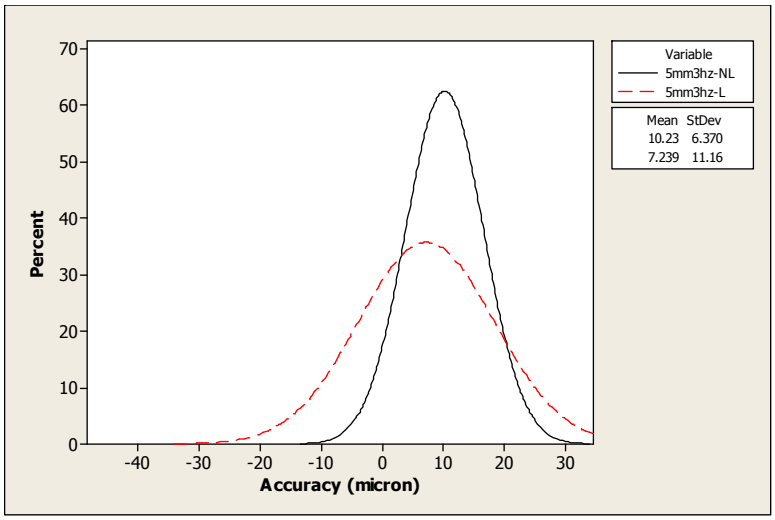
Variable
5mm3hz-NL
5mm3hz-L
Mean StDev
10.23 6.370
7.239 11.16
Percent
Accuracy (micron)

(c)

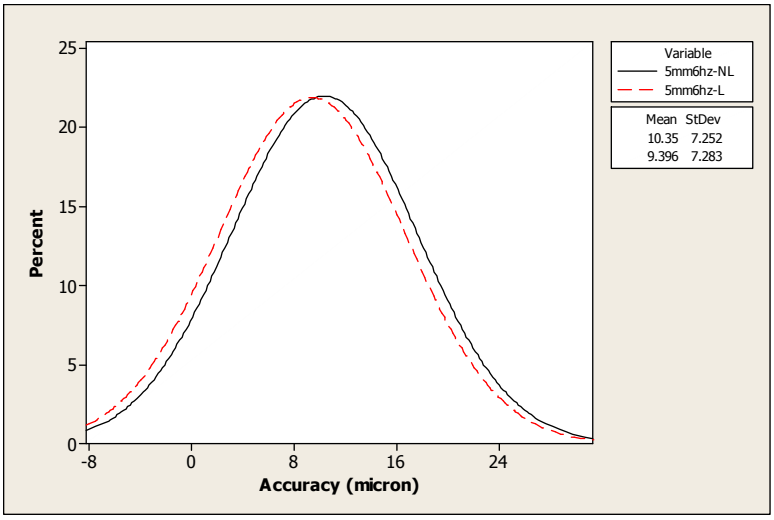
Variable
5mm6hz-NL
5mm6hz-L
Mean StDev
10.35 7.252
9.396 7.283
Percent
Accuracy (micron)

(d)

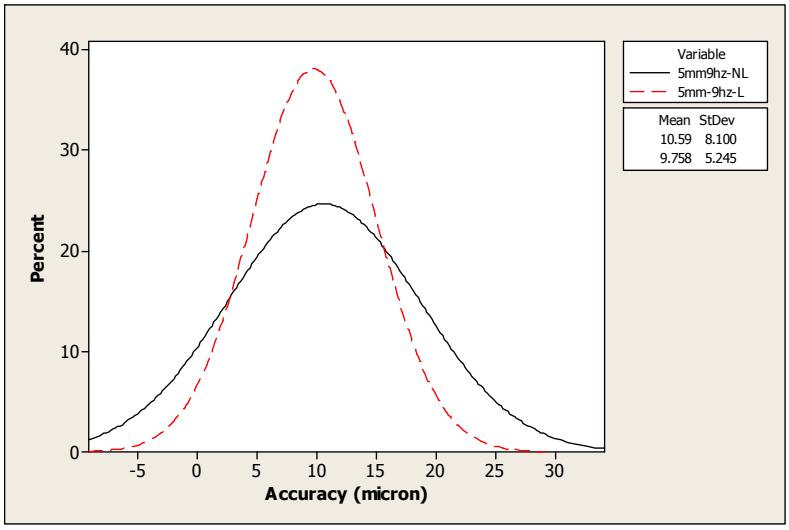
Variable
5mm9hz-NL
5mm-9hz-L
Mean StDev
10.59 8.100
9.758 5.245
Percent
Accuracy (micron)

(e)

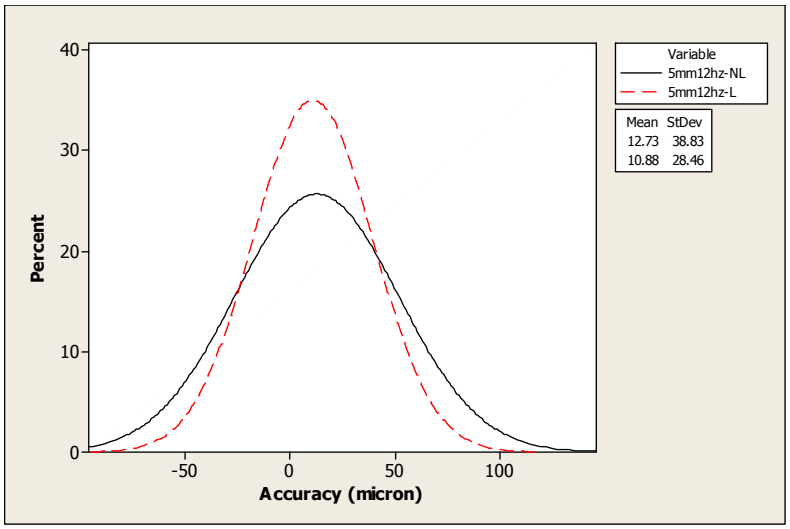

(f)

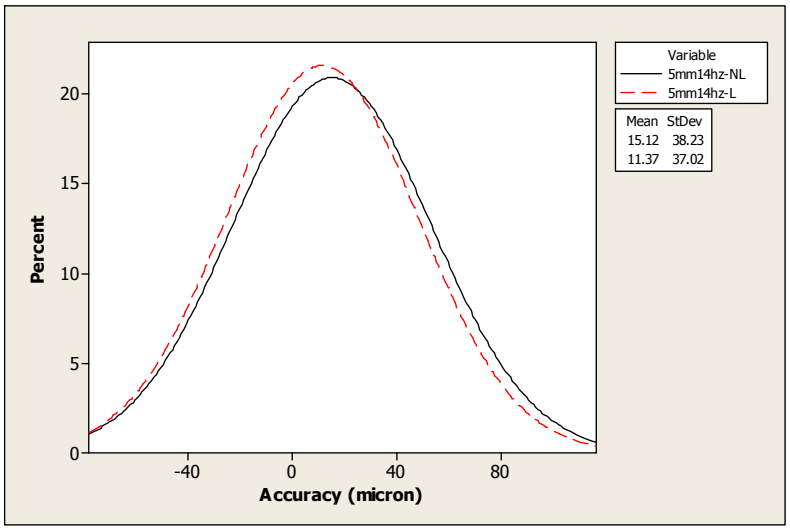

(g)

Fig. 5.14: Recorded positional accuracy for various feed-frequencies at 1mm feed-distance: (a) to (g) represent 1, 2, 3, 6, 9, 12 and 14Hz (representing all frequency-range cases).

5.5.3 Effect of Changes of Strip-Thickness on Positional Accuracy

The thin strip thickness was changed to a thicker strip and the change in to positional accuracy-pattern was observed. In this case, 100µm carbon-steel strip was used to compare with 50µm-thick strip of similar material. A similar feeding-pattern was demonstrated by the 100µm-thick strip with the feeding-pattern as obtained with the 50µm-thick strip.

a) 1mm feed-distance

Based on Fig. 5.15(a), 5.15(b) and 5.15(c), although a better mean positional accuracy was recorded for thinner carbon-steel, a huge deterioration in deviation was recorded for this material when compared to that for thicker strip. The positional accuracy with thinner 50µm-carbon-steel strip was found to be 6.1-6.6µm while the repeatability was found to be ±3.2 to 4.8µm, which demonstrates a consistent mean-positional accuracy and a deterioration of the deviation-patterns proportional to the increase of the feed-frequency, within the category of feed-frequency. Thicker carbon-steel strip, however, demonstrated different positional accuracy- and repeatability-patterns, within the feed-frequency category. At 1Hz feed-frequency, the recorded positional accuracy and repeatability were found to be 6.1µm and ±3.0µm, respectively. At 2Hz, the mean-positional accuracy and repeatability were recorded as 6.6µm and ±2.5µm, respectively. The mean-positional accuracy reduced to 6.6µm for 3Hz feed frequency, but the repeatability improved to ±4.0µm.

In the intermediate feed-frequency category, a similar feed-pattern was observed for 6 and 9Hz feed frequencies for both thinner and thicker carbon-steel strips as shown in Fig. 5.15(d) and 5.15(e). Almost similar mean-positional accuracy and improved repeatability were observed for thinner carbon-steel strip when the feed-frequency was increased from 6 to 9Hz, with a recorded mean-positional accuracy of 7.1µm and a repeatability of ±4.9µm at 6Hz, with 7.2µm mean-positional accuracy and ±4.3µm repeatability at 9Hz feed-frequency. A similar pattern was also observed when thicker carbon-steel strip is used. An almost similar mean-positional accuracy was recorded for both 6 and 9Hz feed-frequency, at 7.1µm at 6Hz and 7.2µm at 9Hz, and likewise for the repeatability, which values were ±3.1µm and ±3.7µm, respectively. Although the mean-positional accuracy of thicker-strip was found to be deteriorate slightly compared to that for thinner strip, the repeatability of the thicker carbon-steel strip was found to be better than that of the thinner carbon-steel strip.

When the high-frequency feeding-category was tested, different mean-positional accuracy and repeatability patterns from those for the intermediate frequency category were observed. As depicted in Fig. 5.15(f) and 5.15(g), the mean-positional accuracy and repeatability of thinner carbon-steel strip were recorded as 8.5µm and

±4.9µm for 12Hz, a similar mean-positional accuracy of 8.5µm and a repeatability of ±4.3µm being recorded when the feed-frequency was changed to 14Hz. A similar trend of the mean-positional accuracy and repeatability as for the intermediate feed-frequency category was observed for thicker carbon-steel strip, with mean-accuracies of 7.4µm and 7.5µm at 6 and 9Hz, respectively and corresponding repeatability of ±4.4µm and ±3.3µm. It can be concluded that not much difference was observed at high feed-frequency category for both thicknesses of strip. However, this finding is different from the low feed-frequency results, where the thicker carbon-steel strip was found to be better in terms of positional accuracy and repeatability when compared to thinner carbon-steel strip.

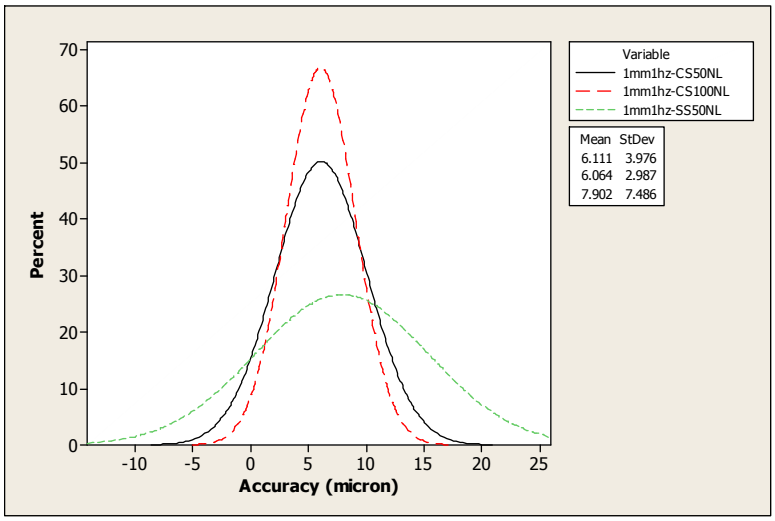

(a)

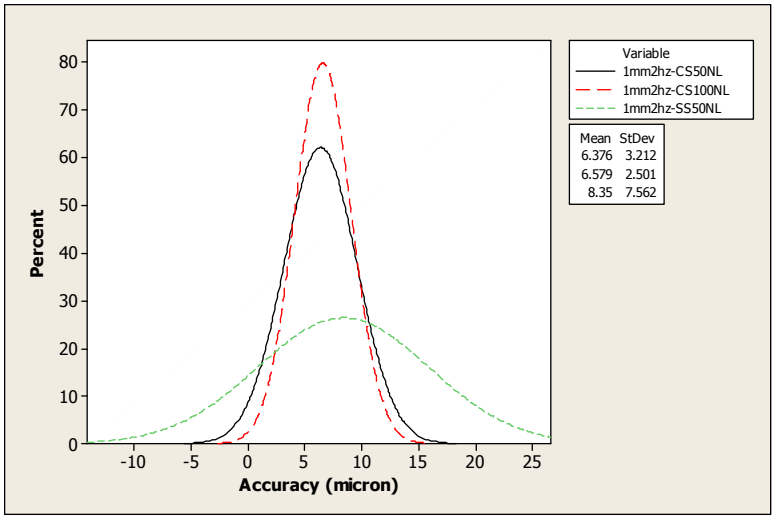

(b)

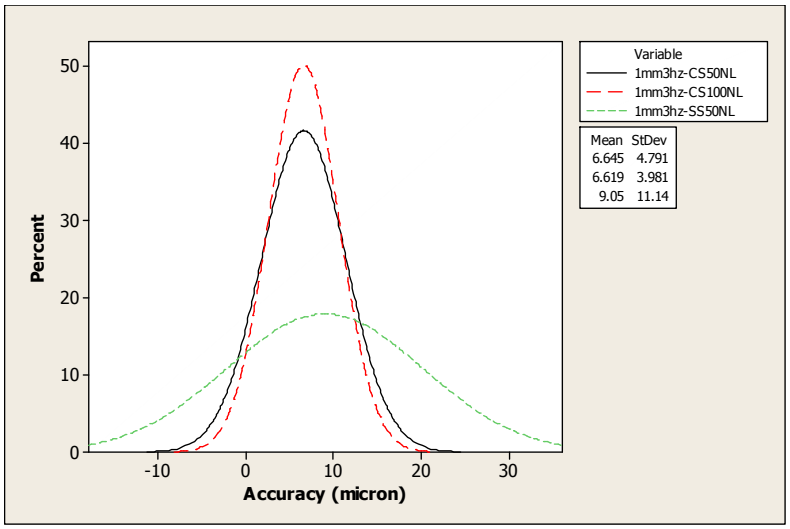
Variable
1mm3hz-CS50NL
1mm3hz-CS100NL
1mm3hz-SS50NL
Mean StDev
6.645 4.791
6.619 3.981
9.05 11.14
Percent
Accuracy (micron)

(c)

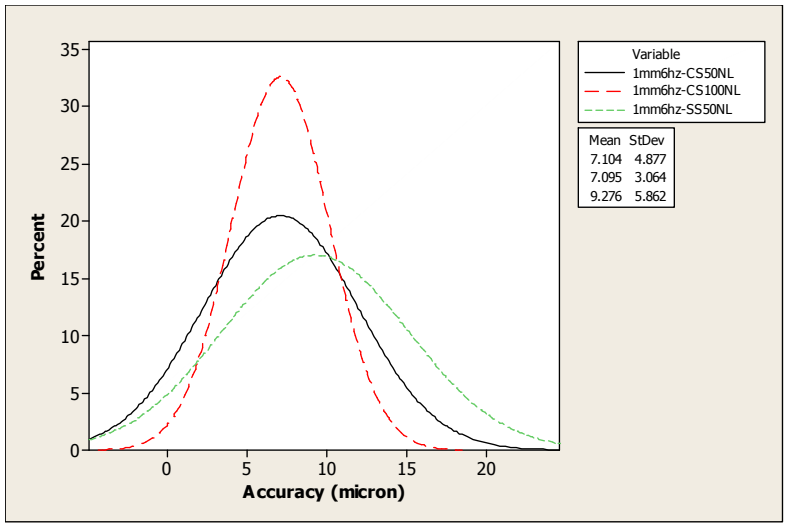
Variable
1mm6hz-CS50NL
1mm6hz-CS100NL
1mm6hz-SS50NL
Mean StDev
7.104 4.877
7.095 3.064
9.276 5.862
Percent
Accuracy (micron)

(d)

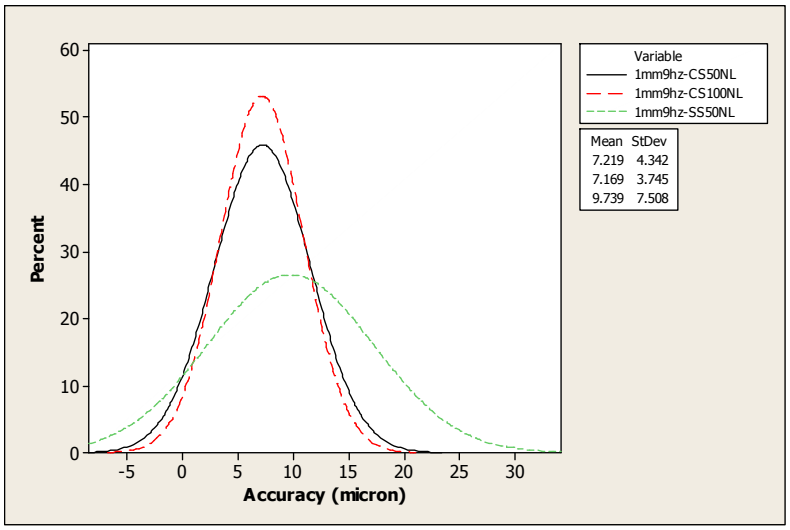
Variable
1mm9hz-CS50NL
1mm9hz-CS100NL
1mm9hz-SS50NL
Mean StDev
7.219 4.342
7.169 3.745
9.739 7.508
Percent
Accuracy (micron)

(e)

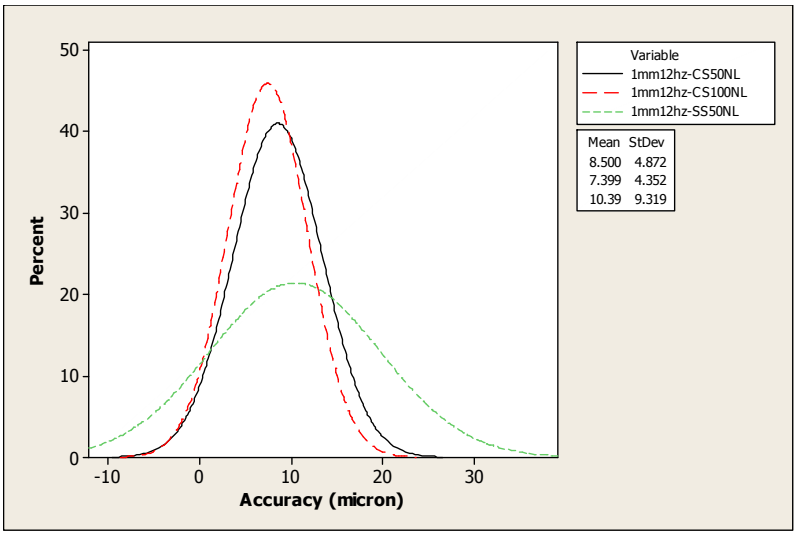

(f)

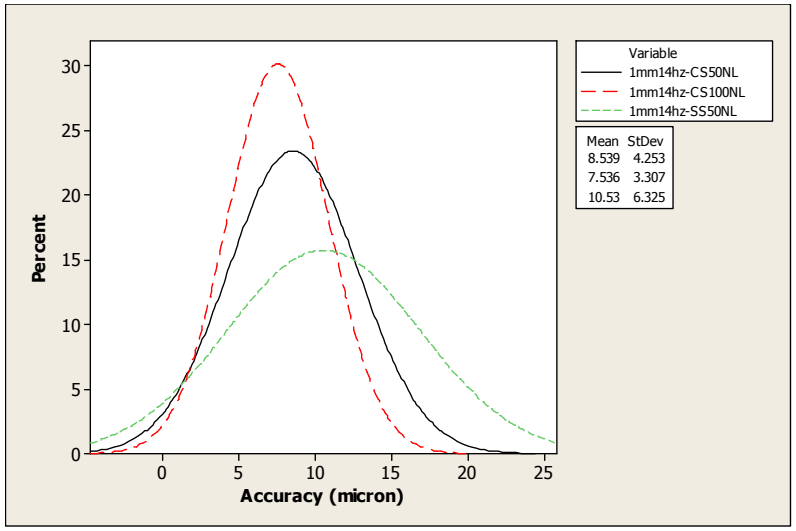

(g)

Fig. 5.15: Recorded positional accuracy for various materials in the non-lubrication case for all feed frequencies and at 1mm feed-distance: (a) to (g) represent feeding frequencies of 1-14Hz, respectively.

(note: CS – carbon-steel, SS – stainless-steel, NL – non-lubricated, L – lubricated, 50 and 100 – thickness in µm)

b) 5mm feed-distance

A significant difference in the mean-positional accuracy and repeatability patterns were observed at this feed distance. As depicted in Fig. 5.16(a), 5.16(b) and 5.16(c), a greater standard-deviation was recorded for thicker carbon-steel strip when compared to that for thinner carbon-steel strip. For the low feed-frequency category, a slightly larger deviation of up to 46% was recorded for thicker carbon-steel strip compared to deviation for thinner strip. The mean-positional accuracy, however,

generally demonstrated that thinner strip has better positional-accuracy compared to that for thicker carbon-steel strip.

For the intermediate-frequency category, as shown in Fig. 5.16(d) and Fig. 5.16(e), 6Hz feed-frequency exhibits a similar pattern of results pattern as for the low feed-frequency category. Almost similar mean positional accuracy and repeatability were observed at 6Hz and 9Hz feed frequencies which were at 10.4µm and 10.6µm respectively with recorded repeatability both at ±7.3µm and ±8.1µm for thinner carbon steel strip, meanwhile for thicker strip CS100, 14.6µm and 14.8µm mean positional accuracy at 6 and 9Hz with repeatability of ±11.3µm and ±10.6µm were recorded.

A slight deterioration in mean-positional accuracy was observed for the high feed-frequency category where, overall, the mean-positional accuracy for both thinner- and thicker-strips were found to deteriorate further, compared to the intermediate and low feed-frequency categories, as shown in Fig. 5.16(f) and 5.16(g). At 12Hz feed frequency, the mean-positional accuracy for thinner carbon-steel strip was recorded at 12.7µm, which was better than for the thicker strip, at 15.3µm. At the same time, the repeatability for thicker carbon-steel strip was found to be far better than for thinner strip, which values were ±11.8µm and ±38.8µm, respectively. At 14Hz, the mean positional accuracy of the thinner and thicker strips deteriorated to 15.2µm and 17.3µm, respectively. The repeatability for both materials was found to be ±38.2µm for thinner strip and ±7.7µm for thicker strip. Due to the large deviation recorded for both strips, the findings suggest that no consistent repeatability was achievable in the feeding process.

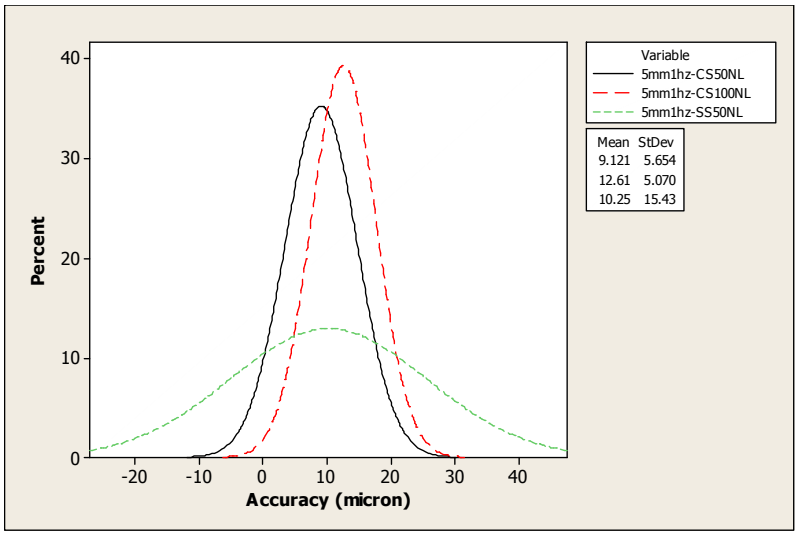
Variable
5mm1hz-CS50NL
5mm1hz-CS100NL
5mm1hz-SS50NL
Mean StDev
9.121 5.654
12.61 5.070
10.25 15.43
Percent
Accuracy (micron)

(a)

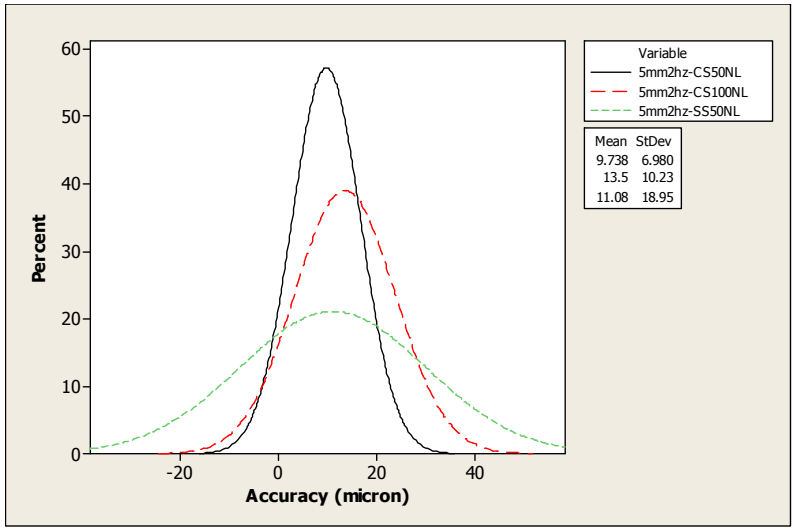
Variable
5mm2hz-CS50NL
5mm2hz-CS100NL
5mm2hz-SS50NL
Mean StDev
9.738 6.980
13.5 10.23
11.08 18.95
Percent
Accuracy (micron)

(b)

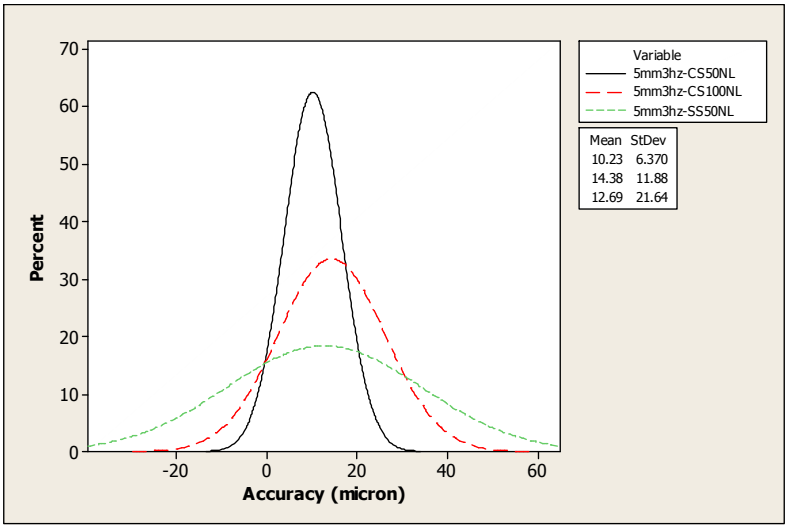
Variable
5mm3hz-CS50NL
5mm3hz-CS100NL
5mm3hz-SS50NL
Mean StDev
10.23 6.370
14.38 11.88
12.69 21.64
Percent
Accuracy (micron)

(c)

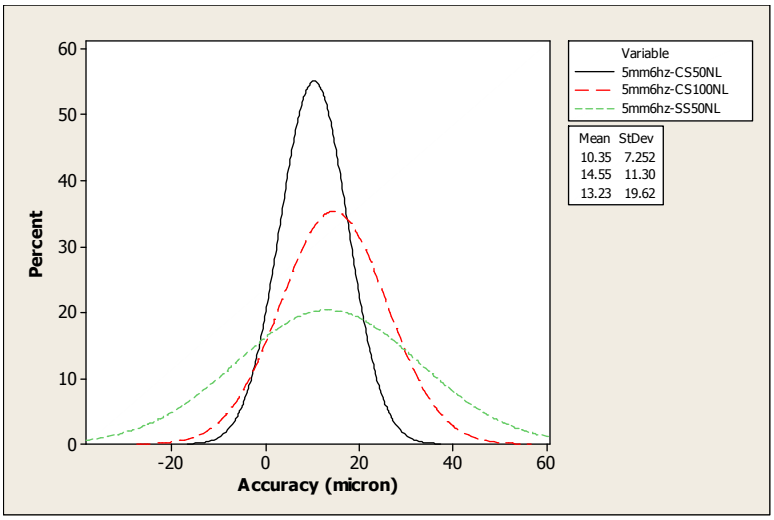
Variable
5mm6hz-CS50NL
5mm6hz-CS100NL
5mm6hz-SS50NL
Mean StDev
10.35 7.252
14.55 11.30
13.23 19.62
Percent
Accuracy (micron)

(d)

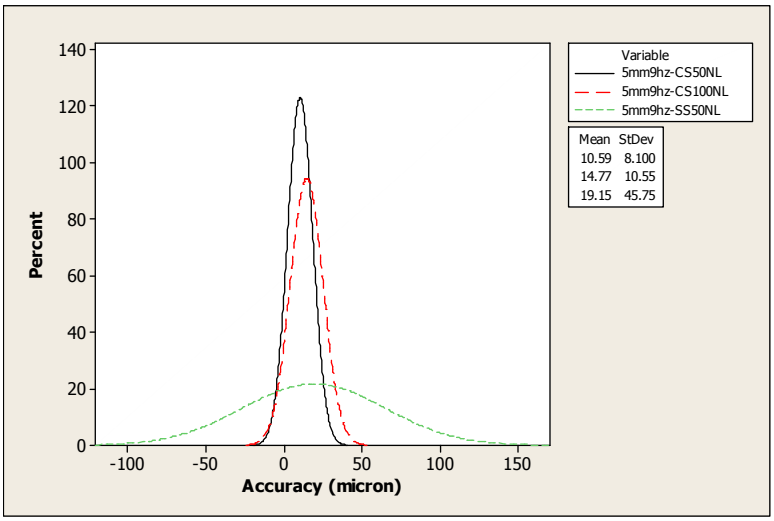
Variable
5mm9hz-CS50NL
5mm9hz-CS100NL
5mm9hz-SS50NL
Mean StDev
10.59 8.100
14.77 10.55
19.15 45.75
Percent
Accuracy (micron)

(e)

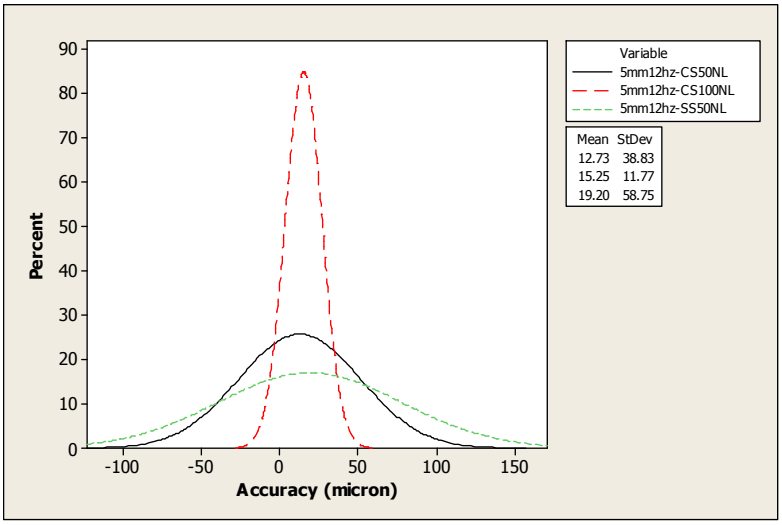
Variable
5mm12hz-CS50NL
5mm12hz-CS100NL
5mm12hz-SS50NL
Mean StDev
12.73 38.83
15.25 11.77
19.20 58.75
Percent
Accuracy (micron)

(f)

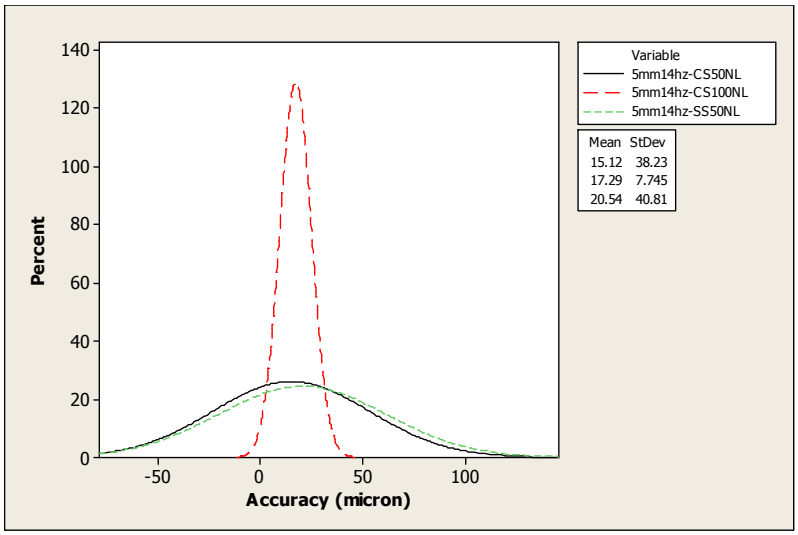

(g)

Fig. 5.16: Recorded positional accuracy for various materials in the non-lubrication case for all feed-frequencies and at 1mm feed distance: (a) to (g) represent feeding frequencies of 1-14Hz, respectively.

5.5.4 Effect of Changes of Strip Material on Positional Accuracy

a) 1mm feed-distance

Based on the experimental results for 1mm feed-distance, the change of strip material to stainless-steel strip with the same, 50µm, thickness did not secure any significant positional accuracy improvement, instead it led to greater inaccuracies and an inconsistent deviation-pattern. As shown in Fig. 5.15(a), 5.15(b) and 5.15(c), within the low feed-frequency category, the-mean positional accuracy for stainless-steel strip was inconsistently recorded between 7.9 and 9.1µm, with a deteriorate range of deviation of repeatability-performance at ±7.5 to 11.1µm. The feed-trend for stainless-steel for this frequency-category was observed to deteriorate even further compared to the deterioration for other materials. This is confirmed by the large deviation-value for each of the frequencies tested.

The intermediate feed-frequency results demonstrated an almost similar trend in mean-positional accuracy as for low feed-frequency, where the positional accuracy reduced to the range of 9.3 to 9.7µm (with a slight deterioration with the increase of feed-frequency) and the repeatability deteriorated to ±5.9µm at 6Hz and ±7.5µm at 9Hz feed-frequency. The large dispersion of the deviation for this material, as shown in Fig. 5.15(d) and 5.15(e), suggested that no consistent positional-repeatability is

achievable.

Change to high feed-frequency demonstrated no improvement of the mean-positional accuracy while at the same time resulting in increase of the dispersion in deviation. Fig. 5.15(f) and 5.15(g) show an almost similar mean-positional accuracy for both 12 and 14Hz feed-frequencies, of 10.4µm and ±10.5µm, respectively, and a large dispersion of within ±6.3 to 9.3µm. The deviation recorded for this material was seen to be little changed from the results for the intermediate feed-frequency category.

b) 5mm feed- distance

Based on the 5mm feed-distance experimental results, as shown in Fig. 5.16(a), 5.16(b) and 5.16(c), a consistent pattern of mean-positional accuracy and deviation-dispersion were observed. At low feed-frequency, the mean-positional accuracy was observed to deteriorate proportionally to the increase of feed-frequency from 1 to 3Hz. The mean-positional accuracy at 1-3Hz was recorded as the following: 10.3µm, 11.1µm and 12.7µm. At the same time the deviation-dispersion was ±15.4µm and ±19.0µm, for 1 and 2Hz feed-frequency, shown in Fig 5.16(a) and 5.16(b). A large reduction in dispersion of deterioration was observed at 3Hz feed frequency, where ±21.6µm repeatability was recorded for the tested frequency, with a mean-positional accuracy of 12.7µm. Overall, the mean-positional accuracy and repeatability for stainless-steel strip were slightly worse than for the 50µm-thick carbon-steel strip.

Fig. 5.16(d) and 5.16(e) demonstrate the results for stainless-steel strip when tested in the intermediate feed-frequency category (6 and 9Hz). A similar pattern of mean-positional accuracy and deviation as for carbon-steel strip were observed at this frequency. A reduction in mean-positional accuracy to 19.2µm was found when the greater feed-frequency of 9Hz was tested, compared to the value at 6Hz, which was 13.2µm: however, at this 9Hz frequency, a very large deviation-dispersion was recorded, which suggested that a high level of repeatability-inconsistency existed during the feeding process of stainless-steel strip. At 6Hz, the repeatability performance was ±19.6µm while at 9Hz the level reduced further to ±45.8µm, which was almost twice that the carbon-steel strip.

The mean-accuracies recorded for 12 and 14Hz in the high feed-frequency category were found to be quite close to each other, with recorded values of 19.2µm and 20.5µm. Both of these values were higher than the numbers observed for carbon-steel strip and suggested that at high feed-frequency, stainless-steel tends to have the worst mean-positional accuracy compared to that for the other materials. At 12Hz feed-frequency, the deviation for stainless-steel was found to be ±58.8µm, which is worse by almost 150% compared to the value a carbon-steel strip of similar thickness and five times worse if compared to thicker carbon-steel strip. At a greater feed-frequency of 14Hz, the deviation-dispersion was observed to decrease to ±40.8µm. Overall, the findings suggest that no repeatability is attainable for stainless-steel material, especially in the intermediate and high feed-frequency categories.

5.5.5 Pilot/Locating Pin-Application

In a high-precision conventional-forming feeding-system, variation in the position of the fed material caused by feeding error is one of the largest sources of error, hence reducing the quality and yield of products. The conventional approach to position the fed material accurately to secure good repeatability is to use a pilot-or locating-pin. The effectiveness of using a pilot pin in other field than forming, such as in the positioning of pallets in multi-station assembly systems, had been studied by Vallance et al., 2004.

According to Vallance et al., 2004, by using a pilot- or locating-pin, the repeatability of the positioning process is confirmed as being better than it is without the presence of a pin. Nevertheless, the experiments conducted have demonstrated that the conventional-approach techniques, which only use locating pins. is often limited by the clearances between dies/bushings and the pins themselves.

Although the locating-pins technique has demonstrated better positioning-precision at the macro-scale, the effectiveness of this technique in micro-scale positioning is still unclear. In order to test the effectiveness of using pilot-pins to improve positional-accuracy and repeatability, pins are installed. Based on the results of the experiments conducted on 50µm-thick carbon steel strip fed by a micro-servo roll-feeder, when pins were employed, mis-location still occurred. The thin-strip tends to

be deformed rather than to be allowed to be aligned properly, hence deteriorating the repeatability. This is depicted in Fig. 5.17.

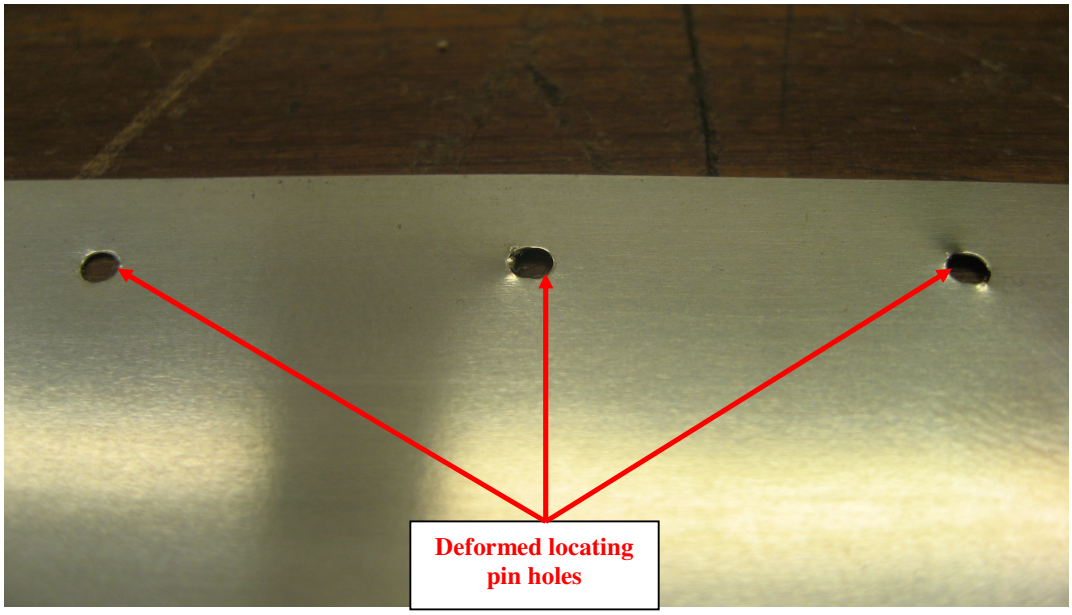

Fig. 5.17: Mis-location of feeding by using a micro-servo roll-feeder. It can be seen clearly that the pilot holes have suffered some deformation during positioned by locating pins.

A detailed examination with the assistance of a visual measuring-machine revealed that relatively 50-150μm of deformation is observed at the-pin holes during positioning-correction, as shown in Fig 5.18. A large deformation is believed to have been caused by positioning-error of the servo roll-feeder in the first place. Based on the experiments done using the servo roll-feeder, the positional accuracy level of the feeder itself shows good agreement with amount of deformation occurring on the fed strip. It may be conclude that pilot pin may be useful to correct feeding position when thicker and stiffer strip is used due to less deformation may be expected from this material.

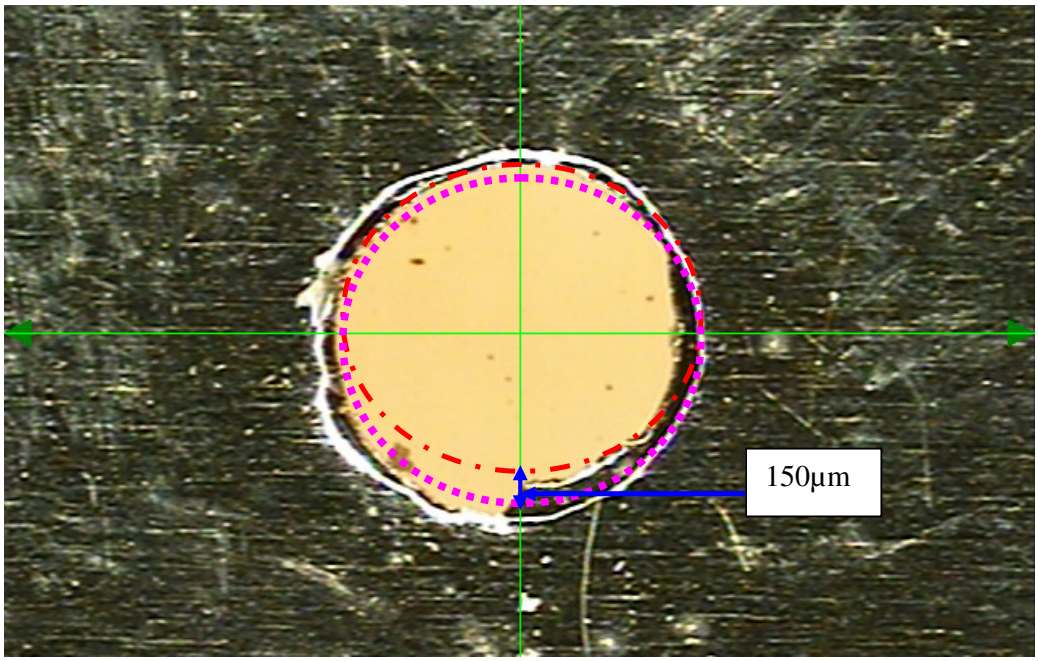

Fig. 5.18: A deformed locating-pin hole.

5.5.6 Optimized-Configuration Results

a) 1mm feed-distance

At 1Hz feed-frequency, as shown in Fig. 5.19(a), the positional accuracy for 50µm-thick carbon-steel was recorded at -3.8µm, with a large repeatability of ±6.2µm. The application of brake-force to the system led to slight deterioration of the mean-positional accuracy, which settled at -4.2µm, but at the same time it improves the positional-repeatability to ±3.2µm. This finding also suggests that brake-force tends to promote a pattern of slight underfeed due to the pulling-force generated and the poor compensation of feeding-force. The Optimized motion also confirms that thicker carbon-steel strip may be positioned more accurate than thinner strip. This is further confirmed by the achieved mean-positional accuracy of -3.1µm, and the surprising repeatability of ±2.7µm, compared to the values recorded for other tests. Change to different material type, which in this case is stainless-steel, demonstrated an almost similar mean positional accuracy to that for carbon-steel strip, a value of -3.7µm being recorded. Nevertheless, better repeatability was observed for stainless-steel, which settled at ±3.8µm.

As depicted in Fig. 5.19(b), changes of the feed-frequency to 2Hz resulted in greater feed-inconsistency for 50µm-thick carbon-steel strip. The mean positional accuracy

for 50µm-thick carbon-steel was found to be -4.8µm with a reduced deviation or repeatability of ±12.0µm. The application of brake-force resulted in good agreement with the findings for the 1Hz feed-frequency tests, where it was established that brake-force can be used to control and improve deviation-dispersion, to secure better and more consistent positional-repeatability. The presence of brake-force caused the deviation to reduce to ±3.1µm. Change to thicker carbon-steel material resulted in a slight reduction of mean positional accuracy, compared to when using 1Hz feed-frequency. The mean-positional accuracy was recorded as -3.6µm, which is 0.6µm above the value for the previously-tested low feed-frequency experiment. Slightly reduced deviation was observed also at 2Hz for thicker carbon-steel strip, where, a difference of 0.5µm from the 1Hz result has caused the repeatability to settle at ±3.2µm. For stainless-steel, an almost similar performance as for 1Hz was observed for 2Hz feed-frequency. The mean-positional accuracy and repeatability were -3.6µm and ±3.8µm, respectively. This finding suggests that stainless-steel was the least accurately-positioned material during the feeding process, compared to the positioning of the other materials.

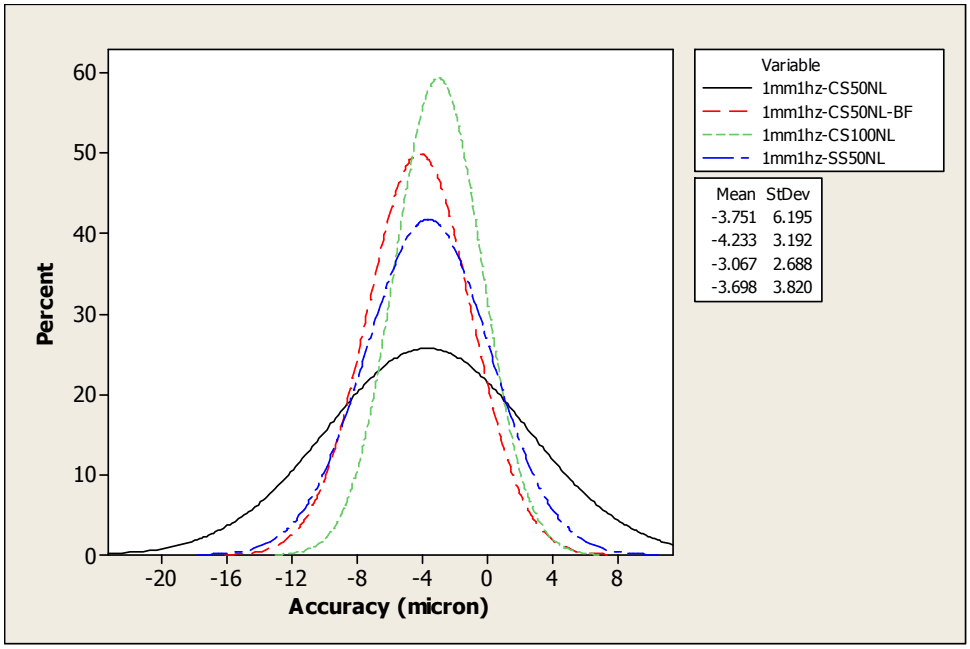

(a)

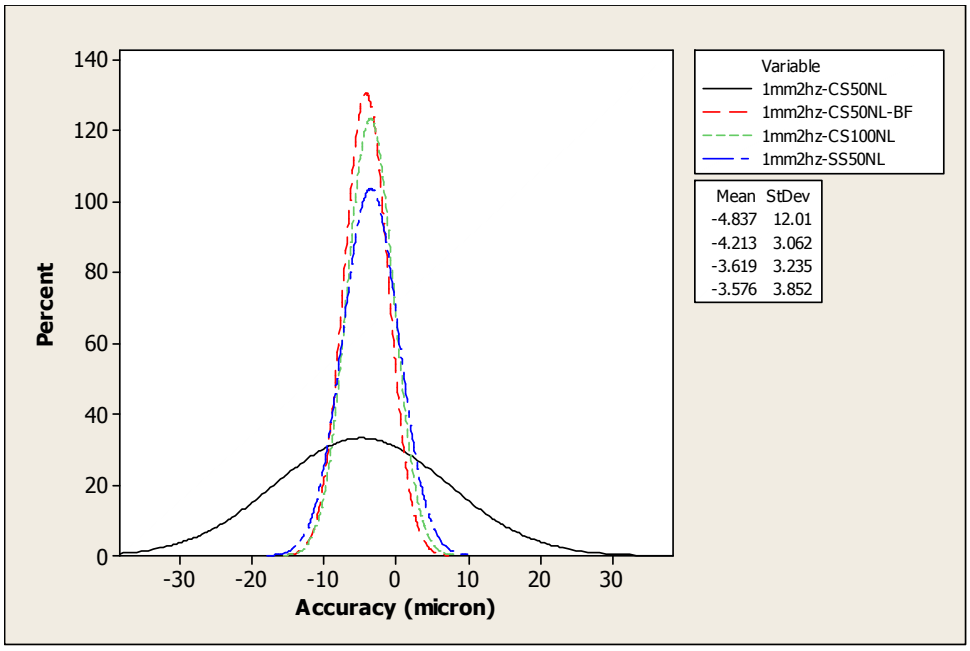

(b)

Fig. 5.19: Feeder performance at 1mm feed-distance for all tested strip-types and thicknesses: (a) 1Hz; and (b) 2Hz.

b) 5mm feed-distance

As depicted in Fig. 5.20(a), at 1Hz feed-frequency, the mean-positional accuracy for 50µm-thick carbon-steel was -1.9µm, with a deviation-dispersion of ±5.3µm. Although the mean-positional accuracy was better than the shorter-feed result, the, deviation recorded was slightly worse than for the shorter feed. This demonstrated a lack of feed-repeatability for longer feed-distance. However, the results of applying brake-force showed good agreement between longer and shorter feed-distances. The application of brake force is seen capable of improving the mean-positional accuracy of the feed to 0.5µm and at the same time reducing the deviation-dispersion, hence a better repeatability of ±4.8µm was recorded. Changing to thicker carbon-steel strip led to a significant reduction of mean-positional accuracy to 9.1µm. Nevertheless, a smaller deviation-dispersion was observed for this material, thus a better repeatability of ±4.5µm was achieved. The lowest mean-positional accuracy of 0.3µm was observed for stainless-steel material. However, the least concentration of repeatability was observed, as the bell-shaped curve for stainless steel was dispersed widely throughout the feed process. The process-repeatability capability was ±11.0µm, which, significantly, suggests that no consistent repeatability may be expected from the fed material.

Change of feed-frequency to 2Hz generally led to deterioration of the mean-positional accuracy and repeatability for all tests, as demonstrated in Fig. 5.20(b). The feed-pattern also demonstrated lack of repeatability-consistency and was reduced to a greater extent than was found at lower feed-frequency. For 50µm-thick carbon-steel strip, the feed-performance was reduced by almost twice as much compared to 1Hz feed-frequency, with a mean-positional accuracy of -3.1µm, however, the process-deviation was similar, at ±5.0µm. The application of brake-force to the system secured a slight improvement in the achieved positional accuracy for the strip. The mean positional accuracy in the brake-force tests was 0.8µm, slightly less compared to that was obtained at 1Hz feed-frequency. Brake force is therefore confirmed as making a significant contribution towards improving the mean-positional accuracy and reducing the deviation-dispersion, thus resulting in better repeatability. Up to ±5.1µm deviation or process-repeatability capability was recorded when brake force was applied. The mean-positional accuracy of the thicker carbon-steel strips was observed to be improved at 6.1µm, when compared to the 1Hz low feed-frequency test results. Nevertheless, at this mean-positional accuracy, the feeder was found unable to maintain the process-deviation at smaller values. Around ±6.6µm repeatability was recorded for the thick strip, which was slightly greater than for the thinner carbon-steel strip. An underfeed pattern was observed for stainless-steel strip fed at 2Hz feed-frequency with a recorded mean-positional accuracy of -0.2µm and a repeatability of ±7.9µm. This large dispersion, above all, confirmed the findings for previous tests, where the lack of repeatability-consistency was observed specifically when dealing with the least-stiff material, stainless-steel.

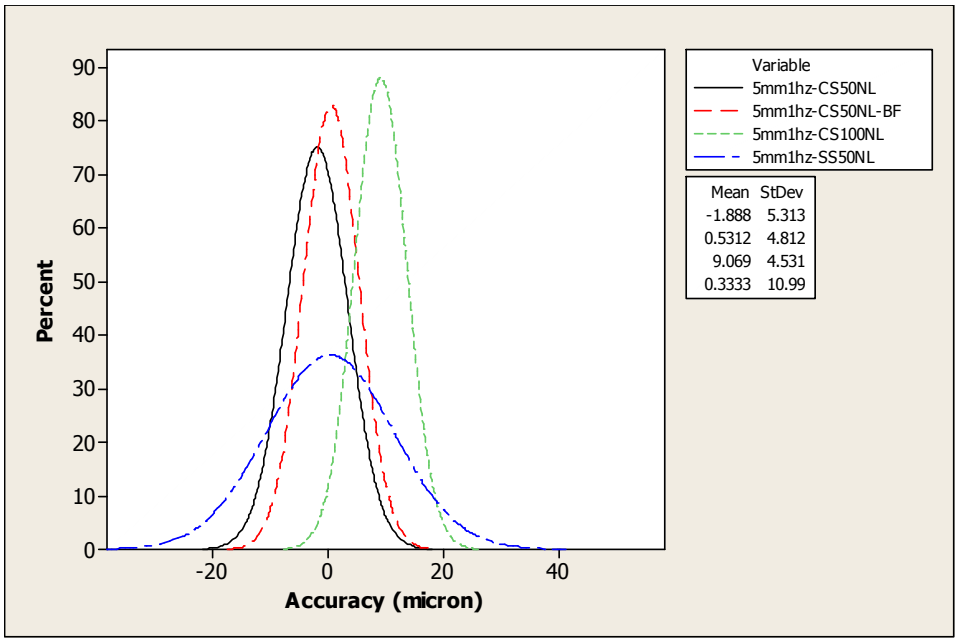

(a)

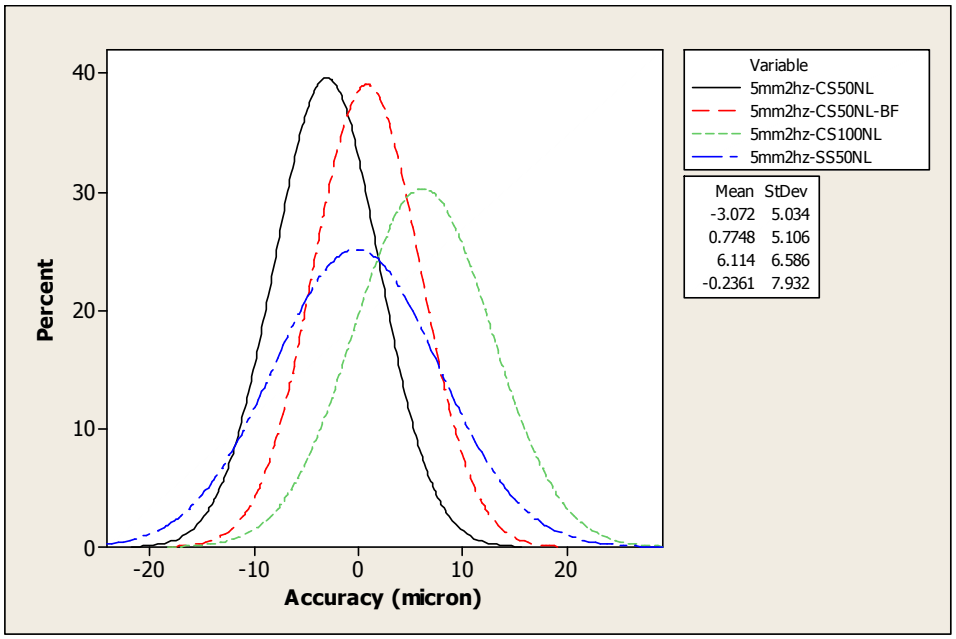

(b)

Fig. 5.20: Feeder performance at 5mm feed-distance for all tested strip-types and thicknesses: (a) 1Hz; and (b) 2Hz.

5.5.7 Air Gripper-Feeder Results

Due to inflexibility in changing the feed-distance of the pneumatic gripper-feeder, only a 5mm feed-distance was tested. At this feed distance, the feed-frequency varied from 1 to 2Hz for the different materials and thicknesses. 50µm-thick carbon-steel strip was fed with a better positional accuracy-consistency at 2Hz feed-frequency,

compared to what was found for 1Hz, as depicted in Fig. 5.21(a). At 2Hz feed-frequency, the mean-positional accuracy was 32.1µm, whilst the process-repeatability lay within the range of ±40.0µm. At 1Hz, positional accuracy-range was observed at 36.5µm with, most of the time, the feeder being able to feed to within ±41.0µm repeatability.

Change to 100µm-thick carbon-steel strip secured an improvement in positional accuracy, where at 1Hz feed-frequency, the mean-positional accuracy was 28.2µm, as shown in Fig. 5.21(b). The positional accuracy at 2Hz feed-frequency was 20.7µm and, most of the time, it was better than for the 1Hz feed-frequency. Both the 1 and 2Hz frequencies showed better repeatability, compared with the thinner carbon-steel strip. Due to its high stiffness, 100µm carbon-steel strip was observed to have a smaller deviation-dispersion which, in turn, led to better positional-repeatability. Although better mean-positional accuracy was recorded for 2Hz, the 1Hz repeatability of ±4.0µm was noted to be much better than the value for 2Hz, which latter was ±7.6µm,

The mean-positional accuracy and repeatability of stainless-steel strip at 1Hz were 40.7µm and ±89.7µm, respectively, while at 2Hz the mean-positional accuracy and repeatability were 31.3µm and ±120.8µm, respectively, as shown in Fig. 5.21(c). This result provides good agreement with the previous test results, where the positioning of the lesser-stiffness material seems worse than for the stiffer material. Based on the previous tests result on 50µm and 100µm thickness carbon-steel strips, 100µm-thick carbon-steel strip tends to be fed with better positional accuracy and repeatability, if compared to the thinner 50µm carbon-steel and 50µm stainless-steel strip. This suggested that the positional accuracy also depends on the material stiffness.

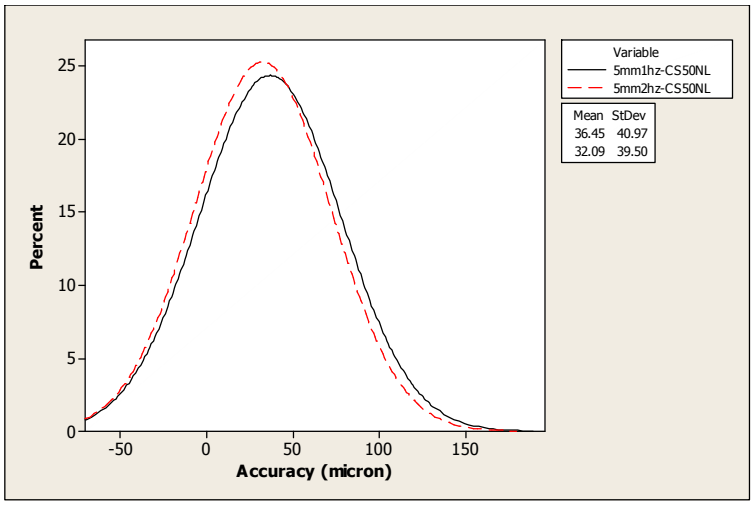

(a)

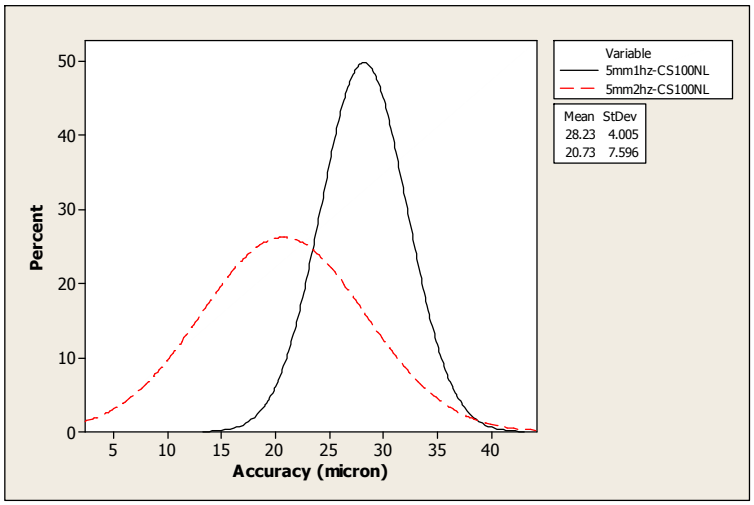

(b)

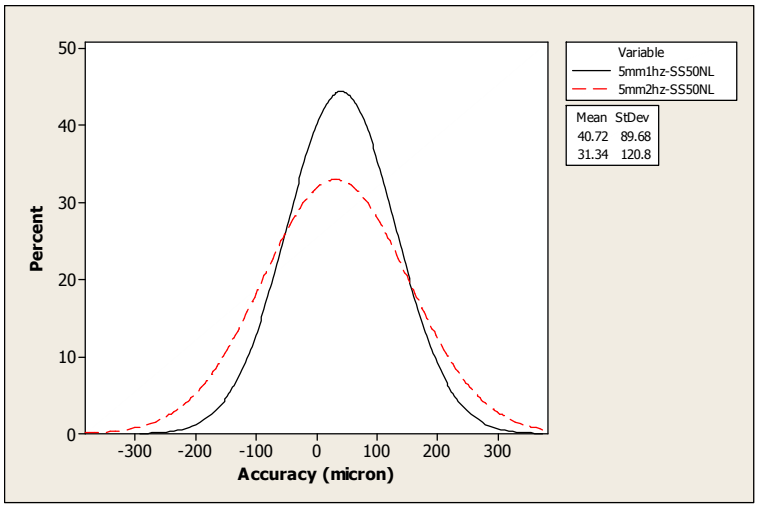

(c)

Fig. 5.21: Air-feeder performance at various feed frequencies for all materials: (a) CS50; (b) CS100; and (c) SS50.

5.6 Discussion

There are several factors which contribute to the feeder performance, specifically in delivering high-positional accuracy and repeatability. Encoder errors, mechanical-transmission errors and mechanical properties of the feed material, have been seen to have an influence on the positional accuracy. These factors are discussed in detail below.

5.6.1 Encoder Errors

A source of great positional inaccuracy is encoder errors [Du et al., 1998]. Encoder non-linearity error and spindle-speed fluctuation are the main contributors towards these inaccuracies, specifically with rotary encoders. According to Lu et al., 2007, when a spindle angle was measured using a rotary encoder, a non-linear error is introduced due to manufacturing-error and misalignment in installation of the encoder, hence, consistent positional accuracy in measurement and repeatability is impossible.

Experiment on a 10000counts/revolution encoder was conducted by Lu et al., 2007 which encoder had the similar specification to that of the encoder used in the micro-servo roll-feeder under examination. The result demonstrated that the maximum error of the encoder was 0.43counts. According to the authors, the source of error was mainly eccentricity and disk-graduation non-uniformity, as well as photo-detector mis-alignment and the threshold of the detection circuit.

5.6.2 Mechanical-Transmission Errors

Another source of great positional inaccuracy and non-repeatability in every experiment conducted is transmission errors. Manin et al., 2007, studied the use of a drive-belt for transmission and find that each portion or segment of the drive-belt does not have a similar longitudinal rigidity and damping value (non-uniform belt-characteristics). According to the authors, the elongation of each section is not similar, where a non-negligible variation is observed for the entire samples tested (i.e. some sections yield more than other sections). The authors concluded that this irregularity is probably due to the manufacturing process (printing, cord-winding, cutting), and generates transmission-error fluctuations. This can be seen clearly, as

illustrated in Fig. 5.22, where the two sides of the belts have a different composition; one side showed a composite line, and while on the other side is was concealed.

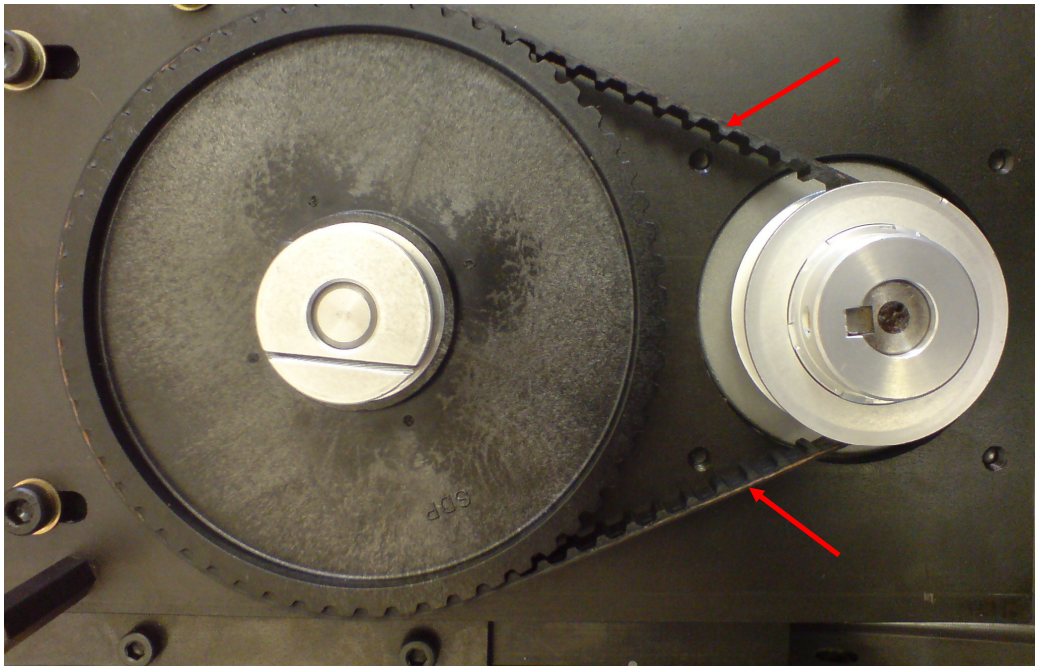

Fig. 5.22:The red arrows show irregularities on the servo roll-feeder drive-belt. A clear difference in belt composition can be seen between A and B.

In addition to such irregularities, according to Manin et al., 2007, slip might occur from the driver- and driven-pulley during power transmission. Although an idler and a belt-tensioner are used to reduce the slip rate, in high-precision motion, this slip rate makes a large contribution towards inaccuracies. This case is demonstrated in Fig. 5.23.

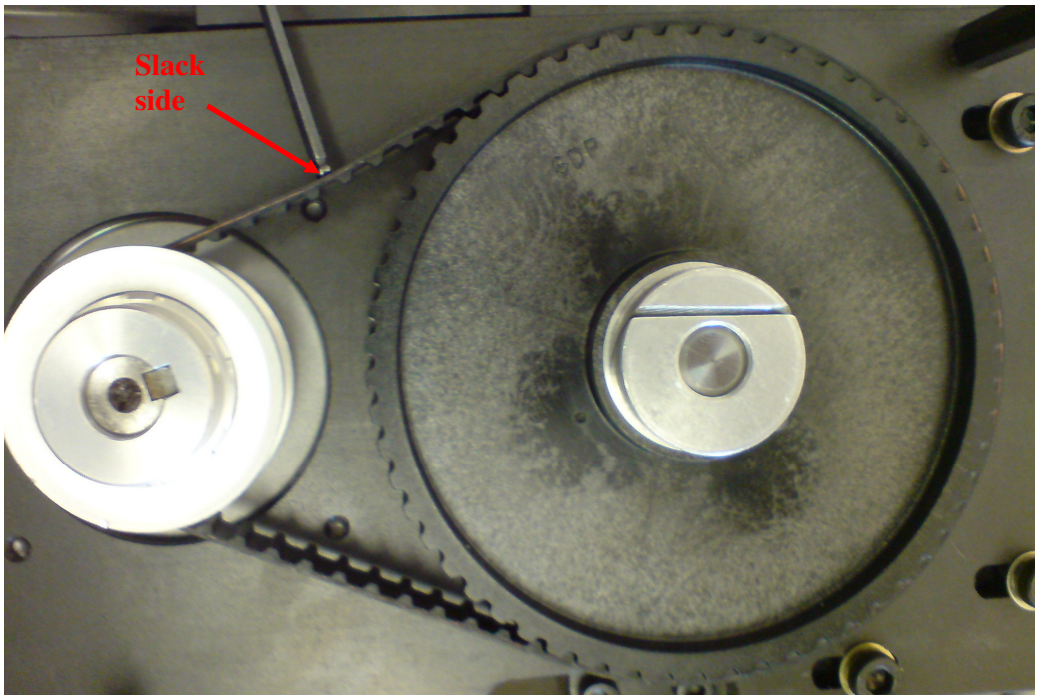

Fig. 5.23: The slack side of the belt and pulley mechanism, which also contributes to positional inaccuracies.

According to Ayax et al. 2003, when the belt is set up on a pulley with clearance, reverse bending is observed between the pulley's groove and the teeth, hence creating a so-called polygonal effect, which generates a transmission error that may cause vibrations and thus alter the behavior of the belt during power transmission, hence promoting inaccuracies under loading conditions. This is shown in Fig. 5.24. This effect is very significant in high-precision motion where, apart from irregularities in belt composition, this phenomenon affects the positional accuracy and positional-fluctuations.

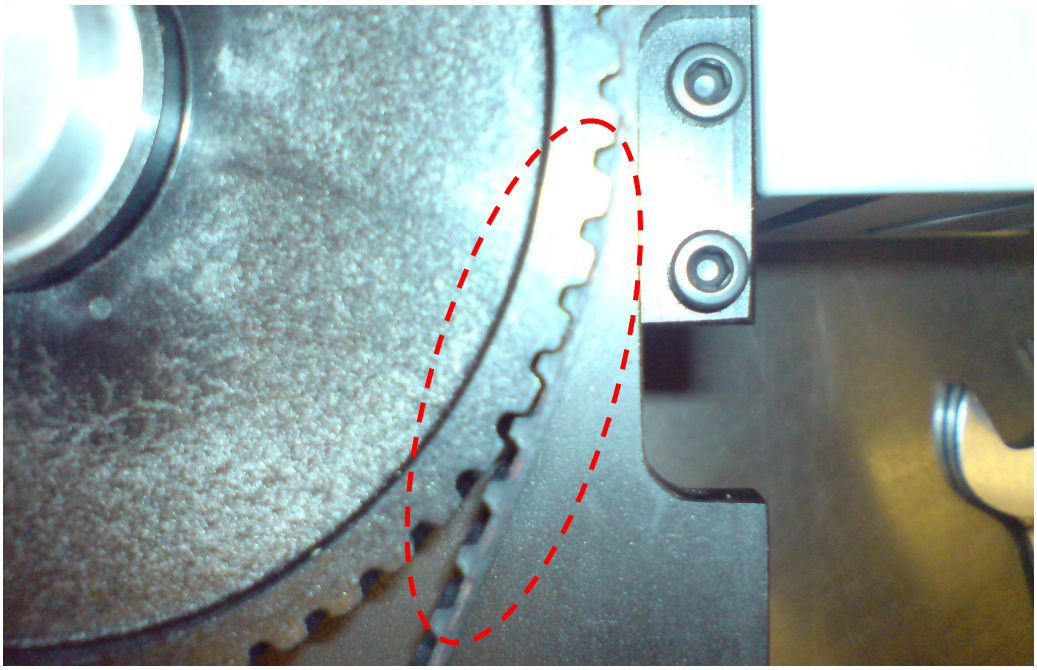

Fig. 5.24: Clearance between the pulley's teeth and the belt's grooves, whichdoes contributes to positional inaccuracies.

5.6.3 Metal–Strip Stiffness

From the results of the experiments, the material stiffness is found to affect the positional accuracy. Stiffer material has a better positional accuracy compared to less-stiff material. A better and shorter settling-time for both 1mm and 5mm feed-distance with a stiffer material provides improved positional-accuracy of the material. This phenomenon is demonstrated in Fig. 5.25. As shown in this figure, carbon-steel strip of 100µm thickness (the stiffest material among the materials tested) has the best settling time, hence the positional accuracy is the best. 50µm carbon-steel strip has a moderate stiffness. A large positional-overshoot was identified with the least-stiff material (50µm-thick strips) for both distances, which resulted in greater positional inaccuracy compared to that for the 100µm-thick strips, which is shown in both Fig. 5.25 and 5.26, particularly for a longer feed-distance and a greater frequency.

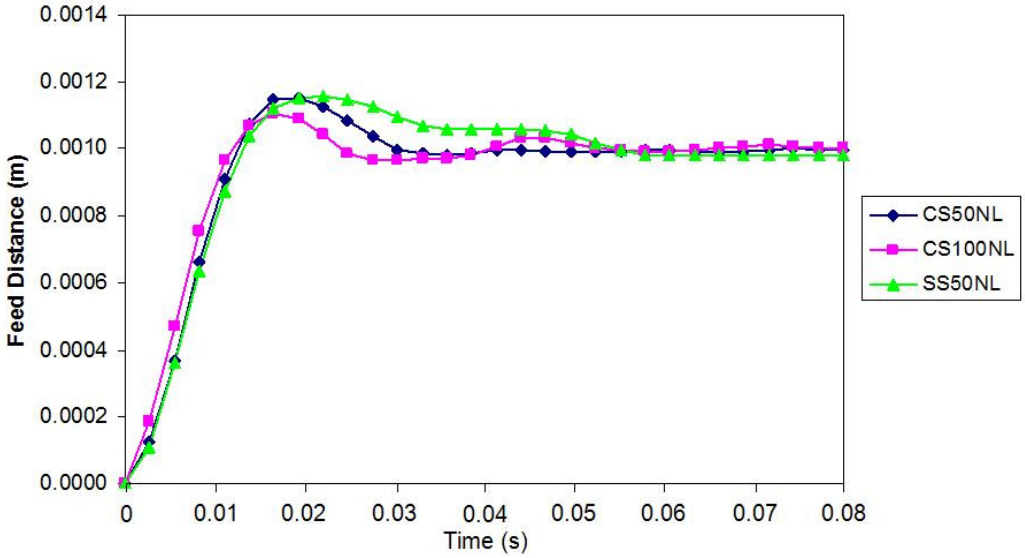

(a)

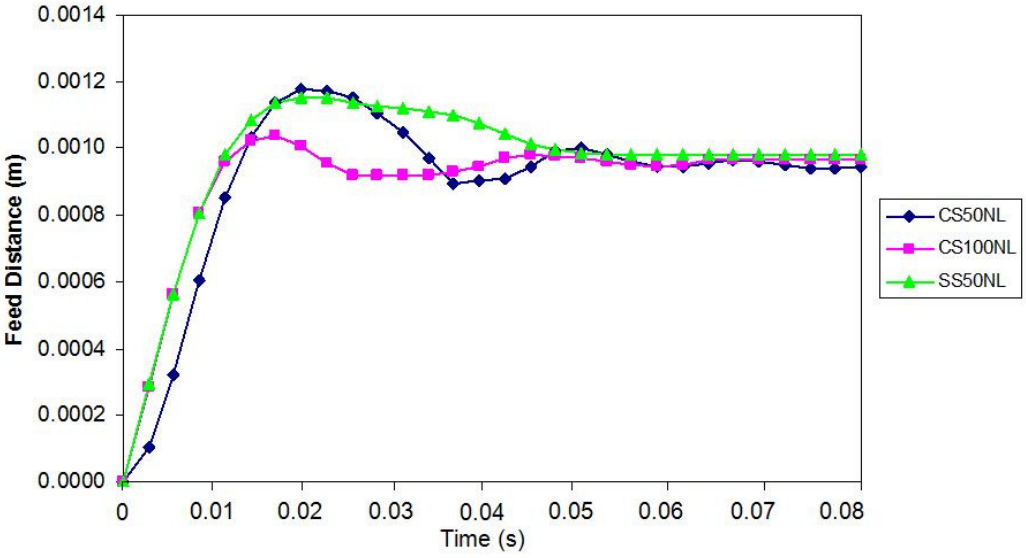

(b)

Fig. 5.25: Overshoot and settling-time at 1mm feed-distance for the non-lubricated case: (a) 1Hz; and (b) 2Hz feeding frequency.

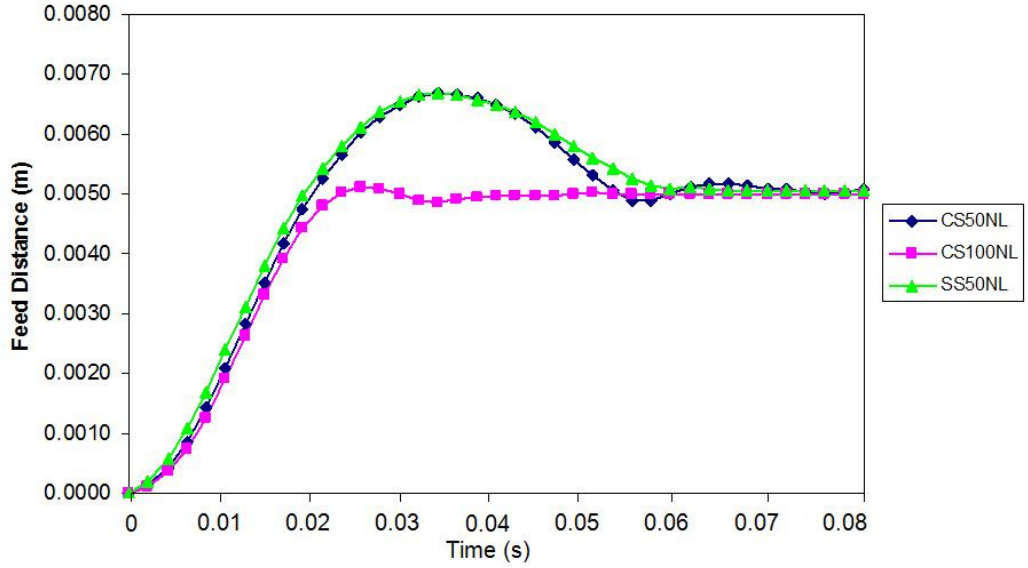

(a)

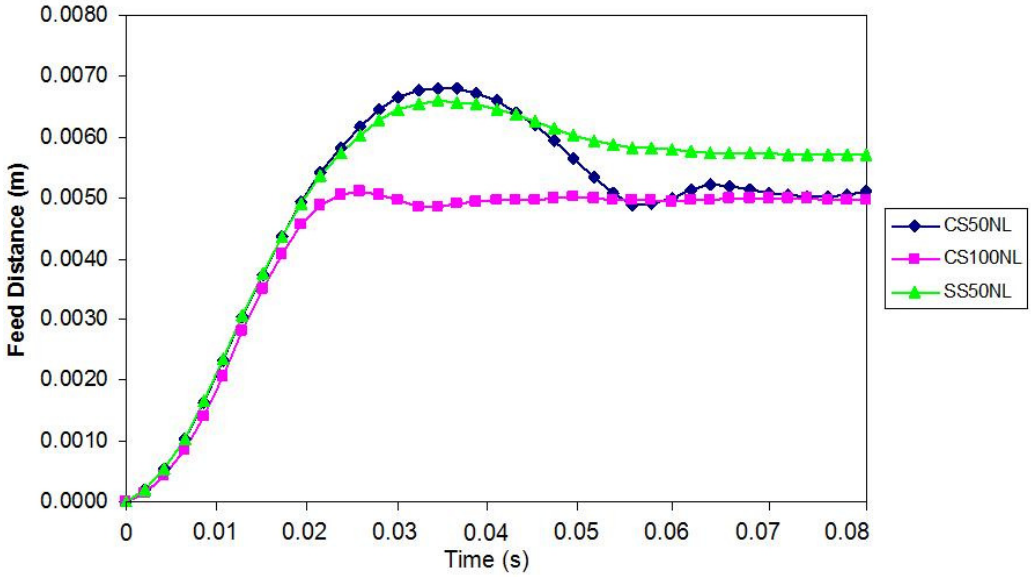

(b)

Fig. 5.26: Comparison of settling time for the tested materials at 5mm feed-distance: (a) 1Hz feeding-frequency; and (b) 2Hz feeding-frequency.

5.6.4 Discussions of Pneumatic Gripper-Feeder Performance

The nature of the pneumatic gripper-feeder, as depicted in Fig. 5.27, when feeding, requires some sort of dead-stop mechanism to stop the fast-moving and high-momentum gripper-block. This dead-stop mechanism is realized by positioning a fixed block immediately rewards of the movable gripper. The movable block/gripper,

as shown in Fig. 5.28, comes to stop suddenly when it hits the fixed block and this, in turn, over a certain time causes a slight dislocation of the fixed block. In addition, not only on the fixed block, dislocation also occurs on the movable block, this being clearly shown in Fig. 5.29(a) and Fig. 5.29(b). The distance between the two represents the travel distance, hence the positional accuracy and repeatability are likely to be affected. Thus, inconsistency of feeding-distance is expected by increased number of feeds. Manual adjustment has to be made in order to set the distance back to the designated distance this certainly affecting the repeatability of the feeding process.

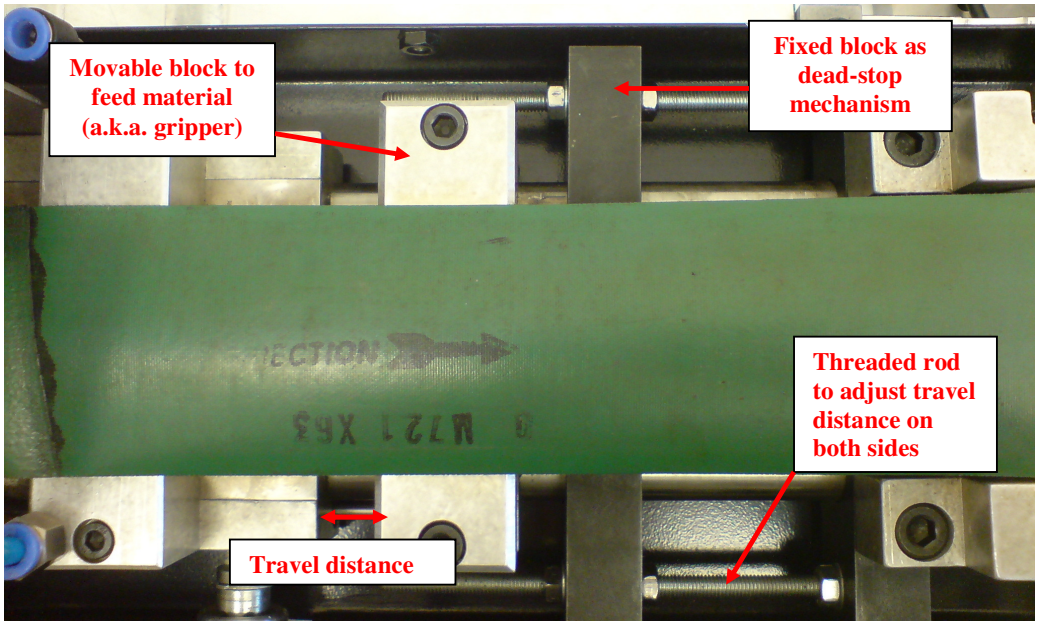

Fig. 5.27: Position of the movable/gripper and the fixed block of the pneumatic gripper-feeder.

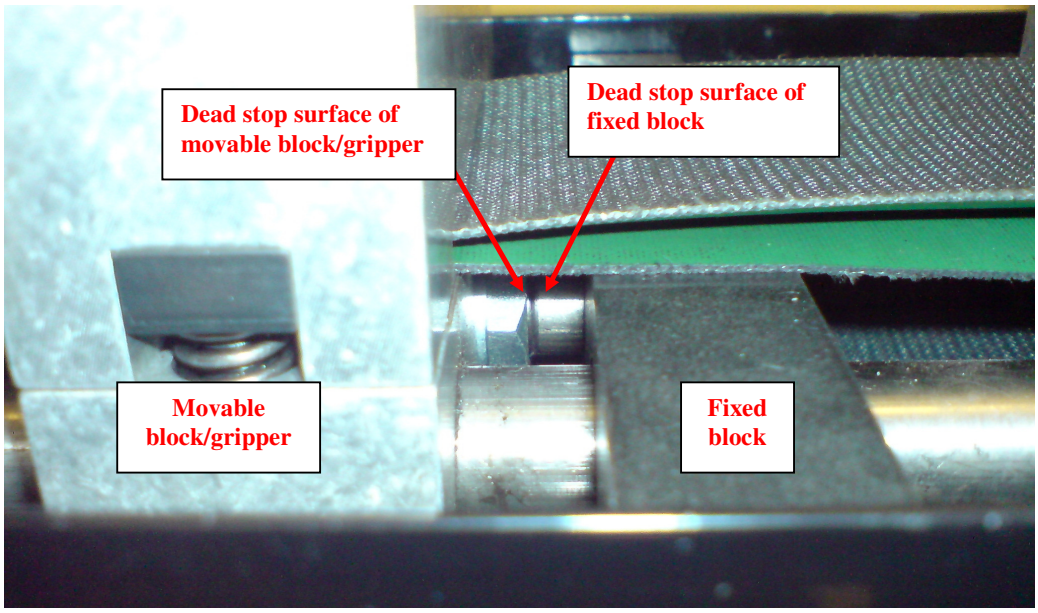

Fig. 5.28: The movable block hits the fixed block during feeding and gradually dislocates the fixed block.

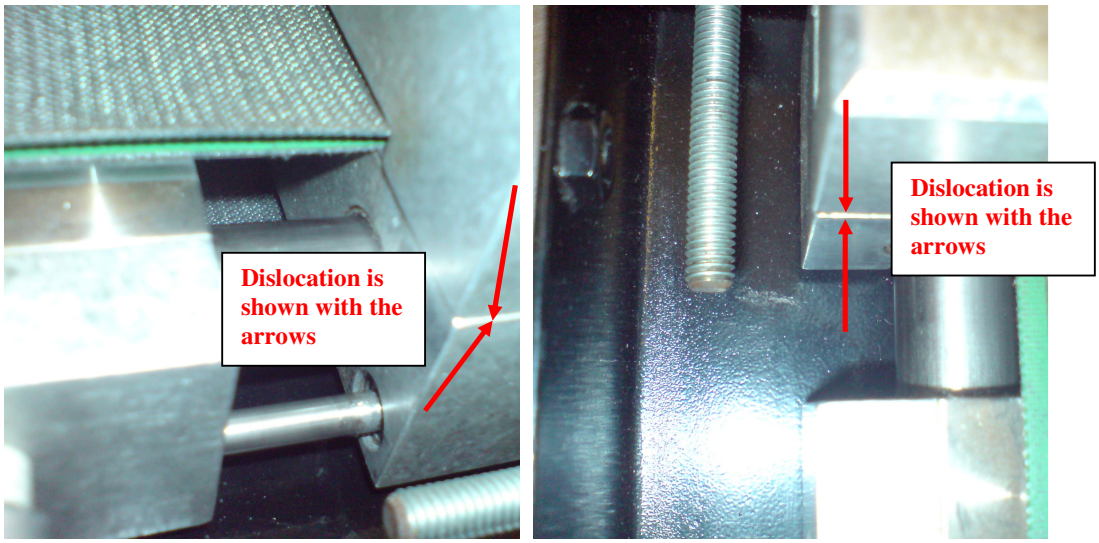

(a) (b)

Fig. 5.29: Dislocation on both the right (a) and the left (b) of the movable block/gripper after several times of feeding.

Due to stop-mechanism being a solid dead-stop device, the change from the acceleration to deceleration phase is very sudden, hence, promoting a very high 'jerk' rate (sudden change of the acceleration to the deceleration phase and vice versa). The high-speed strip is brought to a sudden stop, causing a high inertial

dissipation. This in turn develops a high inertial force to be exerted on the strip and may be identified as one of the main sources of strip-buckling during feeding, hence reducing positional accuracy.

5.7 Conclusions

Based on the results of all of the experiment, the following conclusions may be drawn:

a) The positional accuracy deteriorates proportionally to the increase of feed-distance and feed-frequency, for both feeders.
b) No consistent repeatability is found for the entire range of feed distances and frequencies (speed) for both feeders.
c) Lubrication slightly improves positional accuracy, but its presence does not help significantly in improving repeatability.
d) The positioning accuracy of stiffer material is better compared to that of less-stiff material, for low feed-distance. The least stiff material was found to have the least positional-accuracy and repeatability.
e) A great source of errors makes the servo roll-feeder impossible for use as high-precision feeder for micro-sheet-forming applications.
f) The inflexibility and large errors of the air gripper feeder make the feeder impossible for use in micro-sheet-forming application.
g) Motion 'jerk' or a sudden change of the acceleration-deceleration phase (speed), reduces the positional accuracy. The greater the 'jerk', the greater is the positional-inaccuracy.

High-precision, high-speed strip feeding in micro-forming

(Volume II)

Akhtar Razul Razali

Glasgow, June 2010

High-precision, high-speed strip feeding in micro-forming

Akhtar Razul Razali

This thesis is submitted to the Department of

Design, Manufacture and Engineering Management,

University of Strathclyde

For the degree of Doctor of Philosophy

Glasgow, June 2010

'This thesis is the result of the author's original research. It has been composed by the author and has not been previously submitted for examination which has led to the award of a degree.'

Signed : 

Date : 1st July 2010

Dedication:

The author wishes to dedicate the thesis to his mother, father, his wife, son and daughter without whose support and sacrifice, the thesis would have not been completed.

Acknowledgement

The work reported herein was carried out at the Department of Design, Manufacture & Engineering Management, University of Strathclyde, through full time study funded by the Government of Malaysia through Ministry of Higher Education (MOHE). Permission to register for a PhD degree and financial support provided by the university is gratefully acknowledged.

The author wishes to express his gratitude to Prof. Dr. Yi Qin for his phenomenal supervision of the research, constant support and meticulous checking of the manuscript.

The author would like to thank the colleagues of High-precision Manufacturing Engineering Research Group for their encouragement and constant support. The advice offered by the colleagues is particularly acknowledged.

The author is grateful to Mr. Robert Hay, Mr. Barrie Hunter and Mr. Duncan Lindsay for their assistance in the laboratories. The production of all tools, electronic circuits and electrical connections in the department workshop was of the highest quality for which the author is grateful.

Abstract of the Thesis

A high-precision and high-speed feeder was designed and developed with a view to establishing the greater-precision and accuracy of a handling device for micro-sheet-forming applications. Two types of popular commercial feeder for thin-sheet were tested to quantify their performance in terms of accuracy and repeatability, namely a micro-servo roll-feeder and a pneumatic gripper-feeder, tested using three different strips: carbon steel of 50 to 100microns thickness; and stainless steel of 50microns thickness. A non-contact approach was used to determine the feeders' performance. Several different combinations of the feeding parameters were explored, such as: the employment of various feed distances and feed frequencies; the effect of lubrication; and motion-profile optimization. FE simulations were used to study the feeding characteristic of the feeders. Based on the findings, both of the feeders were found to be unsuitable for micro-sheet-forming application due to their high rate of inaccuracy and their lesser repeatability-capability dealing with very thin sheet. Both empirical results and FE-simulation results show good agreement with the observed feeder-performance.

The research has identified a servo linear-motor gripper-feeder as being suitable for use in micro-sheet-forming applications. This new feeder-concept enables a significant improvement in handling accuracy and repeatability when dealing with very thin sheet. Supported by the results of FE simulations, both empirical and simulation results show good agreement on the feeder performance. In the initial tests, better repeatability was achieved. The success of the initial tests led to an optimization process being conducted to increase the potential for achieving better accuracy, which was designed to be at 5-15% of the strip thickness. The optimization method consists in determining the actual payload acting on the system, the adjustment of the control feedback and the adjustment of the motion-profile curve. The optimization method proved successful, the designated accuracy and greater repeatability being achieved for all of the strips tested, employing a similar test set-up to that when using a roll feeder.

The research continued to develop a finished-part transporting mechanism to transport the finished parts/products by using a pocketed carrier-tape. This transportation concept has proven to be successful in transporting the finished parts/products away from the micro-sheet-forming machine. Both the new feeder-system and new transportation-system were finally integrated with the micro-sheet-forming machine to enable synchronization of operation.

List of Publish Papers

(1) Razali, A., Qin, Y., Harrison, C. and Brockett, A. (2009) 'Investigation of feeding devices and development of design considerations for a new feeder for micro-sheet-forming', *Int. J. Nanomanufacturing*, Vol. 3, No. 1/2, 40-54. (Part of Chapter 6)

(2) Razali, A., Qin, Y., Harrison, C., Zhou, J. and Brockett, A. (2009) 'Non-optimized performance of newly developed linear motor gripper feeder for micro-sheet-forming application' *International Conference on Manufacturing Research (ICMR 2009),* 24-30. (Part of Chapter 8)

(3) Razali, A., Qin, Y., Harrison, C. and Brockett, A. (2008) 'Investigation of feeding devices and development of design considerations for a new feeder for micro-sheet-forming', *International Conference on Manufacturing Research (ICMR 2008),* Vol. 1, 493-504. (Part of Chapter 6)

(4) Razali, A.R., (2008) 'Review, issues and gap in micro-forming development' *Innovative Production Machines and Systems Proceedings, 4th I*PROMS Virtual International Conference,* 276-282. (Part of Chapter 2)

(5) Razali, A.R., Razak, A., & Zahid, M.N.O., (2008) 'Issues and Gap In Micro-Forming Development' *2nd International Conference of Science & Technology (ICSTIE 2008): Applications in Industry and Education.* (Part of Chapter 2)

(6) Razali, A.R., Razak, A., & Zahid, M.N.O., (2008) 'Fabrication and Integration Issues on Custom-Build and Commercial Ironless Linear Motor Stage' Development' *2nd International Conference of Science & Technology (ICSTIE 2008): Applications in Industry and Education.* (Part of Chapter 6)

(7) Razali, A.R., Razak, A., & Zahid, M.N.O., (2008) 'Review And Issues In High-Precision Material Handling Development For Micro-Forming Application' Development' *2nd International Conference of Science & Technology (ICSTIE 2008): Applications in Industry and Education.* (Part of Chapter 2)

(8) Razali, A.R., Razak, A., & Zahid, M.N.O., (2008) 'The Effect of Motion Profile Changes On Linear Motor Stage Sizing Development' *2nd International Conference of Science & Technology (ICSTIE 2008): Applications in Industry and Education.* (Part of Chapter 6)

(9) Razali, A. & Qin, Y., (2010) 'FE Simulation of Sheet-Metal Feeding in Micro-Forming', CAPE 2010 Edinburgh. **(Full paper accepted)** (Part of Chapter 4 and 7)

(10) Micro-sheet-forming and case studies, Metal Forming 2010 **(Abstract accepted)** (Part of Chapter 8)

Contents

Nomenclature

u = initial velocity (m/s)

v = final velocity (m/s)

s = distance (m)

a = acceleration (m/s^2)

t = time (s)

f_p = payload force (N)

f_a = acceleration force (N)

f_g = gravitational force due to inclined plane (N)

f_f = frictional force (N)

f_e = cable-management force (N)

m = mass (kg)

ρ = density (kg/m^3 or g/cm^3)

V = volume (m^3 or cm^3)

μ = coefficient of friction

τ = torque is in N.m

f = force (N)

r = radius (m or mm)

I = inertia ($kg.m^2$)

α = rotational acceleration (rad/s^2)

ω = rotational velocity (rad/s)

h = height (m)

F_{peak} = total peak-force (N)

F_{rms} = total root-mean-square force (N)

R_T = thermal resistance (W/°C)

M_C = motor constant (N/√W)

T = temperature (°C)

BEMF = back electro-motive force (V/m/s)

Exp = expansion

ΔT = change of temperature (°C)

w_t = total weight (kg or gram)

I(amp) = current (A)

w = width (m or mm)

l = length (m or mm)

Subscripts

brake = denotes brake

rms = denotes root-mean-square

reel = denotes reel

coil = denotes coil

composite = denotes composite

outer = denotes outer dimension

inner = denotes inner dimension

cycle = denotes cycle

min = minimum

thermal = denotes thermal

total = denotes total

motor = denotes the motor

2hz = denotes as 2Hz frequency

brakerms = denotes brake rms value

MEMS – denotes microelectromechanical system

nobf – denotes no brake force

BF – denotes brake force

PZT – denotes piezoelectric transducer

N/S – denotes not specified

N/A – denotes not available

Chapter 6

Concept Development of a New Feeder

6.1 Summary

A recent review of micro-forming research and technological development suggested that the trend of the development is focused more on the manufacturing processes, machines and tooling, with efforts on precision material-handling being insufficient. Most of the machines that have been developed were based on stand-alone concepts that do not support efficient integration to make them fully automated and integrated. Material feeding, in most cases, was not of sufficient precision and reliability for high-throughput manufacturing applications. Precision feeding is necessary to ensure that micro-parts can be produced with sufficient accuracy, especially in multi-stage forming, while high-speed feeding is a necessity to meet industrial production-rate requirements. Therefore, the design of a new high-precision and high-speed feeder for micro-forming is proposed. Several possible approaches are examined with a view to establishing feasible concepts. Based on the investigation, several concepts for thin sheet-metal feeding for micro-forming have been generated, these being argued and assessed with appropriate applied-loads and force-analysis. These form a basis for the designing of a new feeder.

6.2 Introduction

Conventional press-feeders have to meet three main criteria to be successful. Firstly, the feeder must be flexible in terms of set-up. Secondly, the delivery of material must be of sufficient precision to satisfy the requirements for forming. Thirdly, the feeders must also ensure feeding at the correct time. All of these criteria are particularly difficult to meet when forming thin sheet-metals, such as those where the thickness is less than 100µm, where the feeding-distance is greater than 10mm and where the feeding-rate is greater than 100 stroke per minute (SPM). These are the requirements for the development of a new machine-system for micro-sheet-forming: Fig. 6.1 shows a 3D model of the machine developed at the University of Strathclyde.

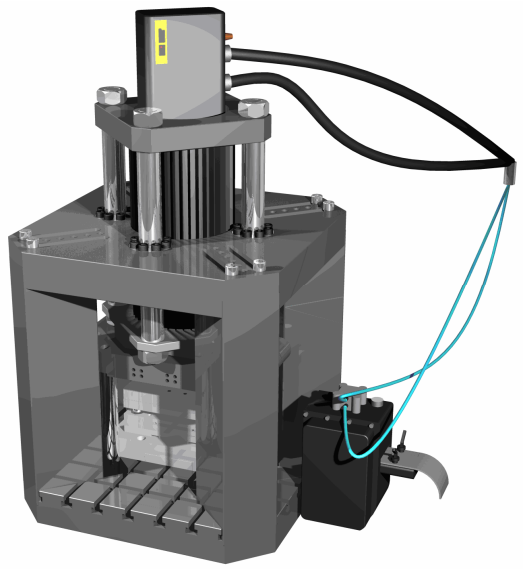

Fig. 6.1: 3D model of the micro-sheet-forming machine.

Two methods of feeding sheet-metals in conventional stamping may be applied to micro-sheet-forming: roller feeding and gripper feeding [Bruderer; PA Industries]. The servo roll-feeder uses an electric servomotor while a gripper feeder mainly uses pneumatic actuation. Although the latter may exhibit limited flexibility in the varying of its travel-distance and feeding-speed, this type of the feeder has the potential to compete with the servo roll-feeder in respect of positional-accuracy and precision. Greater accuracy is achievable due to the possibility of a gripper feeding-mechanism not having a complicated mechanical transmission system and hence, no backlash,

wear, tears, etc., which can contribute towards inaccuracies in feeding. However, an error arising in translation from angular rotation to linear motion in roll feeding contributes towards inaccuracies: this does not occur with a linear gripper-feeder. With the possible use of a servo system, the performance of a gripper feeder could be improved, at the same time giving the flexibility in travel-distance and control-feedback within the system length set-up which ensures better and controllable positional-accuracy.

Three categories of device were identified and found commercially, there being used by most of the micro-manufacturing researchers to position a workpiece or a material accurately and precisely: electromechanical actuators, electrical actuators and piezoelectric-actuators. In this chapter, the analysis of the high-precision and -accuracy handling-strategy used popularly are discussed. A High-accuracy positioning-device is necessary to ensure the best possible positioning or handling of thin sheet-materials for micro-sheet-forming applications. High-repeatability is a necessity to ensure that the next consecutive cycle of positioning/handling of thin sheet-materials retains the same permissible repeatability-tolerance. In addition, to be able to cope with the high-demands of micro-parts/products and being sufficiently reliable for prolonged daily operation, a high-speed positioning-device also may be added as one of the crucial factors for the concept.

The search for a suitable device to serve as the feeder-concept began with determination of the type of linear motor that needs to be used. This was selected through a comparison study on linear motors based on their rated force, acceleration, velocity, achievable-accuracy and size/dimensions. A compact size is necessary due to the limited space of the existing micro-sheet-forming machine-structure. Linear-motor sizing-analysis was conducted to determine the appropriate linear0motor to operate within the rigorous and demanding environment while retaining such features as high-precision, accuracy and speed.

Another factor to be considered for the new feeder-development is its clamping mechanism. A selected high-precision device may be unsuccessful without a proper

strip holding/clamping mechanism. Therefore, a comparison study on holding/clamping device was conducted with a view to identifying the best possible mechanism to be integrated with the new feeder-concept. Selection was made from several devices that were identified as being used popularly commercially and ensuring long-term reliability. The nature of the new feeder-concept requires a clamping device to grip the thin sheet that is also capable of performing the clamping task in a short designated time. A longer clamping-time means that the time for each cycle to be completed is longer, hence limiting the feeder capability to serve a high-yield production-rate. An actuator time of the order of milliseconds is favoured to ensure the success of the concept. Not only being required to be very responsive, the device also has to be capable of generating a strong holding-force to prevent slippage. Slippage, in turn, leads to mis-alignment or positioning of the thin sheet, hence, producing more rejects for both single- and multi-stage tooling-operations. Therefore, a study of the clamping mechanism was conducted, the comparative results are presented in the next chapter.

6.3 Comparison for a High-precision and -Accuracy Device

Three categories of device have been used widely for high-precision feeding: electromechanical actuators [Sato et al., 2008; Erkorkmaz et al., 2007; Chung et al., 2006; Chern et al., 2004; Mei et al., 2003]; electrical actuators [Hsue et al., 2007; Shinno et al., 2007; Yamazaki et al., 2006]; and piezoelectric-actuators [Mracek et al., 2006; Mrad et al., 2004].

6.3.1 Electromechanical Actuators

The use of electromechanical actuators is rapidly replacing the use of hydraulic- and pneumatic-actuators because they save money by reducing unnecessary energy-consumption within the manufacturing facilities,, they have greatly improved control and flexibility, they are suitable for multi-positional tasks, and they incur no health and environmental issues due to high noise-levels. Examples of electromechanical linear-actuation are solenoids and combinations of electrical motors with mechanical transmissions. Solenoids use a magnetic concept to actuate and move the plunger and are used typically in the electrical-transmission field,

specifically as relays in high-voltage switches. The limitations of solenoids are: the travel distance is limited only by limit switches; and they lack controllability of their accuracy/precision. Although solenoids exhibit quite an impressive response-rate, usually in milliseconds, which is suitable for a high-speed punching-process [Chern et al., 2004; Chern et al., 2006b], the overall inflexibility makes this device inappropriate for high-accuracy/precision linear-actuation, due to its uncontrollable nature. The tendency of the electromechanical actuator to spark limits its use in a hazardous environment, and its low power-to-weight ratio limits its usage to low-load application only.

Another type of electromechanical device, which is widely used in industry, is the rotary electrical motor with mechanical transmission such as by the use of lead/ball screws, belts and pulleys, racks and pinions, and gearboxes. Even though this system has a better power-to-weight ratio compared to that of solenoids, this type of electromechanical system exhibits vast inaccuracies in positioning due to backlash, wear and tear of the moving and contacting mechanical-parts etc.

In addition to the inaccuracies due to the rotary-motor, mechanical transmissions such as ball screws, lead screws, toothed rubber drive-belts, racks and pinions, as well as gearboxes, tend to contribute to a large translational-error due to backlash, play, and wear and tear, hence reducing positional-accuracy [Kim et al., 2008].

One of the examples of feeding systems which requires mechanical transmission and is seen as being promising to serve micro-sheet-forming feeding is the servo roll-feeder. Although the micro-servo roll-feeder is encountered commercially and its potential to serve micro press-feeding has been given an opportunity to serve MASMICRO Projects [Masmicro], the feeder's performance in respect of how accurately and precisely the feeder can feed strip-metal has not henceforth been observed and recorded. Indeed, the feeder has been found satisfactory to serve a high-speed sheet-forming operation with a recorded 14 parts per minute, (ppm), but there is no report on its accuracy at this high production-rate and even at 1ppm. An extra effort has to be made to explore the feeder's performance and discover its full

potential for micro-sheet-forming feeding-applications. However, this kind of feeding- and-handling system is still subjected to mechanical wear and tear which definitely contributes to great inaccuracies in the micro-world.

Another type of mechanical-transmission system, which has been used widely as a handling system is the ball/lead screw. In light-load applications, specifically in high-precision handling, the usage of a ball screw is not recommended [Kim et al., 2008]. According to Mei et al., (2003), errors have a great effect on the stiffness of ball-screw mechanisms. The stiffness reduces when a smaller load is applied. The reduction of the stiffness is not because the errors result in the non-contact of the balls, but because of an uneven load-distribution on the balls and uneven contact. This statement is supported by Chung et al., (2006). Based on their studies, the authors found that the contour error of a ball-screw contour also contributes to positional inaccuracies.

Although a study conducted by Erkorkmaz et al., (2007) revealed that the potential linear-positioning accuracy of a ball-screw drive mechanism after compensation for axial vibrations was 2.6µm, this impressive value can be achieved only with the usage of an air-bearing stage at a very-low-velocity transverse motion. Uncontrolled motion/speed increases the accuracy-value to 6.5µm.

An effort made by Sato et al., (2008) demonstrated the potential of a ball-screw positioner to achieve a sub-micron range of positioning-capability. 0.3s is required to settles the position at 0.1µm: longer travel distances require a longer time to settle, for example. up to 0.8s time is taken for 20mm travel. Although the positioner is seen to have better positioning accuracy and precision [Erkorkmaz et al., 2007; Chung et al., 2006; Mei et al., 2003], in terms of high-speed positioning, this system is not a good practical option.

6.3.2 Electrical Actuators

The electrical actuator was invented to overcome the limitations of electromechanical systems. An example of electrical actuators is the linear motor.

This motor is basically similar to the common rotary-motor but instead of having the rotational motion of an ordinary motor, the linear-motor moves in linear motion [Kollmorgen; Rockwell Automation; Copley Controls; Newport; Baldor; Aerotech; Parker Motion; Intellidrives; Hitachi; Linmot; Airex; Yaskawa; Micos; CAlinear]. With this configuration, all mechanical transmissions such as ball/lead screws, racks and pinions, belts and pulleys, as well as gearboxes are eliminated, and this in turn eliminates backlash and compliance and other problems associated with the mechanical transmissions, hence giving a maintenance-free feature. In a linear-motor system, the motor is connected directly to the moving load. Therefore, there is practically no transmission system required between the motor and the load. When the motor moves, the load will move instantaneously. The linear motor has a quite impressive resolution and incremental-motion of up to sub-micron precision, depending on the type and resolution of the encoder used. In terms of acceleration and velocity, a linear motor has outstanding acceleration, where a minimum of 5g is typical and up to 115g (theoretical) maximum acceleration may be achieved [Kollmorgen], 0.2m/s of travel speed are easily achieved. However, linear motor applications are dedicated more on the light machinery industry such as for gantries, CNC machining axes, sub-micro-positioning, etc. Heat build-up may occur in operations that require a long time to be accomplished and in high force-holding processes; therefore with some linear-motors, a cooling system is employed to overcome the problem. Some linear motor exhibit the capability of operating within a rigorous non-stop production environment, which proves to be a good indicator of its robustness, and long life, with average mean-time between failures (MTBF) of 20000 hours [Newport; Kollmorgen; Baldor; Micos]. The linear motor is seen to have substantial potential and becomes one of the best options, as it exhibits the necessary features to be able to realize high-precision/accuracy and high-speed high-precision feeder development.

Using a precision granite table and a linear-motor stage, Kim et al., (2008) reported novel laser-machining tests with micro/nano-machining accuracy for a flat-panel display-industry process. 10nm precision was achieved in high-speed motion of 300mm/s over a long stroke of1.2m.

A comparative study made by Hsue et al., (2007) on conventional rotary-motors and linear-motor-driven wire-EDM machines, reported that a wire-EDM machine equipped with linear-motors performs better than one equipped with rotary motors. They reported that at greater feed-rate, low contouring-errors, better machining-accuracy, and better contouring-machining were achieved using a direct-drive linear motor.

Using a machine equipped with a linear bearing-stage driven by eight linear-motors, Shinno et al., (2007) reported the achieving of a positioning-performance of 1nm accuracy on the X and Y axes in the unloaded condition. This effort has indicated that nanometre positioning-capability in two axes is achievable for super-high-precision-positioning applications.

The development of a 5-axis linear-motor-driven super-precision milling- and turning-machine made by Yamazaki et al., (2006) enabled 10nm-depth nano-step machining to be achieved. Free-form machining with 10nm steps to nanometre-precision and -accuracy was achieved. 1nm positioning-precision was confirmed with the machine temperature maintained to within 1°C.

6.3.3 Piezoelectric-actuators

A later linear-actuation concept is the piezo-actuator [Physik Instrumente; Morgan Electro Ceramics; OAO Piezo]. Piezoelectric-motion comes from the shape change that is generated when a range of crystalline materials are exposed to an electrical field or charge. The most common of these crystals is quartz (SiO_2), but there are more, for example lead zirconate titanate (PZT) and lithium niobate. These materials respond very quickly to changes in the applied voltage and current direction (AC current generates oscillations in the piezoelectric materials). There is also very little variation in the stroke of such actuators, meaning that they have very high accuracy of repeatability. This means that they can be used in devices which demand highly-precise motion and speed. They also exhibit very fast response times and are suitable for applications which require as low as 1ms response time. Piezoelectric materials

are also very efficient and capable of producing a high force-to-weight ratio, and are not affected easily by the ambient temperature. When power is withdrawn they will simply return to a neutral position without the need for any further effort (such as cooling). Typical applications of piezoelectric-actuators focus mainly on very light load application such as in the micro- and nano-positioning area in semiconductors, data storage, photonics, fibre optics, lasers, microscopy, aerospace, precision machining, astronomy and in the micro-systems technology field. One of the well-known piezo-actuators that produce linear motion with a long travel distance is the M-674 PILine® RodDrive integrated piezo linear-motor-drive which was developed by Physik Instrumente. This RodDrive employs a new, patented, ultrasonic drive developed by PI. This highly-compact device measures 160mm in length inclusive of the travel-rod mechanism, 8mm height, and 38mm width, and is integrated with two P-664 piezo-motors which provide acceleration of up to 5g and a velocity of 400mm/s. It has a flexible choice of range of travel from zero up to 100mm. Push/pull force rated at up to 7N (10N is achievable by using different piezoelectric-motors) and a high holding-force when at rest, which results in very high positional stability without the heat dissipation which is common for conventional linear-motors. It has an impressive incremental-motion of 0.05µm, which is a perfect feature for high-accuracy/precision micro-feeder development. There are no backlashes and play, since there are no gears or lead-screws. Nevertheless, other types of mechanical-transmission components are used to translate the elliptical-motion of the piezoelectric actuator to sliding-linear-motion, but these are still subjected to inevitable wear and tear [Mracek et al., 2006]. The main drawback of the RodDrive is that it is not meant for a rigorous constant-production environment, and a high-yield operation is not feasible [Mrad et al., 2004].

Studies made by Mrad et al., 2004 revealed that although a piezoelectric positioner could satisfy positioning-precision requirements, the positioner naturally cannot provide the stiffness, thrust and speed required for constant micro-manufacturing demands. This device tends to fail under such rapid motion due to the nuts and bolts of the equipment becoming loose easily. No bearing system is employed in this RodDrive and the friction force between moving parts is quite high, which leads to

greater heat build-up generated from the rapid motion, which might cause the device to deform and deflect under excessive heat, which would lead to failure.

6.3.4 Qualified Linear Actuator for High-precision Feeding Application

Table 6.1 presents a comparative study made on the discussed high-precision and -accuracy devices. A proper selection of a high-precision system is essential in order to secure high-precision/accuracy for a high-yield feeding application. Linear motors are seen to have superior characteristics among other devices in terms of speed, acceleration, precision/accuracy, robustness, ease of maintenance, etc., as well as being used widely by researchers as an alternative to conventional rotary-machinery [Hsue et al., 2007; Shinno et al., 2007; Yamazaki et al., 2006; Mracek et al., 2006; Mrad et al., 2004; Kim et al., 2008; Chen et al., 2007; Hillery et al., 2005; Cho et al., 2004].

Linear motors are seen to have advantages over other devices in respect of their achievable accuracy with impressive acceleration. Since there is no backlash and play, which will contribute to positioning-inaccuracies in the system, greater accuracy is expected to be achieved. Therefore, a linear motor is seen to be a good platform when considering the feeding design for sheet metal to achieve high-precision and high-rate feeding.

Table 6.1: Types of linear-displacement devices and their suitability for a micro-press feeding-application.

Device	Accuracy and precision	Acceleration rate (g)	Force (N)	Dimension	Reliability
Solenoid	Inflexibility and uncontrollable on stroke distance, hence no accuracy and precision recorded.	Impressive response time and acceleration on short distance.	Fairly high force inversely proportional to stroke distance. The longer the stroke, the less force it produces.	Small and compact hence suitable for constrained space application.	Reliable in terms of mean time between failure (MTBF). 25,000,000 cycles recorded before failure detected. 24/7 production environment is feasible.
Ball/lead Screw, belts & pulleys, gearboxes, rack and pinions and other mean of mechanical transmission.	Flexibility on limited stroke distance hence accuracy and precision is qualified at 6-7µm the best. Nevertheless, due to wear and tear, a greater inaccuracy is expected against time.	Acceleration rate is low due to mechanical transmission involved.	High thrust force is qualified.	Fairly small depends on the force required. The greater the force required, the bigger the system is.	Reliable as demonstrates by most of the machineries nowadays such as milling, turning etc. 24/7 production environment is feasible.
Linear motor and stage	Similar as lead screw. Stroke distance is limited to certain length. Nevertheless if combined with air-bearing, this system produces very high positioning precision and accuracy. No mechanical transmission hence no backlashes to contribute to inaccuracies.	Acceleration rate is very impressive. 5-10g acceleration is typical. 40g is available commercially.	High thrust force is qualified ranges from tenth up to thousands of Newton force.	Fairly small as ball screw system. Force proportional to the coil size. Larger force requires larger n bulkier coil.	Reliable as demonstrated and used by early year 2000's machineries. 24/7 production environment id feasible.
Piezoelectric -actuator (linear motor)	Very accurate and precise as been used in photonics and high precision application but at very limited travel distance.	Response time is better over short distance hence reflecting high acceleration rate. Nevertheless for longer travel distance, 5g is recorded.	Very low force ranging between 7-10N hence limits the application within light weight positioning applications.	Relatively small and compact and suitable for space constrained applications.	Reliability on low speed positioning is acceptable. Nevertheless, for high speed positioning, heat tends to build-up as well as wear and tear. Not suitable for high speed 24/7 production environment.

6.3.4.1 Comparison Study of Ironless and Iron-core Linear Motor

Two types of linear motor are available commercially in today's market; iron-core and iron-less. Each provides characteristics and features that can be optimal and best, depending upon the application. Iron-core motors have coils wound on silicon-steel laminations to maximize the generated force, with a single-sided magnet way. With the advancement in electromagnetic design, iron-core linear-motors have: a high-rated force size-for-size; a high motor-constant value, $K_{m,}$ which in turns reduces thermal losses; and they provide a low cogging-force without the need for skewing of the magnets. The high thrust-forces produced by these motors make them ideal for accelerating and moving high masses, and maintaining stiffness against machining- or process-forces.

Another type of linear motor is iron-less motors. Iron-less motor has no iron, or slots for the coils to be wound on. Therefore, these motors have zero cogging, which is good for high-speed and precise application, a very low mass, and absolutely no attractive force between the coil assembly and the magnet way. These characteristics are ideal for applications that require very-low bearing-friction, the high acceleration of lighter loads, and for maximizing constant velocity, even at ultra-low speeds. The modular magnet-ways consists of a double-row of magnets to maximize the generated thrust-force and to provide a flux-return-path for the magnetic circuit.

The selection of the most-appropriate motor to be used for micro-forming machine's feeder between iron-core and iron-less is made based on several parameters: force density and magnetic attraction; stiffness and settling-times, both dynamic and static force, velocity and stability. Both iron-core and iron-less motors have their respective advantages in terms of the above factors. Therefore, arguments based on these factors for both types of motor will lead to the proper selection of the type of motor which best their feeding application.

The first parameter to be considered in order to choose between iron-core and iron-less motor for a feeding application is force density. The iron-core motor has a twice-

greater continuous-force compared to that of the iron-less motor [Stampfli, 2003]. As the name implies, due to the presence of iron laminations in the forcer of the iron-core motor, extra force is generated by the attractive force from the magnetic track on the forcer on top of the force generated by the electromotive force (emf). The magnetic attraction on iron lamination in the forcer also contributes to the 'cogging' effect of an iron-core motor. 'Cogging' does affect the smoothness and the repeatability of an iron-core motor in achieving outstanding precision such as an iron-less motor might achieve [Yamazaki et al., 2006]. However, the latest technology using a skewed lamination stack [Etel] has enabled iron-core motors to achieve a positional-stability of nanometre precision, but in a greater time as compared to that for iron-less motors.

Gao et al., (2006) used an iron-less linear motor to study the multi-degrees-of-freedom error-motion of a precision linear aerostatic-bearings stage and to determine the achievable precision. An Iron-less motor was used because of the greater precision that is achievable due to there being no 'cogging' effect compared to an iron-core linear motor, which might affect the positional-precision.

In another study made by Park et al., (2006), the authors used an iron-less linear motor to drive an air-bearings stage and determine the precision. Greater precision and repeatability were obtained with the iron-less linear-motor-driven stage.

The next factor is the stiffness of the motor, both static and dynamic, due to the short settling-time and rapid-motion. Short settling-times associated with high dynamic forces or high positional-stability requires stiff mechanical Structures. The epoxy structure in an iron-less motor has low inherent stiffness. The rigidity of the motor is provided by the copper coils inside the forcer, which leads to better overall stiffness. However, the steel structure in an iron-core motor makes it stiffer than the iron-less motor. Nevertheless, according to Cho et al., (2004) and Yamazaki et al., (2006), an ambient temperature controlled to within 1°C may greatly assist the reduction of thermal effects to protect the linear-motor structure from excessive thermal-deformation. Increased stiffness of both the motor structure and the mounting can

eliminate material-deformation which can cause backlash and play during rapid operation. Therefore, a high-accuracy process is feasible. The results of a comparative study made on iron-less and iron-core motors is summarized in Table 6.2, and comparison with an commercial iron-less linear-motor is shown in Table 6.3.

Table 6.2: Suitability of applications and arguments for linear-motor solutions.

Micro-press feeding application	Description	
	Ironless	Ironcore
Continuous force of 150N	Very suitable. Most of the ironless motor has continuous force ranging from 0 – 450N. this indicates that ironless motor only suitable for low load demand for example in application of positioning and light weight feeding mechanism	Very suitable. Ironcore motor usually has two times greater continuous force than ironless which indicates suitability for higher force demand application.
Peak force of 500N	Very suitable for feeding application. Highest peak force rated up to 1600Nm and normally last for a few seconds before the motor starts to overheat and burned.	Very suitable due to higher continuous force leads to higher peak force compared to ironless linear motor.
Smooth motion	Very suitable. No cogging effect and air bearing (gap between forcer and U-channel magnetic tracks) makes non-contact smooth and ultra-precision linear motion is qualified.	Iron lamination inside the forcer will cause cogging effect. Due to magnet attraction force existed, non-smooth motion between forcer and magnetic way experienced. Therefore, this motor is not recommended for high smooth motion.
High precision down to sub-micron order	Sub-micron accuracy/precision and repeatability is qualified and recommended.	Sub-micron accuracy/precision and repeatability is feasible in slow speed and can be used as a cheaper alternative.
Speed stability	Up to 0.1% error at 1kHz measurement which is very stable in speed.	Speed stability is equal to ironless but recommended for cheaper alternative.
Lowest thermal dissipation	Not recommended due to no heat transfer medium. Only rely on air circulation to cool down motor temperature. Controlled ambient temperature might reduce thermal build-up.	Recommended for high heat build-up application due to this motor has water and air cooling mediums.
Tight dimensional constraint	Recommended due to compact size and 200mm x 200mm sized feeder is qualified.	Not recommended due to large and bulky structure. Small and compact feeder is not feasible with this type of motor.
Very high acceleration	Most of the motor has acceleration rate is up to 40g (more than 115g theoretically).	Acceleration rate up to 10g is feasible.
Very high speed	Speed ranges from 0 – 10m/s.	High speed range similar to ironless is achievable.
Stroke < 50mm	Recommended. Moving magnet or moving forcer can be proposed.	Suitable provided moving magnet motion is proposed.
Clean room ready?	Very suitable due to no particle generation (if no moving cable is employed).	Suitable if no moving cable motion is employed.

Table 6.3: Comparative studies on commercial iron-less linear-motors.

No.	Ironless Motor		Feature	Capability									Suitability and Limitation	Cost (£)
	Makes	Model		Peak Force (lb)	Cont. Force (lb)	Max. Accel. (g)	Max. Velo. (m/s)	Max. Travel Range (mm)	Positional Repeat. (micron)	Built-in encoder	Linear Accuracy (micron)	Dim. (mm)		
1	Rockwell Automation	Anorad LZ-075-HT-120	Cogless, 30% higher force, ideal for constant velocity scanning application.	906	181	N/A	10	unlimited*	N/A	No	N/A	136 (L) x 130 (W) x 51.3 (H)	Suitable for micro-press feeding in terms of features and capability. However due to size constraint; which is quite bulky, limits its usage in micro-press feeding application. Separate linear stage needed for micro-press feeder.	N/A
2	Copley Controls	ThrustTube 25 (smallest series)	Tubular design. No attractive force, mount load directly to rugged housing, large airgap eliminates precision alignment, enclosed magnet and coil.	281	51	N/A	9.3	1214	N/A	No	N/A	1214 (L) x 94 (W) x 54 (H)	Not suitable for micro-press feeding due to bulky. Moving cables which will affect motion smoothness, precision and accuracy not specified due to no feedback control stated.	N/A
3	Newport	XMS Series 50 (Linear Stage)	Non-contact direct-drive system, extra large and high efficiency motor to minimize heat generation, cogless for ultra-smooth motion, ripple-free motion, 50nm positional repeatability, sub-nm resolution, no moving cables.	16	N/A	5	0.3	50	0.08	Yes	1.5	125 (L) x 125 (W) x 50 (H)	Suitable for light load feeding application due to low Peak Force. Moving cable might affect positional accuracy and repeatability.	Linear Stage = £4164, Controller = £3875, PWM Drive = £529.
4	Kollmorgen	IL12-100A4-C1	Cogless, no backlashes and play, high stiffness, high positional accuracy, compact size, very smooth velocity.	800	226	106 (T) 10g (Act.)	5	unlimited*	N/A	No	N/A	206.8 (L) x 148.5 (W) x 100 (H)	Suitable for micro-press feeding application. Bulky design limits the application for proposed feeder. Theoratical acceleration is very impressive. However, linear stage needed in order to use as micro-press feeder.	Linear Motor = £1402, Magnetic-way = £332.5, Controller = £1093.28, Encoder = N/A.
5	Baldor	LMCF04F-HCO P	Cogless, no backlashes and play, high stiffness, high positional accuracy, very smooth velocity.	578	191	10	10	unlimited*	N/A	No	N/A	156.2 (L) x 152.4	Suitable for micro-press feeding application. However, linear stage needed in order to use as micro-press feeder.	N/A
6	Aerotech	ANT-LX (Linear Stage)	Non-contact direct-drive system, cogless for ultra-smooth motion, ultra-quiet motion.	10	10	5	0.5	50	0.1	Yes	3	112.7 (L) x 97 (W) x 33 (H)	Suitable for micro-press feeding application. However, due to low Peak and Continuous Force, only light load feeding application is qualified. Moving cable also may affect motion smoothness and accuracy.	Linear Stage = £3165, Controller = £430, Cables = £182

No.	Ironless Motor		Feature	Capability								Suitability and Limitation	Cost (£)
	Makes	Model		Peak Force (N)	Cont. Force (N)	Max. Accel. (g)	Max. Velo. (m/s)	Max. Travel Range (mm)	Positional Repeat. (micron)	Built-in encoder	Linear Accuracy (micron)	Dim. (mm)	
7	Parker Motion	I-Force ML50-2E-NC-MP	Cogless, no backlashes and play, internal air and liquid cooling, vacuum encapsulation allows motors to be used in high vacuums.	847	189	N/A	N/A	unlimited*	N/A	No	N/A	160 (L) x 155 (W) x 50 (H)	Suitable for micro-press feeding application. However, linear stage needed in order to use as micro-press feeder.	Linear Motor = £418, Magnetic-way = £465, Controller = £1778, Encoder = £360.
8	IntelliDrives	LSS-120	Modular design, zero backlashes and play, long travel range.	450	160	N/A	N/A	2000	5 - 50	Yes	0.5 - 10	2000 (L)	Not suitable for micro-press feeding due to bulky. Moving cables will affect motion smoothness.	N/A
9	Linmot	P01-48x240	Tubular design. No attractive force, mount load directly to rugged housing, large airgap eliminates precision alignment, enclosed magnet and coil.	234	150	16	1.8	30 - 180	100	Yes	N/A	350 (L)	Not suitable for micro-press feeding due to bulky. Moving cables will affect motion smoothness. Low positional accuracy.	N/A
10	Airex	P15-4	Cogless, no backlashes and play, configurable connection/cable options.	444	140.4	5	3	unlimited*	N/A	No	N/A	274.3 (L)	Not suitable for micro-press feeding due to bulky. Moving cables will affect motion smoothness.	N/A
11	Yaskawa	SGLGW-60A 253B	Cogless, no backlashes and play, high stiffness, low settling time, very smooth velocity.	440	147	20	5	unlimited*	N/A	No	N/A	253 (L) x 98 (W) x 31.8 (H)	Suitable for micro-press feeding application. However, linear stage needed in order to use as micro-press feeder. Bulky design limits its application for micro-press feeding application which has space constraint.	N/A
12	Micos	LMS-120 (Linear Stage)	Linear recirculating ball system, stiff body structure, inductive limit switches, module combination.	N/A	8	N/A	0.2	40	0.1	Yes	1.5	135 (L) x 115 (W) x 37.5 (H)	Suitable for light load feeding application due to low Continuous Force. Moving cable might affect positional accuracy and repeatability.	Linear Stage = £8000, Controller = N/A.
13	CALinear	4020-2C	Tubular design. No attractive force, enclosed magnet and coil, integral bearing.	1860	363	40	2.5	500	N/A	No	N/A	500 (L) x 183 (W)	Not suitable for micro-press feeding due to bulky. Moving cables will affect motion smoothness. Low positional accuracy.	N/A
14	Baldor	LSC Linear Stage	Cogless, no backlashes and play, stiff structure and compact. Anti creep feature due to crossed roller bearing was used.	270	90	5	0.75	0.3	1	Yes	5	300 (L)	Suitable for micro-press feeding application. However, linear stage needed in order to use as micro-press feeder. Bulky design limits its application for micro-press feeding application which has space constraint.	N/A

+magnetic track length can be varied, depending upon a request.

6.4 Detailed Analyses and Calculations

The correct sizing of a linear-motor during the designing stage is crucial, as this will reflect the entire system's performance and will contribute to the designated production-rate. In order to select which size of motor should be used with the designated load and push/pull force, sizing analysis is conducted. Fig. 6.2 shows the applicable forces which should be taken into account for linear-motor sizing-analysis. Three types of force are identified as contributing to the total -peak and -continuous linear-motor forces.

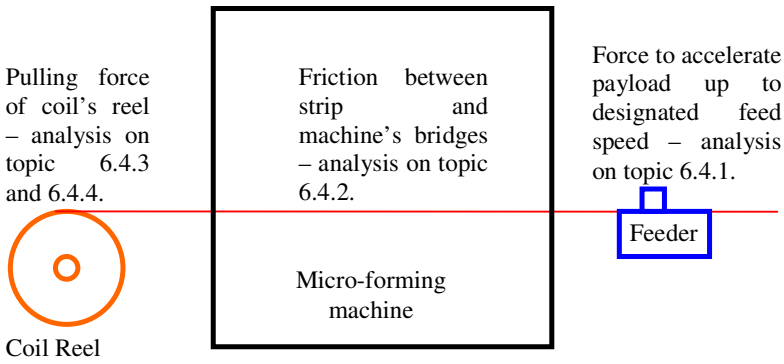

Fig: 6.2: Types of related forces, friction between parts and payloads that contribute to total peak- and continuous-forces calculation.

6.4.1 Calculation of Forces due to Payload

As depicted in Fig. 6.3, about 0.3kg mass/load of clamping mechanism, forcer, linear-motion guide-carriage and table-weight need to be moved. As designed, a 0.3kg payload is required to be moved 5mm in 0.150s, to dwell for 0.050s, to move backward for 0.150s and dwell for 0.050s, and then to repeat the cycle for 2Hz operation [Parkermotion; Kollmorgen; Baldor; Yaskawa; Aerotech]. In this case, the analysis and calculation of the required forces in order to determine the best linear-motor and amplifiers are greatly needed.

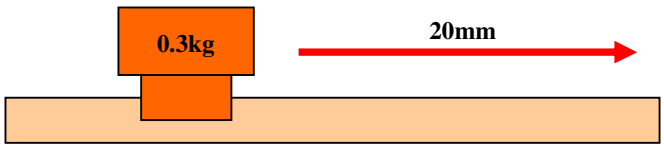

Fig. 6.3: Diagram of the load exerted on the forcer, and the direction and distance of movement.

The first thing to consider is the motion characteristics: the peak speed; the time that is needed to accelerate the mass from the origin to the end point; how long the travel will take; and the dwell-time when the moves finishes. In general, for this type of movement, which is from point-to-point, the basic profile is the trapezoidal move [Chen et al., 2007; Park, 1996]. With this move, time of movement is divided equally between the acceleration and deceleration phase (45% acceleration and 45% deceleration). The first part is acceleration, the second part is constant-velocity and the third part is deceleration. This motion-characteristic should give a balance between speed and acceleration to provide the best motor-combination. Based on trapezoidal motion, the time taken to accelerate is:

$$0.150s \times 0.45 = 0.0675s$$

Then the peak speed required to make the movement can be calculated and, in this case, because the move is symmetrical and divided into three, the equation below is used. The load cannot be accelerated instantaneously from zero to 0.06061m/s, as previously-established: 0.0675s will be needed to reach this speed. Therefore, the acceleration can be calculated as shown in Fig. 6.4:

$$v = \frac{0.005}{0.0675 + 0.015} = 0.06061m/s$$

$$a = \frac{v-u}{t} = \frac{0.06061-0}{0.0675s} = 0.9m/s^2 \approx 0.1g$$

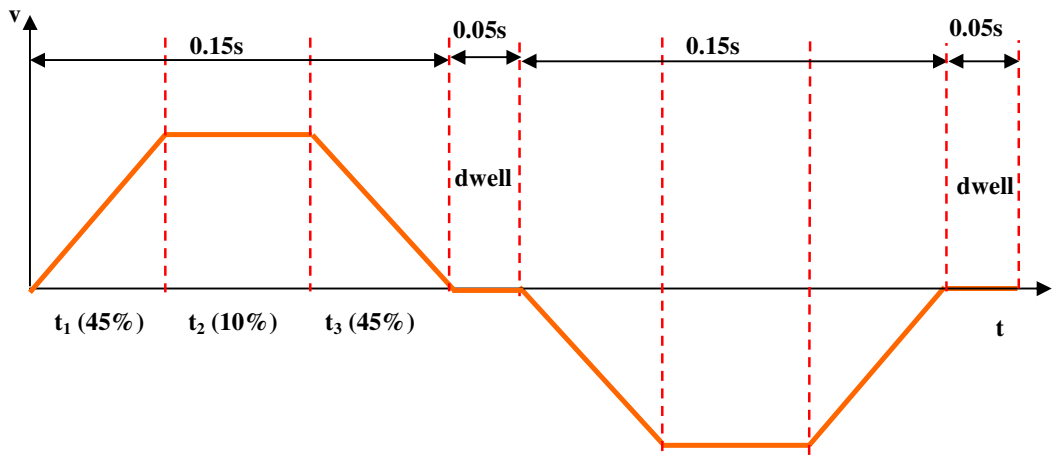

Fig. 6.4: Trapezoidal profile representing the acceleration of the forcer in one cycle.

Then, Newton's third law of motion is used to determine the payload-rating-force, f_p, since the peak rating-force is assessed considering: the frictional-force, f_f, (with the assumption that the recirculating ball-bearing used to carry the load in the system has a coefficient of friction of about 0.002 up to 0.003); the force for acceleration, f_a; and the gravitational force for an inclined plane, f_g; as well as external force, f_e, caused by cable management. Therefore, the payload rating force can be written as:

$$f_p = f_a + f_g + f_f + f_e$$

where f_a represents the force for load, including the forcer mass, and will be used to calculate the final coil-temperature rise, the peak- and continuous-current and the minimum bus-voltage.

$$f_a = ma = 0.3 \times 0.9 = 0.27N$$
$$f_g = \sin(\theta)mg = \sin(0) \times 0.3 \times 9.81 = 0$$
$$f_f = mg\mu = 0.3 \times 9.81 \times 0.003 = 0.01N$$
$$f_e = 0$$
$$\therefore f_p = 0.27 + 0 + 0.01 + 0 = 0.28N$$

By adding a safety-factor of 25% to compensate for the reduction of motor-efficiency, the new force to move payload is therefore calculated to be 0.35N.

6.4.2 Analysis of Frictional Forces between the Sheet Metal and the Machine's Bridges

Frictional forces due to contact between the 50μm-thickness and 50mm-width strip material and the machine can be described and analysed as follows:

Supposing that the width of the machine with which the material makes contact is 500mm, the weight of material in contact with the machine is calculated as:

$$m = \rho V$$
$$V = 0.05 \times 0.5 \times 0.00005 = 1.25 \times 10^{-6} m^3$$
$$\rho = 7.82 \times 10^3 kg/m^3$$
$$\therefore m = 1.25 \times 10^{-6} \times 7.82 \times 10^3 = 9.775 \times 10^{-3} kg \approx 10 gram$$

Frictional coefficient between mild-steel and carbon-steel is given elsewhere as 0.15 [Avallone et al., 2006; Kalpakjian et al., 2006]

$$f_f = \mu ma$$
$$\mu = 0.15$$
$$f_f = 0.15 \times 0.01 \times 9.81 = 0.015N$$

By adding a safety-factor of 25%, the new frictional-force value is 0.02N. This value was added to the calculation of total peak-force for linear-motor sizing.

6.4.3 Analysis of the Coil's Reel-Pulling Force

Another force which contributes to the total peak- and continuous-forces is the force to pull material from its reel, as illustrated in Fig. 6.5. Pulling forces from the coil reel can be estimated as the following:

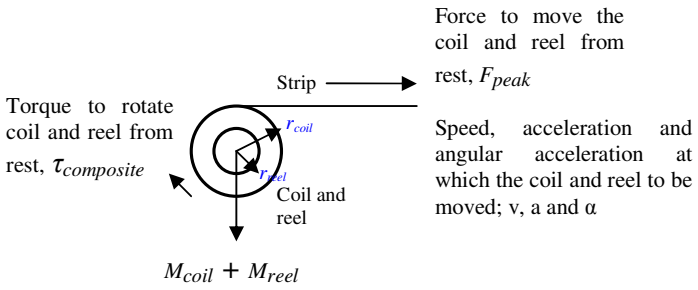

Fig. 6.5: Free-body diagram of the coil and reel producing a total of torque labelled as $\tau_{composite}$.

Knowing that:

$$\tau = fr = I\alpha$$

$$\alpha = \frac{a}{r}$$

$$I = mr^2$$

$$a = \frac{v-u}{t}, v = \frac{3s}{2t}, u = 0$$

And supposing the following:

$$s = 0.005m$$
$$r = 0.0625m$$
$$t = 0.0675s$$
$$u = 0$$

For trapezoidal-motion:

$$v = 0.06061m/s$$

$$a = \frac{0.06061 - 0}{0.0675} = 0.9m/s^2$$

$$\alpha = \frac{0.9}{0.0625} = 14.4rad/s^2$$

Supposing that the coil (made of carbon-steel) and the reel (made of Perspex) have outer diameters of 125mm and 110mm, respectively, by assuming that both the coil and the reel are solid, the inertia of the coil/reel composite can be calculated .

Supposing the following:

$$\rho = \frac{m}{v}, \rho_{coil} = 7820kg/m^3, \rho_{reel} = 1190kg/m^3$$

$$length_{coil} = 50m$$
$$width_{coil} = 0.05m$$
$$thickness_{coil} = 0.00005m$$

$$v_{coil} = 50 \times 0.05 \times 0.00005 = 0.000125m^3$$
$$m_{coil} = 0.000125 \times 7820 = 0.9775kg$$

$$r_{reel} = 0.055m$$
$$h_{reel} = 0.012m$$

$$v_{reel} = \pi \times 0.055^2 \times 0.012 = 1.14 \times 10^{-4} m^3$$

$$m_{reel} = 1.14 \times 10^{-4} \times 1190 = 0.1357kg$$

$$I_{coil} = \frac{m}{2}(r_{outer}^2 + r_{inner}^2)$$

$$I_{coil} = \frac{0.9775}{2}(0.0625^2 + 0.0555^2) = 3.41 \times 10^{-3} kgm^2$$

$$I_{reel} = \frac{mr_{reel}^2}{2}$$

$$I_{reel} = \frac{0.1357 \times 0.055^2}{2} = 2.05 \times 10^{-4} kgm^2$$

$$I_{composite} = I_{coil} + I_{reel}$$

$$I_{composite} = 3.41 \times 10^{-3} + 2.05 \times 10^{-4} = 3.62 \times 10^{-3} kgm^2$$

$$\tau_{composite} = 3.62 \times 10^{-3} kgm^2 \times 14.4 rad/s^2 = 0.052Nm$$

$$f_{composite} = \frac{0.052}{0.0625} = 0.83N$$

Therefore, the total force required for rotating the combination of the coil and the reel is found to be 0.83N. By adding a safety-factor of 25% (to overcome internal frictional-forces), the new total force is calculated to be 1.0N.

6.4.4 Uncoil Braking-Force

Study on the effect of the coil braking-force on the strip tension in the punching process has been conducted by Chern et al., (2006b). However, the study was focused more on the punched hole quality instead of on the feed-accuracy. The relation between strip-tension and feed-accuracy still needs further study. As proposed by Russell, (2003), strip-tension should be kept consistent with the torque needed to coil the strip metal in the first place. Adjustable-braking-force is proposed to make the uncoil-process flexible in terms of adjusting the torque to various values [Chern et al., 2006b]. Supposing that the coiling process requires the same torque as for the uncoiling of the strip metal, given by the previous analysis, the maximum force to uncoil is 1.0N. By taking f_{rms} of the rated force; the designated variable-braking-force for this application is shown below:

$$f_{brake} = \sqrt{\frac{1.0^2 \times 0.0675}{0.2}} = 0.58N$$

For a safety-margin, a safety-factor of 25% is added, so that the braking force becomes 0.73N. Since 0.73N of the force is acting during the whole cycle, this value needs to be included in the final peak- and continuous-force in the sizing of the linear-motor.

6.4.5 Influence of Other Interfacial Forces

Forces which can be neglected in the macro-world can no longer be neglected in the micro-world. The level of micro-forces relative to the weight of micro-parts has about the same value, in the most common situations. However, the micro-forces are greater relative to the weight, where the micro-parts are of $100\mu m^3$ size and smaller. Hence, such parts will stick to the handling mechanism, overcoming the effect of gravity, this resulting in problems in the manipulation process. Three types of micro-forces which have a significant influence on micro-parts are known and are being studied extensively at the present time, these being: adhesive-, van der Waals- and electrostatic-forces. Usually, the adhesive force between particle surfaces is due to the presence of van der Waals- and electrostatic-force [Tomas, 2007; Rougeot et al.,

2005; Fearing et al., 1995; Feddema et al., 1999; Bowling et al., 1986; Bowling et al., 1988; Arai et al., 1995]. However, these forces would not have a significant effect on material handling for the present application, since the handled material is larger than $100\mu m^3$.

6.4.6 Analysis of Peak- and Continuous-Forces

The peak-force can be calculated as follows:

$$F_{peak} = f_p + f_f + f_{composite} + f_{brake} = 0.35 + 0.02 + 1.00 + 0.73 = 2.10N$$

The rms-force is the average force, $f_{rms,}$ from the motor and helps to determine the final temperature that the coil will reach. Based on the above trapezoidal-profile case, the calculation will be as follows:

$$F_{rms} = \sqrt{\frac{F_{peak}^2 \times t}{t_{cycle}}}$$

where:

$t = 0.0675s$

$t_{cycle} = 0.2s$

$$\therefore F_{rms} = \sqrt{\frac{2.10^2 \times 0.0675}{0.20}} = 1.22N$$

The summation of the peak- and continuous-forces is 2.10N and 1.22N, respectively. Both of these forces were used for selecting which linear-motor is most suitable.

6.4.7 Calculation of the Final Coil-Temperature, and the Peak- and Continuous-Current and Minimum Bus-Voltage

6.4.7.1 Final Coil-Temperature Analysis

The final coil-temperature represents the temperature at which the linear motor may be operated without adversely affecting the materials of construction. Therefore this final temperature can be a guideline when choosing which servo-controller is best suited to the designated linear-motor. In order to determine the increase of coil

temperature, the equation below is used. With the assumption of an ambient temperature of 20°C, the increase can be calculated as below.

For the purpose of analysis, some parameter-values are referred to and taken from the linear-motor brochure/catalogue. Using the given values as a guide to conducting the analysis, the rise in temperature of the coil can be determined using the method shown below. For instance, from the Parker Motion I-Force iron-less linear-motor catalogue, parameters were given such as:

Back Electro-motive force (BEMF) = 24.5 V/m/s
Force constant = 21.3 N/amp
Motor constant = 26.3 N/√W
Coil resistance = 0.7 Ω
Thermal Resistance, R_T = 0.64 W/°C

From peak- and continuous-force calculation, both the peak- and continuous-forces were determined as:

F_{peak} = 2.10N
F_{rms} = 1.22N

With the assumption that the ambient temperature is 20°C, the coil temperature-rise can be calculated as below [Aerotech]:

$$T = R_T\left(\frac{F_{rms}}{M_C}\right)^2 = 0.64\left(\frac{1.22}{26.3}\right)^2 = 0.001°C$$

Therefore, the Final Coil Temperature = 20 + 0.001 = 20.001°C ≈20°C

It may be concluded that the effect of temperature rise onto the system is small and may be neglected.

6.4.7.2 Sizing-up the Amplifier

This analysis is conducted in order to determine the most appropriate servo-controller size and type to be used, so the linear-motor can operate at its best performance without suffering from current and voltage drain-out. Based on the given value of the motor's force-constant in the catalogue and the calculated peak- and continuous-forces, the peak- and continuous-current and the minimum bus-voltage can be calculated as follows:

Peak current = F_{peak}/force-constant = 2.10/21.3 = 0.10A
Continuous current = F_{rms}/force-constant = 1.22/21.3 = 0.06A

Drive $\text{Voltage}_{\text{min.}}$ = (peak current x coil resistant) + (velocity x back EMF)
= (0.10 x 0.7) + (0.06061 x 24.50) = 1.6V

Therefore, the servomotor controller must be capable of supplying peak and continuous current minimum of 0.10A and 0.06A respectively.

6.4.7.3 Thermal Expansion due to the Temperature-Rise Effect

The temperature effect which is tolerable in macro-forming is no longer tolerable in micro-forming [Brussel et al., 2000; Aronson, 2004; Cho et al., 2004]. Apparently, a small increment in temperature contributes significantly to the deformation of the parts of the machine. Heat generated by the motor coil, if it is not well controlled, can cause the deformation of contacted parts. Aluminium alloys, mainly found as linear-stage material, typically are used due to their good heat-conductivity, which enables heat to be dissipated efficiently from the linear-motor's coil. [Parkermotion; Kollmorgen; Yaskawa; Baldor]. The analysis below is conducted to understand how much deflection is experienced by the gripper, which is located on top of the stage. Suppose that aluminium alloy 6082-T6 has a coefficient of expansion of 24µm/m°C at 20°C [Society of Amateur Scientists], the thermal expansion due to heat generated by the motor during operation is:

$$Exp_{thermal} = \Delta T \times 24\mu m = (20.001 - 20) \times 24 = 0.024\mu m$$

Suppose for 5mm travel-distance, the expected total thermal-expansion is:

$$Exp_{thermal-20mm} = \frac{0.024\mu m}{1m} \times 0.005m = 0.00012\mu m$$

The thermal expansion due to heat generated by the motor's coil for the gripper is expected to be a maximum of 0.00012µm or 0.12nm for 100% transferred heat. This value is relatively small and negligible, due to having no significant effect on the structural deformation of the system.

6.5 Comparison Study of Holding/Clamping Mechanism

Feeding metal strip by the linear-actuation method requires a mechanism that will hold the strip firmly during the translational process. Enough holding force is vital to avoid slippage of the metal strip, which would cause miss-feed, leading to inaccuracy in feeding. Previously, several methods were used to hold the strip metal during the feeding process: pneumatic and mechanical cam-grippers [Bruderer; PA Industries]; and piezoelectric-actuators [Physik Instrumente]. Three types of device were identified as being suitable to be used for a clamping mechanism for a linear-actuation feeding application: a pneumatic cylinder; a piezoelectric-actuator; and a solenoid. These devices were discussed based on several key parameters which are required to serve a micro-sheet-forming application. The key parameters discussed are in terms of holding-force and travel-distance, response and settling time; and finally, in terms of the system set-up, the controller and the initial costs.

6.5.1 Holding-Force and Travel-Distance Issues

The pneumatic gripper definitely has the required physical capability in term of holding-force within the range of tenths to thousands of Newton. In term of travel distance, the pneumatic cylinder is the best option among the three. Depending on the cylinder size, the travel-distance can be from as low as a few millimetres up to hundreds of millimetres [SMC]. The piezoelectric actuator uses the deformation of piezo-material to generate the holding force. It can generate up to tenths of thousands

Newton force with very precise resolution of sub-micron precision. However, the main drawback of using a piezoelectric actuator as a gripper device is the small travel-distance produced by the large forming force. The maximum travel distance produced is up to 1mm and an average actuator has a travel-range of around 50-200µm. The solenoid usually has a millimetre range of travel distance, with over hundreds of Newton of force, and is size-dependant [Ledex]. Generated force is inversely-proportional to the produced stroke distance. The longer is the stroke distance, the lower is the force generated, due to the lesser magnetic attraction over a large gap.

6.5.2 Response and Settling-Time Issues

The typical response and settling-time for a pneumatic cylinder is 50ms, which is a suitable time for high-speed operation. The greater is the pressure supplied to the cylinder, the greater will be the effect of a faster response and a lesser settling-time. The piezoelectric-actuator has an impressive response-time, which is typically of sub-milliseconds [Physik Instrumente]. This makes it suitable for high-speed micro feed-distance applications, which require sub-micron precision over a short settling-time. On average, 2-10ms is confirmed for a solenoid to reach a travel-distance ranging from 1-5mm. Therefore, the solenoid is seen to have good potential for clamping applications since the stroke produced is quite fast, is longer and is impressive.

6.5.3 System Set-up, Controller and Cost Issues

There is significant increase in capital that has to be paid for a non-stand-alone device such as a piezoelectric-actuator or a pneumatic-system, due to the facility-system required to make them operable and workable. Both of these devices contribute significantly to more cash being required compared to the case with a solenoid. The integration of a piezoelectric-actuator with a machine servo-drive controller is not an easy task. Mainly in open-loop operation, the piezoelectric-actuator is controlled by a pulse-width-modulation (PWM) controller and hence it is difficult to integrate it with the CANbus and Profibus devices that are mainly found in the current technology of a servo-drive controller-interface. Although most

pneumatic-controllers are PLC-base-controlled, and are easily integrated with a servo-drive controller, the necessity for a clean and dry-air facility has made the system more expensive and involving more trouble compared to a stand-alone device. Solenoid is easily controlled by using servo drive controller's logic circuit interface. 24VDV output is usually available on most of today's servo-drive controllers and the easiest solution is to integrate a solenoid with the entire system. Table 6.4 summarizes the findings of the comparative studies made.

Table 6.4: Comparative study of clamping-actuation devices.

No	Clamping Device	Model	Feature	Capability				Suitability and Limitation
				Settling time (ms)	Holding force (N)	Lifetime (duty cycles)	Dimension (mm)	
1.	Air cylinder	Compact cylinder	Simple in design and to be controlled due to no complicated controller required. Open-loop control by pulsing 24VDC and current to the coil. Self-retractable by homing coil spring mechanism.	20	N/A	N/A	25-40 (W & D), 40-60 (L + S)	Suitable for high-speed clamping mechanism, High force to weight ratio is produced. Easy to be integrated with electromechanical machineries due to only require 24VDC signal and compressed air facility.
2.	Solenoid	Low profile and compact (LEDEX 4ECM/4E FM)	Simple in design and to be controlled due to no complicated controller required. Open-loop control by pulsing 24VDC and current to the coil. Self-retractable by homing coil spring mechanism.	4	70-165	5000000	40mm (d) x 38mm (H), 170gram weight	Suitable due to fairly high force to weight ratio. Higher settling time makes it suitable for application where positioning accuracy is no the main concern. Nevertheless, it is not suitable for an application which requires longer travel distance. Force is inversely proportional to the stroke length. Easiest to be integrated with linear motor system via amplified current 24VDC logic circuit.
3.	Piezoelectric actuator	Physik Instrumente	High resolution and controllable short stroke distance.	N/S	50	N/A	60mm (L) x 36mm (W), 280gram weight	Fairly suitable for clamping purposes due to short travel distance of maximum 1mm. Not easily to be integrated with linear motor system since different controller architecture. Hence separate controller is required.

6.6 Conclusions

Based on the studies described above, a linear actuation-method that uses a linear-motor is proposed as a strategy for developing a new feeder for micro-sheet-forming applications. Direct-drive from a linear motor ensures that no mechanical transmission is required, which latter could contribute to play and backlash that affect the accuracy of the feeding in micro-sheet-forming. For the case analysed (the strip materials and micro-stamping process being specified), theoretically, 2.10N and 1.22N peak- and continuous-forces, respectively, are required to serve material feeding for this particular application. At least 1g of acceleration rate is needed to accelerate the payload, i.e., moving the gripper and the strip at up to 120 parts per minute (ppm) in a high-precision operation. The level of precision achieved is significantly greater than that offered by a servo roll-feeder, which typically is 10μm accuracy with inconsistent repeatability.

A solenoid has been chosen to serve the clamping application for the gripper design due to its impressive response time, holding force, ease of integration, etc. The logic output from the servomotor controller is used to control the solenoid, hence giving peace of mind on the integration side by eliminating the necessity of using complicated controller just to control the solenoid. The new feeder for micro-sheet-forming is now being constructed.

Chapter 7

FE Analysis of the Gripper-Feeder

7.1 Summary

Another type of feeding device used in the conventional sheet-forming process apart from the servo roll-feeder is the gripper-feeder. This feeder is cheap to run and the system has a simple structure that is easily integrated with existing forming machines: such features are among the reasons why this type of feeding-device is commonly used. Despite being less-flexible in respect of changes to a longer feed-distance, the gripper-feeder could produce a very-high pulling/pushing force, which would made it suitable for the feeding of thicker- and heavier-sheet. In addition, the lesser mechanical-transmission used in the system itself may be seen as a useful hint as to reducing positional-error. Previous Chapter 6 has defined the new feeder design which uses linear motor as the actuation and solenoid as the clamping devices. In order to understand the feeding characteristic of the feeder, therefore FE-simulations were conducted. This analysis is really useful to determine the system performance of the new feeder, with a view to establishing the feeding-characteristic and the level of success when feeding thin-sheet for the micro-sheet-forming process. FE-simulations were also used to study the strip-feeding characteristic of the feeder with a view to acquiring a better understanding of the system for micro-sheet-forming applications. Various parameters were tested and simulated to obtain an extensive coverage of the feed-characteristics when subjected to different configurations. Based on the results, longer feed distance and higher feed frequency produced better positional accuracy compared to shorter feed distance and lower feed frequency. It is also revealed that brake force application has significant contribution towards improving feeding repeatability but also at the same time affecting positional accuracy. Lubrication on the system was found to have insignificant contribution to improve positional accuracy and repeatability.

7.2 Introduction

The purpose of the present FE-analysis is to study the strip behaviour and the feeding characteristics of the designed feeder. Similar key-factors such as in Chapter 4 has been considered for the analysis. Examination of these factors is seen vital to understand the strip-behaviour during and the feeder's feeding characteristic. The application of brake force to the system was implemented with a view to study its the effect on the uniformity of strip tension throughout the feeding process. Additionally, the effect of brake force on the settled-position of the strip also needs further understanding. The next factor to be explored is the varying of the motion-profile curve. Study had revealed that change in the motion-profile curve affects the positional-stability through the existence of 'jerk'. Therefore, various motion-profile curves were introduced in the analysis with a view to determine their influence on positional accuracy. Change to different strip materials and thicknesses were conducted with a view to study the influence of the mechanical properties on feed-performance. Identification of the correlation between feed-distance and positional accuracy also was conducted. Intensive and detailed studies and analysis by FE are seen vital to the achieving of a sound understanding of feed-characteristics to enable future improvements to be made.

7.3 Procedure

Accurate, wide and various angles-of-geometry may be achieved by simulating the model in 3D dynamics-explicit, compared to a 2D model [Hibbitt et al., 2002a]. Although 3D dynamics-explicit analysis is time-consuming, modelling the thin sheet-metal from a shell and using appropriate meshing-scheme are seen to produce a better approximation of the thin-sheet behaviour and characteristics during the feeding process. This in turn reduces the modelling time-increment and the CPU time (Fig. 7.1).

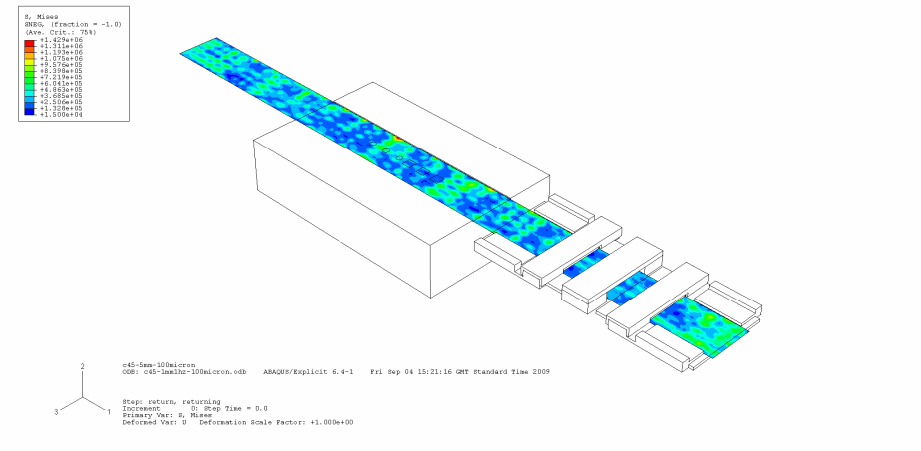

Fig. 7.1: 3D model of the designed feeder.

Several feed key-parameters were identified and considered to establish an intensive FE-analysis of gripper-feeder feeding-characteristics. Analysis was conducted to simulate designed feeder feeding-characteristics at 2Hz feed-frequency. An appropriate feed-velocity at this frequency was determined by trapezoidal-motion profile-analysis. A similar motion-profile curve then was configured on the FE analysis-amplitude as will mimic lifelike feeding conditions. The gripper-feeder model was constructed by ABAQUS/CAE and was based on the actual size.

Each contact-pair was defined with a specific coefficient-of-friction value derived from Chapter 2. A friction-coefficient between a contact pair of aluminium on the gripper and the retainer bodies were defined at 0.3 [Kalpakjian et al., 2006; Lange, 1985], a coefficient-of-friction on the contact pair of the aluminium gripper and a steel strip was defined at 0.20 [Lange, 1985], and a contact pair between the steel strip and the tooling (steel forming-dies) was defined at 0.15 [Roberts, 1978].

The jaws of the upper movable gripper and the jaws of the retainers were subjected to 220N and 150N of clamping force, respectively, which was pre-determined from the solenoid's manual, while the bottom jaws of the gripper and the retainer were constrained in all rotational directions. An appropriate brake-force value was applied to one free end of the strip to represent the brake force generated by the decoiler (discussed in the previous chapter). The movable-gripper structure was subjected to a

designated velocity for each feed-distance, 12.12125mm/s and 60.60625mm/s both for 1mm and 5mm feed-distances, respectively (for a 45-45 motion-profile configuration). The time taken to accelerate was defined by the designated motion-profile curve for each feed-distance. Both 1mm and 5mm feed-distances shared the same value of the acceleration-deceleration phases. Two types of motion-profile curve to define different acceleration-deceleration phases were used, namely as 45-45 and 50-50. The 45-45 motion-profile curve represents 45% of the total time of 150ms being is allowed for acceleration time and another 45% for deceleration time, the remaining 10% of the total time being for the constant-velocity phase, as depicted in Fig. 7.2. Similarly as for 45-45, the 50-50 phase was designed for the model to accelerate for 50% of the total time just for acceleration time and to decelerate for the remaining 50% of the total time, as depicted in Fig. 7.3 with a radial velocity of 13.33340mm/s and 66.66670mm/s for 1mm and 5mm feed-distance, respectively.

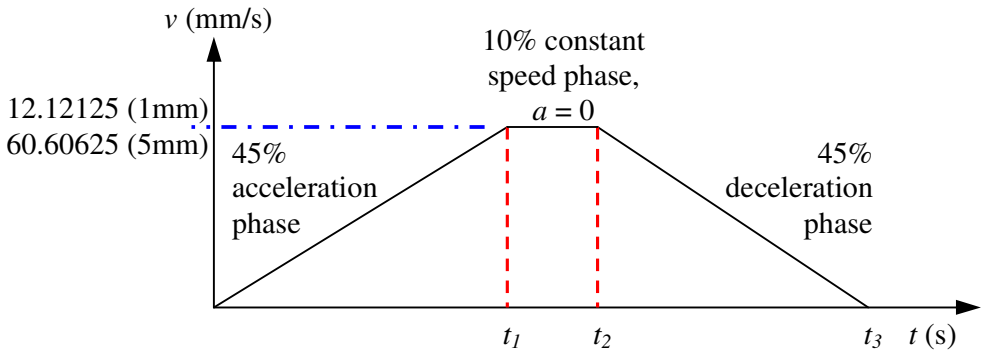

Fig. 7.2: Denotes 45-45 motion profile curve.

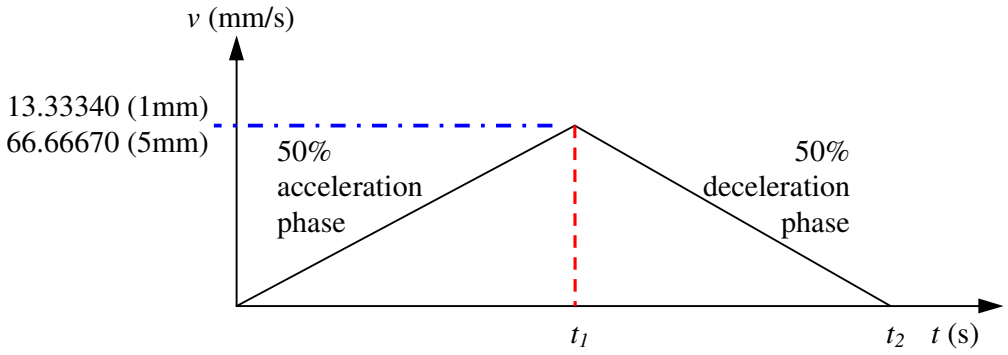

Fig. 7.3: Denotes 50-50 motion profile curve

In the model, gripper, retainers, and tool/die set were assumed rigid and were described by rigid boundary conditions. Thin sheet metal was assumed deformable. The value of the modulus of elasticity/Young's of the thin sheet metal was determined by the uni-axial tensile test, as described in an earlier chapter. Element types of S4R (3D explicit analysis) were used for modelling the thin sheet [Hibbitt et al., 2002b; Hibbitt et al., 2002c]. The simulation was performed using the dynamics explicit procedure to cope with the vast non-linear geometrical-displacement. The decision as to the final mesh was made based on a trial basis, where a compromise between the computing-time, the computer-memory and the simulation-precision is usually required.

Similar nodal-points as for the roll-feeder FE-simulation were used, with a view to establishing a consistent comparison of the overall behaviour of the thin sheet during feeding: one at both of the strip ends; one in the middle; and the other two at the half-distance between the node at the end of the strip and the middle node. The selection of these nodes ensures that the positional accuracy at the die position is also taken into account, hence how large the positional inaccuracy is could be determined directly. In order to avoid difficult and time-consuming 3D-modelling, an appropriate fine mesh was used, which also reduces error generated due to an excessive aspect-ratio.

7.4 Results

7.4.1 Strip-Feeding Characteristics

The feeding cycle for the developed gripper-feeder has several steps, among which are the gripper feeding, and its returning to the home position. Both steps have the same time-frame of 0.15s and are applied for both of the tested feed-frequencies. During the feeding step, the gripper moved the strip by the desired feed-distance. Once the feed-distance is reached, the gripper stops, releases the strip and return to the home position. During the return to the home position, both of the retainers clamp the strip in order to avoid the strip being moved accidentally by the gripper motion. One of the key objectives of this study was to examine and determine the feeding-characteristics of the new feeder, especially the strip behaviour during the return of the gripper to the home position.

Without a good strip-tension, i.e. with no brake force being applied, the feeding characteristic was seen to be to slightly overshoot, especially for CS50 at both feed-frequencies, 1 and 2Hz, as shown in Fig. 7.4 and Fig. 7.5. However, as soon as the designated feed-distance was reached and the feeder stop feeding, a large fluctuation was observed with the CS50 strip. For greater feed-distance, a consistent settling-pattern was observed throughout the feeding process for both of the tested frequencies. as shown in Fig. 7.6 and Fig. 7.7. A uniform starting- and ending-point were observed for all strips, hence better positioning-accuracy was achieved. No significant change in the settling-pattern for the returning of the gripper to the home position was observed, for both the shorter and the longer feed distances.

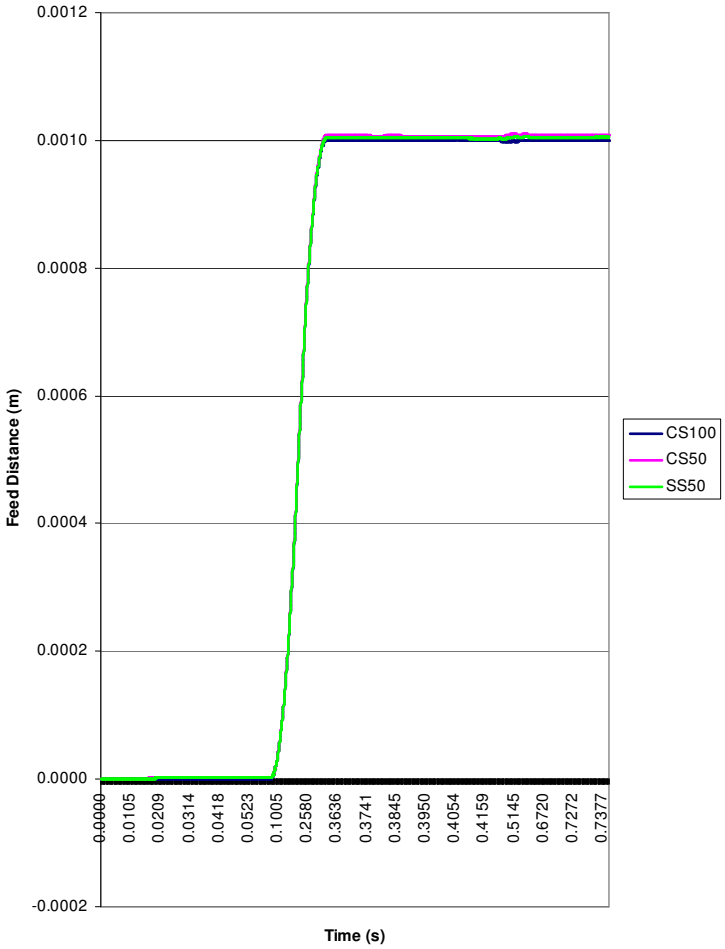

Fig. 7.4: Feeding characteristic for all strips for 1mm feed distance, 1Hz frequency configured at 45-45 motion profile without brake force.

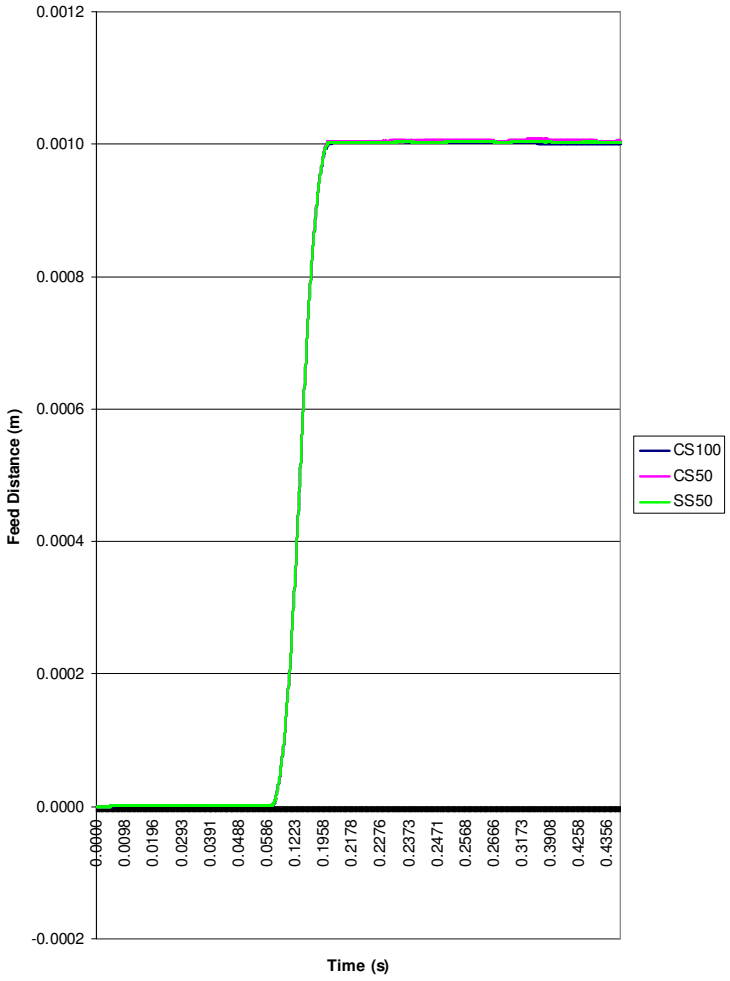

Fig. 7.5: Feeding characteristic for all strips for 1mm feed distance, 2Hz frequency configured at 45-45 motion profile without brake force.

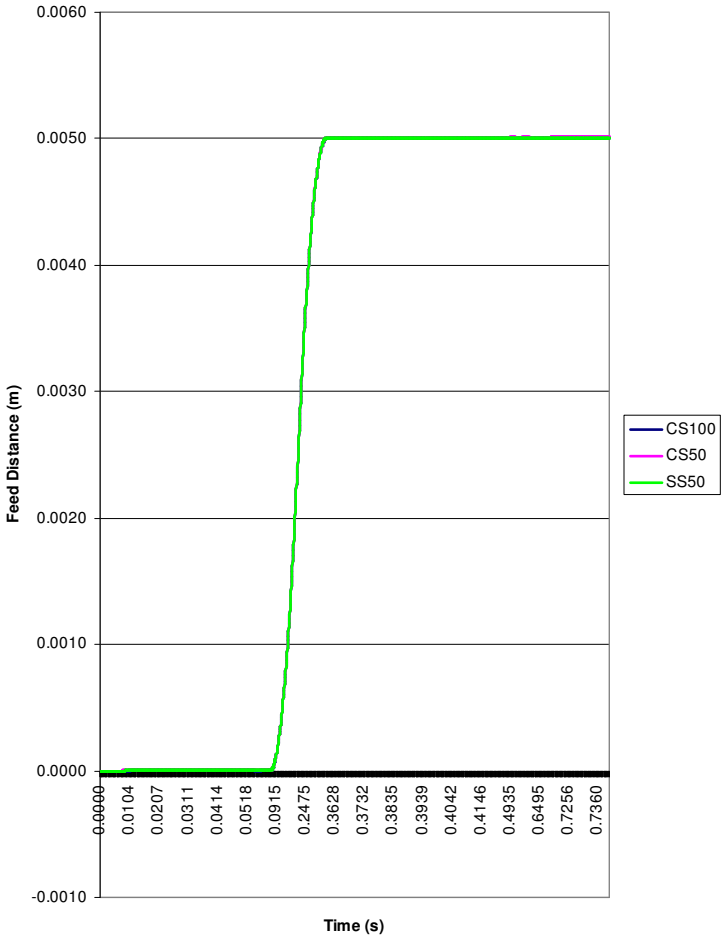

Fig. 7.6: Feeding characteristic for all strips for 5mm feed distance, 1Hz frequency configured at 45-45 motion profile without brake force.

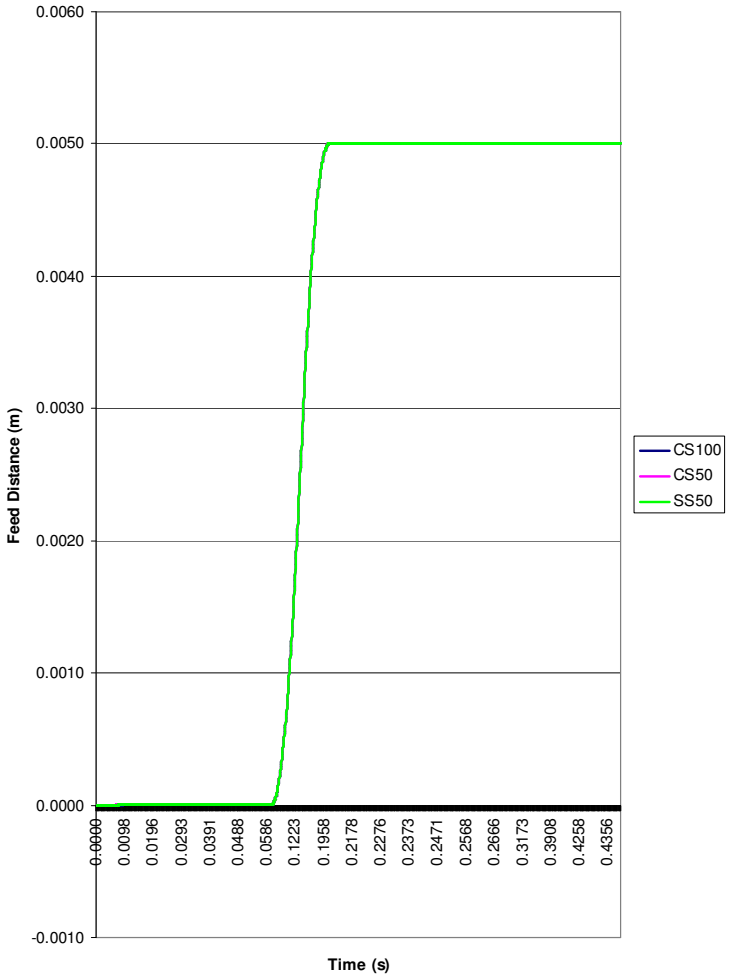

Fig. 7.7: Feeding characteristic for all strips for 5mm feed distance, 2Hz frequency configured at 45-45 motion profile without brake force.

The application of brake force with the 45-45 motion-profile curve resulted in a better settling-pattern throughout the feeding process. A consistent settling-pattern was observed for all strips at both shorter and longer feed-distances and frequencies, as shown in Fig. 7.8, Fig. 7.9, Fig. 7.10 and Fig. 7.11. Due to increase in the strip tension, maintained by the brake force, the strips were seen to be less-easily disturbed, hence promoting a better settling-positional-accuracy. A similar result was found for both frequencies when the motion-profile was change to 50-50, as depicted in Fig. 7.12, Fig. 7.13, Fig. 7.14 and Fig. 7.15. The returning of the gripper to the home position did not interfere with the achieved settled-pattern, for all strips. To

quantify the inaccuracies resulted from the feeding process, close-up observation was carried out, focused on the arresting-step of the gripper.

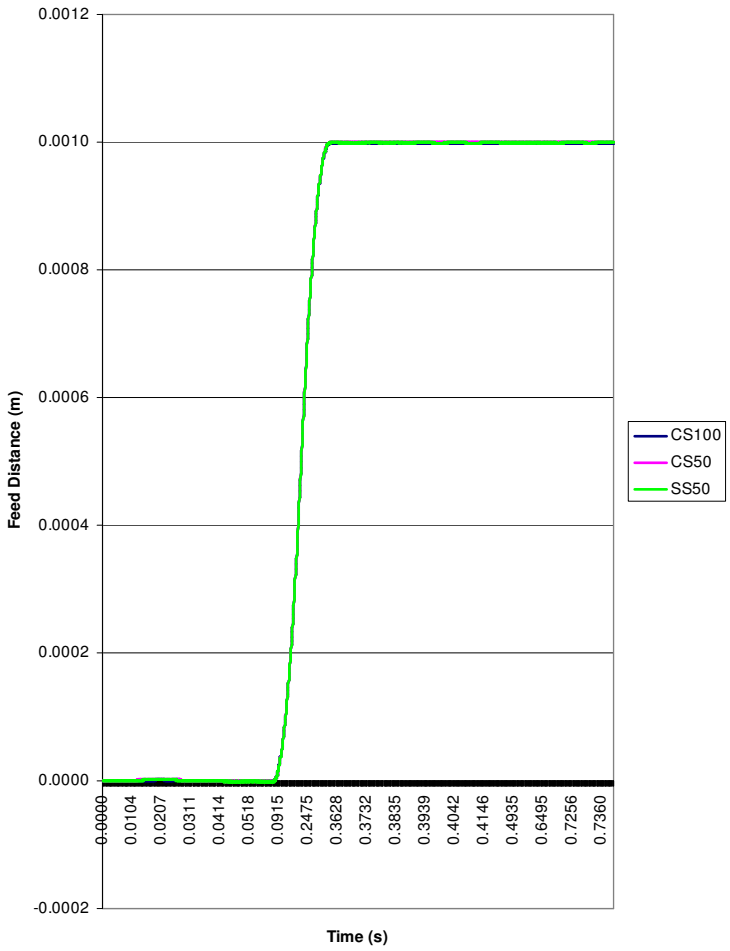

Fig. 7.8: Feeding characteristic for all strips for 1mm feed distance, 1Hz frequency configured at 45-45 motion profile with brake force.

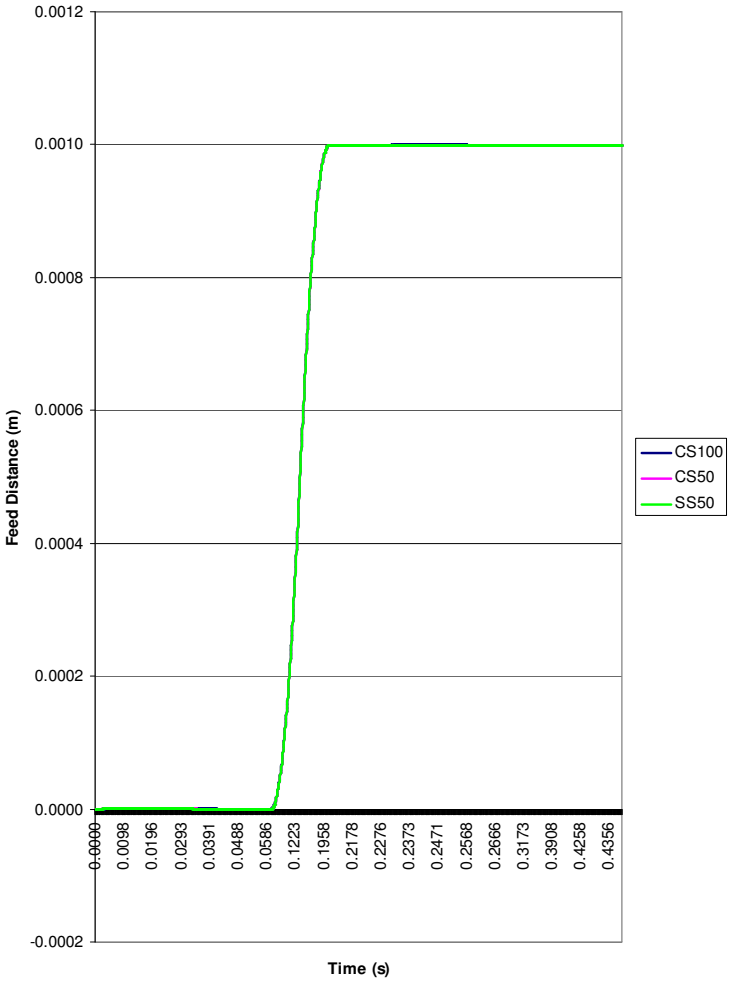

Fig. 7.9: Feeding characteristic for all strips for 1mm feed distance, 2Hz frequency configured at 45-45 motion profile with brake force.

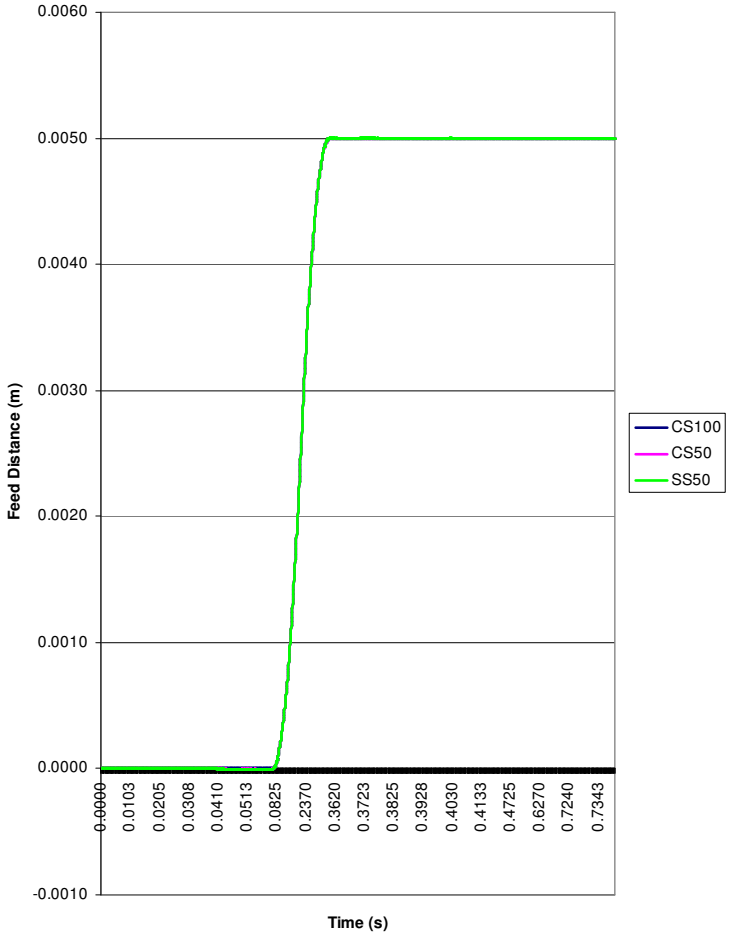

Fig. 7.10: Feeding characteristic for all strips for 5mm feed distance, 1Hz frequency configured at 45-45 motion profile with brake force.

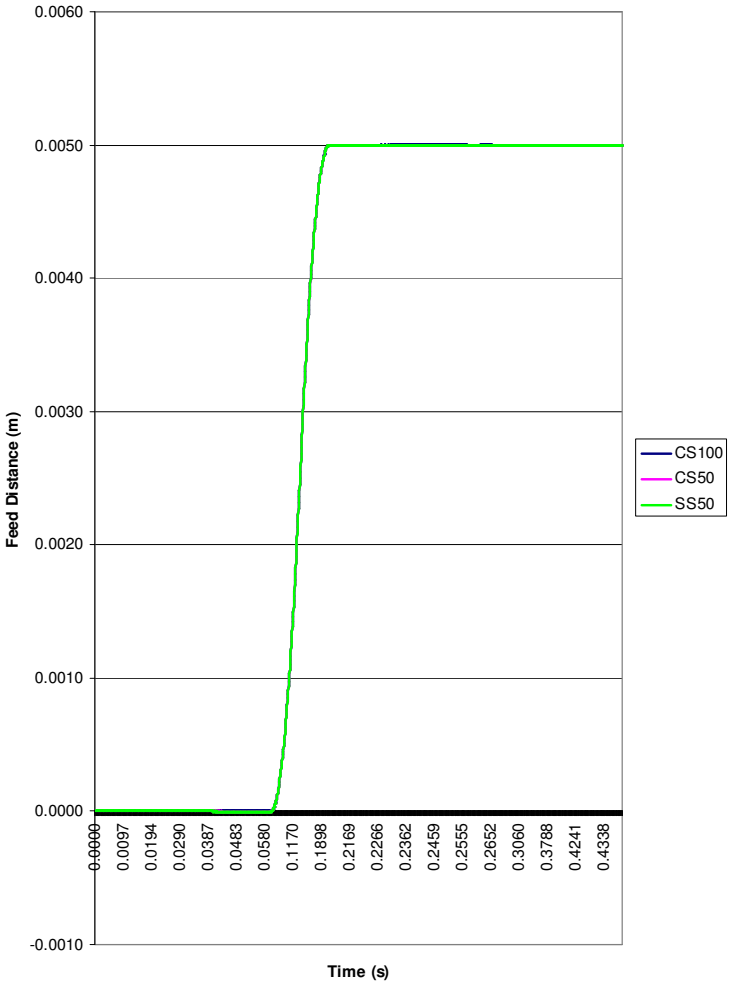

Fig. 7.11: Feeding characteristic for all strips for 5mm feed distance, 2Hz frequency configured at 45-45 motion profile with brake force.

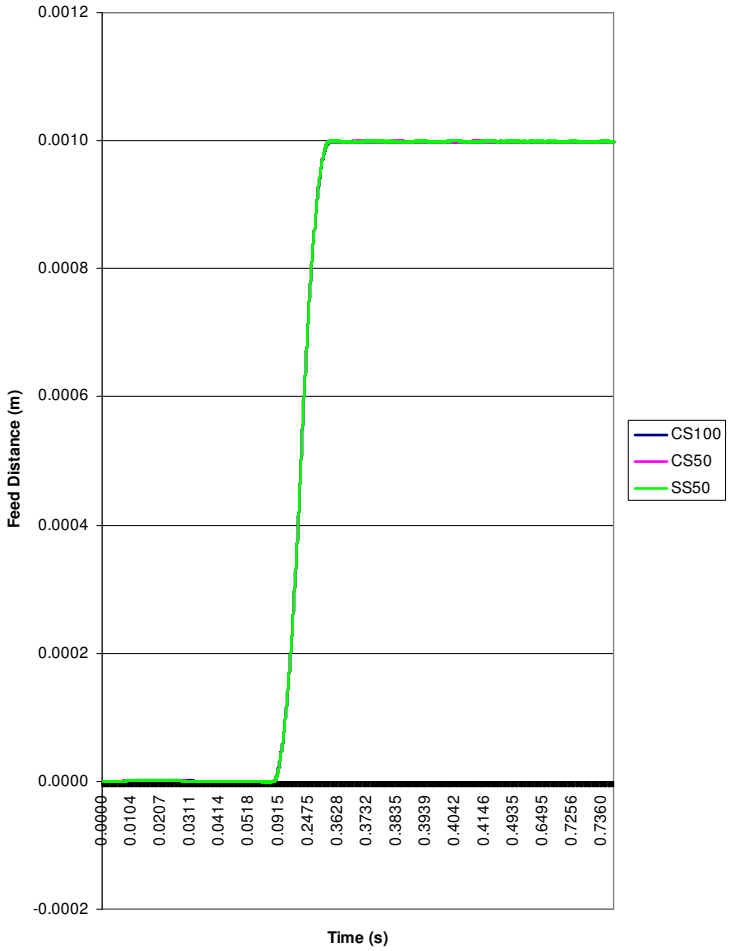

Fig. 7.12: Feeding characteristic for all strips for 1mm feed distance, 1Hz frequency configured at 50-50 motion profile with brake force.

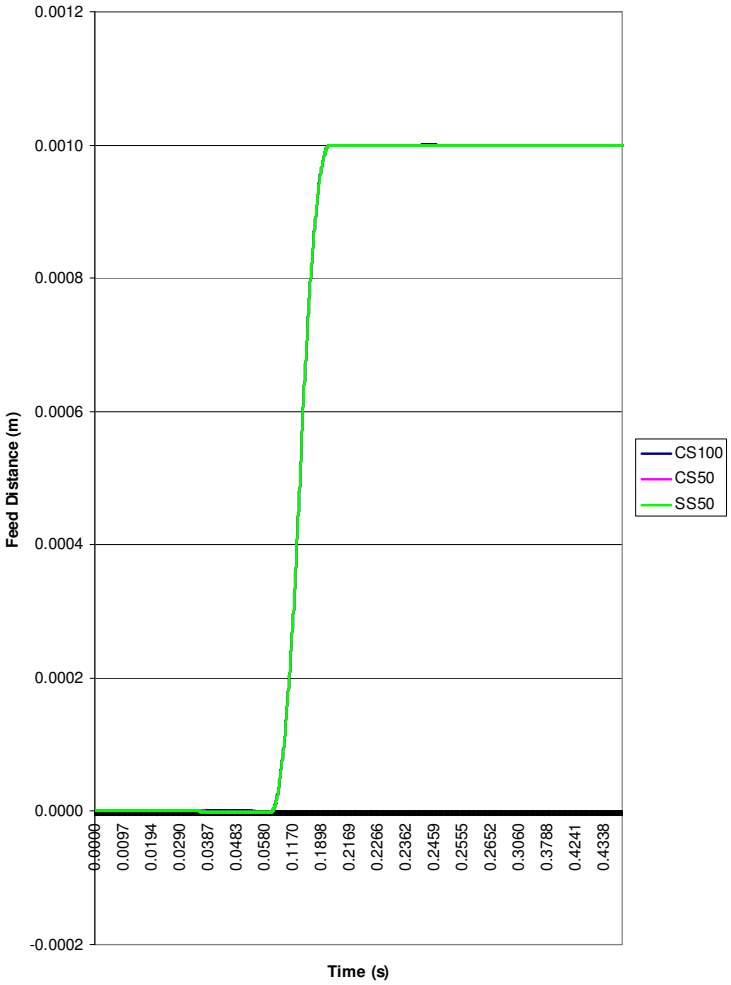

Fig. 7.13: Feeding characteristic for all strips for 1mm feed distance, 2Hz frequency configured at 50-50 motion profile with brake force.

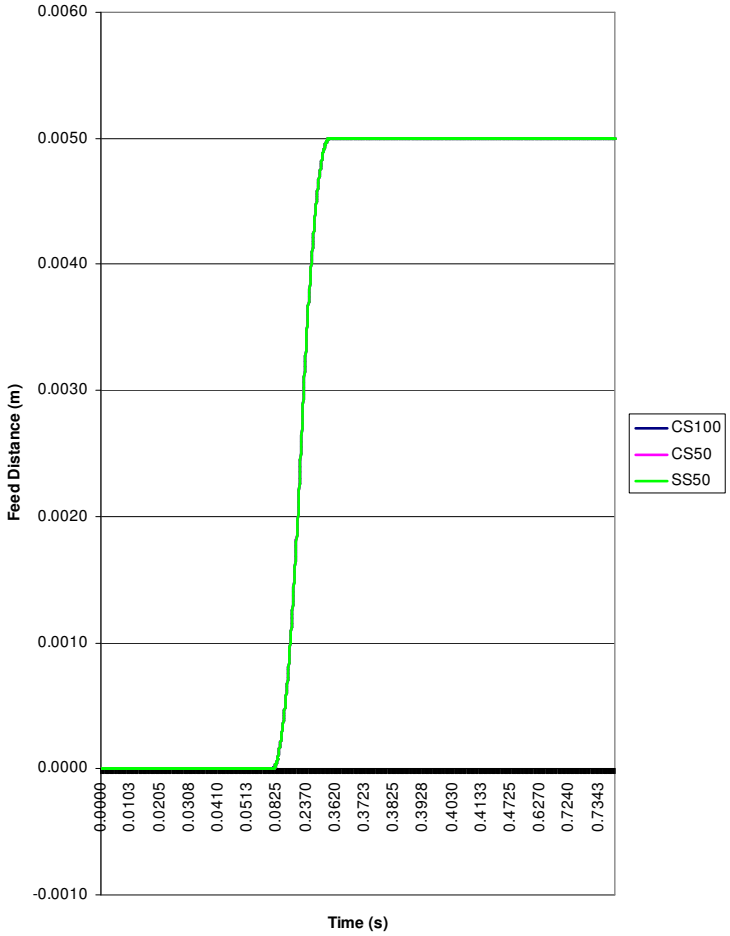

Fig. 7.14: Feeding characteristic for all strips for 5mm feed distance, 1Hz frequency configured at 50-50 motion profile with brake force.

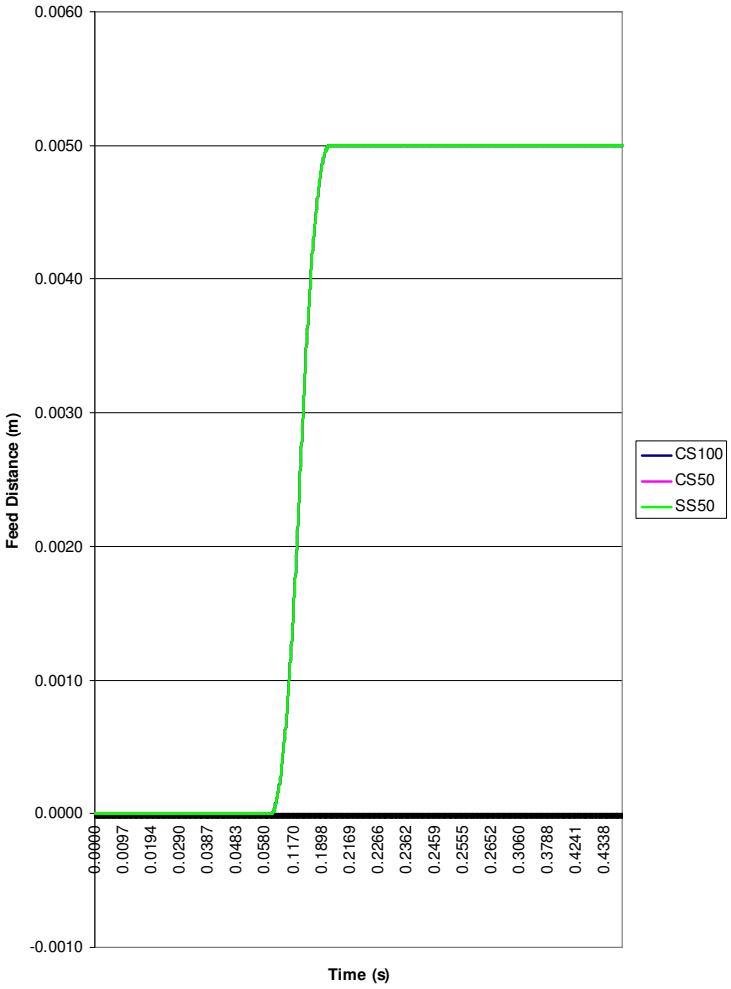

Fig. 7.15: Feeding characteristic for all strips for 5mm feed distance, 2Hz frequency configured at 50-50 motion profile with brake force.

7.4.2 Effect of Brake Force

a) 1mm feed-distance

Fig. 7.16 and 7.17 represent the feeder performance at 1 and 2Hz feed frequency for 50µm-thick carbon-steel (CS50). Based on these figures, without brake force being applied a large positional inaccuracy was recorded for both frequencies, where 1Hz frequency was observed to give a slightly worse positional-accuracy of 8.7µm, compared to that for 2Hz, which was 5.5µm. The positional-settling-trend without brake force was also observed to be unstable, where a large deviation-dispersion was recorded for both frequencies.

The application of brake force was observed to reduce the deviation-dispersion significantly and at the same time to improve the positional-accuracy for both of the frequencies tested, as shown in both Fig 7.16 and Fig. 7.17. Although an underfeed-trend was observed throughout the feeding process at both frequencies, the positional accuracy recorded was significantly better compared to the no-brake-force results. At 1Hz, the positional accuracy when brake force was applied was -0.8µm, and -0.9µm at 2Hz feed frequency. Reduced deviation means that less vibration and waviness was experienced by the strip, which suggests that the strip is more resistant to unwanted force when brake force is applied.

A similar trend was observed also when thicker carbon-steel strip was used (CS100). Without the presence of brake force, a large deviation was recorded, which suggested that the strip is vulnerable to severe waviness due to motion and vibration, as depicted in Fig. 7.18 and Fig. 7.19. Although vulnerable to unwanted forces acting during feeding, the positional-accuracy however, has been recorded to be close to absolute feed distance for both of the frequencies tested.

Fig. 7.18 and Fig. 7.19 also show the feeder-performance when subjected to brake force. Although tighter deviation-dispersion was observed for both of the frequencies, slightly deterioration and an underfeed trend in the positional accuracy was recorded, with 1Hz being observed to have a slightly poorer positional accuracy at -2.3µm when compared to for 2Hz, which was -0.8µm.

A consistent positional accuracy trend was also recorded, as shown in Fig. 7.20 and Fig. 7.21, when 50µm-thick stainless-steel (SS50) strip was used without the presence of brake force. The very large deviation-dispersion suggests that the strip became waved during the feeding-process. At 1Hz the positional accuracy settled at 4.7µm, while at 2Hz the positional accuracy settled at 2.9µm, which was far better.

Similar findings as for CS50 were observed with the stainless-steel strip, where the application of brake force leads to an improved positional-accuracy and at the same

time an improved repeatability. The settled positional accuracy for both 1 and 2Hz frequencies when subjected to brake force was recorded as -1.0µm and -0.7µm, respectively. Again, a similar trend in the results as for CS50 and CS100 was recorded for SS50. Good agreement between the results was found where the application of brake force may cause the positional accuracy pattern to shift to an underfeed pattern.

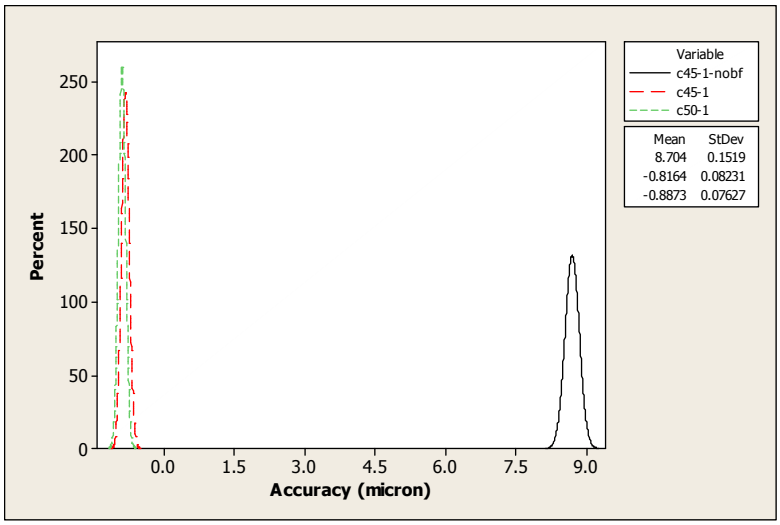

Fig. 7.16: Settled positional accuracy pattern for different motion profile curve and effect of brake force for CS50 strip at 1mm feed distance and 1Hz feed frequency.

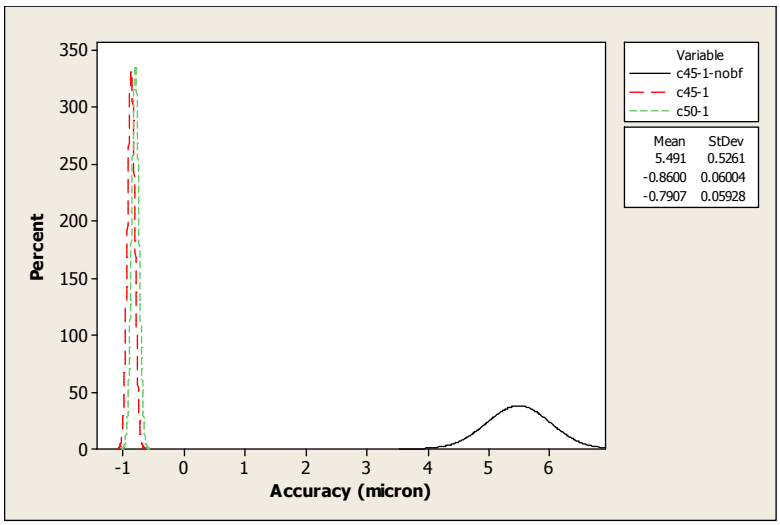

Fig. 7.17: Settled positional accuracy pattern for different motion profile curve and effect of brake force for CS50 strip at 1mm feed distance and 2Hz feed frequency.

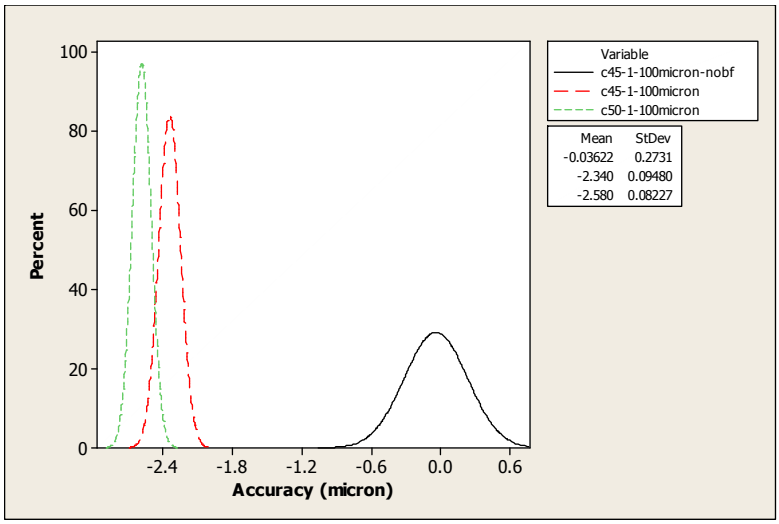

Fig. 7.18: Settled positional accuracy pattern for different motion profile curve and effect of brake force for CS100 strip at 1mm feed distance and 1Hz feed frequency.

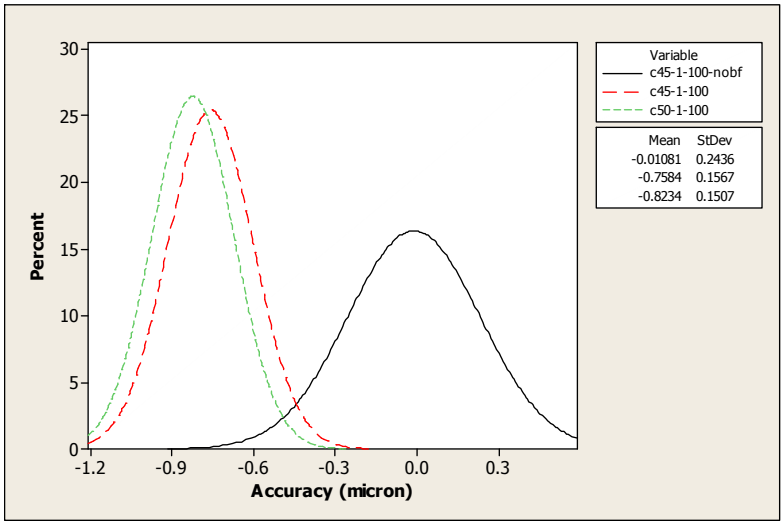

Fig. 7.19: Settled positional accuracy pattern for different motion profile curve and effect of brake force for CS100 strip at 1mm feed distance and 2Hz feed frequency.

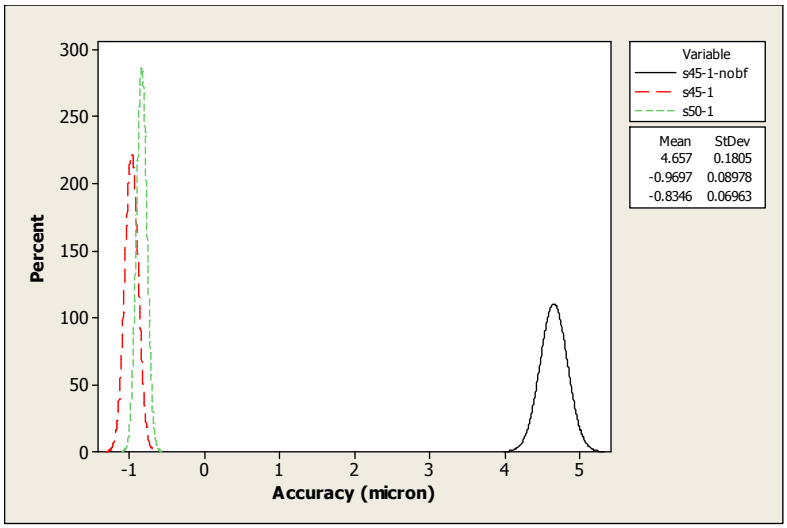

Fig. 7.20: Settled positional accuracy pattern for different motion profile curve and effect of brake force for SS50 strip at 1mm feed distance and 1Hz feed frequency.

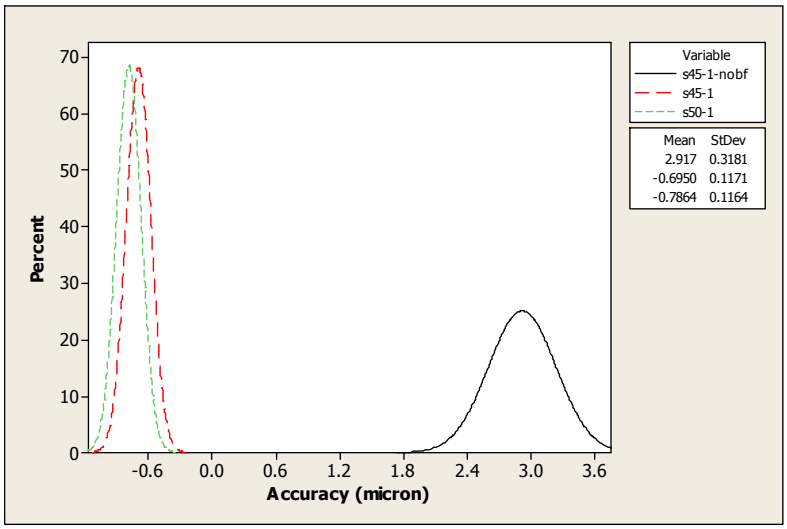

Fig. 7.21: Settled positional accuracy pattern for different motion profile curve and effect of brake force for SS50 strip at 1mm feed distance and 2Hz feed frequency.

b) 5mm feed distance

Fig. 7.22 and Fig. 7.23 show the feeding pattern for CS50 strip at both 1 and 2Hz feed frequencies. Reduced positional accuracy was observed when the feeding of the strip was without the presence of brake force. At 1Hz, the positional accuracy settled at 10.5µm, while at 2Hz feed frequency the positional accuracy was at 5.6µm. Apart from the strip being positioned with less positional accuracy, the absence of brake force resulted in large deviation-dispersion. Instability of the positional accuracy-settling trend was believed to be the main contributor to deteriorate process deviation.

More-controlled and tighter deviation-dispersion was observed when brake force was applied. However, a similar underfeed-settled trend was observed for both 1 and 2Hz frequencies. At 1Hz feed-frequency, the positional accuracy was improved from 10.5µm (without brake force) to almost zero, while at 2Hz, an improvement from 5.6µm to -1.3µm was achieved. Although at 1Hz a settled-positional accuracy was observed, better than for 2Hz and differing from result presented for low feed-distance, the improvement-gap (i.e. the amount of improvement) shows that if the same achieved gap were applied to the 1Hz situation, this would return the positional accuracy to 3.5µm and not to 0µm. Hence, it can be assumed that brake force still has the capability to improve positional-accuracy.

As shown in Fig. 7.24 and Fig. 7.25, for the feeding of CS100 strip without brake force, the positional accuracy settles at 1.5µm and 1.3µm for 1 and 2Hz feed-frequency, respectively. A smaller deviation-dispersion was also recorded at 2Hz feed frequency, which settled at almost 0.2µm, and at almost 0.4µm for 1Hz feed frequency. In addition, the positional accuracy recorded at this feed was slight less, compared to that for a shorter feed-distance.

The presence of brake force improved the settled-positional accuracy, at almost -1.0µm and zero for 1 and 2Hz, respectively. Also, less vibration and waviness of the strip were observed, which was confirmed by the smaller deviation-value compared to that for the no-brake-force case. This is mainly because the strip was a less susceptible to unwanted force acted during the feeding process. A better-settled positional accuracy was also recorded for this 5mm feed-distance when compared to that for 1mm-distance.

The feeding performance of SS50 strip at both 1 and 2Hz feed-frequencies is shown in Fig. 7.26 and Fig. 7.27. Good agreements was found in the findings for with and without the application of brake force, but the strips, were waved, this leading to inaccuracy. At 1Hz feed-frequency, the settled-positional accuracy was 7.1µm and

the deviation was almost 0.2µm. At 2Hz, a settled-positional accuracy of 2.9µm was achieved with a quite large deviation of 0.3µm.

When brake force was applied, an improvement in positional accuracy was achieved: 0.5µm and almost -1.0µm were recorded for 1 and 2Hz, Significant improvement of deviation was also achieved, thus indicating in increase in the strip-resistive-capability to force disturbance. Another good-agreement was achieved, where brake force was seen capable of improving the positional-accuracy, not only for the tested SS50, but also similarly for the other strip-materials, feed-distances and feed-frequencies.

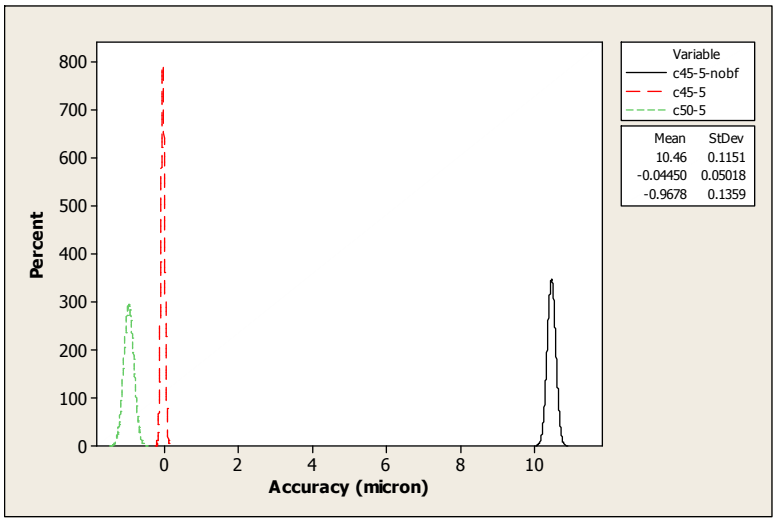

Fig. 7.22: Settled positional accuracy pattern for different motion profile curve and effect of brake force for CS50 strip at 5mm feed distance and 1Hz feed frequency.

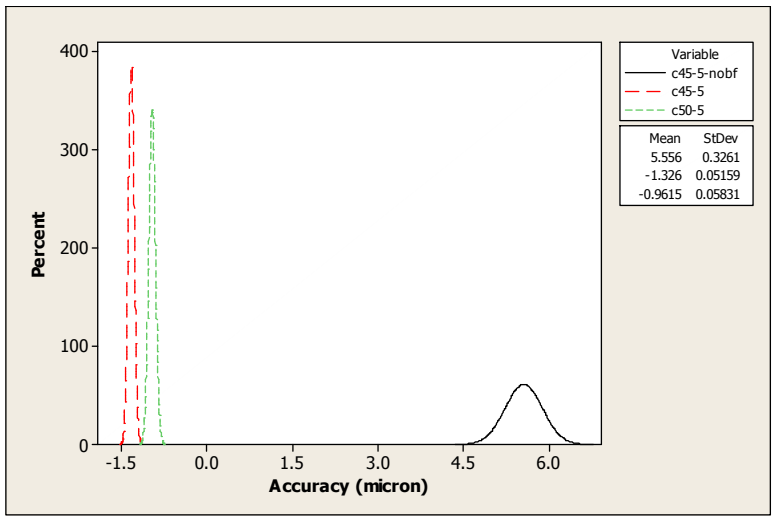

Fig. 7.23: Settled positional accuracy pattern for different motion profile curve and effect of brake force for CS50 strip at 5mm feed distance and 2Hz feed frequency.

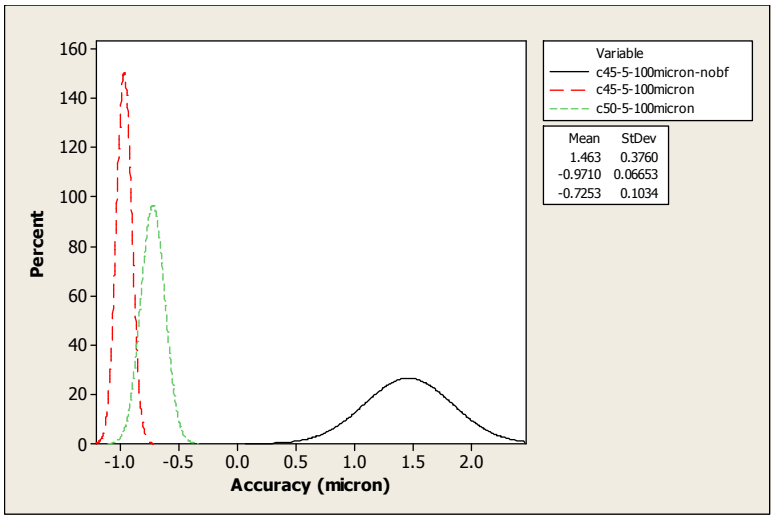

Fig. 7.24: Settled positional accuracy pattern for different motion profile curve and effect of brake force for CS100 strip at 5mm feed distance and 1Hz feed frequency.

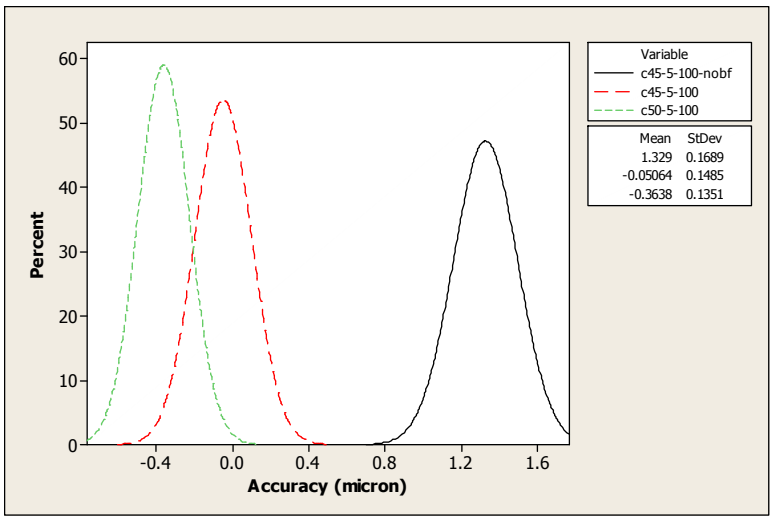

Fig. 7.25: Settled positional accuracy pattern for different motion profile curve and effect of brake force for CS100 strip at 5mm feed distance and 2Hz feed frequency.

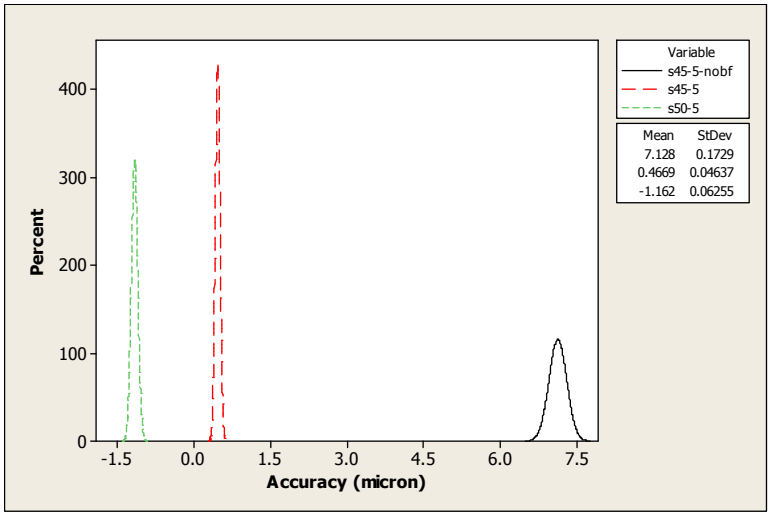

Fig. 7.26: Settled positional accuracy pattern for different motion profile curve and effect of brake force for SS50 strip at 5mm feed distance and 1Hz feed frequency.

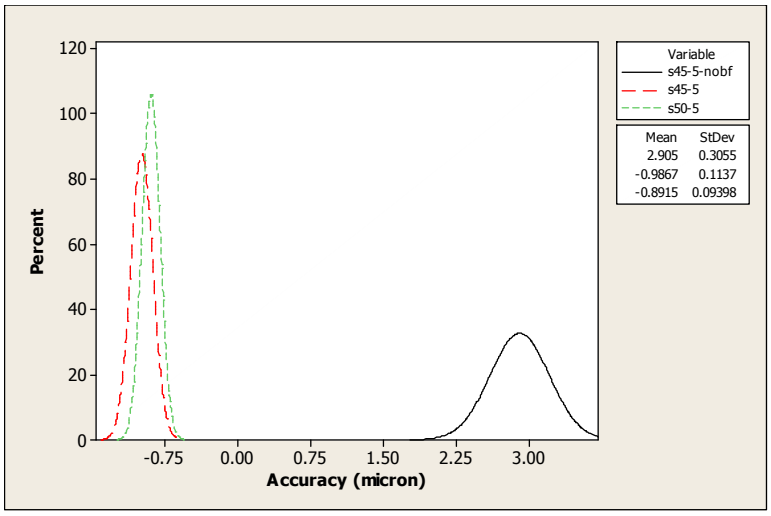

Fig. 7.27: Settled positional accuracy pattern for different motion profile curve and effect of brake force for SS50 strip at 5mm feed distance and 2Hz feed frequency.

7.4.3 Effect of change of the motion-profile

a) 1mm feed-distance

The change of the motion-profile from 45-45 to 50-50 for CS50 strip at both 1 and 2Hz, as shown in Fig. 7.16 and 7.17, did not make a significant contribution to improving the positional accuracy. An almost similar positional accuracy and deviation were recorded for both of the frequencies tested. However, as demonstrated by Fig. 7.18 and Fig. 7.19, slightly better positional accuracy was achieved when the 45-45 motion-profile was used to test CS100 strip at both of the feed frequencies. A similar finding as for CS50 was observed also when the strip material was changed to stainless-steel (SS50), where only a slight improvement was achieved. Based on the results presented in Fig. 7.20, for 1Hz feed-frequency, change from the 45-45 to the 50-50 profile resulted in a slightly better mean-positional accuracy and a tighter deviation-pattern. However, as depicted in Fig. 7.21, at 2Hz, a slight deterioration of the mean-positional accuracy was recorded for the 50-50 profile when compared to the findings for the 45-45 profile. Nevertheless, an almost-similar deviation was recorded for both profiles. These results suggest that no significant improvement can be achieved through a change of the motion-profile curve, especially for less-stiff material such as CS50 and SS50 at short feed-distance. However, with the thicker carbon-steel strip CS100, the positional accuracy might be reduced due to the sharp and steep motion-profile curve.

b) 5mm feed-distance

A significant deterioration of positional accuracy was observed when the 50-50 profile was used on CS50 at 1Hz feed frequency, as depicted in Fig. 7.22. A more-than0twice-wider deviation-dispersion was also observed for the 50-50 profile, which suggests that the strip had suffered from an unstable feeding-process which led to slight waviness, hence reducing the settled-positional accuracy. Differently to the 2Hz results, the steeper 50-50 profile resulted in the mean-positional accuracy shifting slightly to a better settling-position, shown in Fig. 7.23, compared to that for the 45-45 profiles. Nevertheless, an almost similar deviation-pattern was observed, suggesting that no improvement was achieved.

Not much improvement of the positional accuracy and the deviation-pattern was observed when the 50-50 profile was used on CS100 strip at 1Hz feed frequency, as shown in Fig. 7.24. Although a slightly better mean-positional accuracy was achieved by the change, the deviation-dispersion, however, experiencing deterioration, and led to unstable strip feeding. A differ observation was recorded for 2Hz feed-frequency as shown in Fig 7.25, where the use of the 50-50 profile resulted in a quite-significant reduction of the mean-positional accuracy. Moreover, the change also did not have a contribution to improving the process-deviation, where an almost-similar deviation was recorded for both the 45-45 and 50-50 profiles.

At 1Hz feed-frequency, a change from the 45-45 to the 50-50 profile resulted in significant positional inaccuracy, as shown in Fig. 7.26. Not only was the mean-positional accuracy reduced by the change, a little unstable feeding was observed also, indicated by a quite large deviation value. Depicted in Fig. 7.27, the 50-50 profile with 2Hz feed frequency promoted almost no change on the positional accuracy. Although the process-deviation can be seen improved, the increase did not make a big difference between the results for the two different profiles.

Although change of the motion profile may lead to an improvement in positional accuracy at a certain feed-distance and frequency, nevertheless, at the same time this has resulted in deterioration for other of the tested strips (CS50 and SS50). A balance

of the level of improvement achieved and the deterioration caused during the feeding process for both materials (carbon steel and stainless steel) has made a good and a bad contribution to the two profiles, hence, no significant improvement may be expected with the change of motion profile. Nevertheless, the steeper motion-profile (50-50) was seen to have many disadvantages rather than benefits with thicker carbon-steel strip (CS100). Reduction of the mean-positional accuracy and process-deviation was experienced when the 50-50 profile was used. Therefore, the 45-45 profile was seen as giving the most promising solution to improving the positional accuracy and reducing the deviation for the strip. Based on these results, it is suggested that the 50-50 profile may cause unstable feeding characteristic for certain feed-distances and frequencies and abandoning this profile may be a reasonable solution for providing better positional accuracy and lesser process-deviation.

7.5 Discussion

7.5.1 Effect of Brake-Force

The application of brake force has been demonstrated to provide better stability of the settled pattern while keeping the positional-error at a low level. The brake force, which was applied to the ends of the strip edge to represent the decoiler brake-force-effect on the feeding process, resulting in consistent strip-tension throughout the gripper feeder and decoiler, reduced the error and increased the stability during settling. This was achieved by reduction of strip-waviness through proper constraint introduced on one of the strip's end while the other end was kept constrained by the clamping of the retainers and the gripper. Reduced waviness of the strip through maintained- and consistent-tension has made the strip more resistant to disturbance force during the feeding process. The absence of brake force applied to the system, on the other hand, has made the free end of the strip more vulnerable to disturbance, allowing it to absorb unwanted disturbance forces that lead it to become wavier. Due to many constraining points and the greater contact surfaces between the strip and the new feeder, the strip-waviness may be reduced through energy-absorption and damping by the feeder structure.

7.5.2 Effect of Change of the Motion-Profile

Based on the presented results, high 'jerk' motion does affecting the settled pattern and the positional error of the least-stiff material through the increasing of strip-waviness. It is suggested that reduction in jerk promotes a better-settled stability and less positional-error, this is supported by the results of the 45-45 motion-profile curve-configuration. With this configuration, the tendency to a high 'jerk' was reduced by the less steepness of the acceleration- and deceleration-phases, both of which are prone to 'jerking'. According to Newton's Third Law, increases in acceleration rate result in increases in force. Increases of this force may lead to strip curvature-formation as described by Uraoka et al., (2009). According to these authors, the higher the strip motion is, the greater the curvature-formation on the strip will be. The authors also suggested a guide to be used to correct the curvature. However, the simple idea on how to reduce the curvature is to reduce the sharp transition between the acceleration and the deceleration phases. By reducing both of the sharp transitions, 'jerk' may be reduced. This indirectly reduces unwanted transition forces. The reduction of such force in turn leads to reduction of curvature formation of the strip. For the 45-45 motion-profile configuration, minimization of the 'jerk' value led to decreasing of acceleration, hence keeping the reaction force low. Additionally, a low acceleration value leads to lesser strip inertia. This in turn reduces the waviness tendency.

Although the inertia of the strip and the driving-gripper was seen to be greater in value than that of the roll feeder (which could lead to increased strip waviness, although such increase did not occur), the contact-area between the strip and the feeder itself is seen as an advantage. The increase in contact area compared to that of in the roll feeder enabling the dissipation of unwanted inertial energy through the feeder structure. In addition, the presence of brake force increased the strip tension, which increased the resistance of the strip to unwanted disturbance, hence less waviness may be expected.

7.5.3 Effect of Change of Feed-Distance and Frequency

A greater feed-distance requires a high velocity and acceleration to accomplish the feeding process within a similar as for a shorter feed-distance. This indirectly increases the inertia of the gripper and the driven strip. This inertial disturbance is found to be a useful source of compensation for brake force that helped the gripper to move the driven strip as close as possible to the desired feed-distance. Another factor which could possibly increase inertia is the strip's mass. A thicker strip has greater mass than a thinner strip. This in turn leads to increase of the total inertia during the feeding process. Along with the inertial forces produced by the high-speed motion, a greater compensatory effect may be produced to compensate for the brake force acting on the strip.

A shorter feed-distance, on the other hand, requires a lesser velocity and acceleration to achieve the desired distance. This in turn leads to a lesser inertial effect being produced during the feeding process to compensate for the acting brake force. The large positional error found for thinner strip could be explained by its lesser mass. Thinner strip has lesser mass than thicker CS100 strip, which in turn leads to a relatively lesser inertia than that for thicker strip. A lesser mass-inertia along with a lesser inertia due to low-speed motion results in less force to compensate for the acting brake force, hence there is greater positional error.

Similar findings were obtained when the system was subjected to different feed frequencies. The greater feed-frequency (2Hz) requires half the cycle time to accomplish the feed cycle than that for the lower feed-frequency (1Hz). This in turn leads to greater velocity and acceleration being required to achieve the designated feed-position. Although different values of velocity and acceleration between feed-frequency and feed-distance may be calculated, this however leads to a similar consequence, involving the increasing of motion velocity and acceleration. Thus, similar findings between the two configurations (feed-distance and -frequency) may be expected.

7.5.4 Limitation of the FE Software

In general FE-simulations, the work-material is invariably assumed to be perfectly uniform – geometrical and metallurgical defects are assumed not to prevail. This is because in simulation, limitation does exist where everything is considered perfect and this is different to reality. Moreover, the mechanical transmission was assumed to be perfect – no backlash, play, wear and tear were modelled.

In the servo mechanism, the motion step-response usually tends to result in positional overshoot during motion. Positional overshoot could be found more easily in, and is more associated with, high-speed motion. This is mainly because of sudden changes of acceleration-deceleration phase and vice versa. The model was designed based on the S-curve amplitude, where changes of the acceleration-deceleration phase or 'jerk' may be minimized, hence producing better positional accuracy without high positional-overshoot. This was observed when the acceleration-deceleration phase was changed and no excessive positional overshoot was recorded.

7.6 Conclusions

The characteristics of thin-sheet feeding with the new feeder-concept were studied with reference to the changes of: feed distance; material thickness and type; motion-profile curves; and the application of brake force. From the FE-simulation results, it can be concluded that:

i. The new feeder concept may be used for micro-sheet-forming applications due to greater settling-positional accuracy being achieved.
ii. Stiffer sheet-material was positioned better than less-stiff material, with better settling-positional accuracy being achieved for CS100 compared to that for thinner CS50 and SS50.
iii. The application of brake force improved the feed-settling pattern, where better settling-stability and positional accuracy was achieved.
iv. The low-jerk 45-45 motion-profile was the best profile for the feed process due to lesser instability being observed and better positional accuracy being achieved.

Chapter 8

Construction of the New Feeder and its Validation

8.1 Summary

This chapter explains development works of the new feeder. The approach begins with explanation of type of linear motor used to establish the design concept followed by solenoid being used for clamping system. Iron-less linear motor was used as the feeder actuator while clamping system is realized by using three solenoids; two for retaining and another one for gripping mechanism. The works continued with the fabrication of feeder's structure, followed by assembly of the linear motor, and selected solenoids. Linear motor configuration and setup was done by servo drive software while the motion was programmed through Codesys® machine control software. The finished feeder then was successfully integrated to the micro-forming machine developed by the University of Strathclyde [Qin et al., 2008] without any motion optimization is carried out. Validation experiment was carried out with a view to determine the usability of the feeder. Several parameters were tested and being evaluated. This includes change of feed distance and frequency, application of brake force and lubrication. In addition to that, different strip material and thickness were also tested. Based on the results, high positional repeatability was achieved. Load disturbance may be seen as one of the reason in contributing positional error and suggested that the feeder was less in stability.

8.2 Introduction

As what has been discussed previously, an iron-less linear-motor is chosen, as this motor features very-smooth continuous motion and high-precision positioning-capability, compared to the iron-core type. The working nature of the linear motor is to applying load on top of the carrier, which latter is normally known as the stage. As the stage moves, the load also moves. The direct drive of the load exhibits better positioning-accuracy and precision compared to that of a mechanical transmission-system. Comprehensive analysis has been conducted in order to determine the force required to move and transfer the load within the designated travel-distance and time-frame. This ensures that the load is moved within a reasonable time and with good repeatability. Lack of thrust force results in failure to move the load and heat build-up, while over-design leads to a costly system due to an unnecessarily-bulky linear motor being required. The appropriate design has been sought to ensure that the selection is made by considering the best option available. Sometime, design and development-work require systems that are not standard or available commercially. If this is the case, a custom-build system is necessary as a way to achieve a solution. Nevertheless, most researchers tend to avoid this option, as it is a time-consuming option. Not only does this solution require the building of the system piece-by-piece from scratch, but also integrating different parts from different manufacturer is also a tedious and pain-staking process. Machining error from various assembled parts might cause the failure to meet tight design-tolerances due to accumulated machining-errors: the integration of each part has to carried out properly to ensure compatibility, as incompatibility affects the system performance, hence degrading the final outcome. Issues related to the selection of a linear-motor stage for developing a high-precision feeder for a micro-forming machine are considered, specifically with regard to the linear-motor and servo-motor controller, and the linear-motion guideways. This is followed by validation experiments to confirm the operability and performance of the developed feeder. All results were presented, discussed and explained further.

8.3 Procedure

8.3.1 Design and Fabrication Work

Similar to the pneumatic-feeder concept, the new feeder system uses a clamping mechanism to grip and feed, as well as to retain the strip in position during the return stroke. As with the pneumatic feeder, all actuations are realized by pneumatic cylinders. However, for the new high-precision feeder, linear actuation is realized by means of an iron-less linear motor, while the clamping mechanism has a separate stand-alone system. Fig. 8.1 shows the concept of the new feeder. Two separate systems required to establish the feeder are the linear-motor stage and the clamping mechanism.

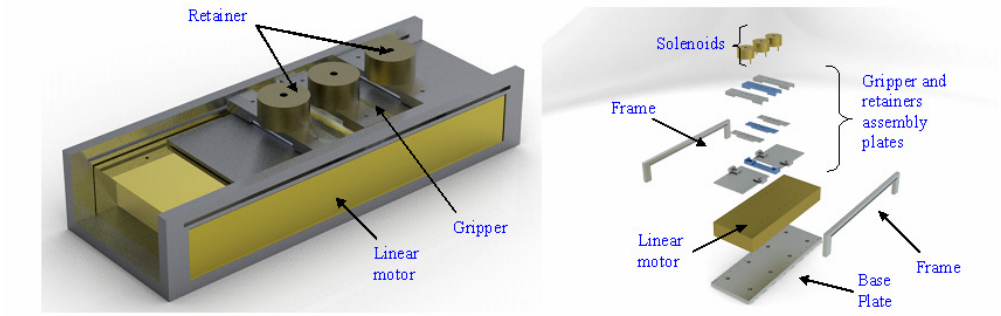

Fig. 8.1: Conceptual design of the high-precision micro-forming feeder.

Based on the design, the retainers are suspended onto a pair of bridges made from aluminium alloy grade 6082-T6. The bridges are bolted securely onto the feeder's base plate with M3 bolts. The gripper is mounted onto the movable stage using a pair of M3 bolts. A flush platform-level is created on the strip-entrance slit of the retainers and the gripper as to enable the strip to rest flat in the system.

Feeding a metal strip by the linear-actuation method requires a mechanism that will hold the strip firmly during the feeding process. Sufficient holding-force is vital to avoid slipping of the metal strip, as this would cause mis-fed which would lead to positional inaccuracy in feeding. Previously, other methods were used to hold the strip metal during the feeding process: a pneumatic gripper, a mechanical-cam gripper [SMC Pneumatics; Bruderer], and a piezoelectric-actuator [Physik Instrumente]. Three types of devices were identified as being suitable to be used for

the clamping mechanism for a linear-actuation feeding-application: a pneumatic cylinder, a piezoelectric-actuator and a solenoid, as discussed in Chapter 6.

8.3.1.1 Introduction to the Proposed Linear-Motor Stage System

Based on the linear-motor sizing-analysis made in the previous chapter, a Parker I-Force linear-motor stage/positioner, model T1D 110-2, was chose as a platform to study the potential of the linear-motor stage as a high-precision and high-speed feeder. Fitted with a 0.1µm Renishaw optical encoder, this stage, as depicted in Fig. 8.2, has a positioning-acceleration and a speed of 5g and 450mm/s, respectively, with 0.1µm motion resolution. High-repeatability potential over a long travel-distance has made this stage suitable for an application which is required to be reasonably fast, but where positional accuracy and repeatability are the main concerns. The stage is capable of delivering 45.2N and 202.5N continuous-force and peak-force, respectively, during operation. The combination of a high continuous-force and a high positioning-repeatability is the key in the selection of this stage for a high-precision feeder for micro-forming-machine applications.

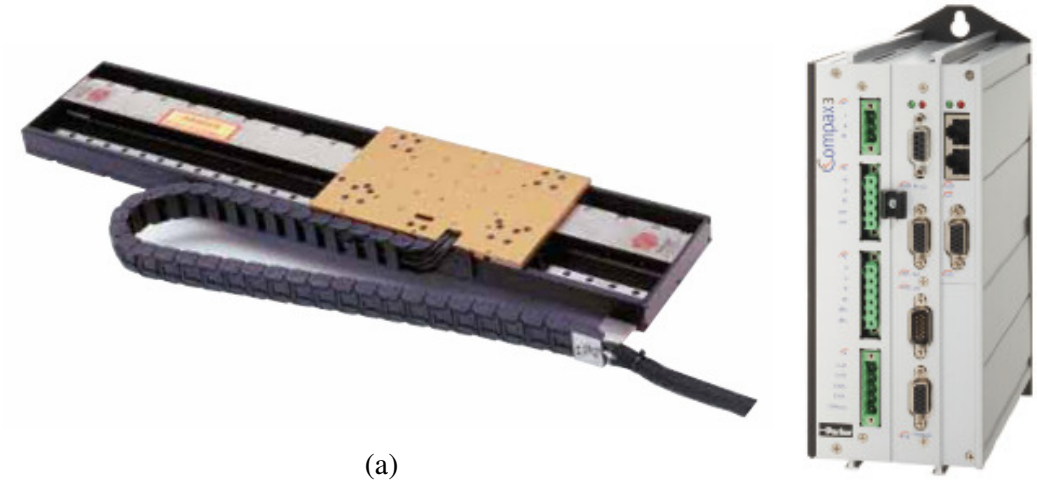

(a) (b)

Fig. 8.2: Parker I-Force products: (a) linear-motor stage/positioner model T1D 110-2; and (b) Compax3 servomotor controller.

The stage's physical dimensions are further advantages compare with other possible stages. Measuring 311mm length, 169mm width and 50mm height, this stage is easily fitted onto the confined space of the micro-forming machine. Being made with a base of flat aluminium ensures that this stage has better flatness and parallelism than can be obtained from extruded aluminium. The stage has dual-bearing guideways and a stiffer structure to ensure better positioning-performance.

The T1D 110-2 stage requires a 240VAC single-phase 50Hz supply to operate, and with the Compax3 servo-drive controller, make the best pair for the system. With its high-performance and modular design, the Compax3 servo-drive controller offers a new level of servo-performance and flexibility. The modular structure of the Compax3 allows options such as intelligent motion-controllers, fieldbus interfaces and industry-standard motor-feedback. Moreover, numerous expansions can be added to the standard Compax3 controller in order to optimize its capabilities, to meet the requirements of demanding servo-applications. A CANbus communication interface on the Compax3 controller enables it to communicate with other types of controller via a master-and-slave hierarchy. This level of machine-control architecture enables the alteration of parameters can be carried out on the master controller, thereby avoiding disturbance to the programme master and the slave controller separately. With this kind of technology, the adjustment or alteration of parameters is a simple and no longer painstaking process.

Being a 240VAC and single-phase 50Hz controller, direct tapping from a domestic 3-pin socket to run the stage is possible: this thus, avoids the necessity to provide a higher-voltage and -current supply such as 240VAC 3-phase as well as 415VAC 3-phase. According to Qin, (2006a), and Okazaki et al., (2002), the development of micro-manufacturing is impeded by large power-supply requirements and a big machine-size. Big or power-guzzling machines are no longer seen as good practice in the micro-manufacturing world.

The pieces were mounted together to form a fully-working feeder before the machine-programming work was started. CoDeSys® machine-programming

software was used to define and program the feeder's home-location and motion-profile. Finally, the feeder was mounted on the existing micro-sheet-forming machine developed by the University of Strathclyde.

8.3.1.2 Introduction to the Selected Solenoids

Of small size and weighing around 170gram, the conical-face-type solenoid selected has a holding force of 71.2N peak, and gradually decreasing over a longer stroke, as depicted in the performance chart of Fig. 8.3. From the chart, the response time for 2mm stroke-length is 7ms, as demonstrated by Fig. 8.4. This impressive response-time has made the solenoid suitable for applications which demand high-throughput operation. This conical-face type-solenoid is used purposely for a retaining mechanism to avoid the occurrence of excessive deformation of the suspended base of the clamping-mechanism structure. Nevertheless, the conical-face-type solenoid is better in an application that requires a longer stroke.

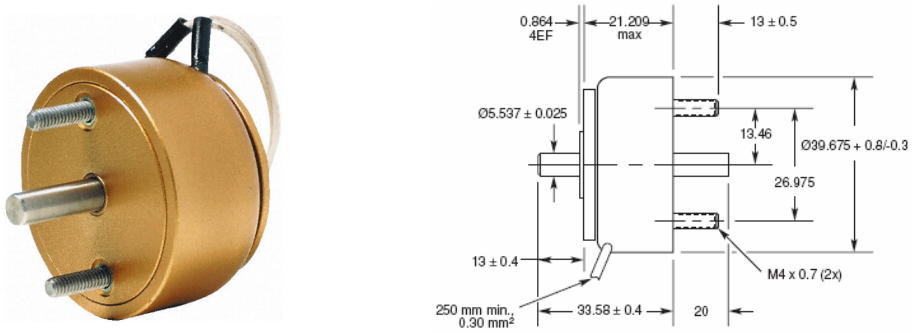

Fig. 8.3: (a) the solenoid used, and (b) solenoid dimensions [LEDEX].

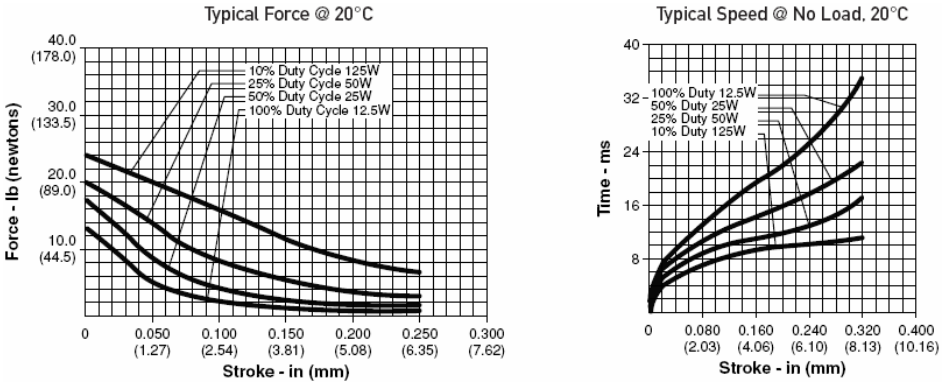

Fig. 8.4: Performance-chart force against stroke-length; and stroke-length against response-time; of the conical-Face-type solenoid [LEDEX].

Another type of solenoid is the flat-face type. Of similar physical-geometry to the conical-face type, this solenoid has greater holding-force: as much as double that of the as conical-face type, being 164.6N, as shown in Fig. 8.5. This type of solenoid is found to be more suitable for use in the gripping mechanism, since the brute force ensures greater holding force to avoid strip-slippage during the feeding process. Moreover, due to the gripping-mechanism design, where there is no suspended section forming the clamping mechanism, the extra force does not have a significant effect in deflecting the base. Up to a 1mm gap for the gripping mechanism has also supported the decision made to choose a flat-face-type solenoid.

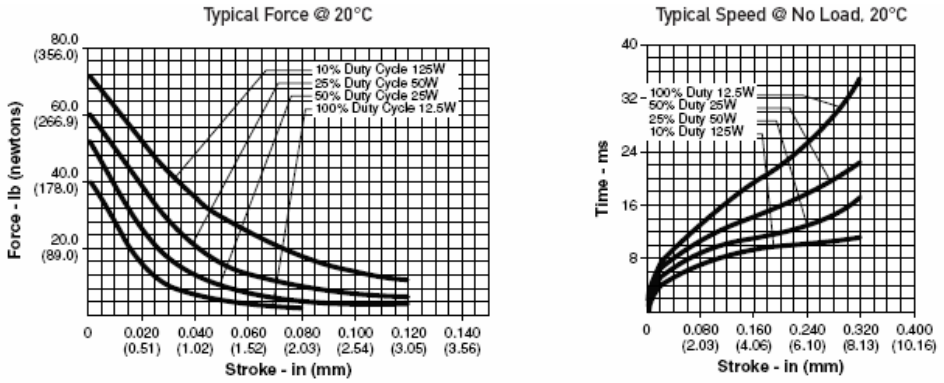

Fig. 8.5: Performance-chart force against stroke length, and stroke-length against response-time; of the flat-face-type solenoid [LEDEX].

8.3.1.3 Assembly of the LMS Frame and the Clamping Devices

a) LMS frame – An assembly of a linear-motor stage and a linear-motor frame/structure

Although the chosen linear-motor has built-in positional feedback (a linear-encoder), mechanical guideways, bearings and a frame to make this stage fit onto the machine, a mounting frame is required. The stage is mounted on the confined micro-forming machine-structure and was set at the same level as the entrance-slit for the strip on the micro-forming-machine, for both the gripper and the retainer mechanism. This has resulted in a long flat surface for the strip to rest flat upon during the feeding process. A mounting frame, which acts as a platform to securely hold the linear motor stage as well as to accommodate the retainer and the strip, was designed as shown in Fig 8.6(a). The motor was secured to the mounting frame by twelve M3 bolts. The handles on each side were each secured with four M3 bolts, as shown in Fig. 8.6(b). The frame and the linear-motor stage were then secured to the machine platform using eight M6 bolts. Slight adjustment to the left or right is possible due to slot mounting having been designed to allow horizontal adjustment to match the slit position of the micro-forming machine. The new platform also acts as a compartment to store the stage inside as a safety precaution, and to avoid dust collecting on the linear-guide bearings-mechanism.

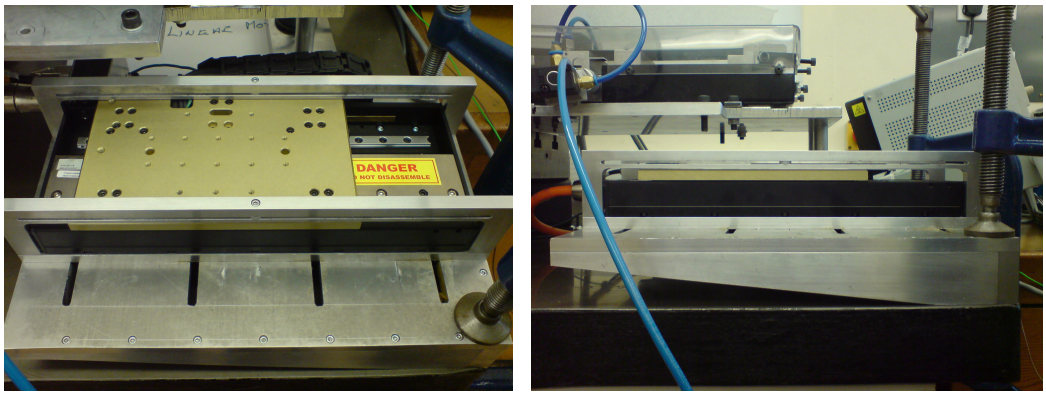

(a) (b)

Fig. 8.6: (a) top view; and (b) side view; of the assembly.

b) Assembly of the linear-motor stage frame and clamping devices

The clamping device consists of two parts, namely the gripper and the retainer. The gripper grips the strip and feeds it to the desired feed-distance, whilst the retainer holds the strip whilst the gripper returns to its original position before the start of the next cycle. As the nature of the motion implies, the gripper was placed on top of the movable-stage platform, while the retainer was placed on the fixed platform. The development work requires two retainers to hold the fed metal-strip securely and a gripper is required to do the feeding process. Both of the retainers were fitted onto the case handles using M3 bolts, with five bolts on both the right and the left side, as depicted in Fig. 8.7(a) and (b). This is to ensure that the clamping devices rest securely on the handle without excessive deformation during clamping process due to the high press-force provided by the solenoids. However, to be on the safe side, a 1.5mm gap was introduced as a safety precaution between the retainers and the movable stage in order to avoid contact under any circumstances, while at the same time keeping the stage safe from accidental damage.

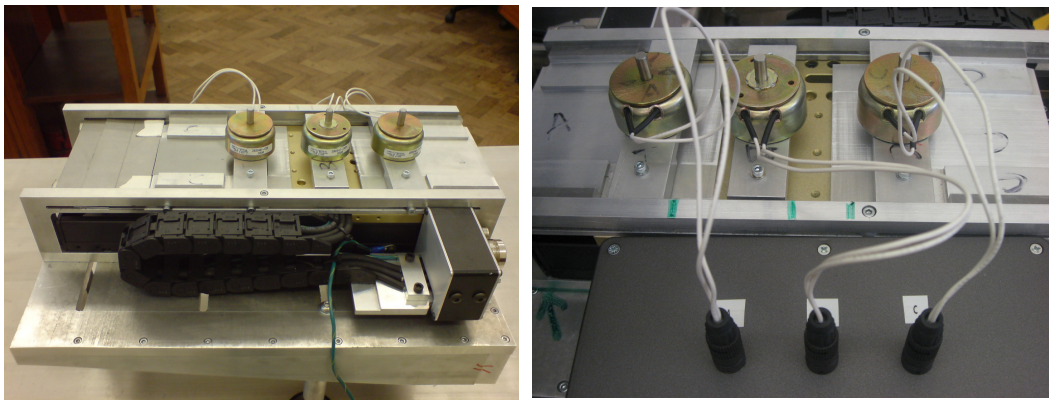

(a) (b)

Fig. 8.7: (a) fully assembled frame; and (b) installed clamping solenoids.

8.3.2 Machine Set-up and Motion-Programming

Although the selected stage is seen as a turnkey solution for the proposed system,, the programming and integration are quite challenging. The proposed feeder was planned to have: a performance and high-commercial value for commercialisation; a wide range of functional-configurations and operating-parameters, and the ability to

operate in a continuous rigorous environment. The next aspects that the servo-drive configuration uses Compax3 servo-manager software, and machine-programming by third-party programming software, so-called CoDeSys.

8.3.2.1 Compax3 Servo-Manager

The C3 Servo Manager Software is a windows-based configuration set-up software for Compax3 servo-motor systems. This software is used to configure the servo-motor drives in terms of linear-motor parameters, i.e. maximum load, brake resistor, travel limits, home position, braking criteria, braking due to errors/faults, etc. The software contents can be categorized into the following configurations:

i) Device selection
ii) Drive configuration
iii) Communication
iv) CoDeSys programming
v) Optimisation
vi) Downloading
vii) Uploading

i) Device selection

In this section, the servo-motor drive-configuration is made specifically on the basis of the power requirements, the feed-back system, and the interfaces used for integration and communication. There are five completed steps, these steps being: Step 1 – Select the Power Level; Step 2 – Select the Feed-back Type; Step 3 – Select the Interface; Step 4 – Select the Technology (Control) Level; and Step 5 – Select Special Options. Usually the selection from options that are available in each step can be made easily by retrieving the servo-motor drive's order-number, which is available on the drive's name plate.

ii) Drive configuration

Every servo-motor drive has to know what type of actuation it needs to control. In this case, the selection of the appropriate linear-motor is carried-out using the 'drive

configuration' option. Due to the linear-motor used not being in the Compax3 Servo Manager Software library, the key parameters of the motor were defined in the C3 Motor Manager. This configuration includes the determination of: the right servo-drive controller to drive the servo motor; the brake-resistor settings; the external-load definition; the travel-distance unit-selection; the homing-mode selection; the travel-limits settings; the jerk ramp-control criteria for emergency stopping; the limit-settings for maximum permissible-error of the defined linear-motor stage; the configuration of the encoder; the sources of error and type of reaction to be taken, and finally downloading the drive configuration onto the servo-drive controller.

iii) Communication

This setting was used to enable configuration of the communication interface being made between the computer's RS232 serial port and the servo-drive's communication port. Usually, a PC does come with a RS232 serial port and is automatically assigned to the com1 port. In the present case, two RS232 serial ports were used, the port being assigned as com1 and com2, in order to avoid conflict.

iv) CoDeSys Programming

Third-party software CoDeSys, was used as the machine programming language to define the machine's motion. This configuration enables the linking of a pre-programmed machine-motion program in CoDeSys format to Compax3 software for conversion and before being downloaded to the drives. This option also shows details such as the date and time of programming of the current programming-file that has been downloaded to the drive, hence making it easier to retrieve and counter-check what was programmed previously.

v) Optimization

This setting enables advanced optimization of the servo-drive settings in terms of classical P-D feedback manipulation and more advanced acceleration and current feed-forward controls. Adjustment of P-D control feedback was realized in this setting, where several designated parameters were adjusted and uploaded directly into the servo-drive controller.

vi) Download

This option enables written CoDeSys machine-programming language to be downloaded into the servo drives. Machine programming was done with the help of the graphical user-interface or GUI in CoDeSys. The machine program then was pre-checked and compiled in CoDeSys software and downloaded from the Compax3 software environment before being uploaded to the servo-drive controller.

vii) Upload

This option enables the retrieval of the contents of the current servo-drive configuration, as well as details of the programming language downloaded to the PC. The feeder configurations and written machine program was uploaded into the feeder's servo-drive controller for permanent storage and automated running. Having been uploaded once, the feeder may be operated automatically and synchronized with the micro-forming machine.

8.3.2.2 CoDeSys – Machine's Motion-Programming Software

CoDeSys is a third-party machine language-programming software which complies with the IEC61131-3 standard. This enables CoDeSys to be used to programme almost all of the current servo-drives from various manufacturers. There are three well-known programming methods which CoDeSys has to offer: ladder logic programming; C++ language programming; and graphical user interface (GUI) programming. For this research purpose, GUI programming method was used as it is proven easier and faster to programme the whole cycle compared to native C++ programming. Due to many steps and devices being involved, GUI seems very promising to solve the problem by step-by-step GUI plotting. There are three main steps taken to design the feeding-programming-language sequence: understanding the cycle; sketching the cycle flowchart and time-frame chart; and lastly GUI programming.

The numbers and types of devices involved during the feeding cycle for the linear-motor stage are two retainers and a gripper. Except for the linear-motor stage, all the

retainers, grippers and input commands were assigned with respective output and input from the Compax3 logic circuit. In order to initiate the cycle, a signal from the micro-forming machine is required, fed into linear-motor stage logic-circuit input. This is assigned as 'Input 0' on the servo-drive inputs. Two retainers were placed on both sides of the gripper in order to maintain strip tension. Both of these retainers are assigned to Outputs 1 and 3 on the servo-drives, and at the same time the gripper is assigned to Output 2.

In order to obtain a better view of controlling the devices and initiating each device in the correct sequence, a cycle flowchart was designed, shown in Fig. 8.8. Based on the flowchart, as soon as the feeding system receives a signal from the micro-forming machine, both of the retainers start to clamp the strip metal. This ensures that strip-metal tension is retained for the gripper to grip for the entire feed-cycle. 10ms time is allocated for the retainers to settle. As soon as the retainers are settled, the gripper starts to clamp the strip firmly. In this case, due to the nature of a solenoid, which requires settling time, 10ms are allocated for the gripper to grip the strip and settle. As 10ms of gripper clamping-time elapse, the retainers release the strip in 10ms in preparation to feed. The linear-motor stage then moves from the designated zero position by the designated travel-distance. When the linear-motor stage reaches the designated position, another 10ms settling time is allocated for the stage to properly correct its position as a means to improve the positional accuracy. As soon as the 10ms of the linear-motor-stage settling time elapse, both of the retainers start to clamp over the 10ms allocation time. When the retainers are settled, the gripper then begins to release the strip over 10ms time before the linear-motor stage returns to its zero position (home position) and settles over 10ms. At this stage, the linear-motor-stage drive triggers a signal to the micro-forming machine servo-drive as an acknowledgement of the completion of the cycle: only then does the next press cycle commence. The whole cycle repeats, depending on the setting of the feeding frequency on the linear-motor-stage drive.

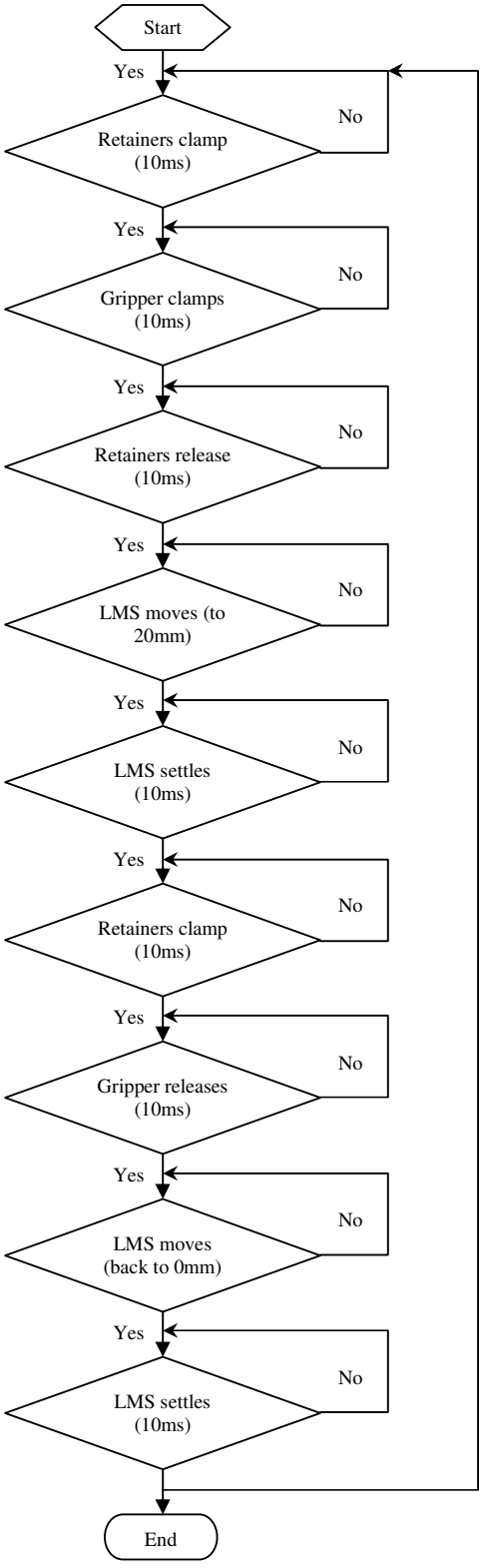

Fig. 8.8: Cycle-sequence flowchart for the feeding process.

The integration of all those devices with a linear-motor stage and when to initiate each of them is discussed further. For 2Hz feed-operation, each cycle has less than 0.5s in which to be completed. Due to the nature of this feeder, which employs reciprocating motion for the feeding process, the allocation of 0.5s now applies for both moves of the strip: to the designated position and the home-return operation. Thus it can be concluded that for one each cycle, a maximum of 0.25s is required for both the back and the forth operation. For this total of 0.5s, the time-triggering sequence for each device and linear-motor-stage motion was designed, as shown in Fig. 8.9. Due to the entire cycle relying on the signal triggered by the micro-forming-machine servo-drive, the initiation of this signal is considered as the input to trigger the whole feeding-cycle and named the 'start bit' on 'Input 1', as shown in the figure. From the analysis conducted and presented in the previous chapter, the speed and acceleration required to move the load for 20mm distance were found at 0.38m/s and 4.75m/s^2, respectively. The motion profile was divided into three sections, namely the acceleration, constant velocity and deceleration phases. The acceleration and deceleration phase was set at 40% of the 0.2s total linear-motor-stage moving-time while the constant-speed phase was set at 20% of the 0.2s. This may be simplified as the acceleration and deceleration phases taking 0.08s each to be completed, with 0.04s for the constant-speed phase. From this analysis, a time-trigger and sequence graph was plotted. Based on the graph shown, the feeding cycle was initiated immediately the linear-motor stage received the signal from the micro-forming-machine servo-drive. The time taken for each device to operate is also shown. Based on the sketched flow- and time-based chart, the machine programming was written using CoDeSys software and is shown in Fig. 8.10.

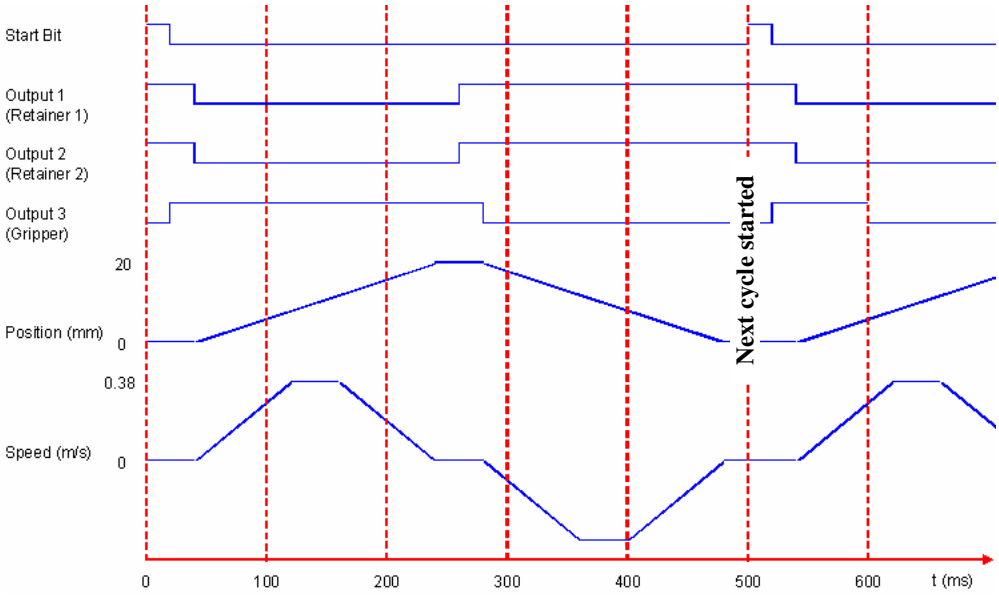

Fig. 8.9: Time-based control- and trigger-sequence.

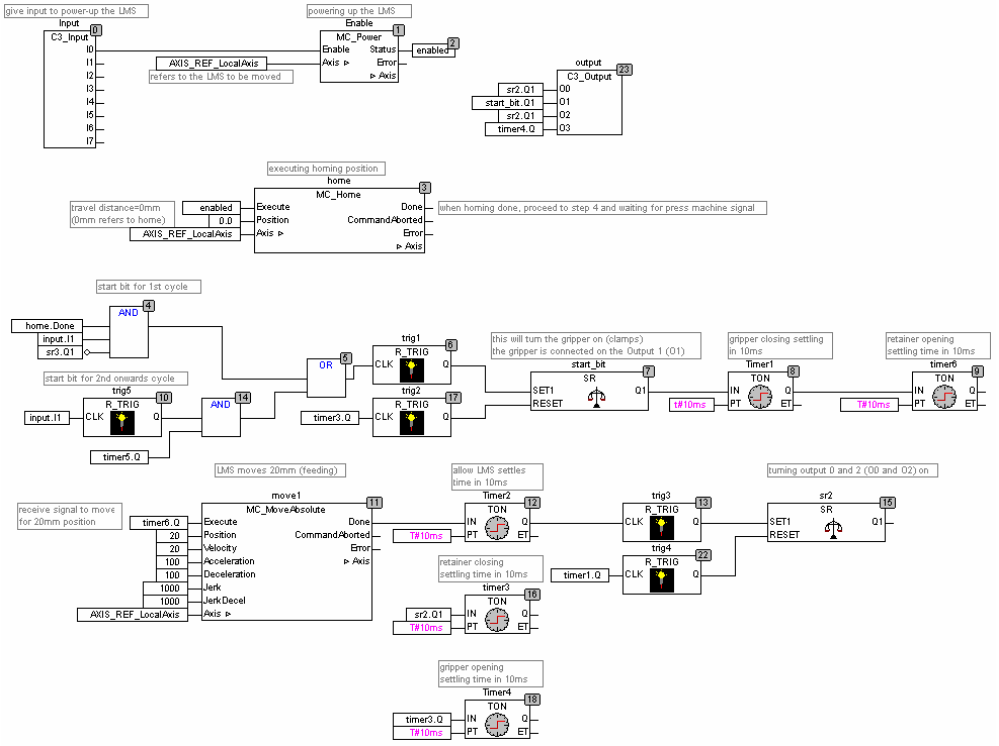

Fig. 8.10: CoDeSys GUI programming for the high-precision feeder.

8.3.3 Integration with the Developed Micro-sheet-forming Machine

The completed developed feeder is shown in Fig. 8.11(a). An acrylic cover complying with the IP52 standard was used, as shown in Fig 8.11(b), to conceal the moving parts in order to avoid injury and to comply with the University's Health and Safety Policy [University of Strathclyde]. Integration of the machine-control system, which is biased towards electrical circuits and connections is explained further in this section. Various power-supplies were used in this development work. There were two-times of stepping-down of the voltage done on the machine control-box: 415VAC 3Ø to 240VAC 1Ø, and then to 24VDC. 415VAC 3Ø was used to energize the micro-forming linear-motor, while 240VAC 1Ø was used to power-up the developed feeder's servo-drive. The developed high-precision linear-motor-stage feeder only take 24VDC, which was reduced from 240VAC 1Ø by a step-down transformer. Fig. 8.12 below describes all of the connected parts and devices.

(a) (b)

Fig. 8.11: (a) complete assembled feeder integrated with the clamping solenoids systems; and (b) the protective cover used to prevent injury and dust pollution.

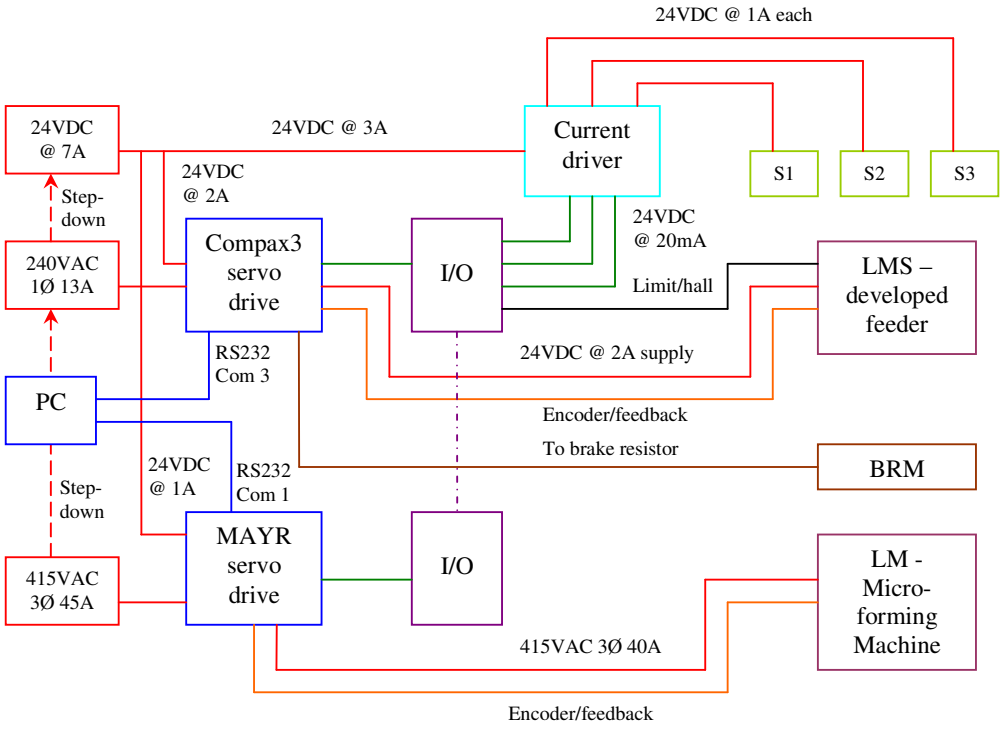

Fig. 8.12: Schematic diagram of the connections of the developed feeder with the micro-forming machine.

As shown in the figure, the development of the new high-precision feeder uses three solenoids to actuate the clamping mechanism where two are for retaining and the third is for gripping. These solenoids receive a signal from Compax3 servo drive to actuate. However, a circuit-driver is required to boost the 20mA currents supplied by the servo-drive up to 1A. This was done by switching on a high-current relay-circuit to enable the solenoids to perform at their best. An opto-coupler transistor was used as a relay to power-up the high-current circuit. An electrical-connection schematic-diagram of the solenoid-driver circuit is shown in Fig. 8.13.

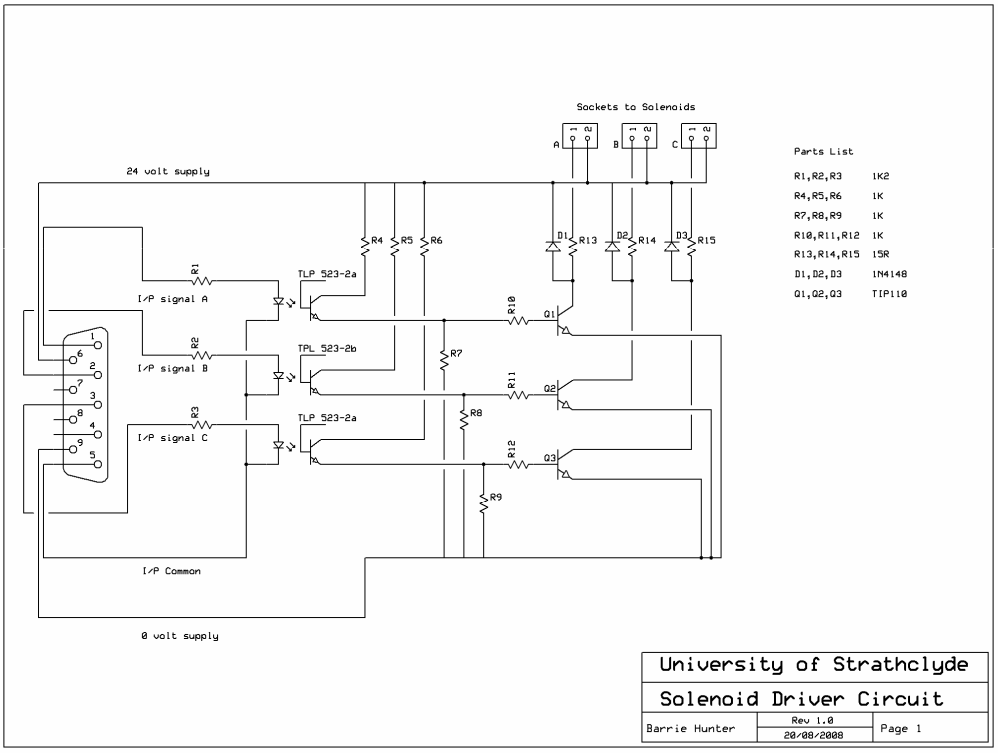

Fig. 8.13: Solenoid-driver circuit which uses an opto-coupler as a high-current switch-over relay.

The principle of the solenoid-driver circuit requires two different sources of supply which is 24VDC at 20mA supply from the Compax3 servo-drive was used to power-up the low-energy opto-coupler transistor, while other 24VDC supply, but at 1A, was used to actuate the solenoids. The opto-coupler transistor worked by completing the other, high-current circuit when only the low-current circuit is in the closed position; thereby, the high-current circuit is completed, allowing high-currents to flow to the solenoids. This circuit-method proved to avoid excessive time-delay, as only microsecond delay times are required to complete the circuit. The actuation time then can be shortened and saved, which has been proven better than using electromagnetic relays that may cause higher dwell-times due the 10-15milliseconds required energize and de-energize the relays. The solenoid circuit-driver was secured in an anti-static and magnetic box, as depicted in Fig. 8.14(a), and connected to the Compax3 servo-controller via its logic circuit shown in Fig. 8.14(b).

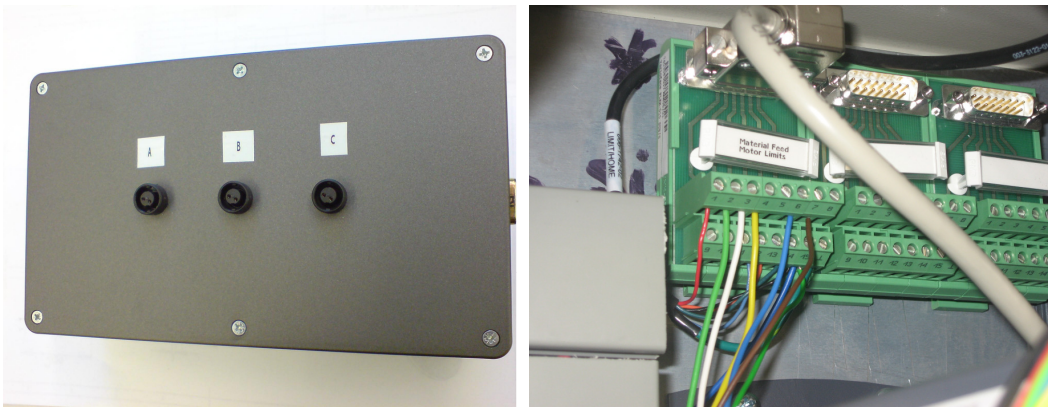

(a) (b)

Fig. 8.14: (a) the solenoid driver circuit box uses an RS232 interface to communicate with the Compax3 servo-drive through an I/O terminal in (b): the 3 sockets connect the retainers and the gripper solenoids.

As mentioned in previous sections, most of the servo-drives available commercially at the present time require an extra 24VDC power-supply to power-up their logic circuits. The Compax3 servo-drive is no exception, this drive receiving a 24VDC supply stepped-down from a 240V 1Ø supply. This 24VDC source also powers-up the linear-motor stage.

A brake-resistor motor, or BRM, was used in the system to avoid the current backflow that is generated during the deceleration of the linear-motor stage. Although the present servo-drives have the capability of accepting the backflow current, the capability is limited: any backflow current might cause the drive to trip and short-circuit. Hence, a brake-resistor motor is introduced to the system to minimize the possibility of backflow current to avoid catastrophic consequences occurring with the Compax3 servo-drive. A backflow current than exceeds the Compax3-drive-limits is diverted automatically to the brake-resistor motor. This backflow current is converted to heat, which dissipates easily into the environment via the BRM coil.

The developed high-precision feeder is actuated automatically when it receives a 24VDC logic signal from the micro-forming machine servo-drive. This low-level communication is chosen due to no other device/sensor being used during the forming process. In the case of other devices/sensors needing to be associated with the feeder system, communication via CANbus is feasible for both controllers. The process of actuating the feeder begins when the micro-forming-machine ram reaches the designated position, its logic circuit then sent a signal to the Compax3 servo drive to start actuating the feeder. As soon as the feeder has completed the feeding cycle, a feedback signal is sent back to the micro-forming servo-drive to actuate the next forming cycle.

8.3.4 Experiments

Validation experiments were conducted to demonstrate the working of the feeder and to validate the initial performance without servo-drive optimization. Similar parameters as the previous micro-servo roll-feeder's optimization experiments were used in order to be able to accurately compare the performance of the two feeders. Non-contact measurement [Gao et al., 2006] using linear encoder carried out to determine the positional accuracy and repeatability of the feeder.

Control feedback (PID) was not varied with a view to enabling the observation of just the effect of changes of feed distance and frequency, strip thickness, material and lubrication, on the positional accuracy and repeatability of the feeder. A similar feeding-time-frame as for the micro-servo roll-feeder experiments was used to create a fair basis for comparison.

The experiments started with 50µm-thick carbon-steel strip (CS50) being fed by the feeder without the presence of lubrication for both feed-distances, 1 and 5mm, at 1 and 2Hz feed-frequencies. This was followed by carbon-steel strip of 100µm thickness, CS100, which was tested at a similar configuration as for CS50. The strip material was changed to stainless-steel to examine the achieved positional-accuracy and repeatability. Finally, lubrication was introduced to the system for CS50 strip. The results are discussed and explained in the following.

8.4 Results

a) 1mm feed distance

As shown in Fig. 8.15(a), at 1Hz feeding-frequency, the results demonstrate that a thicker strip was positioned less accurately compared to a 50µm-thick strip. Based on the trend of the curve, 100µm-thick carbon-steel strip, CS100NL, was positioned with almost three-times the positional inaccuracy compared to the thin CS50NL. For 100µm-thick carbon-steel strip, the mean-positional accuracy was recorded at 11.7µm with ±1.9µm repeatability, while for 5µm carbon-steel strip the positional accuracy was 3.8µm, with repeatability of ±1.0µm.

The positioning of less-stiff material also demonstrated lesser positioning-accuracy compared to a stiffer and more-rigid material such as carbon steel. Based on the positional accuracy curve, 50µm stainless-steel strip, SS50NL, only half as accurate, and slightly less in repeatability compared to CS50NL, with an positional accuracy of 8.7µm and ±1.9µm repeatability over one sigma process capability.

The presence of lubrication presence for this low feed-frequency effected a large deterioration of positional accuracy. The positional accuracy was noted to reduce to one third of that for the non-lubricated case. 12.6µm mean-positional accuracy was recorded for 50µm-thick lubricated carbon-steel strip, CS50L. Nevertheless, this did not affect the repeatability-performance, which was still ±1.9µm.

Analysis of the repeatability performance was conducted, as shown in Fig. 8.15(b). A lesser deviation-dispersion was recorded when lubrication was introduced into the system, which suggests that lubrication may improve the repeatability of the feed process. Changes to different strip-thickness and material-type resulted in changes in the repeatability pattern. This suggests that each material has different feed-characteristics, which may be improved correspondingly by lubrication.

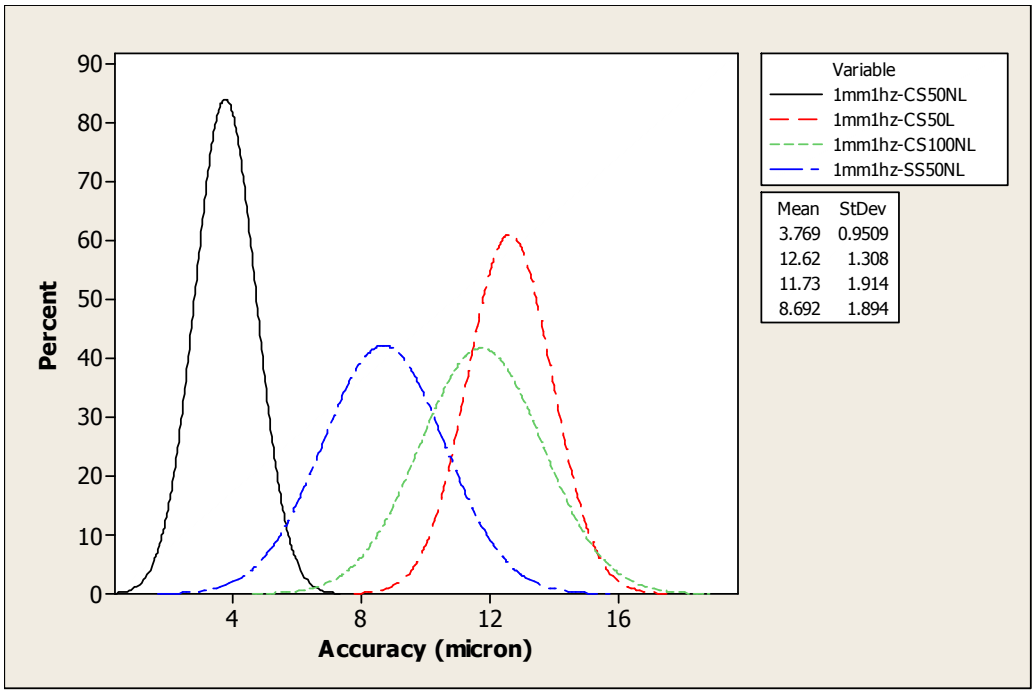

(a)

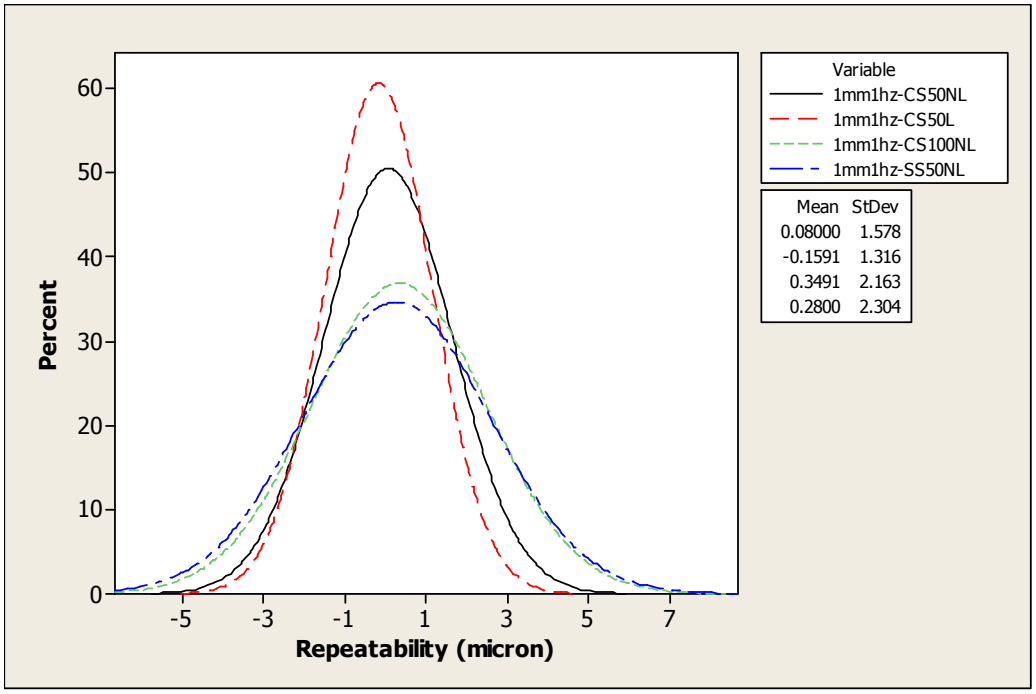

(b)

Fig. 8.15: Feeding performance at 1mm feed-distance and 1Hz feed-frequency: (a) positional accuracy; and (b) repeatability.

For 2Hz feed-frequency, depicted in Fig. 8.16(a), the positional accuracy deteriorated and the curve demonstrates a consistent underfeed-trend for all of the experiments. Based on this figure, the CS50NL positioning accuracy is -23.2µm, this is almost six times deterioration compared to that for 1Hz feed frequency positional accuracy. Slight deterioration in repeatability was observed also for CS50NL, with a value of within ±4.2µm, as shown in Fig. 8.16(a).

The positioning of thicker material, CS100NL, was observed to be slightly better compared to that for CS50NL, with recorded positional accuracy of -19.4µm and a repeatability of ±2.3µm. The positioning accuracy of less-stiff material, SS50NL was recorded at 20.4µm, which is slightly better than for CS50NL, but shared a quite similar repeatability as for CS50NL, of ±3.9µm. Nevertheless, based on the trend, lubrication was observed to make a slight contribution at higher feed-frequency. The mean positional accuracy of S50L was found to be 17.0µm. Moreover, the presence of lubrication was seen to improve the feed repeatability. A consistent repeatability-performance of ±2.7µm was recorded for CS50L.

Similar repeatability findings were observed as in the previous test, where the presence of lubrication in the system can improve the repeatability of the feeder. This is confirmed by the tight deviation-dispersion, as depicted in Fig. 8.16(b). Comparison between the bell-shaped curves of CS50NL and CS50L may be used to confirm the lubrication effect. Good agreement in the results was found when compared to the 1Hz experiment results. The change to greater strip-thickness was observed to secure better deviation dispersion, this suggesting that stiff material tends to be positioned with high repeatability. The different strip-materials used have resulted in a wider deviation-dispersion, which suggests that the least-stiff strip-material tends to promote repeatability-inconsistency.

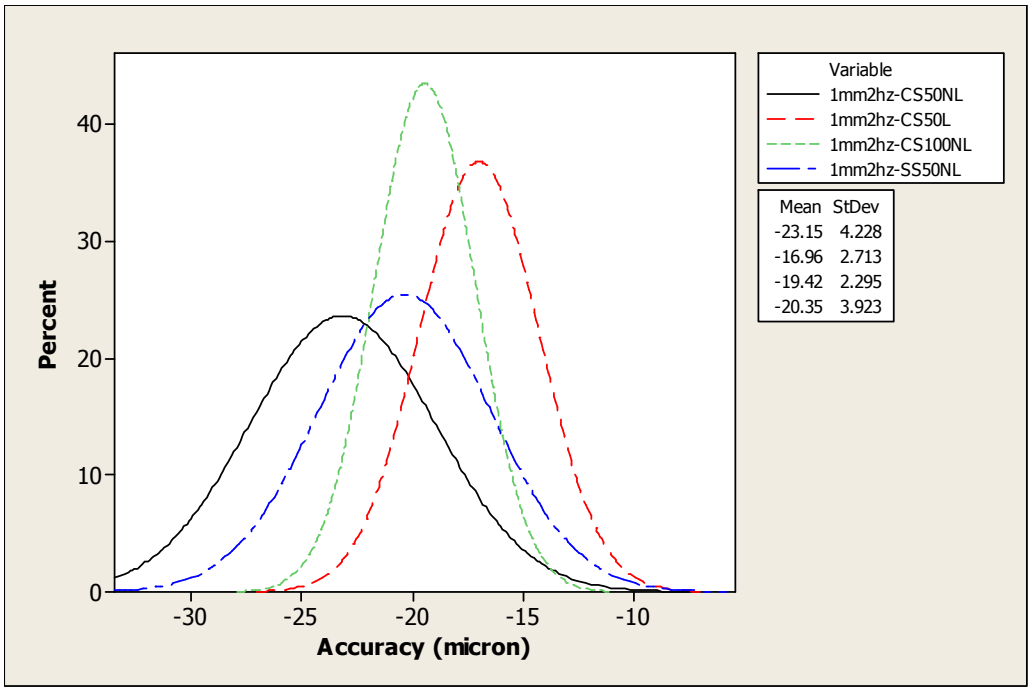

(a)

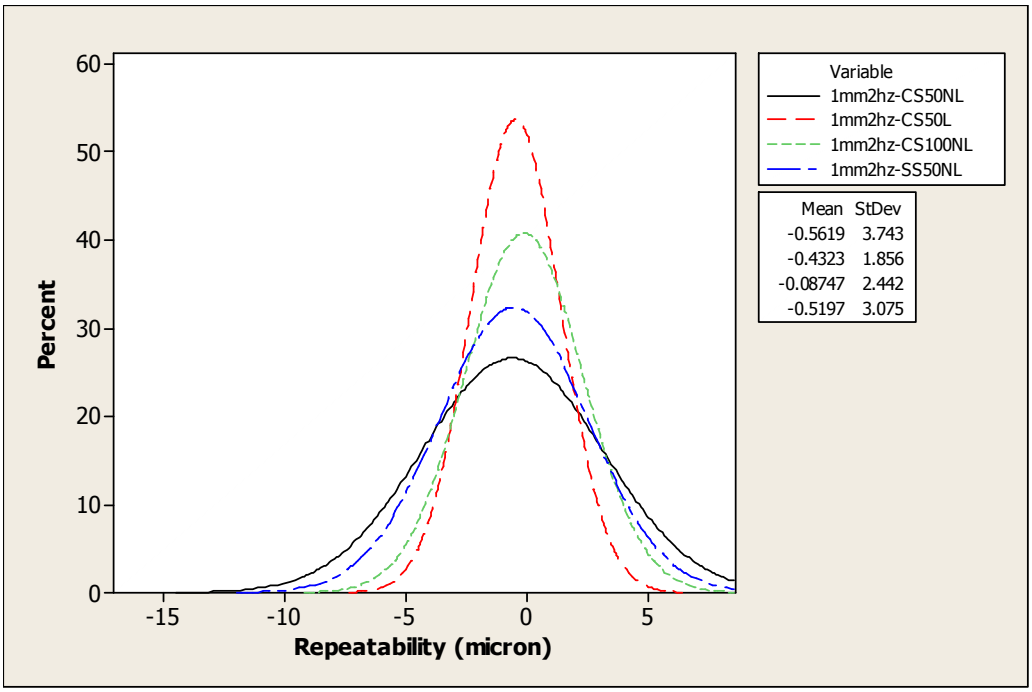

(b)

Fig. 8.16: Feeding performance at 1mm feed-distance and 2Hz feed-frequency: (a) positional accuracy; and (b) repeatability.

b) 5mm feed distance

Both the mean-positional accuracy and repeatability with 5mm feed-distance at 1Hz feed-frequency are shown in Fig. 8.17(a). The trend demonstrates a significant deterioration of both mean-positional accuracy and repeatability. Although the mean-positional accuracy recorded for CS50NL strip was 1.8µm, a large dispersion of deviation was obtained at ±3.6µm, and thus slightly worsened repeatability. For thicker CS100NL, the mean positional accuracy was observed to be reduced at 15.4µm, with significant deterioration of repeatability at ±3.6µm, which latter was almost twice that of the shorter feed repeatability performance for the shorter, 1mm, feed-distance. Change in the feed material to SS50NL resulted in half the mean positional accuracy when compared to the results for the same feed-frequency at shorter, 1mm, feed-distance. An obvious deterioration of repeatability at ±5.8µm was observed which was three times the repeatability value of that for shorter feed-distance.

At low feeding-frequency, the presence of lubrication did not contribute towards improving the positional accuracy: instead, causing it to decrease. Significant deterioration in positional accuracy was noted, a mean-positional accuracy of 12.6µm was recorded. However, lubrication did not affect improvement in repeatability also. This is confirmed by the similar repeatability for CS50NL and CS50L, with the recorded value being ±3.6µm.

At longer feed-distance, lubrication did not have a significant effect on improve repeatability, as shown in Fig. 8.17(b). However, the repeatability pattern for stiffer material was observed to be better compared to the results for less-stiff material. A tighter dispersion was observed for CS100NL compared to those for CS50NL, CS50L and SS50NL. Change of strip material however, tended to result in large inconsistency in repeatability, as the deviation of SS50NL was found to be widely dispersed, compared to the results for the similar-thickness carbon-steel.

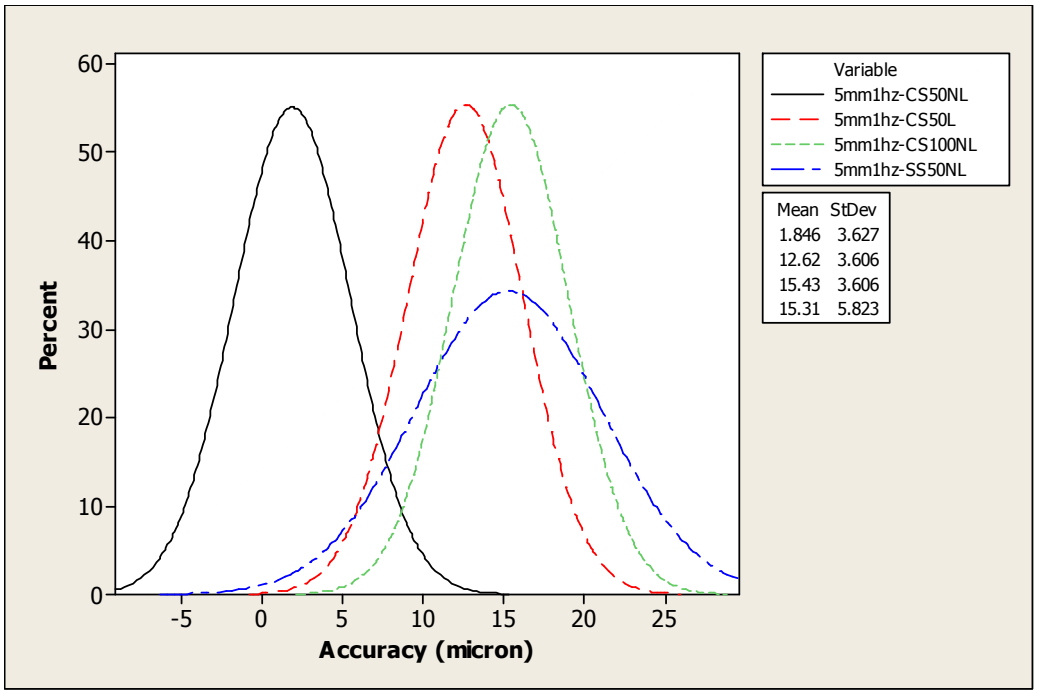

(a)

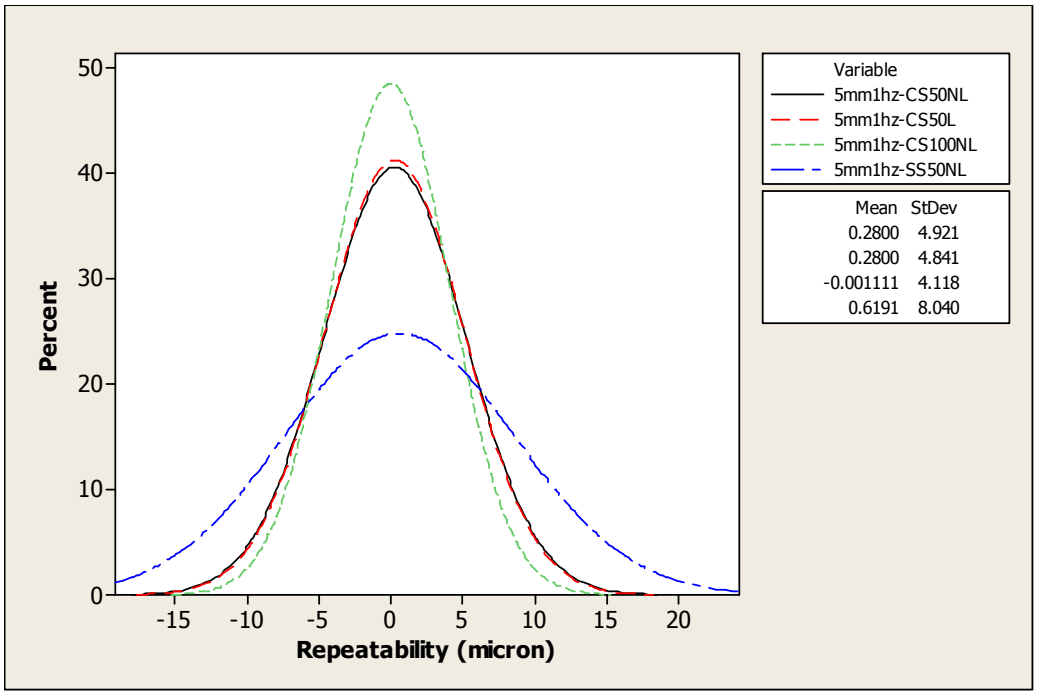

(b)

Fig. 8.17: Feeding performance at 5 mm feed-distances and 1Hz feed-frequency: (a) positional accuracy; and (b) repeatability.

Change to 2Hz feed-frequency showed good in the positional accuracy trend, as depicted in Fig. 8.18(a). From this figure, the mean positional accuracy for CS50NL was recorded as 2.2µm, with repeatability at ±2.1µm. Change to thicker CS100NL resulted in a mean-positional accuracy of 2.5µm being achieved and very tight deviation-dispersion of ±1.8µm. However, change to softer material, SS50NL, in turn leading to an almost similar mean-positional accuracy as for CS50NL, which at 2.0µm, but a significantly-deteriorated repeatability at ±6.5µm. Fig. 8.18(b) confirmed the finding for the stiffer and the least-stiff material, where stiffer material tends to promote better positional-repeatability compared to that for the least-stiff material. The least-stiff material on the other hand tends to result in greater in deviation-dispersion, in turns led to large repeatability-inconsistency. The presence of lubrication, however, was found not to have a significant contribution towards improving the feed-positional accuracy and repeatability. Revealed by the figure, the presence of lubrication led to worsened deviation-dispersion, hence worse repeatability was found.

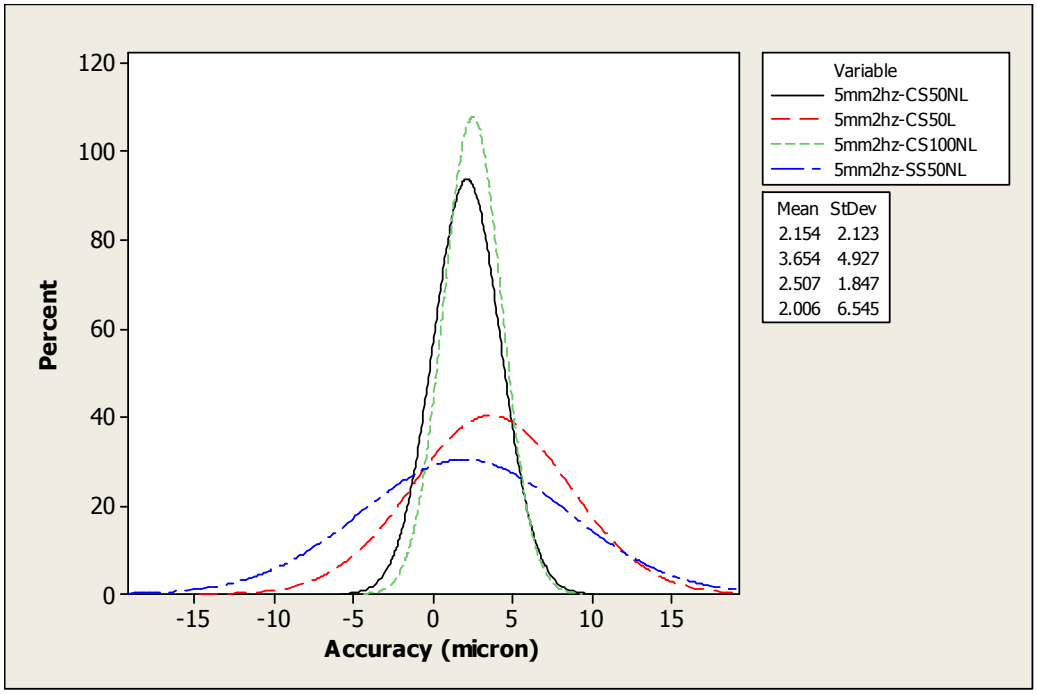

(a)

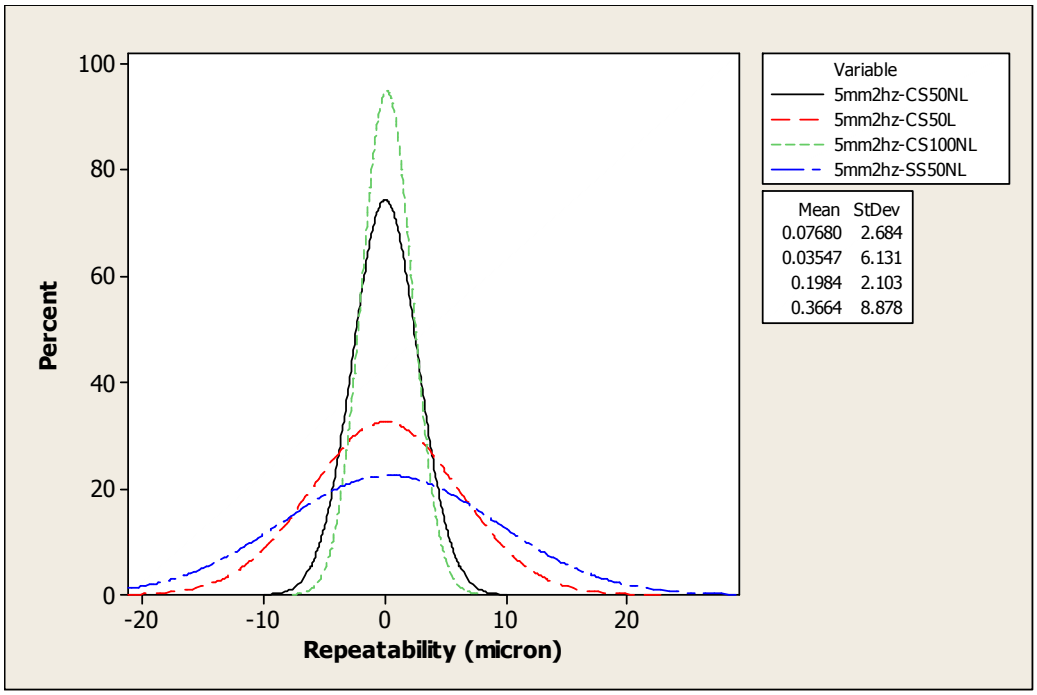

(b)

Fig. 8.18: Feeding performance at 5 mm feed-distances and 2Hz feed-frequency: (a) positional accuracy; and (b) repeatability.

8.5 Discussion

8.5.1 Load Disturbance

Although the direct-feed drive employed on this feeder could result in better positional accuracy, direct contact between the actuator and the strip itself was sometime becomes a disadvantage, which could also reduce the positioning accuracy. Direct contact between the moving mass and the actuator in the feeder may cause load disturbances in the system. Although the payload of the feeder may be considered fixed, still inconsistency of interfacial/external forces such as friction between contacts pairs, and changes of strip material, can contribute towards load disturbance. This suggests that each strip has to be respectively 'motion-optimised' in order to properly compensate for the load disturbance. Proper compensation by use of an optimising feedback controller is suggested as the way to achieve better positional accuracy and repeatability. 75% reduction of positional/tracking error may b- achieved with proper adjustment of the feedback controller, which reduction is realized by good adjustment of the P-D term [Gao et al., 2006]. Another effort made

elsewhere [Yen et al., 2004] has successfully shown that primitive PID gain-adjustment may be a good choice in reducing load disturbance, compared to other compensation-control techniques.

8.5.2 Stability of the Feeder

The feeding patterns from the experiments still showed significant positional/tracking errors. These errors during feeding may suggest that the servo-mechanism itself has a lack of sufficient stiffness, thus, lack of sufficient motion-stability. The instability increases with the increasing of the feeder's velocity and results in deterioration of positional accuracy, specifically at higher feed-frequency. To combat the motion-instability and hence to improving the positional-accuracy, a larger dynamic stiffness is required in the servo-control loop [Breambussche et al., 1996; Alter et al., 1994; Alter et al., 1996]. Effort made by [Yen et al., 2004] has successfully shown that servo-stiffness may be easily achieved by proper tuning of the PID gain. Various compensatory-techniques have been used to control servo-stiffness such as PDF, and advanced derivative model-based techniques have been used with the main purpose of increasing the dynamic stiffness of the servo. Although the other compensation models tested have shown improvement in increasing servo-stiffness, PID compensation-techniques were observed to produce better stiffness-control compared to the other techniques. Therefore, adjustment of the proportional and derivative (PD) gain and the feed-forward feedback-loop of the feeder controller is seen as a promising solution to the achieving of better servo-stiffness control and may be the simplest solution to increasing the feeder-stiffness and indirectly to improving positional accuracy and repeatability.

8.6 Conclusions

Based on the results of all of the experiments conducted, the following conclusions are drawn:

i. Lack of servo-stiffness has resulted in inconsistent positional-accuracy and repeatability being recorded.
ii. Dedicated control-feedback-optimization for each strip may be useful in improving positional-accuracy and repeatability.
iii. The lubrication of the system promotes improved positional accuracy and repeatability, specifically with a shorter feed-distance and a greater feed frequency.
iv. The repeatability deteriorates proportionally to the increasing of the feed-distance and the feed-frequency.
v. The greater positional accuracy and precision achieved in the experiments show the good potential of the developed feeder for use in micro-forming applications.

Chapter 9

Optimization of the Feeder's Performance

9.1 Summary

This chapter focuses on the optimization works carried out on the newly developed feeder. Several optimization strategies were identified; load identification, motion profile optimization and feedback control compensation. Detail load identification analysis was conducted with a view to determine the accurate load acted on the system. With this analysis, better servo stiffness was achieved. The optimization works continued with testing of different motion profile to produce better positional positional accuracy and stability. Result from the works concluded that sharp transition in motion may not have significant effect to improve positional accuracy and repeatability. Conventional feedback control compensation technique was employed to further improve the positional accuracy and repeatability. Proportional and derivative compensation were used to achieve better servo stiffness and damping performance. This method is proven to have significant contribution to improve the feeder performance. Validation experiment was also conducted based on the selected proportional and derivative compensation value with a view to observe the effect of optimization works towards improving positional accuracy and repeatability. Several parameters were tested to qualify the feeder performance in detail. This includes change of feed distance and frequency, usage of different strip materials and thicknesses. The experiment was also conducted with and without the presence of brake force and lubrication to study their effect on the feeder performance. Based on the thoroughly series of testing, the feeder was proven to have greater positional/feeding accuracy and repeatability and may be used to serve micro-forming application.

9.2 Introduction

For decades, the positional accuracy of servo-driven direct-drive devices has been limited by the performance of the mechanical design. This is due to the frictional and stictional forces existed on the mechanical guideways that have a significant effect on the stability of the positional-accuracy and the yield-stability. The achievable performance of a direct-drive linear-motor feeder system that is actuated by a permanent magnet is unavoidably limited because of the effect of the sliding surface, load changes as well as variation in the parameters of the system. Therefore, how to compensate for these non-linear force-disturbances, which directly impose and affect the positional accuracy and repeatability is very important knowledge for this high-precision application. Until recently, servo-technology was employed as a method for going beyond mechanical-accuracy limits and to partially overcome the non-linearity problem in the actuation system.

Servo-technology enables the performance and efficiency of a developed feeder to be adjusted to produce an accurate and precise process. This is because the two major goals for a feeding process are positional accuracy and repeatability. Therefore, an excellent motion-control system can meet these goals and can effectively demonstrate the efficiency of the driven feeder. This is only achievable through an optimisation process of the servo controller.

Optimization is necessary to improve positioning accuracy and reduce tracking error for better and more consistent feeding performance. This is to ensure that the feeder feeds the strip metal as accurately as possible, and with good repeatability. There are two types of conventional feedback-controllers often used and adjusted to achieve better positional accuracy and repeatability through frictional compensation, namely the Proportional-Integral-Derivative (PID) controller and the feed-forward feedback controller. The PID compensation usually can be found in chemical-process-plant, where the chemical-mixing processes require some sort of PID compensation to achieve the final solution-ratio. Sometimes, in a machine-control system, typically P-D compensation is favoured and has sufficient effect to improve the system's performance [Bose; Parkermotion]. Nevertheless, P-D compensation is also called PID compensation to avoid confusion. The combination of PID compensation with

some other advanced methods to obtain better results has been were proposed in recent years, these advanced methods including: friction-observer; robust control; adaptive friction compensation; sliding-mode control; and neural and fuzzy control. Nevertheless, none of these advanced-control methods have been employed in the present work, or discussed and explained in this chapter.

9.3 Procedure – Optimization Strategy

The most popular optimization of a servo-motor is by using conventional feedback-compensation such as P-D and feedforward feedback. Nevertheless, the selection of the proper load is very crucial in the prior adjustment of P-D gain to ensure that the system is able to provide a certain level of stiffness, thus achieving the designated position. Moreover, the selection of a proper motion-profile could ensure a more-controlled positional-overshoot. Based on the three factors mentioned earlier, these methods are adopted as the way of optimizing the performance of the developed feed. The methods are identified and categorized as load identification,; motion profile; and adjustment of the feedback controller, and are explained in the following.

9.3.1 Load Identification

Load identification enables the servo-drive system to determine: the load; the characteristic value of the gripper mass; the required pulling-force and its payload; and the compensation of the loads for better positional-accuracy. In automatic configuration, this is executed by exciting the system with an excitation signal, which is then is fed into the control loop. The control loops dampens the excitation signal, therefore the superimposed control-loop is set slowly by reducing the stiffness, and thus the measurement is not influenced. Hence, better positioning stability can be obtained.

For the purposes of this research, load identification is accomplished with a view to establishing accurate load-identification to enable absolute precision-positioning [McCarthy, 2006] by determining: the exact weight of the live payload, which consists of the gripper device, and the pulling force required to feed. The total weight

of the payload is estimated based on the following analysis, considering all the weights involved, as depicted as in Fig. 9.1.

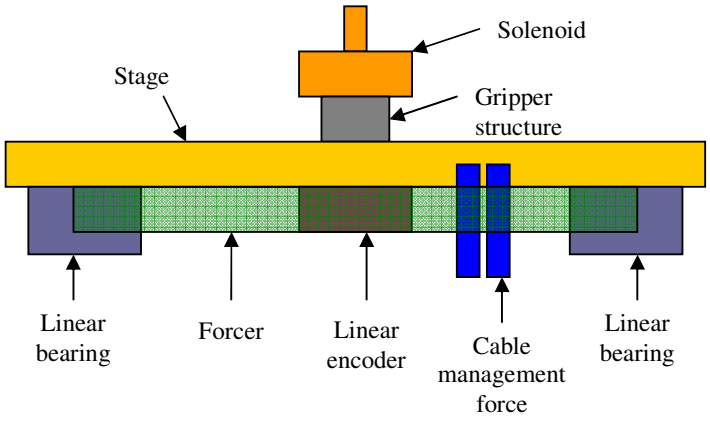

Fig. 9.1: Side-view anatomy of the developed feeder and payload estimation.

The analysis of each part that contributes to the total payload is as follows:

i. Gripper weight

The gripper weight is calculated as the following:

length (l) = 110mm, width (w) = 25mm, and height (h) = 14mm

$$volume, v = 100 \times 25 \times 14 = 35000 mm^3$$

$$known, \rho = 2.73 g / cm^3$$

$$\therefore m = \rho \times v = 2.73 \times \frac{35000}{1000} \approx 96 g$$

Therefore, the gripper weight is calculated to be 96g

ii. Solenoid weight

The solenoid is weighted at 170gram

iii. Stage weight

The stage mass is calculated as the following:

length (l) = 200mm, width (w) = 128mm and height (h) = 10mm,

$$volume, v = 200 \times 128 \times 10 = 256000 mm^3$$

$$known, \rho = 2.73 g / cm^3$$

$$\therefore m = \rho \times v = 2.73 \times \frac{256000}{1000} \approx 700 g$$

Therefore, the stage weight is estimated as 700g.

iv. Linear-bearings weight

Each of the linear-bearings is estimated to weigh 150g [THK]. Therefore, the four bearings give a total weight of 600g.

v. Forcer/coil weight

The forcer weight is estimated as 220g (www.parkermotion.com)

vi. Linear-encoder weight

The weight of the linear-encoder is estimated as 11g (www.renishaw.com)

vii. Force due to cable management

The force to overcome cable-management was found experimentally to be 4.5N, which is equivalent to 450g. This force was measured by driving the feeder to the home position with no load onboard. The maximum plotted actual-force required to retain its position was considered as the cable-management force.

Total weight (w_t) = 96 + 170 + 700g + 600g + 220 + 11 + 450 = 2247g

Including the weight of the few M3 bolts used in the system, the total weight is rounded to the nearest 100g and thus becomes 2300g. This value is used to configure the servo-drive load-optimization. With the declared weight onboard, the system automatically determines the best servo-drive control-configuration to gain better positioning-accuracy.

9.3.2 Motion-Profile Optimisation

The effect of the motion profile on reducing the tracking error is also studied. Very-tight windows of acceleration and deceleration result in high jerk in the system due

to sudden change of the acceleration and deceleration phases, hence reducing the ability to achieve better positional-accuracy, specifically when the load in onboard. At the same time, an excess of time for acceleration and deceleration could somehow result in delay in reaching the target position within the designated time-frame.

Experiments were conducted to observe the best possible time-frame for the acceleration and deceleration phases. The feeding process was designed to be accomplished within 300ms for 1Hz feeding-operation and consists of acceleration-, constant speed- and deceleration-phases. Each acceleration and deceleration time-frame was fixed at the same value due to the repetitive motion not requiring positional accuracy during feeding and homing. In addition, this makes the time-frames easier to be controlled. Four types of time-frame configuration were used: 15-15%; 30-30%; 45-45%; and 50-50%; which carry 45ms, 90ms, 135ms and 150ms of acceleration-deceleration time, respectively.

9.3.3 PID Compensation

A PID, or proportional-integral-derivative, controller mainly is one of the best industrial process controllers because of its simple structure and robust performance in a wide range of operating conditions [Petrov et al., 2002; Huang et al., 2000; Braembussche et al., 1996]. PID controller usually consists of three different types of gain: so-called proportional gains; integral gains; and derivative gains. All gains are denoted by their first letter.

P-terms, or proportional gains, are usually associated with the stiffness of the system. The adjustment of this parameter is required to control positional overshoot, which can slightly deteriorate the positional-accuracy. The greater is the proportional-gain value, the stiffer is the system and vice versa. Greater gain reduces the settling time and excessive positional-overshoot, which is shown clearly and explained in the next section.

Although PIDs are not seen to be adequate controllers for non-linear problems, the combination of a PID and feedforward-feedback appears to be a promising solution to reducing non-linearity and tracking-error [Wang et al., 2006]. Most servo-motion-

control researchers and designers still rely on this traditional feedback-compensation as a mean to improve positional-accuracy.

Some efforts have been made towards more advanced control of linear-motor drive-systems to suppress the effect of non-linear force disturbances. Mekid et al., (2000) has proposed the adjustment of PID gain-value along with Internal Model Controller (IMC) to automatically compensate for un-modelled mechanical-behaviour such as pre-rolling phenomena.

In another effort, Yan et al., (2008) designed a modified feed-forward controller to reduce the tracking errors of a direct-drive system. Based on the experiment made, the author managed to reduce the contour error of circular motion from 8.5μm to 3.2μm when the modified feed-forward controller was used together with the adjustment of PID gain.

Chen et al., (2007) reported that the elimination of period tracking-error can be achieved via the design of a discrete-time repetitive controller. A repetitive Controller is used to control repetitive-motion accurately and, according to the authors, with the use and adjustment of speed and acceleration feed-forward commands, it can enhance the tracking-ability of the repetitive controller and reduce tracking-error.

An attempt made by Wu et al., (2007) on a voice-coil servo-motor-driven system for a non-circular machining application demonstrated that the feed-forward error-compensation controller improved the machining tracking-precision. Two types of experiments were conducted, the results illustrating a control-system synthesis procedure which involved the variation of the feed-forward controller. The experiment results showed substantial improvement of the tracking error when compared to the effort of correcting it by the use of a linear active-disturbance-rejection controller.

Zhao et al., (2005) reported the effectiveness of a developed and experimentally tested control scheme, to reduce the effect of force ripples on linear motor. Force

ripples have a significant influence on positional accuracy, since they have a similar effect as friction, i.e. they cause lack of smoothness and an imprecise motion-profile. The control scheme consists of a PID feedback component, feed-forward compensation, and another adaptive feed-forward component. The results of the simulation and experimental work carried out, verified that high-precision motion-tracking was achieved.

Due to the significant capability of PID compensation to improving positional accuracy, an experiment was designed to establish the best PID compensation-value for better feeder-positional accuracy and -precision. Different PID-values was explored with different types of material, as material stiffness is found to affect positional accuracy, as explained in the previous chapter. The results demonstrated that less-stiffness materials tended to be positioned slightly less accurately than stiffer materials.

Some classic methods of tuning PID gains are identified as Routh Herwitz, Ziegler-Nichols [Kim et al., 2006; Su et al., 2005; Tang et al., 2004] and Tyreus-Luyben [West et al., 2008]. These methods use a trial-and-error basis by determining the ultimate-gain, through experimentation, at which the system becomes unstable and oscillates. When the ultimate gain is achieved, this parameter is then used to calculate the best controller-output-value by using a general-control equation. Nevertheless, these methods are seen more favourable for a liquid-mixing plant rather than for manipulating a motion-control scheme [Thornhill et al., 2008; Jillson et al., 2008]. Contrarily, experimentally trial-and-error PID values are the most favourable method of most recent manufacturers and researchers worldwide, to -control servodrive systems [Wang et al., 2006; Petrov et al., 2002; Huang et al., 2000; Adams et al., 1997; BOSE; Parkermotion].

For the present research purposes, several ranges of proportional- and differential-gain values were adjusted and categorized into two categories, namely: a Fixed-D and Fixed-P. In the Fixed-D category, the differential gain was fixed at 100% and adjustment was carried out on only the proportional gain, and vice versa. The main purpose of the Fixed-D method is to observe the effect of positional accuracy with

the increasing of proportional gain from 50-200% in 50% increments. A similar method is applied for Fixed-P case, where the proportional gain is fixed and the differential gain is varied from 0-200% at 50% increment. The effect of servo-controller damping on positional accuracy was observed and the best PID-value was determined by the best positional-accuracy. All of these configurations were repeated for all of the materials used, i.e. 50 and 100µm-thick carbon-steel strip without lubrication, 50µm-thick stainless-steel strip without lubrication and 50µm-thick carbon-steel strip with lubrication. The feed-frequency was varied from 1-2Hz for both 1 and 5mm feed-distances for all materials and conditions.

9.3.4 Validation Experiments

The three methods described above were adjusted and the results verified through a series of experiments. Although an insignificant effect on performance was found in previous chapters, lubrication was also considered for these experiments. A similar experiment set-up as for the previously-conducted experiments was used to validate the feeder performance. 1 and 5mm feed distances were used at both 1 and 2Hz feed-frequency for all strips. The experiments were repeated with the application of brake-force after the best P-D configuration had been identified.

9.3.4.1 Actual Acting Brake-Force

Based on the coil- and reel- inertia-analysis made in the previous chapter, the inertia of the rotor and stator of an additional DC-motor were also taken into account in assessing the total inertia acting during uncoiling. Based on the inertia given by Maxon DC motor-specification paperwork of 0.00000335kgm^2 [Maxon], the uncoil force at 2Hz feeding-frequency was calculated as follows:

$$I_{total} = I_{composite} + I_{motor} = 3.62 \times 10^{-4} + 3.35 \times 10^{-6} = 0.00362335 kgm^2$$

At 2Hz feeding-frequency, based on an analysis made on Compax3 motion-profile software and using the trapezoidal curve depicted in Fig. 9.2, the acceleration is 2.25m/s^2. Therefore, the radial acceleration is:

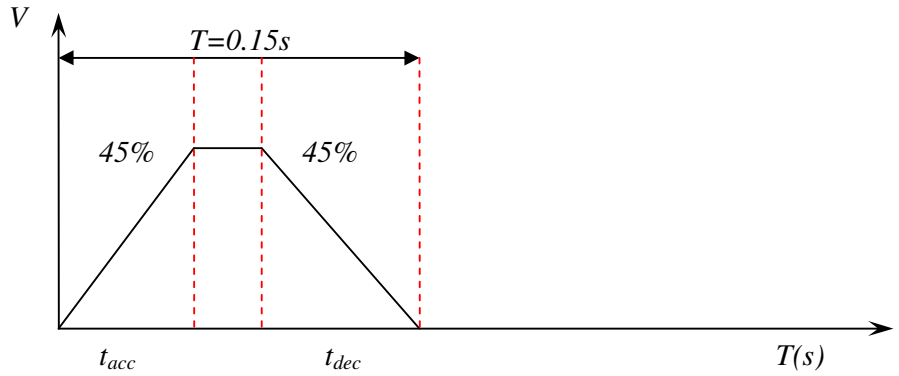

Fig. 9.2: Acceleration and deceleration time-frame for the 2Hz feeding-frequency motion-profile.

$$\alpha_{2hz} = \frac{a_{2hz}}{r_{coil}} = \frac{0.9}{0.0625} = 14.4 rad \cdot s^{-2}$$

Hence, the total torque- and force- required to uncoil the coil and reel are:

$$\tau_{total} = I_{total} \times \alpha_{2hz} = 0.00362335 \times 14.4 = 0.0522 Nm$$
$$f_{total} = \frac{\tau_{total}}{r_{coil}} = \frac{0.0522}{0.0625} = 0.84 N$$

By applying a safety factor of 25% to the above analysis, the new total-force is almost 1.0N. As discussed in the previous chapter, the uncoil braking-force was kept the same as the uncoil force. Hence, the maximum uncoil-braking-force acting instantaneously on the system was 0.84N. By taking f_{rms} as the maximum force, continuous uncoil-braking-force was determined as below:

$$f_{brake\,rms} = \sqrt{\frac{{f_{total}}^2 \times t_{acc}}{T}} = \sqrt{\frac{1.0^2 \times 0.0675}{0.2}} = 0.58 N$$

Again applying a safety factor of 4, about 0.73N of braking force was required to maintain the strip in good tension. Hence, $\tau_{brake\,rms}$ is:

$$\tau_{brake\,rms} = f_{brake\,rms} \times r_{coil} = 0.73 \times 0.0625 = 0.046 Nm$$

Based on the Maxon DC motor model 310005 specification depicted in Fig. 9.3(a), the torque constant is 0.0139Nm/A. For 0.046Nm torque, at 12VDC, the motor needs to draw a total current of:

$$I(amp) = \frac{0.046}{0.0139} = 3.3A$$

The complete brake-force system is shown in Fig. 9.3(b). In the system, a 30V-10A DC power supply was used to regulate the designated voltage and current so as to match the desired force-output, as illustrated in Fig. 9.4. A series of further experiments was designed to study the effect of uncoiler/decoiler braking-force on positional accuracy. Based on the best P-D configuration for CS50NL found earlier, experiments with the same configurations were repeated with uncoiler/decoiler brake-force introduced into the system. The experiment began with 1mm feed-distance at 1 and 2Hz feed-frequency both at the best-determined configuration, followed by 5mm feed-distance and 1 and 2Hz feed-frequency at the best configured/adjusted configurations, respectively.

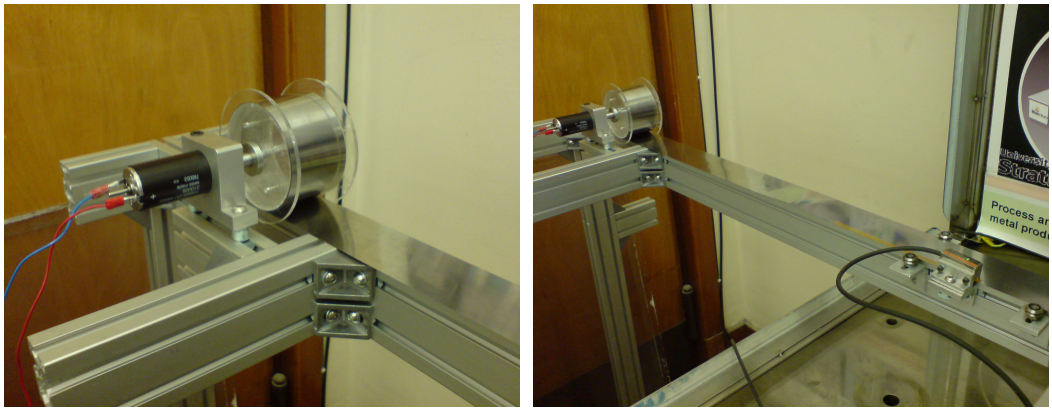

(a) (b)

Fig. 9.3: (a) the DC motor is used to generate brake-force which is transferred to and acts on the reel; and (b) the whole brake-force and linear-encoder system.

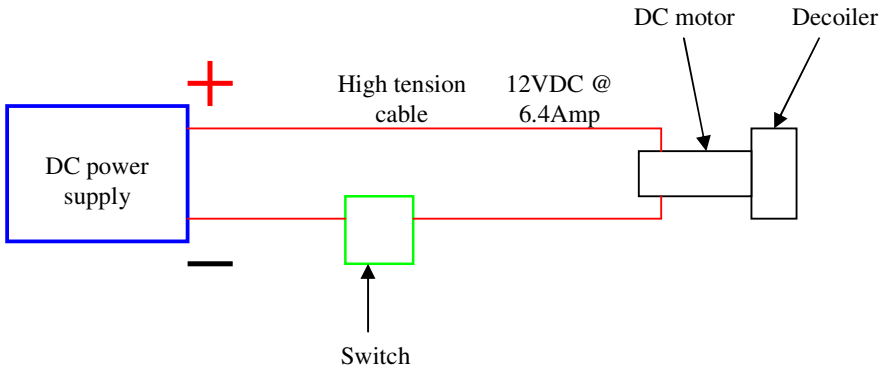

Fig. 9.4: Schematic diagram of the controlling brake force exerted by the DC motor on then uncoiler/decoiler.

9.4 Results

9.4.1 Load Identification Optimization Results

Several experiments were conducted to study the effect of change of optimized weight. Various weights were used and their effect on feeder positional-accuracy was studied. The experiment results have demonstrated that a well-optimized loads produced better positional-accuracy, this being done by comparing the actual and the target-position of the feeder, as shown in: Fig. 9.5(a) to Fig. 9.5(d). In Fig. 9.5(a), the load was set at 300g to represent the weight of the gripping device. Each square division is equal to 5µm of positional accuracy. Based on the figure, the feeder was unable to produce a better positional-accuracy of less than 30µm error. 1000g represents the weight of the gripper and the moving stage. At this load, as depicted in Fig. 9.5(b), the actual position of the feeder was seen slightly better. Nevertheless, a large positional-tracking error was observed. A significant improvement was observed when the servo-drive load-configuration was set to 1500g, as shown in Fig. 9.5(c). With this load, the actual position was seen to reach the same value as the target position. However, the positioning-capability was able to be sustained for only a very short period of time. Better positional-accuracy was achieved when the servo configuration was properly tuned, as the load-analysis suggested. Fig. 9.5(d) demonstrates a slight positional-overshoot of 5µm when load was configured at 2300g. Nevertheless, this can be overcome with proper configuration and optimization of the gain of the feedback control, i.e. the PID gain.

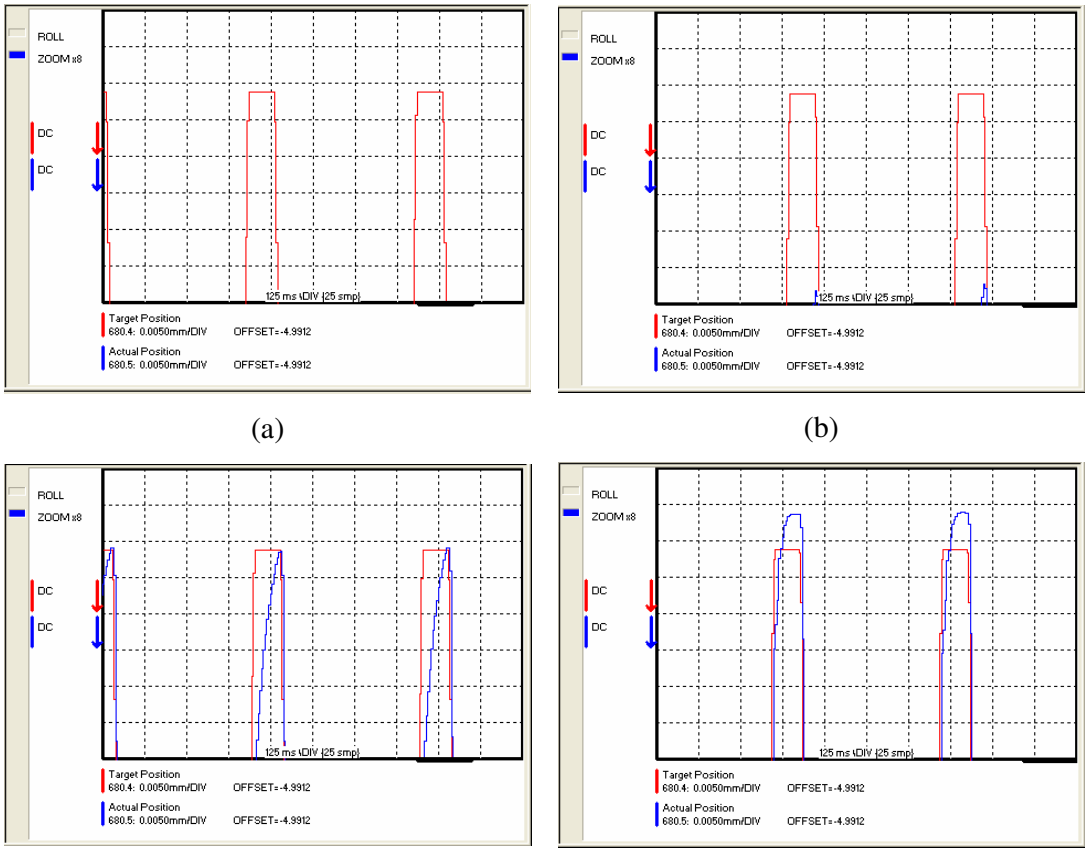

Fig. 9.5: Various load configurations tested for better positional accuracy: (a) 300g; (b) 1000g; (c) 1500g; and (d) 2300g.

9.4.2 Motion-Profile Optimization Results

As depicted in Fig. 9.6(a), for the 15-15% motion-profile, the system took some time to position the feeder to the designated target-position due to very short time given for the system to accelerate. A longer time to reach the target position was seen as the main reason for inaccuracy, because the system uses the rest of the remaining positional-time to reach as close as possible to the target position to overcome 'jerk' overshooting-error. This phenomenon still occurred with the 30-30% profile (Fig. 9.6(b)), but with a slightly lesser time to reach the target position. With the less-steep acceleration curve, as depicted in Fig. 9.6(c) and Fig. 9.6(d), the feed-curve pattern was seen to be more stable in reaching the target position.

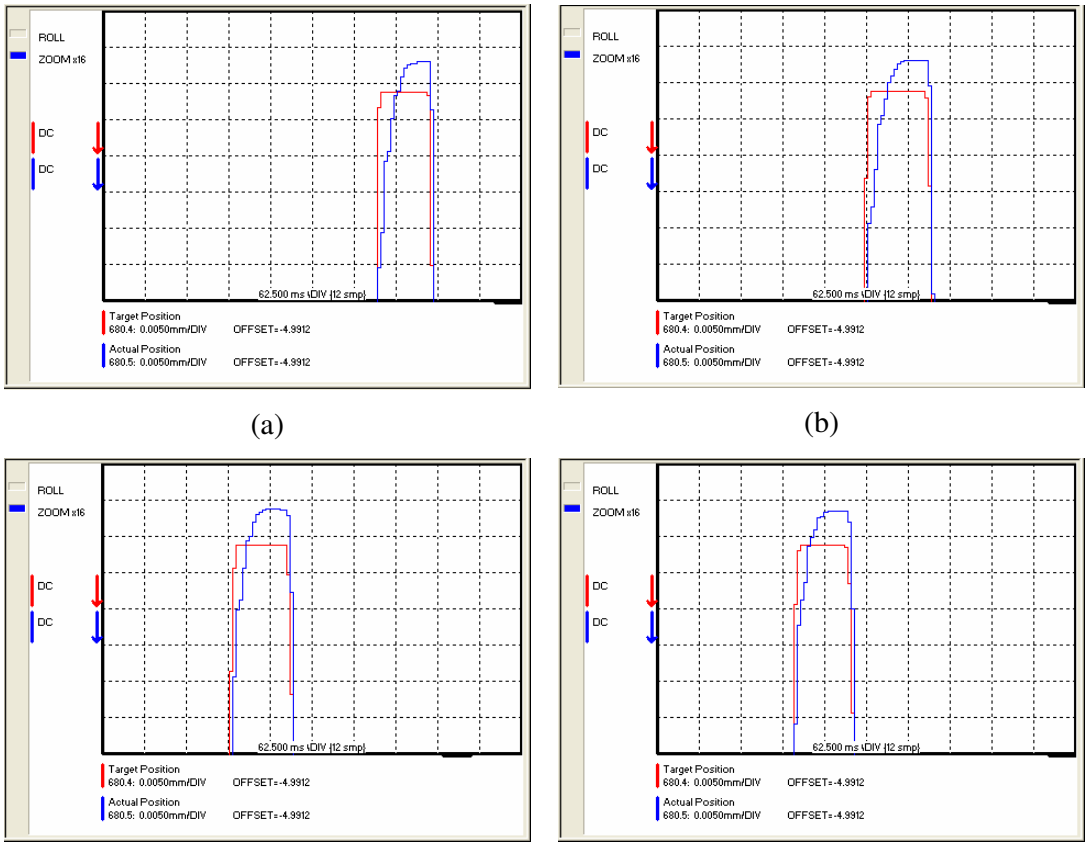

Fig. 9.6: The response of the feeder to various motion-profile time-frames: (a) 15-15%; (b) 30-30%; (c) 45-45; and (d) 50-50%.

9.4.3 P-D Compensation Results

9.4.3.1 Fixed-D Results

a) 1mm feed-distance

At 1Hz feed-frequency, the pattern for all material types and thicknesses seems to be consistent. The results demonstrated that stiffer material was positioned more accurately than less-stiff material. As shown in Fig. 9.7, for 50µm-thick non-lubricated carbon-steel strip, CS50NL, the mean-positional accuracy and repeatability were observed to be 0.8µm and ±0.6µm with P100-D100 gain. Greater P-term gain resulted in reduction of positional accuracy, however, the repeatability remained the same. The effect of low P-term gain had a similar consequence as for P=100, around 1.4µm mean-positional accuracy being observed with ±0.6µm repeatability. For 100µm-thick non-lubricated carbon-steel strip, CS100NL, the positional accuracy and repeatability were better than for CS50NL. A mean-

positional accuracy of -0.6µm and a repeatability of ±0.5µm were obtained for P200-D100 compensation-gain, as depicted in Fig. 9.8. Based on this figure, low P-term gain results in the inability of the system to reach the designated target-position. The stability increased with the increasing of the P-term gain and resulted in a greater number of feed attempts being made as reach as close as possible to the target position. All of the adjusted P-term gains demonstrated the underfeed phenomenon. A similar effect of low P-term gain on positional-accuracy was also demonstrated for stainless-steel material, but in an overfeed situation values of mean-positional accuracy and repeatability of -0.2µm and ±1.1µm, respectively were recorded, as shown in Fig. 9.9 when feeding 50µm-thick non-lubricated stainless-steel strip. For the lubricated 50µm-thick carbon-steel case, CS50L, as shown in Fig. 9.10, slight deterioration of positional accuracy occurred at low P-term value. The best mean-positional accuracy and repeatability were recorded for P100-D100, at 2.1µm and ±0.7µm, respectively.

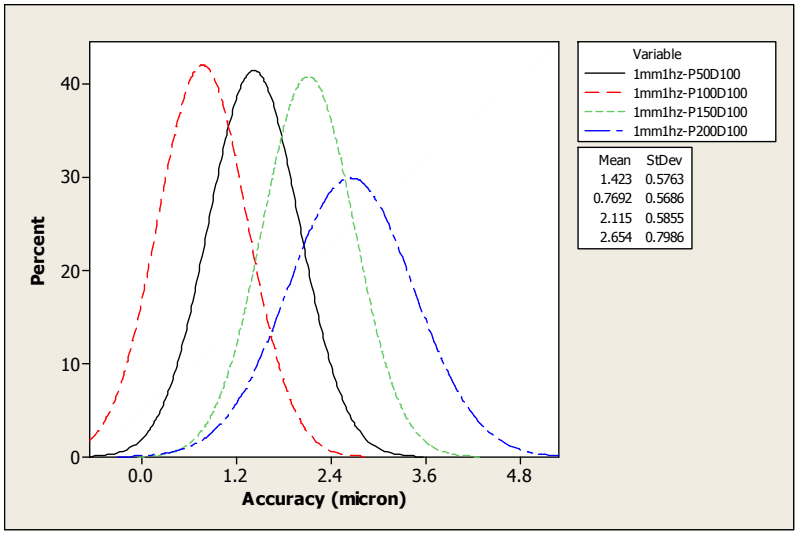

Fig. 9.7: Optimized-positional accuracy for non-lubricated 50µm-thick carbon-steel at 1Hz feed-frequency.

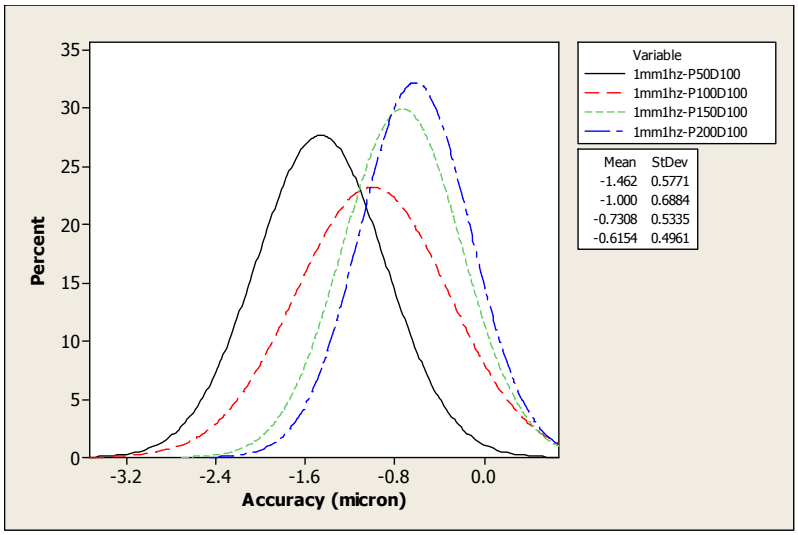

Fig. 9.8: Optimized positional accuracy for non-lubricated 100µm-thick carbon-steel at 1Hz feed-frequency.

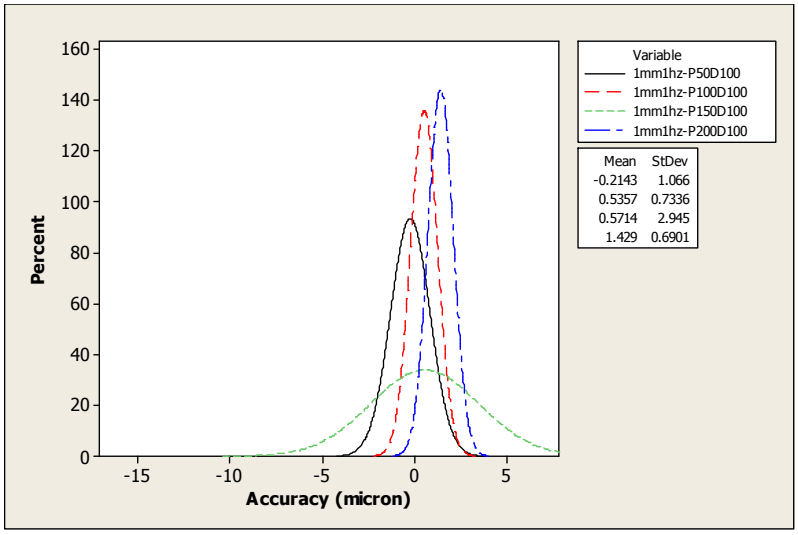

Fig. 9.9: Optimized positional accuracy for non-lubricated 50µm-thick stainless-steel at 1Hz feed-frequency.

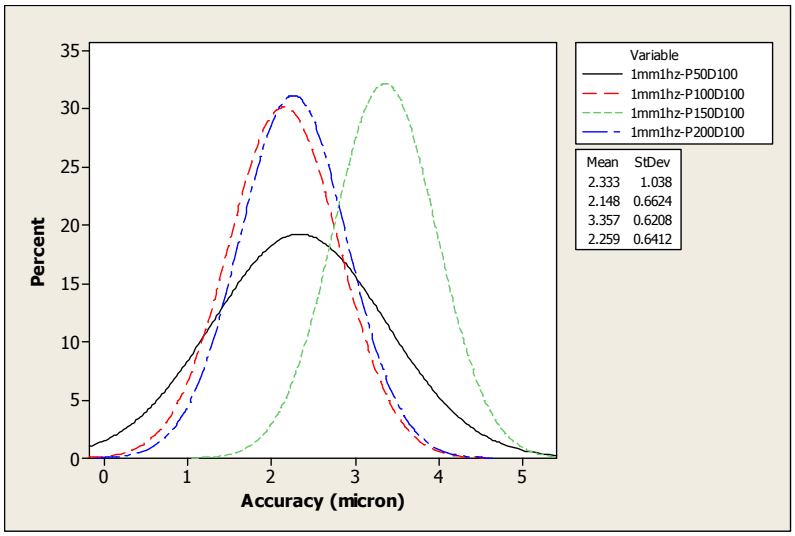

Fig. 9.10: Optimized positional accuracy for lubricated 50µm-thick carbon-steel at 1Hz feed-frequency.

At 2Hz feed-frequency, for all tests, as depicted in the Figs. 9.11, 9.12 and 9.13, mainly slight deterioration of positional accuracy and repeatability performance were recorded The system was seen unable to repeat the same positional accuracy-level performance as 1Hz feeding-frequency. For the CS100NL test, the positional accuracy tends to demonstrate a greater overfeed-phenomenon, in comparison with the greater underfeed for the 1Hz-feeding-frequency test. However, good positional accuracy and repeatability were still maintained for CS50NL with P50-D100 configuration, at 1.4µm and ±1.1µm respectively; for CS100NL with P200D100 configuration, at -0.2µm and ±0.5µm, respectively; and for SS50NL with P50D100 configuration, at 0.7µm and ±0.9µm, respectively. Slight improvement of repeatability was observed with CS50L, when compared to CS50NL, as shown in Fig. 9.14, however, the positional accuracy demonstrated a slight deterioration at 4.1µm, with a repeatability of ±0.4µm.

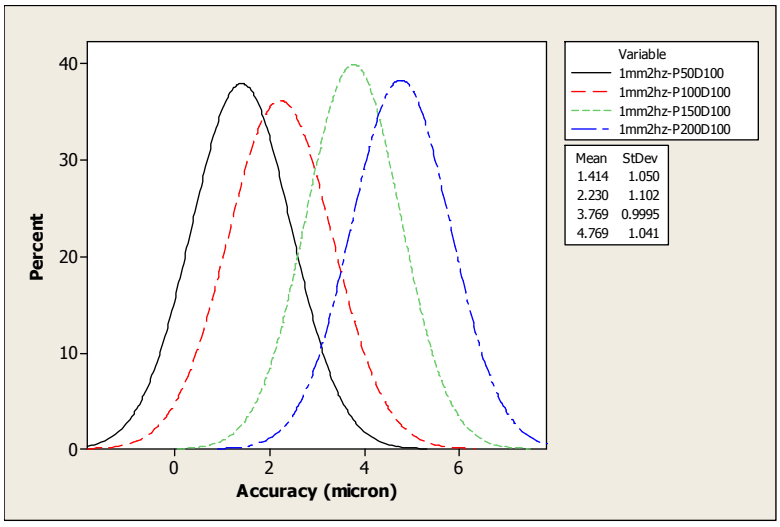

Fig. 9.11: Optimized positional accuracy for non-lubricated 50µm-thick carbon-steel at 2Hz feed-frequency.

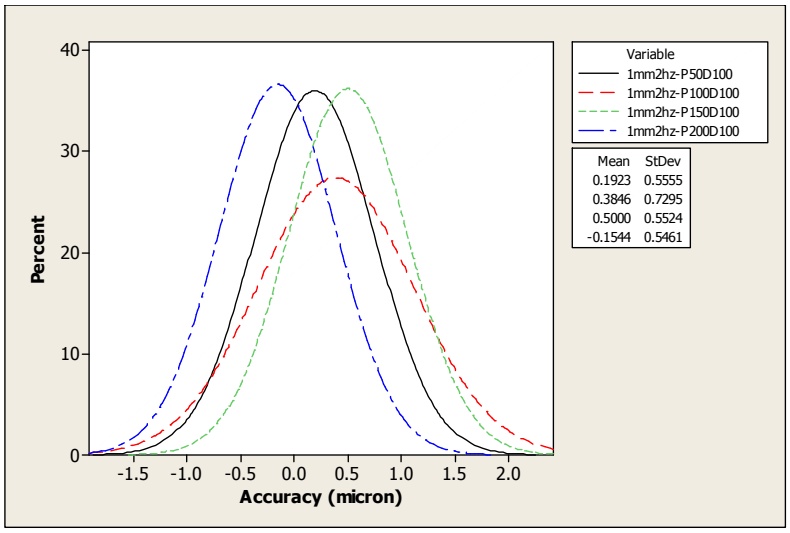

Fig. 9.12: Optimized positional accuracy for non-lubricated 100µm-thick carbon-steel at 2Hz feed-frequency.

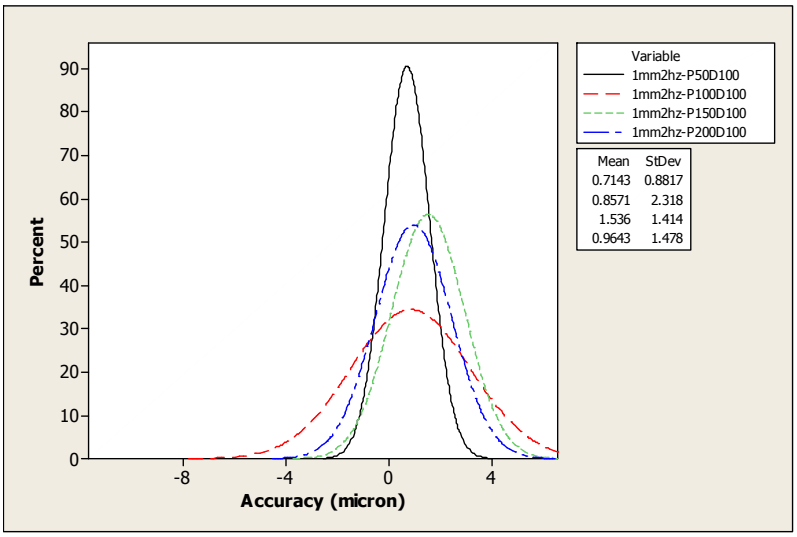

Fig. 9.13: Optimized positional accuracy for non-lubricated 50µm-thick stainless-steel at 2Hz feed-frequency.

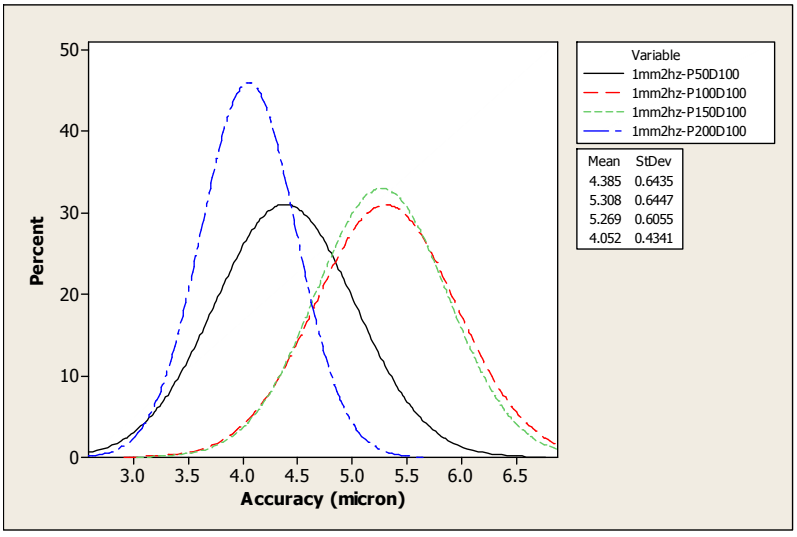

Fig. 9.14: Optimized positional accuracy for lubricated 50µm-thick carbon-steel at 2Hz feed-frequency.

b) 5mm feed-distance

At 1Hz feed-frequency, the experiment results showed a slight deterioration of positional accuracy and repeatability for all of the tested materials and thicknesses. As shown in Fig. 9.15, CS50NL experienced slight deterioration of positional accuracy from 0.8µm at 1mm feed-distance to 2.7µm mean-positional accuracy. Repeatability was also recorded at ±1.4µm. Change of the P-term gain-value promoted the same effect as in previous tests. Too-low a P-term gain-value resulted in the system being unable to maintain the desired -target-position and repeatability. Too-high a P-term gain-value promoted better repeatability but, on the other hand, proportionally increased the error-level of the system.

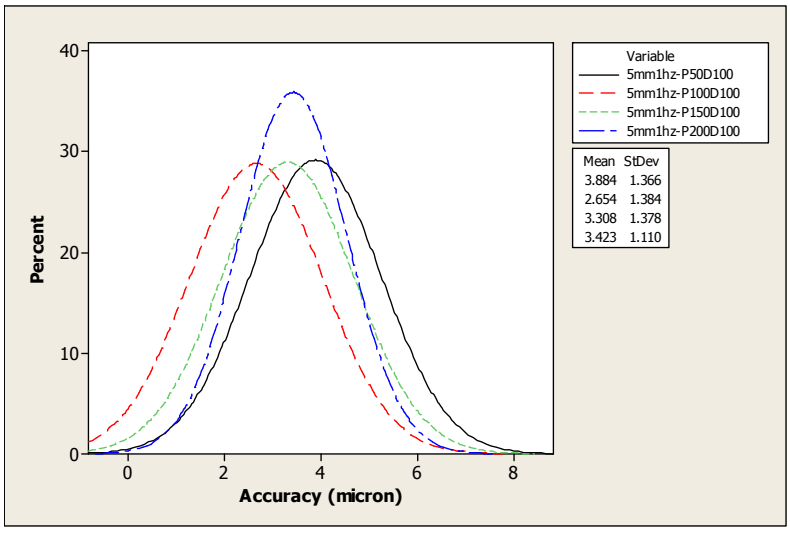

Fig. 9.15: Optimized positional accuracy for non-lubricated 50µm-thick carbon-steel at 1Hz feed-frequency.

No significant effect of the increase of the P-term gain-value on positional accuracy was observed for the CS100NL tests. Based on the tests, shown in Fig. 9.16, there was some slight deterioration of positional accuracy and repeatability of the system in comparison to the results for 1mm feeding-distance. However, a reasonably good mean-positional accuracy of 1.2µm was achieved, apart from the ±0.7µm average-repeatability found with the P50D100 configuration.

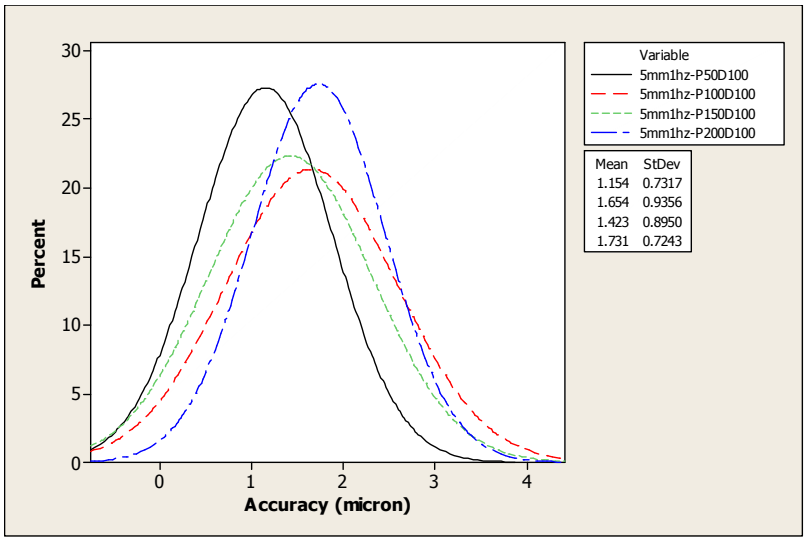

Fig. 9.16: Optimized positional accuracy for non-lubricated 100µm-thick carbon-steel at 1Hz feed-frequency.

Significant loss of repeatability of the system was observed when SS50NL strip was tested. Based on Fig. 9.17, the system tried to maintain positional-repeatability at around ±2.1µm to ±2.5µm for each feed. Change on the P-term gain to higher values did not promote improvement positional accuracy and repeatability, as shown by the similar patterns demonstrated for all adjusted P-term gains.

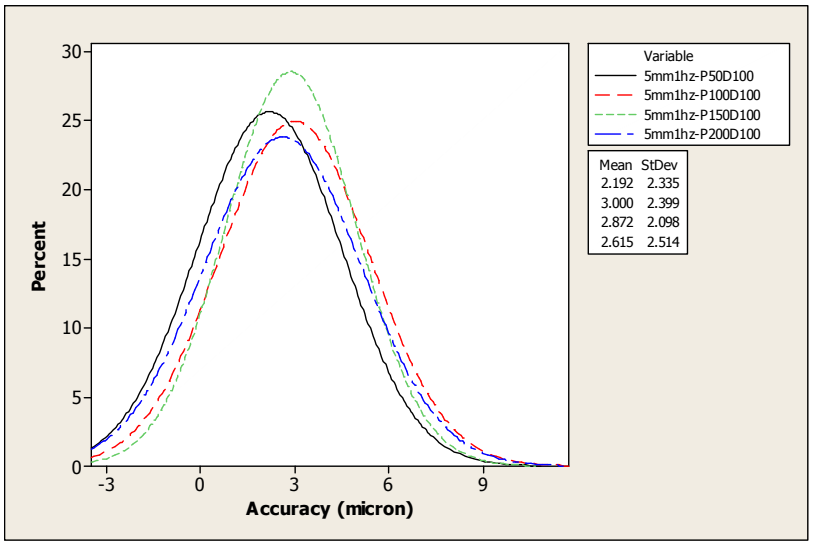

Fig. 9.17: Optimized positional accuracy for non-lubricated 50µm-thick stainless-steel at 1Hz feed-frequency.

As shown in Fig. 9.18, the presence of lubricant promoted stability in the system when 50µm-thick carbon-steel strip was used. For the P200D100 configuration, 1.9µm and ±1.1µm positional accuracy and repeatability, respectively, were recorded. Some slight under- and overfeed-patterns were observed for the lowest P-

term value of 50%. At the same time, the rest of the higher-values of the P-term-gain resulted an overfeed tendency of the system.

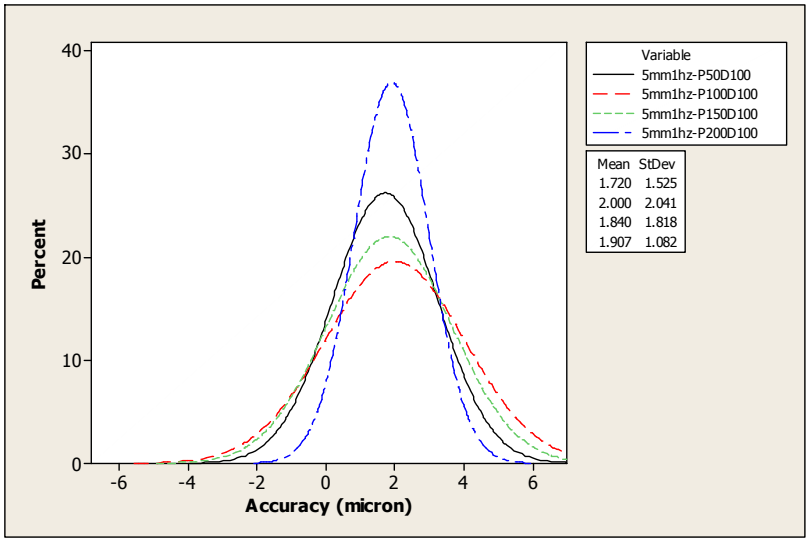

Fig. 9.18: Optimized positional accuracy for lubricated 50µm-thick carbon-steel at 1Hz feed-frequency.

At 2Hz feed-frequency, significant deterioration of feeder's positional accuracy and repeatability were observed for the whole of the material types and thicknesses tested. As shown in Fig. 9.19, for P150-D100, the positional accuracy recorded for CS50NL was observed to be the best among all of the other adjusted P-term gain-values. For this configuration, 4.3µm mean-positional accuracy and ±0.8µm repeatability were recorded. Slight better positional accuracy was observed when CS100NL was used, as demonstrated by Fig. 9.20. For P50D100 adjusted proportional gain, the recorded mean-positional accuracy and repeatability were 0.2µm and ±0.8µm, respectively. For the lowest P-term gain-value of the P50-D100 configuration, the feeder tends to underfeed. A similar phenomenon was observed when the P-term gain was increased to 100%. The tendency to underfeed reduced slightly at this higher proportional-gain-value. For both 150 and 200%, the trend changed to more positive feeding-positional accuracy, with little underfeeding being experienced.

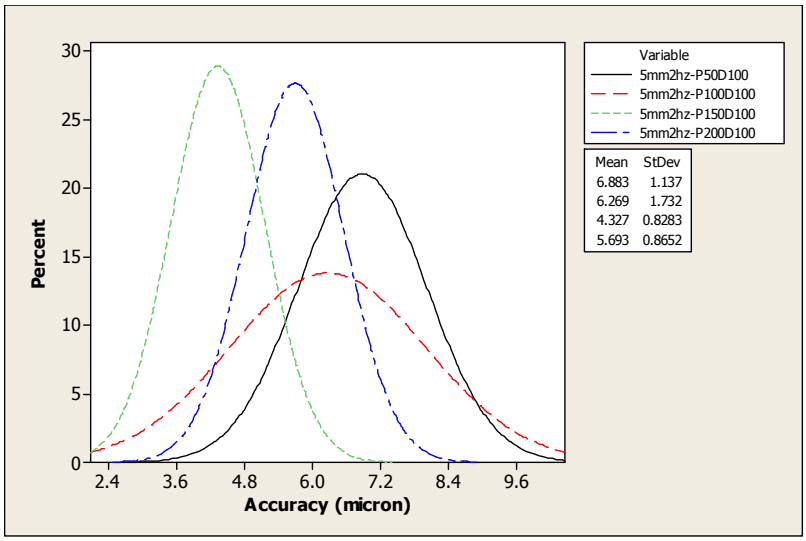

Fig. 9.19: Optimized positional accuracy for non-lubricated 50µm-thick carbon-steel at 2Hz feed-frequency.

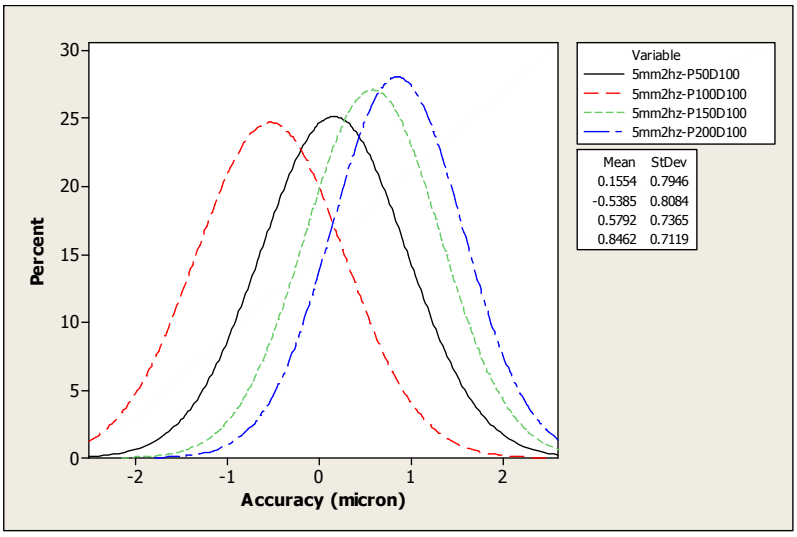

Fig. 9.20: Optimized positional accuracy for non-lubricated 100µm-thick carbon-steel at 2Hz feed-frequency.

About the same range of positional accuracy as that of CS50NL was demonstrated by SS50NL, as depicted in Fig. 9.21. However, the recorded pattern showed a slightly worse performance, with an achieved mean-positional accuracy of 2.8µm, and ±1.7µm repeatability was maintained by the feeder throughout the feeding process. Contrarily, with CS100NL, the mean positional accuracy for all of the adjusted proportional-gain values for both CS50NL and SS50NL was increased.

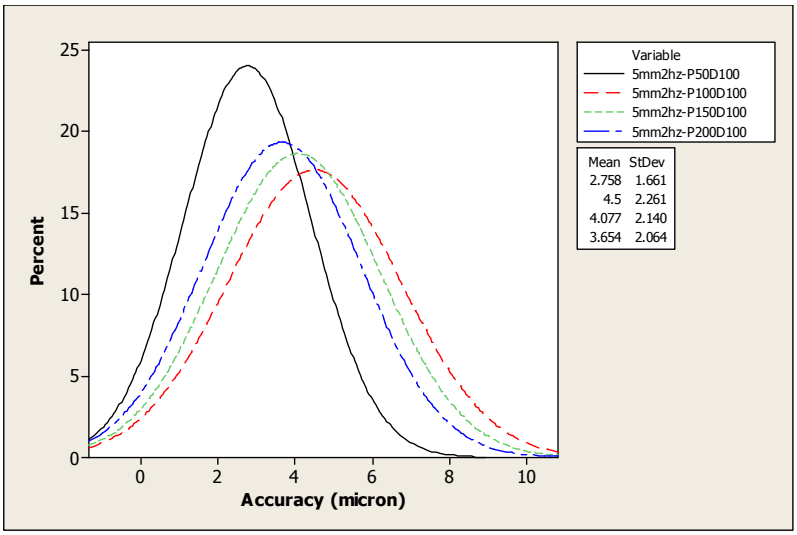

Fig. 9.21: Optimized positional accuracy for non-lubricated 50µm-thick stainless-steel at 2Hz feed-frequency.

From the lubrication experiment of CS50L, repeatability improvement was observed, as shown in Fig 9.22. A smaller range but large repeatability was recorded, compared to the values for the non-lubricated tests. However, the level of positional accuracy for all adjusted proportional-gains remained consistent for all values, deteriorating slightly to ±5.5µm with ±1.6µm repeatability, when compared to the findings for CS50NL.

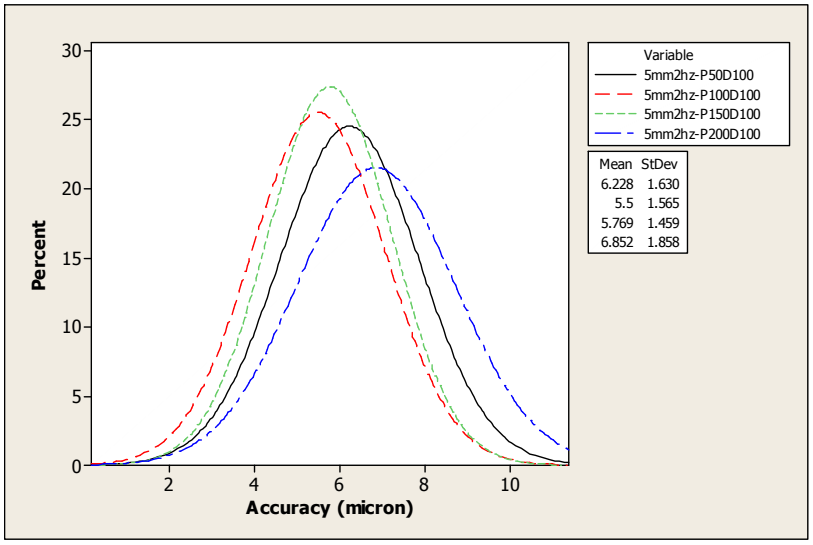

Fig. 9.22: Optimized positional accuracy for lubricated 50µm-thick carbon-steel at 2Hz feed-frequency.

9.4.3.2 Fixed-P Results

a) 1mm feed-distance

At 1Hz feeding-frequency, changes in the damping-gain D-term value did not promote any improvement in positional accuracy, as depicted in Fig. 9.23. An average of 2-3µm positional accuracy was recorded for most of the adjusted damping-gain values. Hence, the effect of changing the damping-gain on positional-positional accuracy was, significantly, not to improve positional accuracy, rather than deteriorating it. However, the repeatability settled mostly at ±0.6µm for the P100D100 configuration.

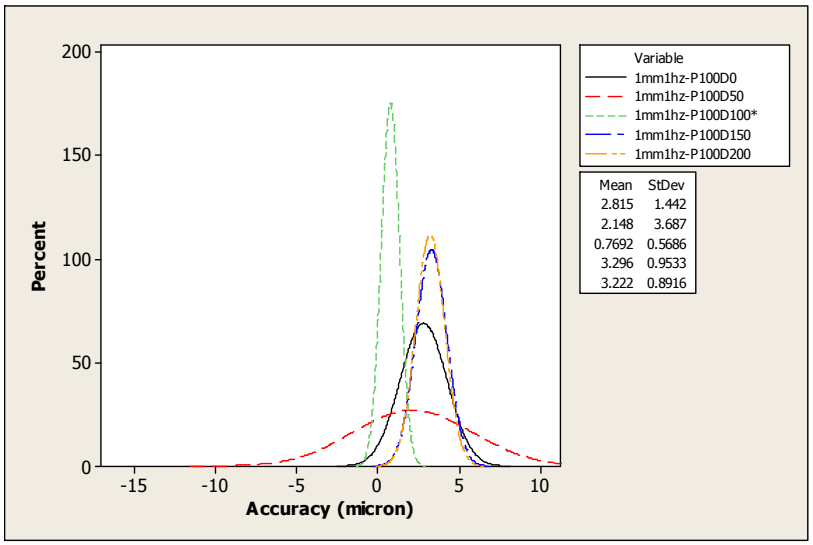

Fig. 9.23: Optimized positional accuracy for non-lubricated 50µm-thick carbon-steel at 1Hz feed-frequency.

Significant improvement on positional accuracy was observed when thicker carbon-steel strip was used. For CS100NL strip, as shown in Fig. 9.24, increase in damping gain produces positive positional accuracy but at the same time proportionally increases the positional errors. When the damping gain was configured to 100%, there was a tendency towards negative positional error of -1µm mean-positional accuracy and with consistent repeatability at ±0.7µm. The-lowest damping-gain configured, 0%, demonstrated better mean-positional accuracy started at -0.2µm and reducing to ±0.6µm repeatability.

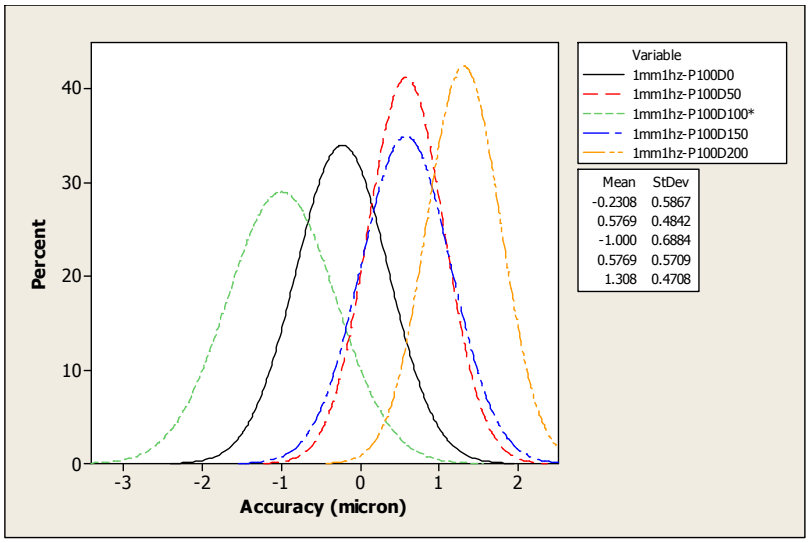

Fig. 9.24: Optimized positional accuracy for non-lubricated 100µm-thick carbon-steel at 1Hz feed-frequency.

A contra-effect was demonstrated when stainless-steel strip CS50NL was used. Proportionally with the increase of damping gain, the positional positional accuracy was improved to a better value than that when configured at a low value, as demonstrated by Fig. 9.25. A repeatability of ±0.7µm was recorded when the system was configured at P100D100 damping-gain. For this compensation-rate, the average-positional accuracy was recorded as 0.5µm. The lowest damping-gain-value of 0% clearly reduced the performance of the system, with mean-positional accuracy of 1.8µm and ±1µm repeatability.

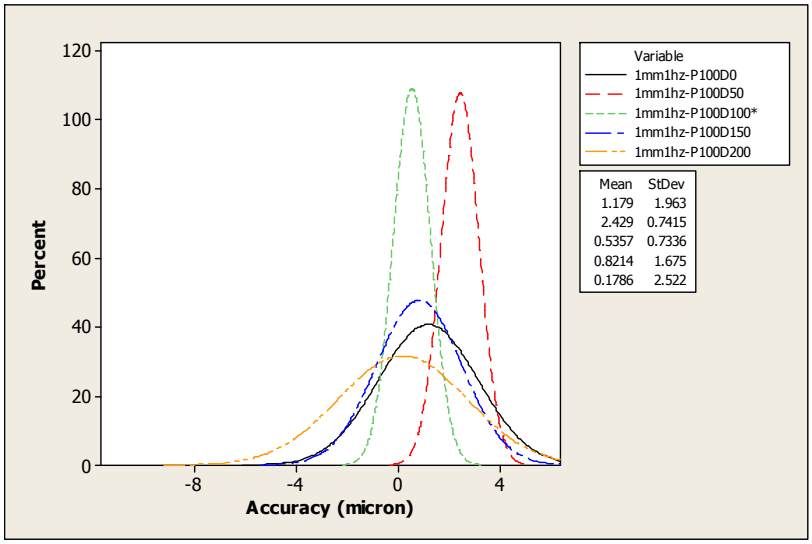

Fig. 9.25: Optimized positional accuracy for non-lubricated 50µm-thick stainless-steel at 1Hz feed-frequency.

In the presence of lubricant for CS50L strip, as depicted in Fig. 9.26, a similar trend of positional accuracy pattern as that for CS50NL was observed. However, the observed positional accuracy at 100% damping gain was slightly reduced and settled at 2.1µm with repeatability at ±0.7µm. Further increase in the damping-gain value proportionally increased the positional-error to 4µm average, with a repeatability of ±0.7µm; while the lowest-configured damping-gains settled mostly at 1.8µm mean-positional accuracy and ±1.0µm repeatability.

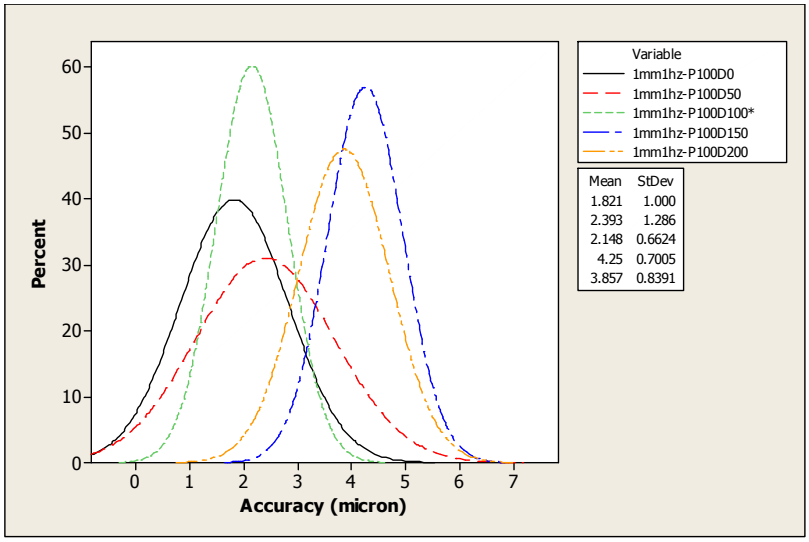

Fig. 9.26: Optimized positional accuracy for lubricated 50µm-thick carbon-steel at 1Hz feed-frequency.

At 2Hz feed-frequency, greater levels of damping-gain did not produce similar results to those obtained at lower damping-gain. For CS50NL, as shown in Fig. 9.27, on average, mean-accuracies of 6.1µm and 5.1µm, and ±0.6µm and ±2.6µm repeatability were achieved for the smallest and the largest damping-gain, respectively. For 100% damping-gain, better positional accuracy and repeatability were recorded, with an average of 2.2µm mean-positional accuracy and ±1.1µm repeatability.

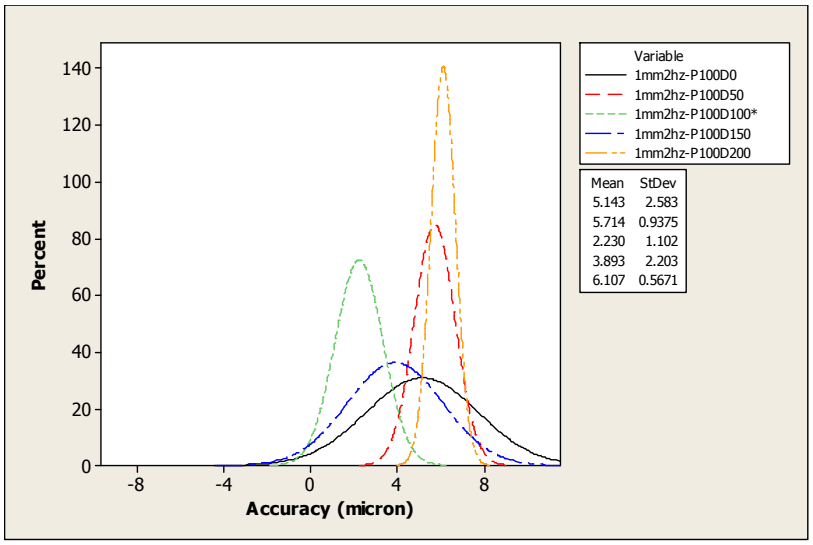

Fig. 9.27: Optimized positional accuracy for non-lubricated 50µm-thick carbon-steel at 2Hz feed-frequency.

Changes on damping-gain did not promote significant changes in the feeder performance when feeding CS100NL material. Based on the experimental results presented in Fig 9.28, almost all of the adjusted damping-gain results lay within -0.1µm to -0.6µm mean-positional accuracy, with an average repeatability-range of from ±0.5µm to ±0.7µm. However, a negative positional accuracy-pattern was recorded when the damping gain was configured at 0%. At this configuration, the settled mean-positional accuracy and repeatability were recorded as -0.2µm and ±0.5µm, respectively, without overshooting of any point by more than a ±1µm range.

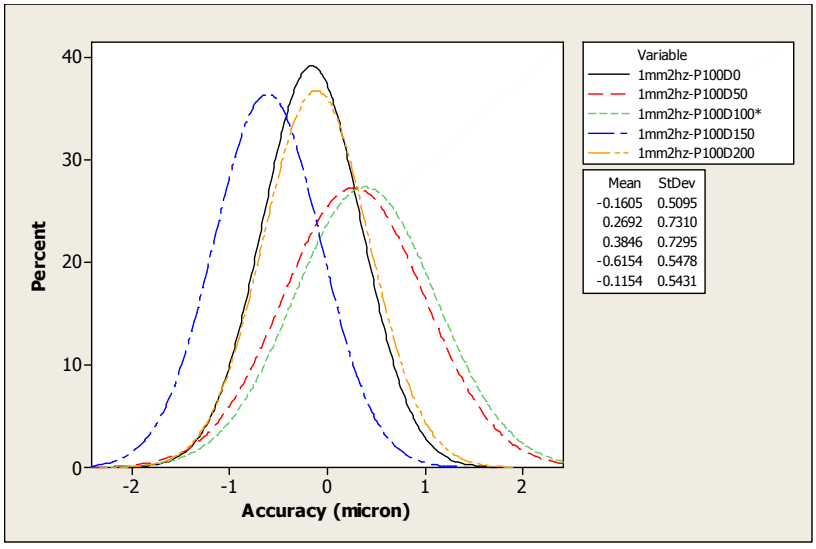

Fig. 9.28: Optimized positional accuracy for non-lubricated 100µm-thick carbon-steel at 2Hz feed-frequency.

A similar phenomenon of insignificant influence of damping-gain on positional accuracy and repeatability was recorded when the strip material was changed to stainless-steel, as depicted in Fig. 9.29. At a damping-gain configuration of 150%, SS50NL showed a better positional accuracy compared to that for the others. At this configuration, a mean-positional accuracy of 1.1µm and ±0.6µm repeatability was recorded.

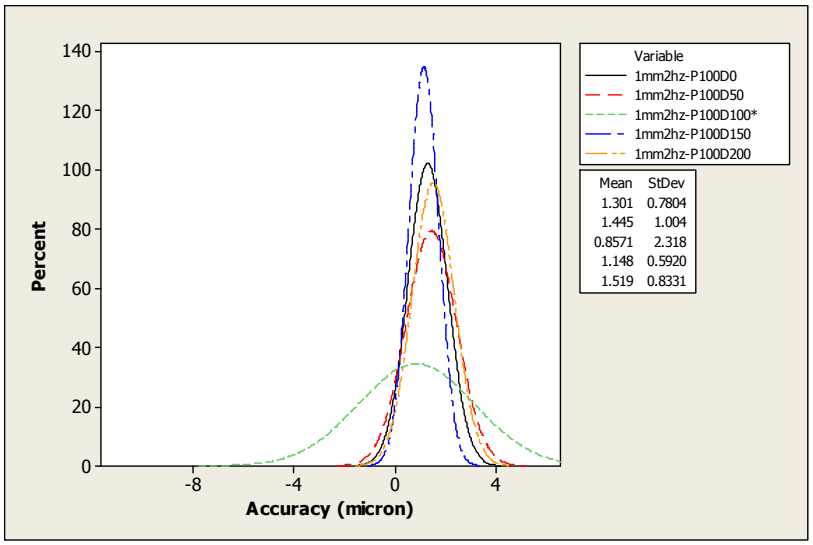

Fig. 9.29: Optimized positional accuracy for non-lubricated 50µm-thick stainless-steel at 2Hz feed-frequency.

Deterioration of the positional accuracy was experienced when lubrication was introduced to the system, as shown in Fig. 9.30. However, slight improvement in repeatability was observed throughout the feed process. An positional accuracy and repeatability of 5.3µm and ±0.6µm, respectively, were recorded when the damping gain was configured to 100%. At this configuration, no tendency to overshooting- and undershooting-repeatability beyond ±1µm range occurred. Although contributing little towards improving the feeding performance of the feeder, lubrication was believed to slightly improve repeatability-consistency.

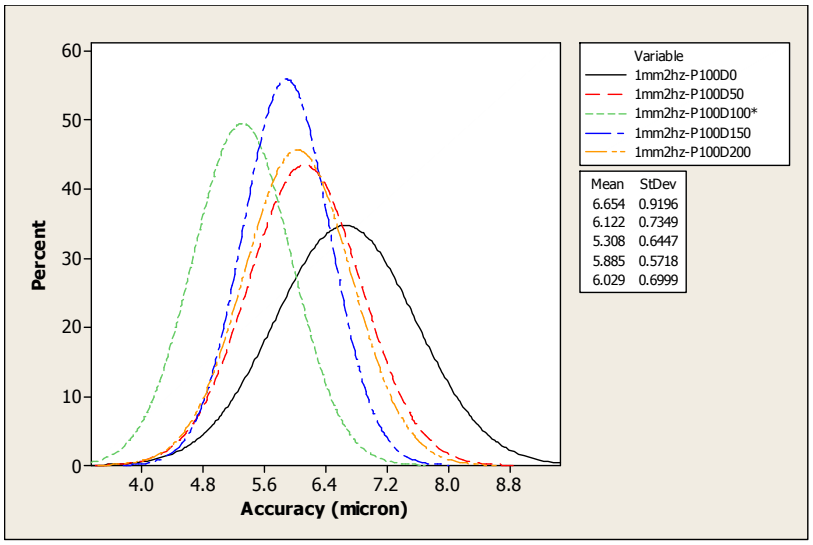

Fig. 9.30: Optimized positional accuracy for lubricated 50µm-thick carbon-steel at 2Hz feed-frequency.

b) 5mm feed-distance

At 1Hz feed-frequency over a longer feed-distance, similar pattern of positional accuracy and repeatability as for 1mm feed-distance at 2Hz feed-frequency was observed. The deterioration on both parameters was significant throughout the entire range of adjusted damping-gain. As depicted in Fig. 9.31, the feed-performance of CS50NL was recorded as an average of 2-2.7µm mean-positional accuracy and ±1.4µm repeatability. A pattern in the repeatability was identified when the damping gain was configured at 0%. Increase of the damping value of the system tends to promote inconsistency in the repeatability pattern, hence resulting in slight overshooting and undershooting of repeatability of up to ±1.4µm.

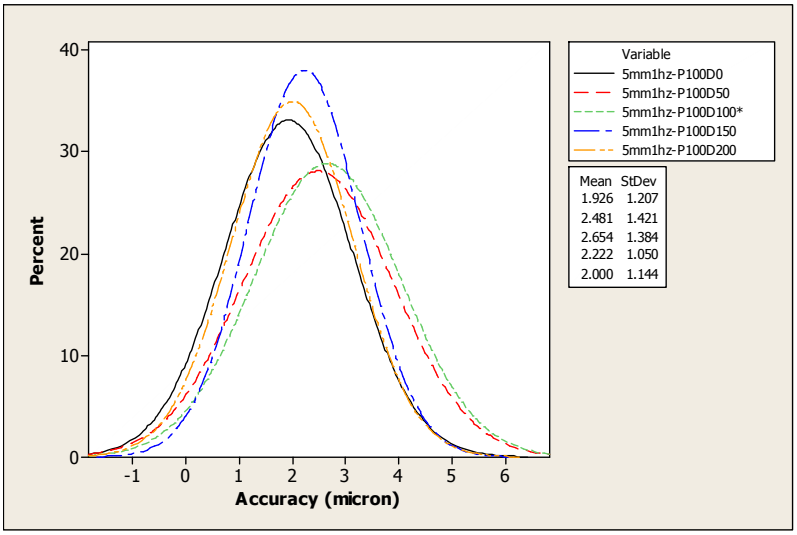

Fig. 9.31: Optimized positional accuracy for non-lubricated 50µm-thick carbon-steel at 1Hz feed-frequency.

Insignificant improvement on positional accuracy was also recorded when the material thickness was changed to 100µm-thickness. As demonstrated by Fig. 9.32, on average, about 1.5-1.7µm mean-positional accuracy and between ±0.7-0.9µm repeatability were recorded when the damping gain of the system was varied. Slightly better repeatability was recorded when the damping-gain was configured at 200%, with an achieved mean-positional accuracy of 1.5µm and ±0.7µm repeatability.

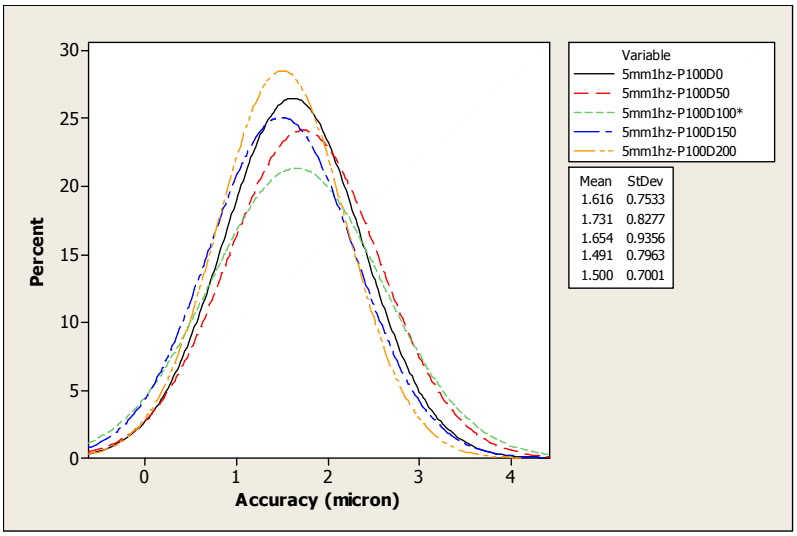

Fig. 9.32: Optimized positional accuracy for non-lubricated 100µm-thick carbon-steel at 1Hz feed-frequency.

When the material was changed to stainless steel, as illustrated in Fig. 9.33, a deteriorated repeatability was observed, along with some slight deterioration of positional accuracy-performance compared to the values for short-distance feeding. The best mean-positional accuracy was 1.8µm, with ±1.9µm repeatability, when damping-gain was increased to 150%. Switching the damping-gain to a lower value did not contribute to the improvement of mean-positional accuracy and repeatability: instead, it slightly reduced them. At the same time, too-high damping-gain at 200% resulted in wider deviation-dispersion, which in turn led to reducing repeatability.

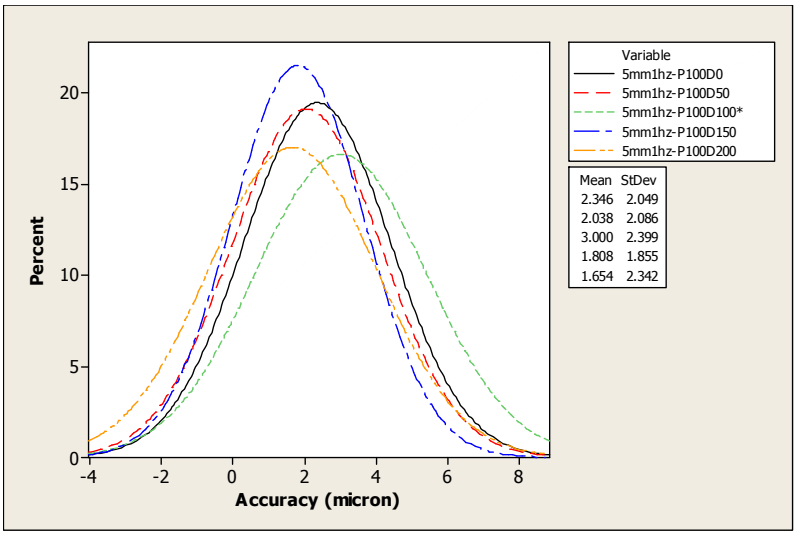

Fig. 9.33: Optimized positional accuracy for non-lubricated 50µm-thick stainless-steel at 1Hz feed-frequency.

Tight deviation-dispersion was observed with the presence of lubrication on the system, as shown in Fig. 9.34. Nevertheless, slight deterioration on positional accuracy was observed when the damping gain was increased to the greatest value. Although tighter and more-controlled deviation-dispersion was observed with the presence of lubrication, this however, did not contribute to any improvement in positional accuracy: instead, it reduced it slightly.

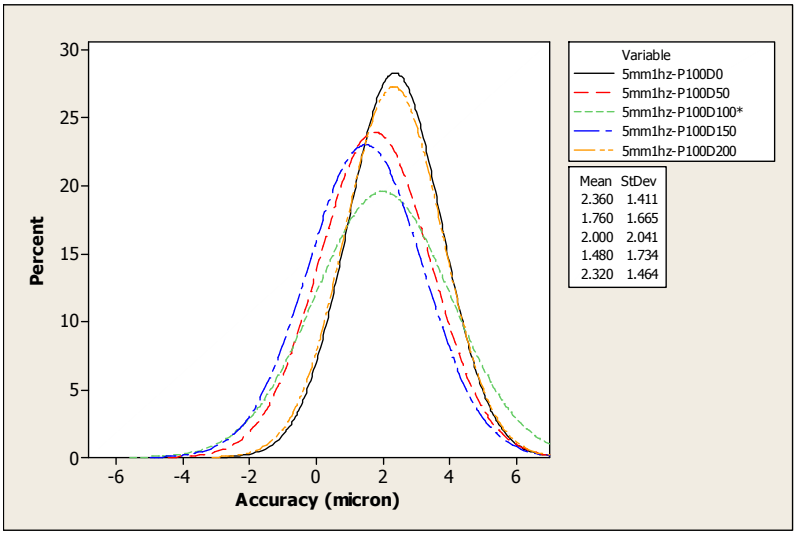

Fig. 9.34: Optimized positional accuracy for lubricated 50µm-thick carbon-steel at 1Hz feed-frequency.

At 2Hz feed-frequency, an obvious deterioration in positional accuracy was experienced, where the positional accuracy level worsen to the highest value of 6.3µm, at P100D100 along with some consistent repeatability-patterns at ±1.7µm,

for CS50NL, as shown in Fig 9.35. Positional accuracy instability was observed when the damping gain was configured at 100%. The positional accuracy tends to gradually decreases with the increases in the number of feeding. A low damping-gain at 50% promoted more positional accuracy of damping stability and consistent-repeatability, with a recorded positional accuracy and repeatability of 3.1µm and ±0.9µm, respectively.

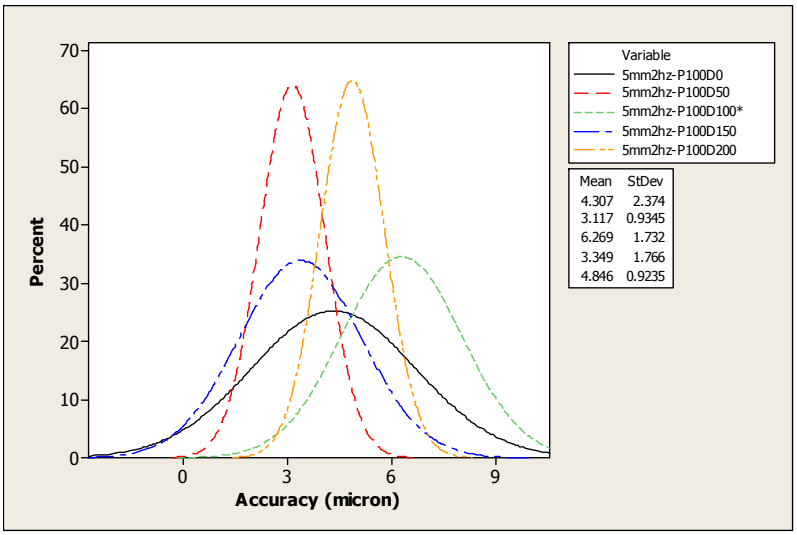

Fig. 9.35: Optimized positional accuracy for non-lubricated 50µm-thick carbon-steel at 2Hz feed-frequency.

The effect of different values of damping gain on thicker strip, CS100NL, demonstrated various responses in the positional accuracy and repeatability performance, as depicted in Fig 9.36. The best positional accuracy and repeatability were recorded at 0.5µm and ±0.6µm, respectively, when the damping gain was configured to 0%. Greater damping gain tended to promote overshooting and undershooting of the positional accuracy and repeatability beyond the best value. The positional accuracy tended to deteriorate to 2.2µm when subjected to 200% damping-gain.

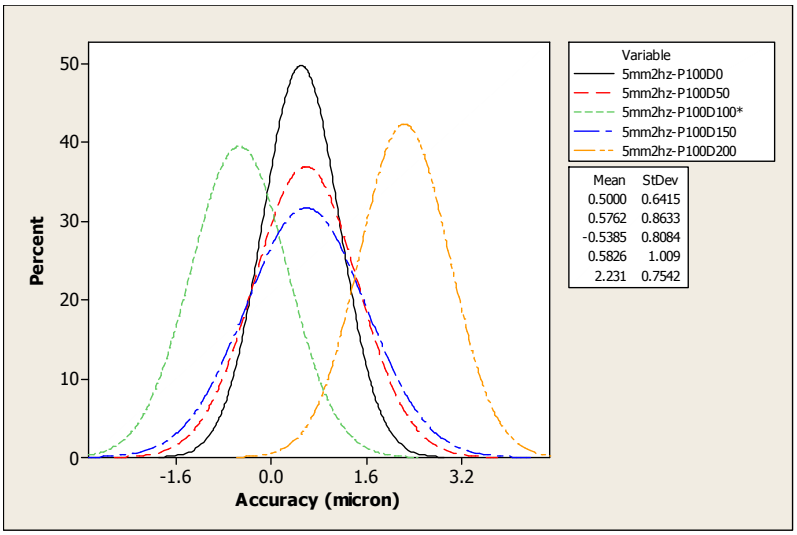

Fig. 9.36: Optimized positional accuracy for non-lubricated 100µm-thick carbon-steel at 2Hz feed-frequency.

A similar positional accuracy and repeatability pattern for SS50NL as for 1Hz feed pattern was observed, as shown in Fig 9.37. A greater damping-gain of 150% tended to slightly improve the positional accuracy, but decreased it when 200% damping-gain was used. Nevertheless, a quite similar repeatability-pattern was observed, where the deviation-dispersion for the entire range of damping-gain tested settled within ±2.0-2.4µm. It can be concluded that no significant improvement may be expected with the change of damping-gain.

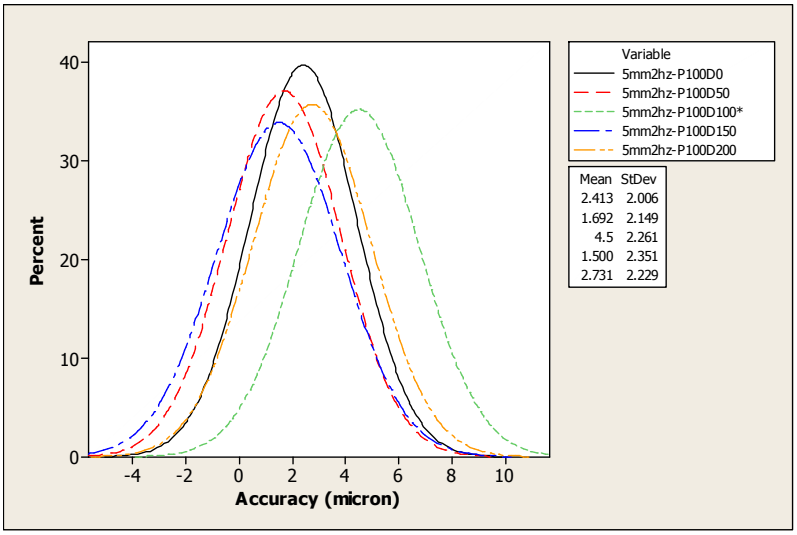

Fig. 9.37: Optimized positional accuracy for non-lubricated 50µm-thick stainless-steel at 2Hz feed-frequency.

Further positional accuracy-deterioration was experienced by carbon-steel strip when lubrication was introduced into the system, as shown in Fig 9.38. The best achieved

positional accuracy and repeatability for this case was when the damping-gain was configured at 50%, which gave around 5.2µm mean-positional accuracy and almost ±1µm repeatability. Greater damping-gain promoted instability of the system, hence further reducing the positional accuracy.

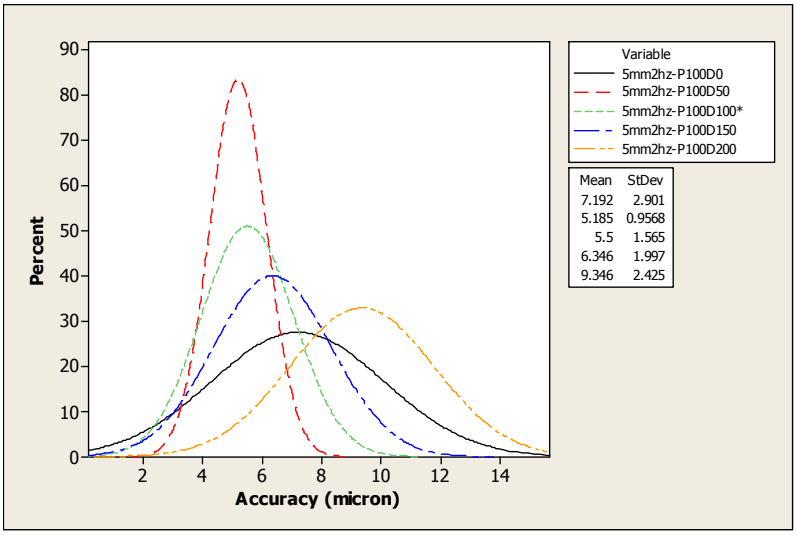

Fig. 9.38: Optimized positional accuracy for lubricated 50µm-thick carbon-steel at 2Hz feed-frequency.

9.4.4 Brake-Force Application Results

a) 1mm feed-distance

At 1mm feed-distance, a similar trend and pattern for both 1 and 2Hz feed-frequencies were observed. At 1Hz feed-frequency, as depicted in Fig. 9.39, the presence of brake-force promoted very slight deterioration inaccuracy. The feeding process tended to demonstrate an underfeed pattern. This also happened when feed frequency was changed to 2Hz. Although the tendency to underfeed was observed to be significant for both cases, an obvious improvement on positional accuracy was observed -n the 2Hz test, as shown in Fig. 9.40. The best mean-positional accuracy when brake-force was applied was -0.4µm with an average repeatability of ±1.2µm. Compared to the results for 1Hz, most of the time the feed pattern showed underfeed when subjected to brake-force, whereas at 1Hz, the mean-positional accuracy was 0.4µm with a repeatability of ±1.0µm. Nevertheless, at this 2Hz feed-frequency, a slightly better mean-positional accuracy was recorded compared with the results observed in the absence of brake-force, where the recorded mean-positional accuracy and repeatability were 2.2µm and ±1.1µm, respectively.

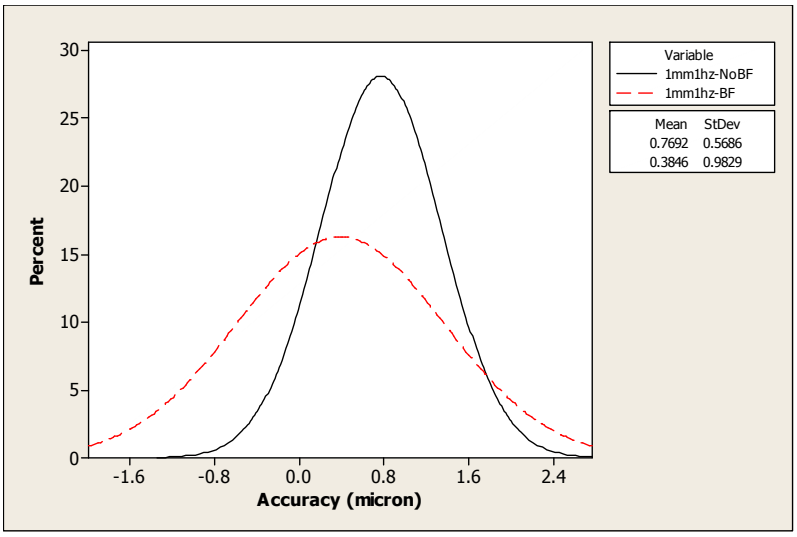

Fig. 9.39: Positional accuracy and repeatability at 1mm and 1Hz feed-distance and frequency, respectively.

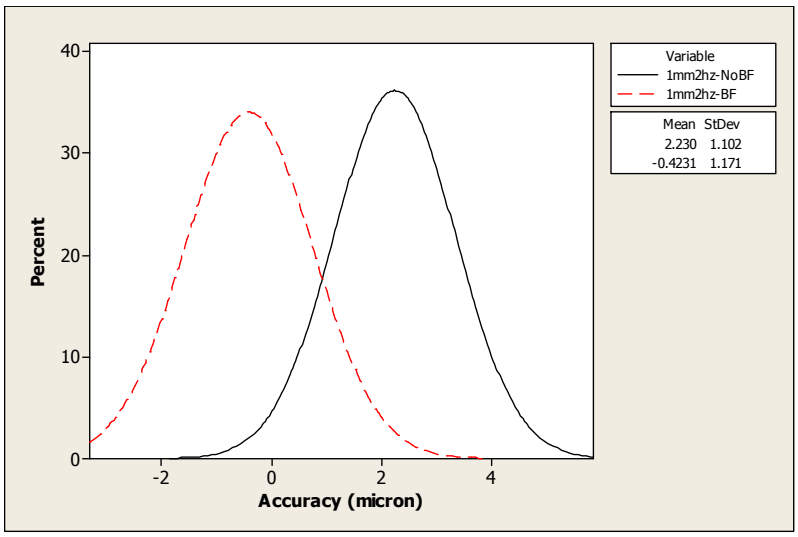

Fig. 9.40: Positional accuracy and repeatability at 1mm and 2Hz feed-distance and frequency, respectively.

b) 5mm feed-distance

Applying brake-force over longer feed distance demonstrated improvement in positional accuracy. Observation of the results presented in Figs. 9.41 and 9.42 however, showed that no improvement in repeatability was recorded. At 1Hz feed-frequency, the positional accuracy pattern tended to shift from positive positional accuracy to negative positional accuracy of -1.2µm mean-positional accuracy and to ±1.3µm repeatability, as shown in Fig. 9.41.

For the greater feed-frequency of 2Hz, as depicted in Fig. 9.42, the brake-force positional accuracy pattern showed slight improvement compared to the test results

obtained in the absence of brake-force. A similar repeatability-pattern was observed between the-with- and without- brake-force results, but with slight deterioration when the system was subjected to brake-force. For this configuration, the system repeatability was ±1.4µm with a mean-positional accuracy of 1.3µm.

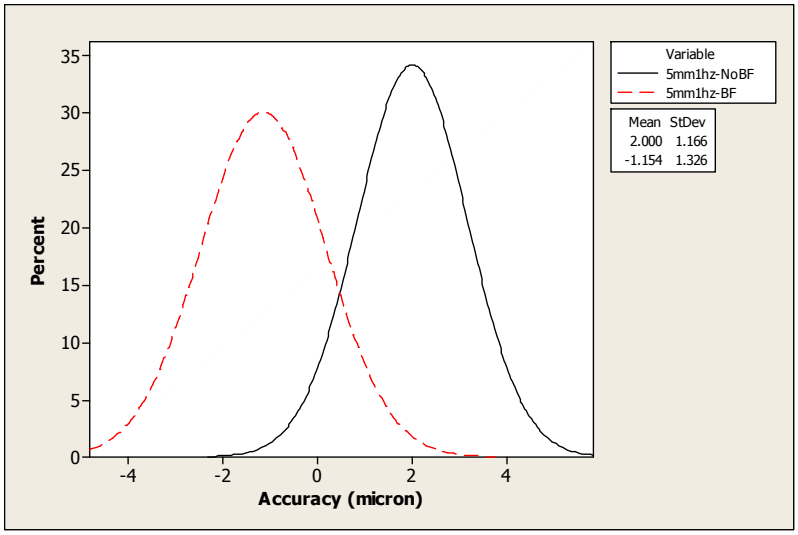

Fig. 9.41: Positional accuracy and repeatability at 5mm and 1Hz feed-distance and frequency, respectively.

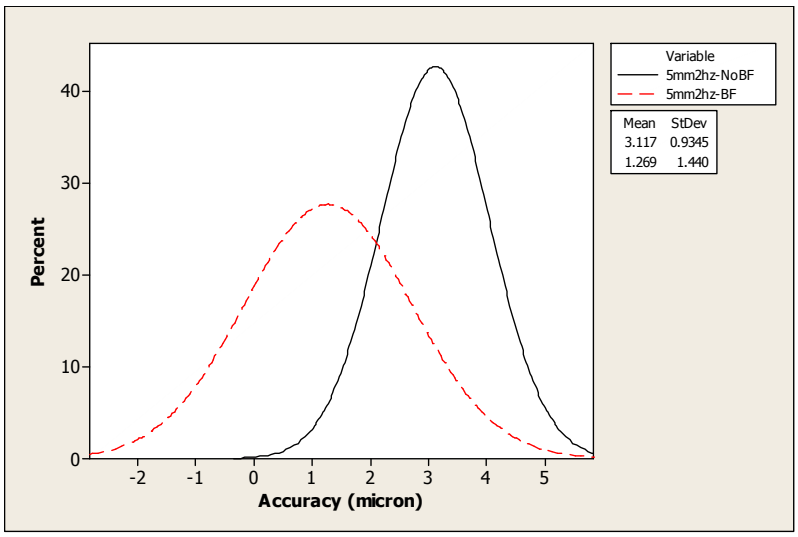

Fig. 9.42: Positional accuracy and repeatability at 5mm and 2Hz feed-distance and frequency, respectively.

9.5 Discussion

9.5.1 Linear-Encoder and Tape Errors

For a system which employs a linear-motor as the means of actuation, the acceleration and velocity of the system is strictly limited by its encoder bandwidth [Braembussche et al., 1996]. Therefore, it is suspected that amongst the sources of inaccuracies identified in the developed feeder's performance, one caused by error and limitation of the linear-encoder readhead capability. The readhead was designed to give a best measurement and reading-repeatability of ±1µm [Renishaw]. Hence, most of the readings were taken with the best repeatability of almost ±1µm. Moreover, the linear-tape used in the system was subjected to 3µm error at 1m travel-distance. At 1 and 5mm feed-distances, this is equivalent to 0.003µm and 0.015µm error. Although the error-contribution is relatively small, the accumulation of all such errors however, did reduce the performance of the feeder.

9.5.2 Linear-Motion Guideways Issues

9.5.2.1 Contact and Non-Contact Issues

The presence of excessive and over-constrained contact in conventional mechanical-bearings guideways (effects from lubricants, preload variation, recirculating ball cogging, retainer creep, ball-cage creep etc.) prevent such guideways from coming close to matching both the static and dynamic performance of air-bearings guideways. On top of that matter, cable management due to the moving cable is also seen to contribute to inaccuracy. The residual effect of a moving cable contributes to a small force, for which the servo-integrator develops an equal and opposing force to cancel the contributed force of the moving cable [McCarthy, 2006]. In low-speed motion, this cancellation may be working to improve positional accuracy. Nevertheless, in high-speed motion, inertia from the moving cable is of sufficient magnitude to affect the final settling effort, which ultimately reduces the positional-accuracy.

Friction in mechanical-bearings guideways is a highly non-linear effect and degrades the performance of servo-control loops, since the servo-controller is constructed based upon linear-system theory. In addition, although mechanical-bearings guideways are made to support a high load, their motion-accuracy and precision are

often affected and limited because of the presence of non-linear guide-friction [Chen et al., 2003].

According to Elfizy et al., (2005), ripple-force has also demonstrated a contribution to positional error, not only with the iron-core-type motor but also with the iron-less motor. As a result, this limits the feeder's potential when it comes to sub-micron positional accuracy. In addition, stick-slip friction could also affect the precision, especially when the feeder is about to execute high-precision positioning.

9.5.2.2 Motion and Velocity Issues

As to what has been described in the previous chapter, although efforts in achieving greater positional-accuracy of direct-drive linear-motors have demonstrated success with the range of sub-micron or nanometre capability [Gao et al., 2006; Shinno et al., 1999], all of the efforts were conducted very cautiously and at a very low positioning-speed. Issues such as bearing friction, pre-load variations, recirculator cogging and lubrication issues make mechanical linear-bearings guideways-systems fraught with problems in securing perfect constant-velocity and smooth motion. With such systems there is also the need to wait until the servo-loop integrator overcomes the problems and restores the best absolute position. Low positioning-speed gives servo-controllers adequate time to gradually correct the positioning errors to the lowest possible value, thus improving positional accuracy and repeatability.

Differently to low-speed feeding at 1Hz, high-speed feeding at 2Hz requires positioning to be completed in 50% of the time for 1Hz, hence requires a shorter settling time and a greater velocity to be able to accomplish the task. Moreover, in high-speed positioning, fluctuation of the velocity in mechanical-bearings-based stages occurs during the zero acceleration in the trapezoidal motion. This inconsistency affects the motion smoothness, where constant-velocity motion is barely achievable. As a result, the deterioration of positional accuracy at 2Hz is greater than that at 1Hz.

A change to longer feed-distance also causes deterioration of positional accuracy and repeatability, even though the operational feed-frequency is fixed. This is mainly

because a longer feed-distance requires a greater velocity and acceleration compared to that for a shorter feed-distance due to the given time-frame for both feed-distances being similar at 1Hz. Therefore, a similar consequence as for 2Hz feed-frequency in terms of positional accuracy was observed.

9.5.2.3 Positional Accuracy and Repeatability Issues

The positional accuracy of linear-motion mechanical-guideways can be specified in terms of running parallelism, dimensional tolerance for height and width, and height and width differences between a pair when two or more linear-motion carriage are used on the same rail, or when two or more rails are mounted on the same plane. Parallelism on the travel axis can be as low as 1µm for 50mm travel-distance and also on the other two axes [THK; SBC Slide], while both height and width tolerances are up to 8µm maximum. This indirectly contributes to inaccuracy during the feeding process.

9.6 Conclusions

Based on the results of the experiments conducted, the following conclusions are drawn.

i. The payload acting on the feeder has a significant effect on the positional accuracy and repeatability performance of the feeder
ii. The motion-profile does have significant effect towards on the positional accuracy and repeatability performance of the feeder.
iii. The positional accuracy and repeatability of the developed feeder was optimized and seen to be improved with proper adjustment of the P-D gain.
iv. Each strip has a different P-D configuration to achieve high positional accuracy and positioning repeatability. Better feed-performance is achieved when proper optimization work has been carried out for each strip material used.
v. The presence of brake-force on the system promotes improved positional accuracy and repeatability for both of the feed-distances and feed-frequencies explored.

Chapter 10

Part Transport – *Transport-Micro*™

10.1 Summary

Based on the present-day trend in micro-forming trend, effort is being focused more into establishing the micro-machine in order to be able to produce micro-parts/products without there being sufficient research and development into material handling. A micro-forming machine alone, without a proper handling-system, is seen impractical for meeting industrial demands. Continuous production requires not just an efficient manufacturing cell, but also autonomous synchronization between the machine and the material-handling system itself. This is inclusive of the way in which the machine automatically transports the finished parts/products away from its working environment and automatically packs the parts/products for shipment. The purpose of this part of the research programme is to investigate the handling-strategy for the finished parts/products machined by the micro-sheet-forming machine developed by the University of Strathclyde. This effort is focused more into the investigation of handling devices and the development of design considerations for a new transportation system for micro-sheet-forming applications. FE simulation by ABAQUS is used as a tool to study the characteristics of carrier-tape feeding as well as feeding accuracy. This is followed by development work on the part-transport system that was validated experimentally. Finally, the system is integrated with the existing micro-forming machine developed at the University of Strathclyde.

10.2 Introduction

It is also identified that more efforts are needed to address the transportation strategy for the finished thin-sheet-material parts/products of the manufacturing systems and production lines for micro-forming. It is shown that the handling of existing finished-parts/products from sheet forming was realized by the collection of parts directly from the tooling itself. Hence, inefficient and time-consuming manual-intervention is required to remove the finished parts/products from the machine.

Although most of the automation system use robotic arms as a handling strategy, it is too difficult to integrate robotic system into a small machine with limited access and space constraint. Moreover, if finished parts are to be produced by involving a process of transfer from one machine cell to another cell, an integrated handling and packaging system which can satisfy industrial needs is the best option. With this problem in mind, the development of an autonomous high-precision finished-parts transportation system has been initiated.

A servo roll-feeder was used to develop a system which capable of feeding carrier tape into the tooling. Finished parts/products are discharged from the tooling and directed to the embossed pocketed carrier-tape. Fairly-high positioning accuracy is required to ensure that the empty pockets of the carrier-tape remain accurately in place at the bottom of the lower-die opening. Huge inaccuracy may lead to misalignment between the carrier-tape pocket and the exit of the die opening which could result in mis-placement and cause the parts to stack together. This in turn leads to jam and failure of the collection system. Due to difficulty of employing the same accuracy-measurement technique as used in previous chapters, FE simulation is seen as a useful tool to quantify the system's accuracy. Several key parameters were tested and adjusted with a view to establishing the relationship between the feeding-characteristics and the feeding-frequency and motion-profile, as well as the presence of brake-force.

10.3 Equipment and Materials

10.3.1 The Micro-forming Machine

Experiments were performed on a micro-forming-machine system (Fig. 10.1) developed at the University of Strathclyde [Qin et al., 2008]. The machine uses a high-power linear-motor to directly drive a stamping/forming ram. The direct-drive linear-actuation of the machine is capable of generating a peak thrust-force of 5000N. With this large force, the machine is able to achieve has a production rate of up to 16 parts per second. Various types of tools may be used on the machine: these include easy- and simple- shape-creation by single-stage tooling, or enable the production of more advanced micro-parts through the use of multi-stage tooling. As discussed in the previous chapter, amongst the possible commercially-available sheet-metal feeders for sheet-forming, the micro-servo roll-feeder was the one that was identified as being the most suitable for micro-sheet-forming part-transport applications due to its compact design, easy control-features and high accuracy.

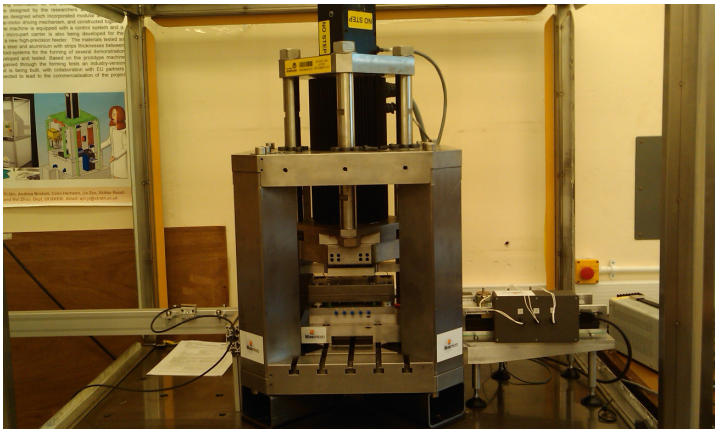

Fig. 10.1: Micro-forming machine developed at the University of Strathclyde.

10.3.2 The Servo Roll-Feeder

The servo roll-feeder uses a belt-transmission system to transfer rotational motion from the motor to the feeder rollers. Basically, the servo motor is controlled by a closed-loop operation where a rotational incremental-encoder is used for positional feedback. An effort has been made to assess the suitability of the performance of the feeder, as being presented in the previous chapter. Based on the studies made, the feeder exhibits a large positional-error, which makes it unsuitable for strip feeding.

The achieved accuracy, however, was seen to be suitable enough for micro-sheet-forming part-transport applications. Due to the use of a large pocketed carrier-tape, t accuracy is not the main concern. A similar technique as for the feeding of thin strip was used, where the carrier tape is pulled into the machine in order to avoid the occurrence of buckles and wrinkles during the transporting process [Jacques et al., 2007].

10.3.3 Pocketed Carrier-Tape

A pocketed carrier-tape, also known as an embossed carrier-tape, has the greatest production volume due to its flexibility in application. The use of a carrier-tape is one of the most common methods in the packaging of electronic components such as IC to LCD cells. The anti-static and mass-production-capability features obtained from this tape have been established through its dominance in electronic industries worldwide, compared to other packaging methods/techniques. Not only may thousands of sensitive- and fragile- electronic components be stored, packaged and safely protected against moisture and electro-static effects, they may be shipped out to the market directly, using such tapes.

The huge demand for this type of packaging has resulted in more effort being made to improve the existing system and materials [Yen et al., 2007]. Irrespective to the potential of this packaging technique, it has been extended to non-MEMS production application. Due to the system employed in this technique being relatively easy and simple, it has used as a means of transporting formed/processed parts/products out of the micro-sheet-forming machine. The type of tape used for the research is a pocketed/embosses carrier-tape (Fig. 10.2), with pocket measurements of 10mm width, 10mm length and 2mm depth, set at a pitch-distance of 12mm and within a total width of 16mm. The tape is made from polycarbonate having a density of 1270kg/m^3.

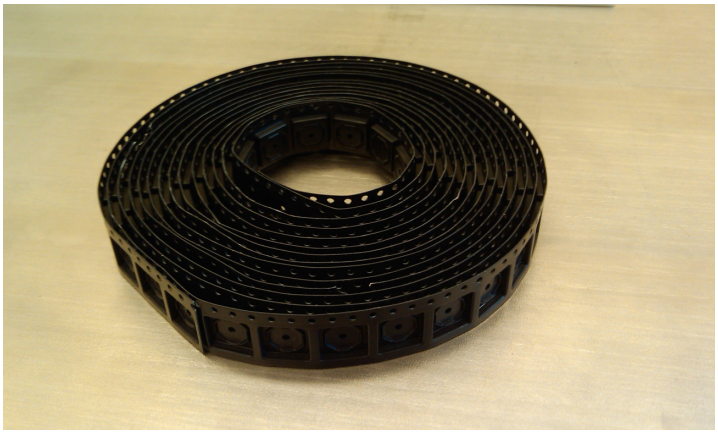

Fig. 10.2: Pocketed/embossed carrier-tape used for the tests.

10.3.4 75µm-thick Stainless-steel Strip

75µm stainless-steel strip grade AISI 316L (Fig. 10.3) was used as for study, where a part of simple round geometry was punched by the micro-sheet-forming machine. The strip composition is: of 69% iron; 18% chromium; 10% nickel; and 3% molybdenum. The strip is ductile due to having been annealed and shearing/punching was carried out using multi-stage tooling. The carrier-tape was placed underneath the die exit, where the produced parts will easily fall into the pockets of the tape.

Fig. 10.3: Stainless-steel strip used for part-transport testing.

10.3.5 Machine Control Architecture

The control architecture of the micro-forming machine used for the testing along with the servo roll-feeder is illustrated in Fig. 10.4. The heart of the machine is a

MAYR control-box which receives a signal from a linear-encoder to control and position the linear ram. At certain designated encoder-increments, a 24VDC signal is pulsed from the logic circuit of the MAYR box to both the part-transport servo-drive and the developed feeder-controller box. A triggered open-loop signal activates the part transport to feed the carrier tape to the designated distance. C++ programming language and a RS232 interface were used to create the forming and part-transport program as well as to control the machining parameters and other communication aspects (downloading/uploading). The position of the ram is controlled by a linear encoder embedded inside the linear-motor used for actuation. The encoder also notes the home position, which represents the starting point of the ram before it is moved. The motion-frequency of the ram is considered as the forming speed and counted as the number of strokes per minute (spm). SPM is referred to as a number at which the machine to be operated, and can be amended through program-editing. The adjustment of the process-frequency or any other command, if required, is done in the communication terminal software before being downloaded to the servo-controller drive via an RS232 communication port. The program is stored in the servo-drive ROM for the operation, which may be carried out automatically. The actual real-life system is shown in Fig. 10.5.

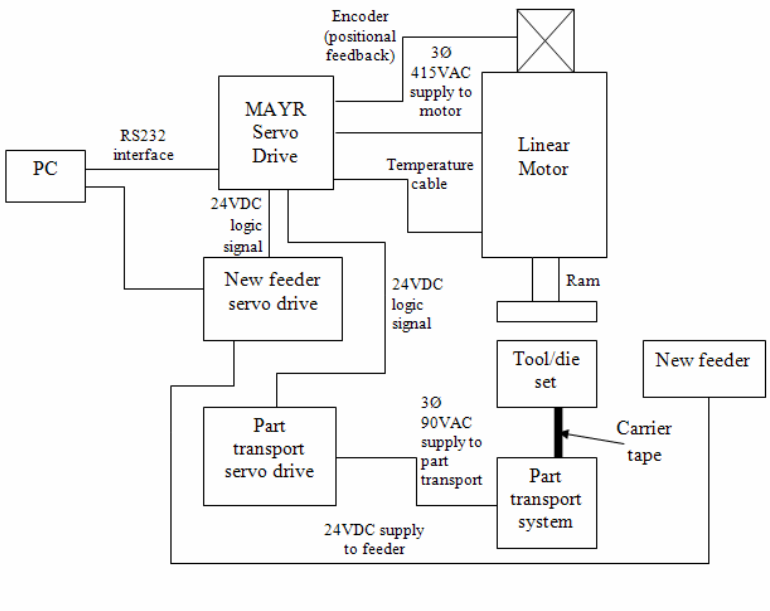

Fig. 10.4: Integrated feeder and part-transport system of the micro-sheet-forming machine.

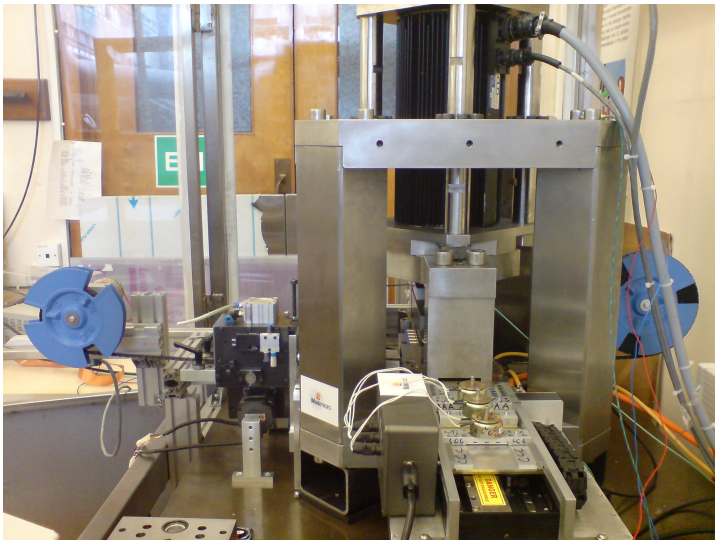

Fig. 10.5: Part-transport system developed for the handling of finished micro-parts.

10.4 Procedure

The concept of the finished parts/products transportation system was initiated based on its counterpart; the feeding system. Differently to the feeding system, which requires feeding with high-accuracy and precision each and every time during the feeding process, transporting the finished parts/products from the micro-sheet-forming machine does not require such accuracy. Tenth to hundreds of microns accuracy may be required for the system to work.

Similarly to the feeding system, instead of moving a strip metal, the transportation system is expected to move- and position-accurately a pocketed carrier-tape on the tool/die set during the forming process. The system consists of a decoiler to uncoil the carrier tape; the carrier tape itself; and a motor-powered coiler to wind back the carrier-tape. Force-analysis was conducted in order to determine the required pulling- and braking-forces acting during the transporting process, which include the forces required to accelerate the payload to match the feed-speed; the friction between the contact surface of the carrier-tape and the machine's structure (tooling, machine bridges, and other structures in contact); and finally the braking-force required to maintain tension within the tape.

The rotary servo-roll system uses a pair of rollers to move material to the desired pre-configured distance. Usually one roller acts as a driver while the other remains free to be driven. The top roller has to be loosened initially to accommodate different thickness of material for gripping and threading purposes. Non-symmetry and profiled materials such as the carrier-tape require some modification to be made to the rollers to accommodate a profiled shape nicely between the two rollers: this is to preserve the pocketed tape, which contains formed micro-parts/products, from being squashed during the transporting process.

Differently to the materials-feeding system, which requires high precision and accuracy in positioning the material for forming, transporting out the finished parts from the machinery is seen to be less difficult. Usually a tenth to hundreds of microns accuracy may be needed for the system to work, so placing the micro-parts accurately into the pocket of the carrier tape is not a major issue. Nevertheless, the transporting system must not accumulate each feed-error during transportation. The accumulation of positional error or inaccuracy may lead to great mis-alignment of the carrier-tape in the next cycle. Although some inaccuracy is allowed for the system to work, to ensure that no mis-alignment has occurred, each successive cycle has to eliminate the variation arising in the previous cycle. To achieve this, usually a second type of feedback system is required. A camera or laser-measurement system can be used to measure how much the inaccuracy is and feedback can be applied to the system to correct the position to within the designated tolerance.

An experimental method was used to validate the transportation of micro-parts/products by means of the carrier-tape. The transportation system was interfaced with the feeding system and controlled automatically from the micro-sheet-forming machine. Initially, to prove the concept, 1Hz feed-frequency was used to validate the transporting process.

10.4.1 Forces Analyses

Correct sizing of the rotary servo-motor is crucial, as this will have an impact on the entire transportation system in terms of it performances and efficiency. Associated

considerations also include the designated load and push/pull force. Fig. 10.6 shows the applicable forces are taken into account for motor-sizing analysis. Three types of forces contributing to the total peak force and the continuous linear-motor forces were identified for this particular application.

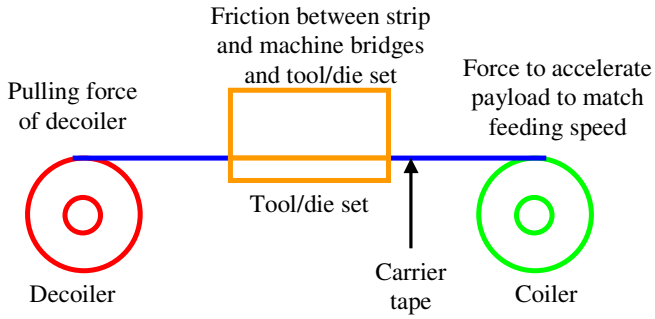

Fig. 10.6: Types of forces acting on the transportation system.

10.4.1.1 Forces due to the payload

The carrier-tape (Fig. 10.7a) was required to be moved by 12mm in 0.20s, then to dwell for 0.10s (Fig. 10.7b), to make it well synchronized with the feeding system. In this case, analysis and calculation of the required forces in order to determine the peak and continuous forces was required to realize the system.

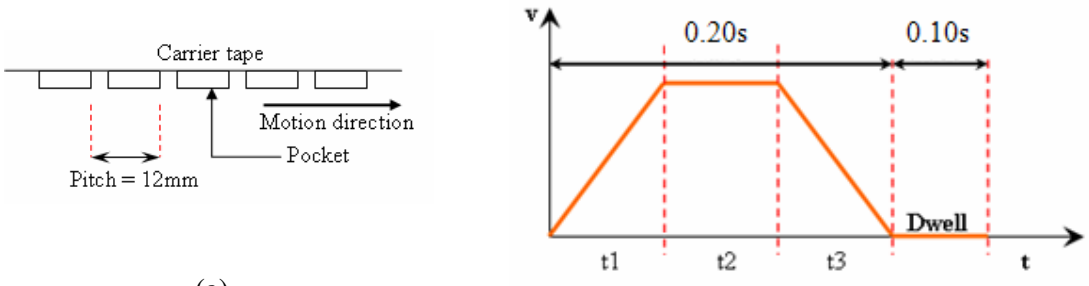

(a) (b)

Fig. 10.7: (a) the load exerted on the forcer, and the direction and distance of movement, and (b) trapezoidal profile representing the acceleration and deceleration of the coiler in one cycle.

The first factor considered was the motion characteristics - the peak speed needed to accelerate the mass from the origin to the end point, time duration which the travel takes, and the dwell when the moves end. In generator this type of motion characteristics which is from point to point, the basic profile is trapezoidal. [Erkorkmaz et al., 2001; Rogers et al., 2005]. With this profile, the move time is equal for the acceleration and deceleration phases (45% acceleration and 45% deceleration). The first part is acceleration, the second part is constant velocity, and the third part is deceleration. Such a motion characteristic should ensure a balance between the speed and acceleration to give the best motor combination. Based on trapezoidal motion, the time taken to accelerate is calculated as;

$$0.20 \times 0.45 = 0.09s$$

Then the peak speed required to make the move is calculated and in this case, because the move is symmetrical and divided into three parts, the equation below is used. The load cannot be accelerated instantaneously from 0 to 0.2m/s, but takes 0.09s to reach this speed. Therefore the acceleration is calculated as shown in Fig. 10.7b.

$$v = \frac{3s}{2t} = \frac{3 \times 0.012m}{2 \times 0.09s} = 0.20m/s$$
$$a = \frac{v-u}{t} = \frac{0.20m/s - 0}{0.09s} = 2.22m/s^2 \approx 1.15g$$

Newton's third law of motion was used to determine the payload rating force, f_p, since the peak rating force considers frictional force, f_f, (with the assumption of a single-row ball bearing being used to support the carrier-tape collection-coil in the system, having a coefficient of friction of about 0.0015), the force to accelerate, f_a, gravitational force for an inclined plane, f_g, as well as external force, f_e, caused by cable management. Therefore, the payload rating force can be expressed as:

$$f_p = f_a + f_g + f_f + f_e$$

f_e was neglected due to there being no cables attached directly to the movable coiler. The weight of the carrier-tape collection-coil, the carrier-tape and the finished parts/products was estimated at 450g and acts on a flat surface.

$$f_a = ma = 0.45 \times 2.22 = 1.0N$$
$$f_g = \sin(\theta)mg = \sin(0) \times 0.45 \times 9.81 = 0$$
$$f_f = mg\mu = 0.45 \times 9.81 \times 0.0015 = 0.007N$$
$$f_e = 0$$
$$\therefore f_p = 1.0 + 0 + 0.007 + 0 \approx 1.0N$$

By adding a safety factor of 25% to compensate for degradation of the motor efficiency, the new force to move the payload was calculated to be 1.25N.

10.4.1.2 Frictional Forces

Friction forces due to the contact between the carrier-tape and the structure of the machine structure and the tool/die set (300μm-thick strip, 16mm width and contact length 500mm) was analyzed as follows. The mass of material in contact was calculated as:

$$m = \rho V$$
$$V = 0.016 \times 0.5 \times 0.0003 = 2.4 \times 10^{-6} m^3$$
$$\rho = 1.06 \times 10^3 kg/m^3$$
$$\therefore m = 2.4 \times 10^{-6} \times 1.06 \times 10^3 = 25.4 \times 10^{-3} kg \approx 25 gram$$

The coefficient of friction between the carrier tape (polycarbonate) and the steel surfaces of the machine and the tooling were given as 0.36 [Fadeeva et al., 2005], therefore:

$$f_f = \mu ma$$
$$\mu = 0.36$$
$$f_f = 0.36 \times 0.025 \times 9.81 = 0.088N$$

By adding a safety factor of 25%, the new frictional-force value is found to be 0.11N. This value will be added to the calculation of the total peak force for linear-motor sizing.

10.4.1.3 Carrier-Tape Coil's and Reel-Pulling Force

Another force which contributes to the total peak force and the continuous forces is force for pulling the material from its reel, as illustrated in Fig. 10.8. It can be estimated and calculated as follows:

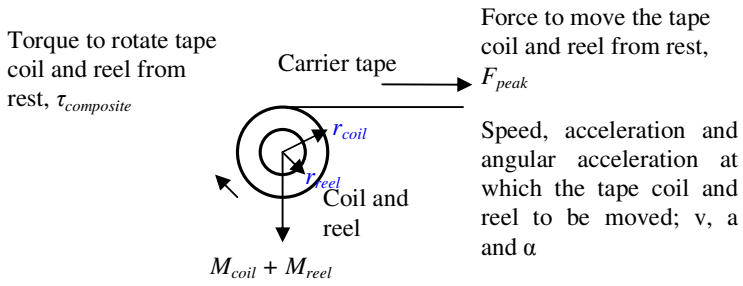

Fig. 10.8: Free-body diagram of the coil and the reel producing a total torque labelled $\tau_{composite}$.

Knowing that:

$$\begin{aligned} s &= 0.012m \\ r &= 0.165m \\ t &= 0.09s \\ u &= 0 \end{aligned}$$; Suppose the followings,

$$\tau = fr = I\alpha$$
$$\alpha = \frac{a}{r}$$
$$I = mr^2$$
$$a = \frac{v-u}{t}, v = \frac{3s}{2t}, u = 0$$

for trapezoidal motion:

$$v = \frac{3 \times 0.0120}{2 \times 0.09} = 0.20m/s$$
$$a = \frac{0.20 - 0}{0.09} = 2.22m/s^2$$
$$\alpha = \frac{2.22}{0.165} = 13.5rad/s^2$$

Suppose that the coil (carrier-tape) and reel can be assumed to be a thin solid cylinder with an outer diameter of 330mm and a total thickness of 20mm (the reel thickness was 2mm on both sides), therefore system's inertia can be calculated as:

Suppose the following:

$$\rho = \frac{m}{v}, \rho_{coil} = 1060kg/m^3, \rho_{reel} = 1040kg/m^3$$

To simplify the analysis:

$$length_{coil} = 50m$$
$$width_{coil} = 0.016m$$
$$thickness_{coil} = 0.0003m$$

$$v_{coil} = 50 \times 0.016 \times 0.0003 = 0.00024m^3$$
$$m_{coil} = 0.00024 \times 1060 = 0.254kg$$

$$radius_{reel} = 0.165m$$
$$thickness_{reel} = 0.002m$$

$$v_{reel} = \pi r^2 h = \pi \times 0.165^2 \times 0.002 = 0.00017m^3$$
$$m_{reel} = 0.00017 \times 1040 = 0.18kg$$
$$m_{system} = 0.254 + 0.18 = 0.434kg$$

$$I_{system} = \frac{m_{system}}{12}(3r_{system}^2 + h_{system}^2)$$

$$I_{system} = \frac{0.434}{12}(3 \times 0.165^2 + 0.02^2) = 2.97 \times 10^{-3} kgm^2$$

; $\tau_{system} = 2.97 \times 10^{-3} kgm^2 \times 13.5 rad/s^2 = 0.04Nm$

$$f_{system} = \frac{0.04}{0.165} = 0.243N$$

Therefore, the total force required for rotating the combination of the coil and the reel is found to be 0.24N. By adding a safety factor of 25% (to overcome internal frictional forces, etc), the new total force is calculated to be 0.30N.

10.4.1.4 Decoiler Braking-Force

Study on the effect of the coil braking-force on strip-tension during the stamping process was conducted in previous chapters. A similar analytical concept was applied to calculate the decoiler braking-force. Suppose that the coiling process requires a similar level of torque as for uncoiling the carrier-tape, given by the previous

analysis, the maximum force to uncoil is 0.3N. By taking f_{rms} of the rated force; therefore, the designated variable braking-force for this application was determined as follows:

$$f_{brake} = \sqrt{\frac{0.3^2 \times 0.09}{0.3}} = 0.16N$$

Since 0.16N force acts during the whole cycle, this value needs to be included in the peak force in linear-motor sizing.

10.4.1.5 Qualified Peak and Continuous Forces

Based on the analysis presented above, the peak force can be calculated as follows:

$$F_{peak} = f_p + f_f + f_{system} + f_{brake} = 1.25 + 0.11 + 0.30 + 0.16 \approx 1.82N$$

Based on the above trapezoidal profile, the rms force, f_{rms} is calculated as follows:

$$F_{rms} = \sqrt{\frac{F_{peak}^2 \times t}{t_{cycle}}} \qquad t = 0.09s \quad t_{cycle} = 0.30s \quad \therefore F_{rms} = \sqrt{\frac{1.82^2 \times 0.09}{0.30}} = 1.0N$$

New summations of the peak-force and the continuous-forces are 1.82N and 1.00N respectively. Both of these forces were considered when selecting a suitable servo-motor.

10.4.2 FE Analysis of Part Transport

Accurate, wide and various angles of geometry may be achieved by simulating the model in 3D dynamics explicit, as opposed to the 2D model [Hibbitt et al., 2002a]. Although 3D dynamics explicit analysis is time-consuming, modelling the thin sheet-metal from a shell and using an appropriate meshing-scheme are seen to produce a better approximation of the behaviour and the characteristics of the thin sheet during the feeding process, this reduces the modelling time-increment and CPU time.

Several key parameters were identified and have been considered in establishing an intensive FE analysis of the feeding characteristics of the part transportation system. Analysis was conducted to simulate the transporting characteristic at 1 and 2Hz transporting-frequency. An appropriate travel-velocity at this frequency was determined by trapezoidal-motion profile-analysis. A similar motion-profile curve then was configured in the FE analysis amplitude so as to mimic a life-like transporting condition. The part-transport model was constructed by ABAQUS/CAE and was based on the actual size.

Each contact-pair was defined with a specific coefficient-of-friction value gathered elsewhere [Rothbart et al., 2006; Roberts, 1978; Fadeeva et al., 2005]. The friction coefficient between the contact pair of the upper roller, which was made from polyurethane rubber, and the carrier-tape was defined as 0.8. The coefficient of friction of the contact pair of the bottom steel-roller and the carrier-tape was defined as 0.36. The contact pair between the polycarbonate carrier-tape and the bottom die-plate was defined as 0.36. The contact-pair coefficient of friction between the rollers was defined as 0.7.

The upper synthetic-rubber roller was subjected to 220N of clamping force, which was pre-determined from the servo-roll-feeder's manual, while the bottom roller was constrained in all direction. Both the bottom- and top-roller were subjected to a designated rotational speed for each fixed transporting distance: 6.98rad/s for 12mm feed-distance. The time taken to accelerate was defined by the designated motion-profile curve.

In the model, both the bottom and the top rollers, and the bottom die-plate set were assumed rigid and were described by rigid boundary-conditions. The carrier tape was assumed to be deformable. The values of the modulus of elasticity/Young's of the carrier-tape were given by a uni-axial tensile test conducted by the manufacturer. Element types S4R (3D explicit analysis) were used for modelling the carrier-tape [Hibbitt et al., 2002b; Hibbitt et al., 2002c]. The simulation was performed using the dynamics explicit procedure to cope with vast non-linear geometrical displacement.

The decision regarding the final mesh was made on a trial-basis, where usually a compromise is required between computing-time, computer-memory and simulation-precision.

Different nodes were selected with a view to establishing the n overall transporting behaviour of the carrier-tape; at both ends, and in the middle. The selection of these three nodes ensures that the travel-accuracy at the bottom die-position is also taken into account, hence how great the inaccuracy is could be determined directly. In order to avoid difficulty and time consuming 3D modelling, an appropriate fine-mesh was used, which also reduces error generated due to excessive aspect-ratio.

10.4.3 Validation Experiments

One of the key issues in monitoring the travel accuracy of a pocketed carrier-tape is flat-surface constraint. The nature of carrier-tape geometry itself has made adhering to a linear-encoder scale tape impossible. A commercial techniques use different approach to minimize the travel error of the pocketed carrier-tape. Instead of having a motor that pulls the tape onto a reel, the driving system of commercial carrier-tape machinery is placed underneath the filled pocket. This technique ensures the direct measurement of travel mis-alignment of the tape. A different technique was employed in the present research, in adapting the system to meet the space-constraint of the micro-forming machine. A powered pulling-reel was used instead of the commercial technique. This concept was tested for travel-frequency of 1 and 2Hz both with and without brake force being applied to the reel. 45-45 motion-profile was used to reduce ‘jerk’ in the system. Moreover, since in the previous work, a steeper motion-profile (50-50) did not make a significant contribution to improving travel accuracy, this was neglected. Due to the difficulty in employing the same accuracy-measurement technique as used previously, FE simulation was used as a general means of establishing the feeding-accuracy.

10.5 Results

10.5.1 Feeding Characteristics

1Hz Feed-Frequency

One of the key objectives of this study was to examine and determine the feed characteristics of the part-transport system, specifically the behaviour of the carrier-tape during transporting process. Fig. 10.9 shows the feed characteristics inn the preliminary analysis-step, just before the feeding started. Both for without and with brake-force, the analyses shows similar characteristics up to 0.1s. Without the presence of brake-force, the tape was seen to be slightly vulnerable to the pressure of the rollers pressure and continues to suffer waviness beyond 0.1s time. Nevertheless, the application of brake-force beyond the 0.1s period reduced the waviness and at the same time served to settle the tape at the origin. A similar result was observed also when motion profile was changed to 50-50, as shown in Fig. 10.10. Although the 50-50 profile was used, due to no motion being initiated in the step, similar disturbance-characteristics were experienced by the tape as for the 45-45 motion-profile.

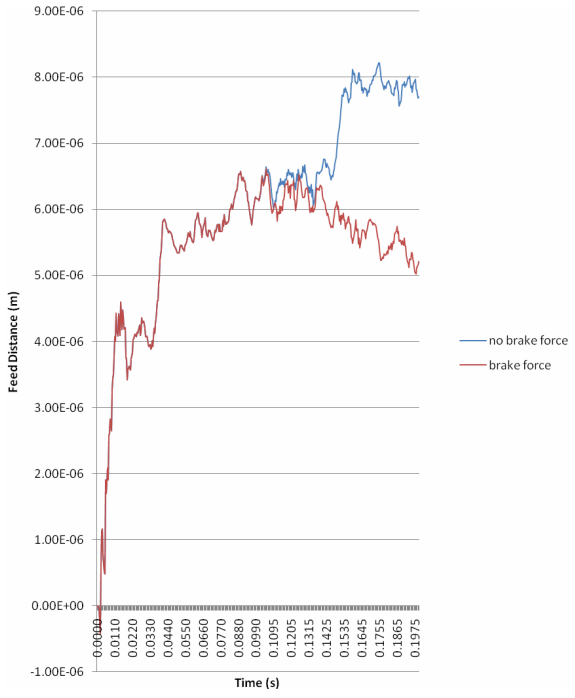

Fig. 10.9: FE analysis results for the preliminary step just before feeding starts for 1Hz feed-frequency and 45-45 motion-profile.

Fig. 10.10: FE analysis result for the preliminary step just before feeding starts for 1Hz feed-frequency and 50-50 motion-profile.

Similar feed characteristic for both without and with brake-force was observed for the 45-45 motion-profile, as shown in Fig. 10.11. The feed-process was seen to begin at an almost similar position, for both without brake-force and with brake-force, and ended up with quite large positional error. Nevertheless, detail observation has indicated that better settled-accuracy may be achieved without brake-force being applied to the system. Results for the 50-50 motion-profile (Fig. 10.12) confirmed this finding, where the presence of brake-force resulted in a large set-back of positional accuracy, when compared to the without-brake-force result. Although similar feed characteristics were observed at the beginning of the process, brake-force caused the system to settle far from the designated feed-position.

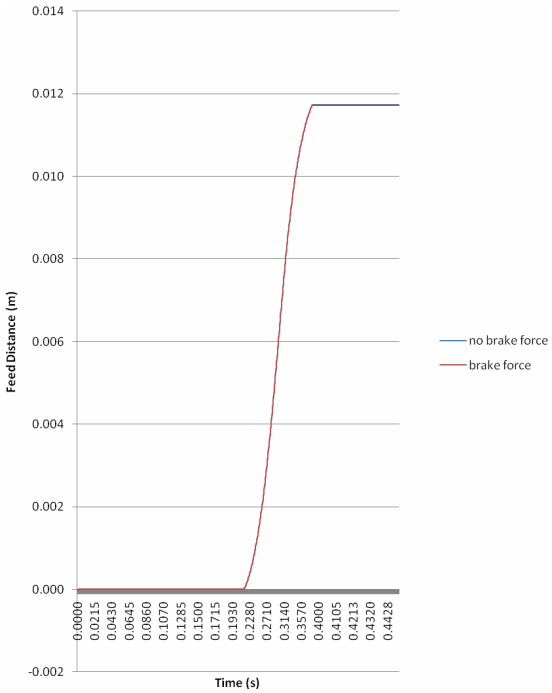

Fig. 10.11: Feed characteristics for 1Hz feed-frequency and 45-45 motion-profile.

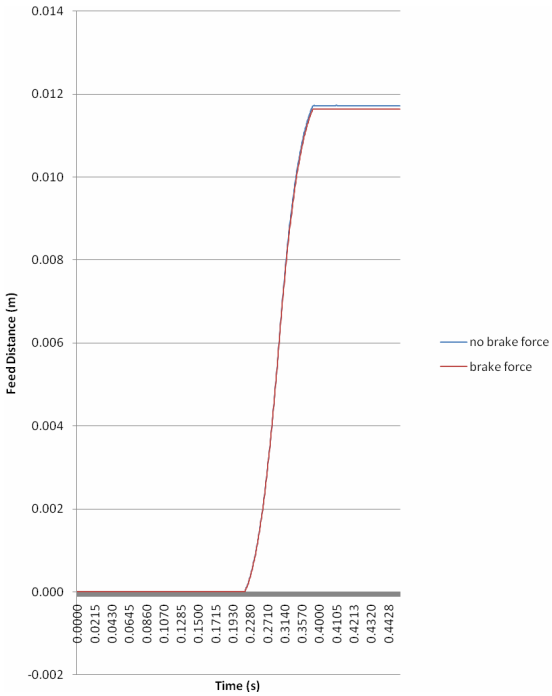

Fig. 10.12: Feed characteristics for 1Hz feed-frequency and 50-50 motion-profile.

2Hz Feed-Frequency

Similar types of steps and step-time as for the 1 Hz feed-process were used to study feeding characteristics at 2Hz feed-frequency. Due to the 45-45 and 50-50 motion-profile having similar step-times, similar feeding-characteristic were obtained, as shown in Fig. 10.13 and Fig. 10.14. Without brake-force being applied, the tape was more vulnerable to disturbance, hence resulting in slight offset from the starting point. The application of brake-force nevertheless, was seen to reduce the disturbance. Due to well-maintained tension being created by the brake-force, the tendency to be disturbed may be reduced, thus resulting in more-stable feeding-characteristics.

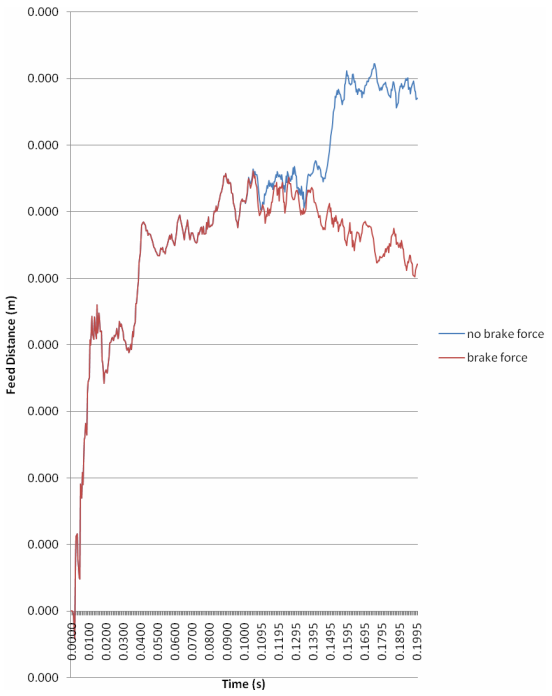

Fig. 10.13: FE analysis results for the preliminary step just before feeding starts for 2Hz feed-frequency and 45-45 motion-profile.

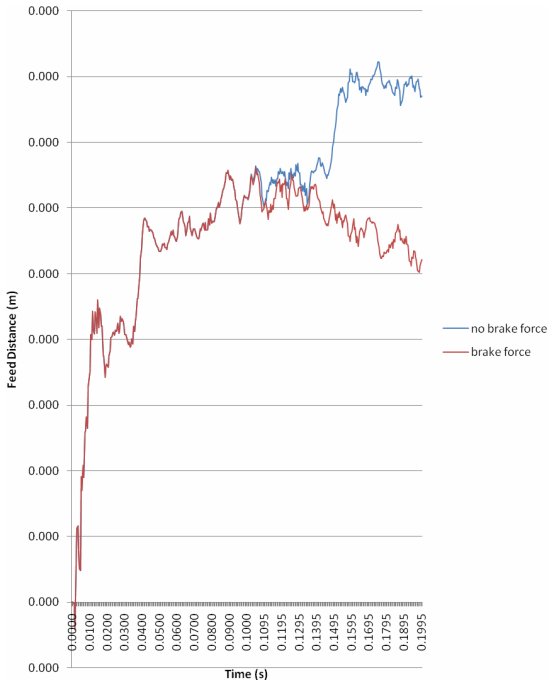

Fig. 10.14: FE analysis results for the preliminary step just before feeding starts for 2Hz feed-frequency and 50-50 motion-profile.

At this feed-frequency, the feeding-characteristics and -performance were observed to be slightly better when compared to the 1Hz feed-frequency results. With the 45-45 motion-profile, as depicted in Fig. 10.15, both without and with brake-force shared a similar feeding-curve and settled fairly close to the designated feed-distance. In the 50-50 motion-profile analysis, as shown in. 10.16, the analyses for without and with brake-force showed a similar feeding-pattern. Nevertheless, a different settling-pattern between the two was recorded at the end of the feeding-process. When no brake-force was applied, the tendency was to settle closer to desired feed-position compared to when brake force was applied. In addition, the 50-50 profile produced slightly greater offset from desired feed-distance when compared to that for the 45-45 profile. Hence, it is suggested that the 45-45 profile may result in better positional-accuracy.

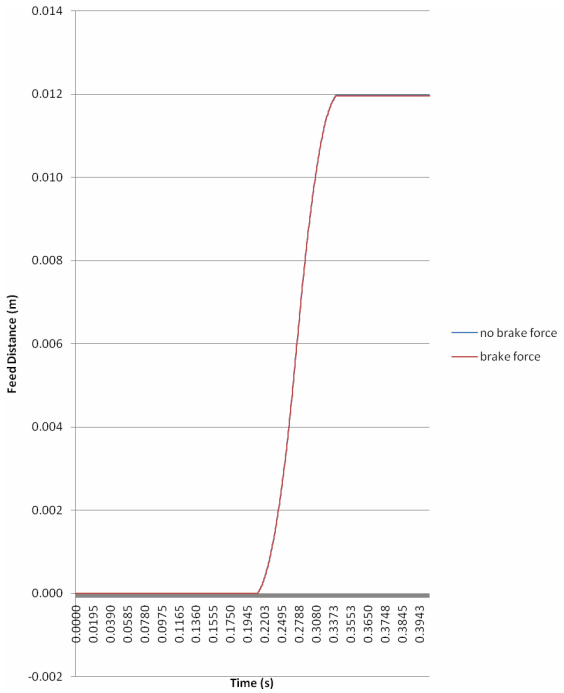

Fig. 10.15: Feed characteristic for 2Hz feed-frequency and 45-45 motion profile.

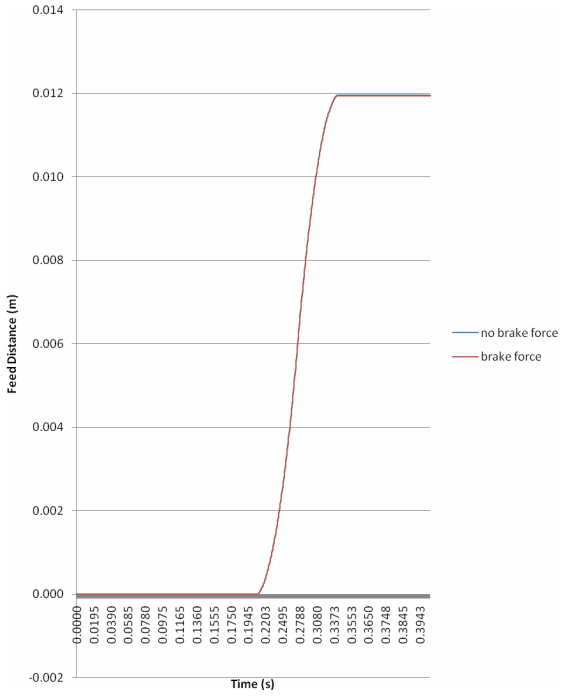

Fig. 10.16: Feed characteristics for 2Hz feed-frequency and 50-50 motion-profile.

10.5.2 Effect of Brake-Force

1Hz Feed-Frequency

Fig. 10.17 shows the effect of brake-force on the settled-accuracy for both motion profiles. A long feed-distance may be confirmed as one of the reason for the increasing of positional error. The tape has a complex and irregular geometry with prominent edges, thus, the contact area between the tape and the system's structure may increase the resistance force during feeding due to high friction, hence a lesser achievable accuracy being recorded. For all cases presented in Fig. 10.17, all attempts achieved just under 12mm in underfeed settling-pattern. For the 45-45 motion-profile, without the presence of brake force, the system positioned the tape with -266.8µm of error. The positional-error remained the same with the presence of brake force and with the same motion-profile, with a settled-accuracy of -277µm. Nevertheless, due to the low brake force applied to the system, poor resistance to force disturbance was encountered. As indicated by a smaller deviation pattern, this established the insignificant effect of very low brake-forces on improving the resistance to disturbance of the system. This indicates that the tape was likely to have better resistance to disturbance with the application of brake-force.

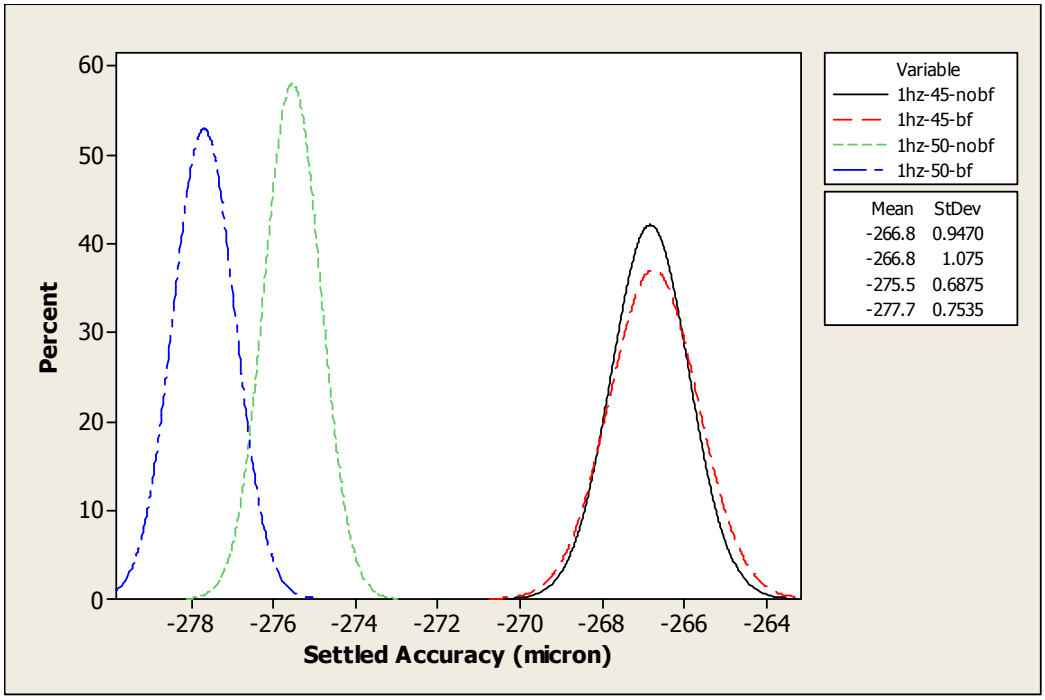

Fig. 10.17: The effect of brake-force for both motion-profiles at 1Hz feed-frequency.

Change of the motion-profile to 50-50, however, resulted in deterioration of the achieved positional-accuracy. Without the presence of brake-force, the 50-50 motion-profile managed to settle the tape at about -275.5µm. Slight deterioration of accuracy was observed when the 50-50 motion-profile was used with brake-force, settling at -277.7µm. Although the accuracy settled at a slightly worse value than found without brake-force, low brake-force however, is shown to have no significant effect on improve positional-repeatability. In addition, differently for the 45-45 motion-profile, the change of the motion-profile to 50-50 did not promote improved positional accuracy, instead of deteriorating it.

2Hz Feed-Frequency

Fig. 10.18 shows the feeding performance at 2Hz feed-frequency. Based on the figure, for the 45-45 motion-profile, although greater positional-accuracy may be achieved, a large dispersion of the process-deviation was inevitable due to the lesser resistance to disturbance. On the other hand, the presence of brake-force, which in the previous chapter was found to be useful in improving positional-repeatability, was found to be useless for this purpose. Although the positional-accuracy is slightly reduced, the deviation-dispersion showed good agreement with the accuracy pattern, where no improvement in positional repeatability was achieved.

Similar findings as for the 1Hz results were observed when the motion-profile was changed to 50-50. Without the presence of brake-force, the process-capability was recorded at -44.5µm. Differently to the repeatability performance achieved with the 45-45 motion-profile, the change to a steeper motion-profile resulted in substantial change to the process-deviation which was improved by almost a factor of two, but with a large positional-offset when compared to without the presence of brake-force. Consistent findings achieved throughout the analyses confirmed that the brake-force applied to the system did not improve precision, but jeopardized accuracy.

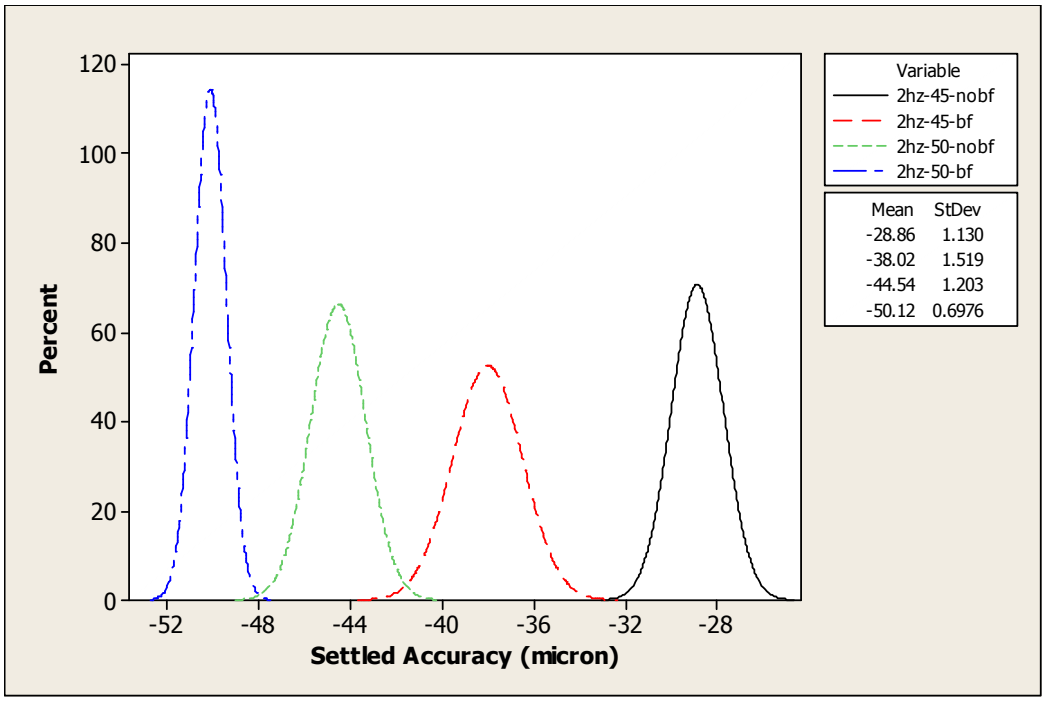

Fig. 10.18: The effect of brake-force for both motion-profiles at 2Hz feed-frequency.

10.5.3 Validation-Experiment Results

One of the key issues in the handling of micro-parts is that of the interfacial forces which act on the part itself. Many studies elsewhere [Arai et al., 1995; Arai et al., 1997; Feddema et al., 1999; Rollot et al., 2000; Fearing et al., 1985; Bowling et al., 1986; Bowling et al., 1988; Tomas et al., 2007] have revealed that when micro-parts having a dimension of less than $1mm^3$ are produced, gravitational force no longer is seen as the dominating force. Interfacial forces such as adhesion played a great role for parts with these dimensions. The parts tend to stick together or adhere onto the manipulator rather than to be moved or adjusted. Nevertheless, this adhesive effect may be neglected for parts having a dimension of greater than $1mm^3$. In this research, for the purposes of the validation of the part-transport system, simple round disc were blanked from 75µm stainless steel strip using multi-stage tooling and discharged directly from the tooling into the pocketed carrier-tape.

Experiments at 1Hz feed frequency, Fig. 10.19, proved successful, where good synchronization was achieved between the part-transport system and the other systems of the micro-forming machine, i.e. feeder and the forming-machine itself.

No mis-placed/dropped components were encountered. Observations made at 2Hz frequency, Fig. 10.20, also recorded similar results, where no tendency for mis-placement was found. The parts settled perfectly in the pocketed carrier-tape without any tendency to land elsewhere.

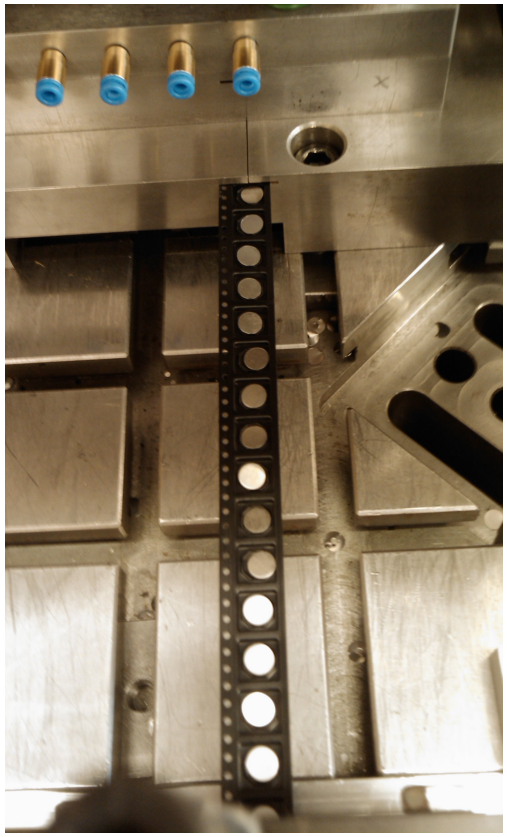

Fig. 10.19: Collection of parts/products at 1Hz feed-frequency.

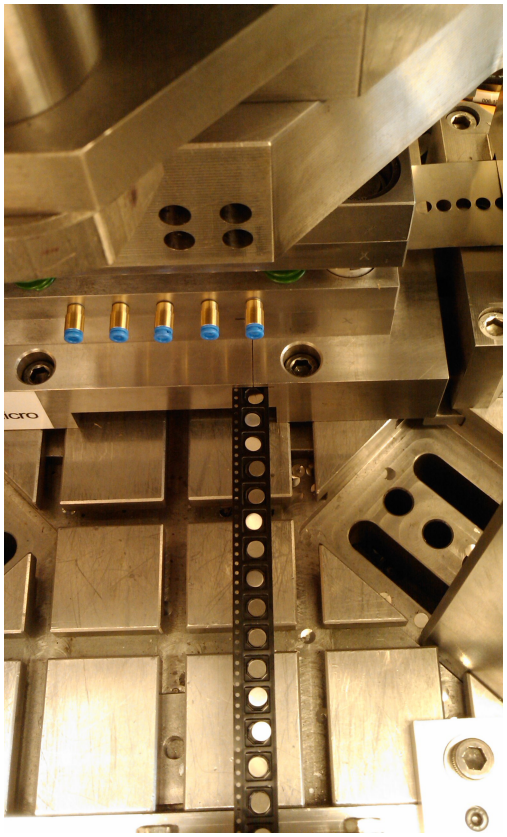

Fig. 10.20: Collection of parts/products at 2Hz feed-frequency.

10.6 Discussion

10.6.1 Effect of Brake-Force

The application of brake-force demonstrated better stability of the settled-pattern while keeping the positional error at a low level. Brake-force applied to the end of the tape edge to represent the decoiler brake-force effect on the feed process, resulted in consistent tension throughout the roll-feeder and the decoiler, hence reducing error and increased stability during settling. This was achieved by reduction of tape waviness through proper constraint introduced on one of the tape's end while the other end was kept constrained by the rollers. Reduced waviness of the tape through maintained and consistent tension made the tape more resistant to disturbance forces during the feed process. Without brake-force being applied to the system on the other hand, makes the free end of the tape more vulnerable to disturbance and allows the strip to absorb unwanted disturbance forces that led to increased waviness.

10.6.2 Effect of Change of Motion-Profile

Acceleration is defined as change of the velocity rate. 'Jerk' on the other hand is defined as changes of the acceleration rate. High 'jerk' is usually associated with high-speed motion. Based on the present results, high 'jerk' affects the settled-pattern and positional-error of the least-stiff material through increasing strip waviness. It is suggested that reduction in 'jerk' promotes better-settled stability but less positional-error, which was supported by the results for the 45-45 motion-profile curve. With this configuration, the tendency to high 'jerk' was eliminated by introducing a constant-velocity phase, hence, reducing any sharp transitions during change of acceleration and deceleration. According to Newton's Third Law, increases in acceleration rate results in increases in force. Sudden change of this force resulted various curvature-formation on the tape, as explained elsewhere [Uraoka et al., 2009], hence leading to waviness. Additionally, the waviness tends to propagate along the body of the strip and gradually dissipate. Nevertheless, in a high-speed process, waviness may not be damped fast enough to settle the tape accurately within the specification. Moreover, high 'jerk' motion in turn leads to greater sudden change of force that may cause large curvature during feeding. For the 45-45 motion-profile configuration, minimization of 'jerk' led to decrease of acceleration, hence

keeping the reaction force low. Additionally, a low acceleration value leads to low strip inertia, low 'jerk' consequently reducing tape curvature-formation, this in turn reducing the waviness tendency.

10.7 Conclusions

Based on the results of the experiments and the FE analyses, the following conclusions are drawn.

i) A servo roll-feeder may be used to drive the part-transport system.

ii) A high-jerk motion-profile does not contribute to improved accuracy, but instead reduces it.

iii) Low brake-force was found to be of no use in increasing resistance to unwanted disturbance of the feed material, and hence did not improve positional-repeatability.

iv) Carrier-tape application for transporting and packaging micro-parts was proven to be successful.

v) The developed part-transport system and technique may be used for micro-forming applications.

Chapter 11

Conclusions and Recommendations For Further Work

11.1 Conclusions

Research was conducted to develop a high-precision and high-speed feeder for micro-sheet-forming applications. One of the key issues identified was related to the automation of the forming process by the continuous feeding of thin sheet-metals with micron-range accuracy and good repeatability, especially for multi-stage micro-stamping. Another identified issue was related to the feeding speed/frequency, where apart from the precise feeding that is necessary to ensure that precise micro-parts can be produced in multi-stage micro-stamping, high-speed feeding is essential for high-throughput production.

Micro servo-roll and pneumatic gripper-feeders were identified as a possible current strategy for the handling of thin metal sheets for micro-sheet-forming. A pneumatic feeder however, was seen unsuitable for use in serve micro-sheet-forming due to inflexibility in changing the feed-distance and the large positional-error obtained with manual feed-distance adjustment. Detailed and extensive tests were conducted to assess the feeder performance of a micro-servo roll-feeder for micro-sheet-forming applications. Results from FE simulations of the micro-servo roll-feeder had demonstrated that the feeder was unsuitable to be used for micro-sheet-forming applications specifically in conjunction with producing micro-hat parts described in Chapter 1. These results were supported by experimental results which confirmed the finding. A non-contact approach using a high-precision linear-encoder was used to assess the accuracy- and repeatability- performance of the feeder.

Several strategy used in high-precision and high-accuracy positioning were identified for the development of the new feeder to replace the micro servo roll-feeder. A high-precision iron-less linear-motor was chose as a strategy to feed thin sheet-metal with higher accuracy and repeatability. FE simulations were conducted to explore the feeding-characteristic of the concept. Results from FE simulation suggested that high-accuracy feeding may be achieved with the linear-motor actuation. The concept was developed and tested experimentally to determine its performance. Initial experimental results confirmed the FE simulation results, better accuracy and repeatability being achieved by the new concept of a linear-motor gripper-feeder

compared to those for a micro-servo roll-feeder. The feeder was optimized and it was confirmed that greater feeding-accuracy and -repeatability were achieved by the system. This finding has become the promising solution for high-precision feeding to produce micro-hat parts discussed previously.

The new feeder was integrated with the existing micro-sheet-forming machine, which enabled automatic, synchronized and harmonic running of the stamping and feeding processes. A part-transportation system was developed as a mean of collecting the finished parts/products from the machine. Experimental effort has successfully validated the use of a pocketed carrier-tape to collect and store the finished parts/products for packaging.

11.2 Recommendations for Further Work

The research reported in this thesis has resulted in a better understanding of current issues in micro-sheet-forming, and the feeding characteristics of different types of feeders for micro-sheet-forming applications. The results provide useful guidelines for the design of a new high-precision and high-accuracy feeder for micro-sheet-forming. Some fundamental aspects will have to be addressed to support the successful work in micro-sheet-forming engineering carried out to date, these being as follows:

i. Correlation between high-accuracy feeding and stamping-quality

At the present time systematic correlation between the high-accuracy achievable during the feeding process and the achievable stamping quality has not been explored. The study should refer to all feasible process-configurations, including possible variations of tool-kinematics, tool-geometry, tool-tolerances, strip thickness and different strip-materials. Single-stage tooling may be used in an initial effort to study such correlation, supported by FE simulations. The efforts should be continued to cover multi-stage tooling operations where most of the parts/products are nesting closely to each other during the stamping operation, hence the disturbance experienced by the nesting neighbour should be examined.

ii. Correlation between control-loop feedback and strip-stiffness for better positioning- accuracy/repeatability.

Initial work carried out in this research has demonstrated the feasibility of correlation between the optimization of the control-loop feedback and the positional-accuracy, for different strip stiffness. Nevertheless, the correlation could not be confirmed as further and intensive experimental work needed done to confirm the correlation. Due to the different waviness patterns of different strip thickness and materials, a different PID-configuration and set-up are necessary according to each stiffness category, in order to be able to achieve better positional-accuracy Exotic materials may be studied to good advantage.

iii. Correlation between the material properties of thin sheets determined through electron-backscatter-diffraction analysis (EBSD) and the stamping quality obtained.

A lot of effort has been carried out to study the correlation between material properties and forming quality [Peng et al., 2009; Lai et al., 2008; Peng et al., 2007]. Nevertheless, the effort has been more focused on an examination of mechanical properties through conventional uniaxial tension/bending/shearing tests without a significant effort being made to study the actual grain–boundary-pattern and size through electron-backscatter-diffraction (EBSD) analysis. Not only being capable of scientifically determine the grain size of a material, the EBSD technique is also capable of the mapping of grain boundaries and direct observation of asymmetrical grain patterns. Accurate grain-boundary-orientation may be worthy of study, as the effect of different grain-boundary-orientation has not been dealt with extensively.

iv. A fully-integrated and centre-base CNC control interface

In order to serve rigorous and prolonged industrial demand, the machine set-up should be reliable, yet easy for maintenance work and also accessible through a centred-based control-system. A user-friendly control-interface which can be handled by a low-skilled worker may be a good choice, as CNC controllers that are difficult to program and handle require highly-skilled technicians to operate them. Fully-

accessible control should be provided to enable for remote-control operation while maintaining a human-interface handheld-device for threading and troubleshooting purposes.

v. Gravitational deformation of the features of the micro-parts/products due to transportation

It is still not clear what the effects are of free-fall due to gravity on the micro-features of the produced parts/products. The collection of the produced parts/products in the part-transport described in the previous chapter relies on gravitational force. However, this force is no longer negligible, as it was of main concern as an unwanted source of deformation of micro-featured parts having dimensions of millimetres range. FE simulation may be useful in studying the deformation of micro-featured parts/products, along with some empirical experiments to validate the findings.

References

ADAMS, G. P. & STONE, J. W. (1997) Determination of friction and feed forward tuning for a DC servomotor-driven slide table. *IEEE Industry Applications Society.* New Orleans, Louisiana, IEEE.

ALTER, D. M., TSAO, T. (1994) Stability of turning processes with actively controlled linear motor feed drive, *ASME Journal of Engineering for Industry,* 116, 298–306.

ALTER, D. M., TSAO, T. (1996) Control of linear motors for machine tool feed drives: design and implementation of H1 optimal feedback control, *ASME Journal of Dynamic Systems, Measurements, and Control,* 118, 649–655.

ARAI, F. & FUKUDA, T. (1997) A new pick up and release method by heating for micromanipulation. *IEEE.* Nagoya, 383-388.

ARAI, F., ANDO, D., FUKUDA, T., NONODA, Y. & OOTA, T. (1995) Micro manipulation based on micro physics - Strategy based on attractive force reduction and stress measurement. *Proc. IEEE/RSJ.* 2, 236-241.

ARONSON, R. B. (2003) The new world of micromanufacturing. *Manufacturing Engineering*. 140, 4.

ARONSON, R. B. (2004) Micromanufacturing is Growing. *Manufacturing Engineering. Manufacturing Engineering.* 132, 4. http://findarticles.com/p/articles/mi_qa3618/is_200404/ai_n9397440/print

ATAKA, T. (1999) The Experimental Microfactory System in Japanese National R&D project. http://websrv2.tekes.fi/opencms/opencms/OhjelmaPortaali/Paattyneet/Presto/fi/Dokumenttiarkisto/Viestinta_ja_aktivointi/Seminaarit/Seminaari0601/.

AVALLONE, E. A., BAUMEISTER, T., SADEGH, A. M. & MARKS, L. S. (2006) *90th Anniversary Edition Marks' Standard handbook for Mechanical Engineer*, McGraw Hill professional.

AYAX, E., HUOT, S., PLAY, D. & FRITCH, N. (2003) Numerical simulation of timing belt camshaft layout. *ABAQUS User's Conference.* ABAQUS. Munich, Germany.

BAEUMLER, F. (2001) Keeping pace with today's punching requirements: Advancements in tool design, metallurgy lead to more accurate holes, improved part quality. *Punching Article.* http://www.thefabricator.com/article/punching/keeping-pace-with-todays-punching-requirements

BOWLING, R. A. (1986) Detection, Adhesion and Removal. *Proceedings of the Symposium on particles on surfaces 1.* Plenum Press. San Francisco.

BOWLING, R. A. (1988) A theoretical review of particle adhesion. *Particles on Surfaces I - Detection, Adhesion, and Removal.* Plenum Press. New York.

BRAEMBUSSCHE, P. V. D., SWEVERS, J., BRUSSEL, H. V. & VANHERCK, P. (1996) Accurate tracking control of linear synchronous motor machine tool axes. *Mechatronics,* 6**,** 507-521.

BRITISH STANDARDS INSTITUTION (1984) Manual of British Standards in Engineering Metrology. Hutchinson & Co.

BRUSSEL, H. V., J. PEIRS, REYNAERTS, D., DELCHAMBRE, A., REINHART, G., ROTH, N., WECK, M. & ZUSSMAN, E. (2000) Assembly of microsystems. *Annals of the CIRP,* 49**,** 451-472.

BYUNG, -. Y. J., RHIM, S.-H. & OH, S.-L. (2005) Micro-hole fabrication by mechanical punching process. *J. Mats. Proc. Tech.,* 170**,** 593.

CASTRO, H. F. F. (2008) A method for evaluating spindle rotation errors of machine tools using a laser interferometer. *Measurement,* 41**,** 526-537.

CHEN, J.-S., CHEN, K.-C., LAI, Z.-C. & HUANG, Y.-K. (2003) Friction characterization and compensation of a linear-motor rolling-guide stage. *International Journal of Machine Tools & Manufacture,* 43**,** 905-915.

CHEN, S.-L. & HSIEH, T.-H. (2007) Repetitive control design and implementation for linear motor machine tool. *International Journal of Machine Tools & Manufacture,* 47**,** 1807-1816.

CHERN, G.-L. & CHUANG, Y. (2006a) Study on vibration-EDM and mass punching of micro holes. *J. Mats. Proc. Tech.,* 180**,** 151-160.

CHERN, G.-L. & RENN, J. C. (2004) Development of a novel micro-punching machine using proportional solenoid. *J. Mats. Proc. Tech.,* 25**,** 89-93.

CHERN, G.-L., WU, Y.-J. E. & LIU, S.-F. (2006b) Development of a micro-punching machine and study on the influence of vibration machining in micro-EDM. *J. Mats. Proc. Tech.,* 180**,** 102-109.

CHO, D.-W., KIM, J.-J. & JEONG, Y. H. (2004) Thermal behavior of a machine tool equipped with linear motors. *International Journal of Machine Tools & Manufacture,* 44**,** 749-758.

CHUNG, S.-C. & KIM, M.-S. (2006) Integrated design methodology of ball-screw driven servomechanisms with discrete controllers. Part I: Modelling and performance analysis. *Mechatronics,* 16**,** 491-502.

CLAESSEN, U. & CODOUREY, A. (2002) Microfactory. *Section Head CSEM CH 6055 Alpnach Switzerlan.* Switzerland.

DAVIM, J. P., VILARINHO, C., SOARES, D., CASTRO, F. & BARBOSA, J. (2005) Influence of the chemical composition on the machinability of brasses. *J. Mats. Proc. Tech.,* 170**,** 441-447.

DU, S. & RANDALL, R. B. (1998) Encoder error analysis in gear transmission error measurement. *Proc. Instn. Mech. Engrs,* 212**,** 277-285.

ELFIZY, A. T., BONE, G. M. & ELBESTAWI, M. A. (2005) Design and control of a dual-stage feed drive. *International Journal of Machine Tools & Manufacture,* 45**,** 153-165.

ENGEL, U. & ECKSTEIN, R. (2002) Microforming — from basic research to its realization. *J. Mats. Proc. Tech.,* 125-126**,** 35-44.

ERKORKMAZ, K. & ALTINTAS, Y. (2001) High speed CNC system design. Part I: Jerk limited trajectory generation and quintic spline interpolation. *International Journal of Machine Tool and Manufacture*, 41, 9, 1323-1345.

ERKORKMAZ, K. & KAMALZADEH, A. (2007) Compensation of axial vibrations in ball screw drives. *Annals of the CIRP,* 56.

FADEEVA, V. S., LAZAREV, G. E., YAKHONTOVA, N. E. & ABRAMOV, L. K. (2005) Investigation of the external friction coefficient of foamed polystyrene *Chemistry and Materials Science,* 4**,** 751-753.

FARZIN, M., TEHRANI, M. S. & SHAMELI, E. (2002) Determination of buckling limit of strain in cold roll forming by the finite element analysis. *J. Mats. Proc. Tech.,* 125-126**,** 626-632.

FEARING, R. S. (1995) Survey of Sticking Effects for Micro Parts Handling. *Proceedings of the IEEE/RSJ Intelligent Robots Systems.* IEEE. 2, 212-217.

FEDDEMA, J. T., XAVIER, P. & BROWN, R. (1999) Micro-Assembly Planning with Van Der Waals Force. *Proceedings of the 1999 IEEE International Symposium on Assembly and Task Planning.* Porto, Portugal, IEEE. 32-38.

GAO, N., WANG, S. C., UBHI, H. S. & STARINK, M. J. (2005) A comparison of grain size determination by light microscopy and EBSD analysis. *Journal of Materials Science*. 40, 18, 4971-4974.

GAO, W., ARAI, Y., SHIBUYA, A., KIYONO, S. & PARK, C. H. (2006) Measurement of multi-degree-of-freedom errors motions of a precision linear air-bearing stage. *Precision Engineering,* 30**,** 96-103.

GAO, W., TANO, M., ARAKI, T., KIYONO, S. & PARK, C. H. (2007) Measurement and compensation of error motions of a diamond turning machine. *Precision Engineering,* 31**,** 310-316.

GAUGEL, T., DOBLER, H., MALTHAN, D., BENGEL, M. & WEIS, C. (2001) Minifabrik für Laserdioden und Biochips. 1-7.

GEIGER, M., KLEINER, M., ECKSTEIN, R., TIESLER, N. & ENGEL, U. (2001) Microforming. *CIRP Annals - Manufacturing Technology,* 50**,** 445-462.

GEIGER, M., VOLLERTSEN, F. & KALS, R. (1996) Fundamentals on the manufacturing of sheet metal microparts. *Annals of the CIRP,* 45(1)**,** 227-282.

GHAYESH, M. H. & KHADEM, S. E. (2008) Rotary inertia and temperature effects on non-linear vibration, steady-state response and stability of an axially moving beam with time-dependent velocity. *International Journal of Mechanical Sciences,* 50**,** 389-404.

GRANT, B. (2001) Examining press feeding options: Considerations that determine a feed's effectiveness. *Stamping Journals(R).* http://www.thefabricator.com/article/stamping/examining-press-feeding-options--considerations-that-determine-a-feeds-effectiveness

GRANT, B. (2006) Understanding press feeds - A primer for the 'nontechie'. *Press Feeding Article.* http://www.thefabricator.com/article/pressfeeding/understanding-press-feeds

GROCHE, P. & SCHNEIDER, R. (2004) Method for the optimization of forming presses for the manufacturing of micro parts. *Annals of the CIRP,* 53(1)**,** 281–284.

HERNANDEZ, J. J., FRANCO, P., ESTREMS, M. & FAURA, F. (2006) Modelling and experimental analysis of the effects of tool wear on form errors in stainless steel blanking. *J. Mats. Proc. Tech.,* 180, 143-150.

HESS, A. (2000) Piezoelectric driven press for production of metallic microparts by forming. *7th International Conference on New Actuators.* Bremen.

HIBBITT, KARLSSON & SORENSON INC., (2002a), ABAQUS/Explicit Example Problems Manual.

HIBBITT, KARLSSON & SORENSON INC., (2002b), ABAQUS/Standard Example Problems Manual.

HIBBITT, KARLSSON & SORENSON INC., (2002c), ABAQUS/Standard User's Manual.

HILLERY, M. T. & GORDON, S. (2005) Development of a high-speed CNC cutting machine using linear motors. *J. Mats. Proc. Tech.,* 166**,** 321-329.

HSUE, A. W.-J., YAN, M.-T. & KE, S.-H. (2007) Comparison on linear synchronous motors and conventional rotary motors driven wire-EDM processes. *J. Mats. Proc. Tech.,* 192-193**,** 478-485.

HU, Z., VOLLERTSEN, F., NIEHOFF, H. S. & THEILER, C. (2004) State of the art in micro forming and investigations into micro deep drawing. *J. Mats. Proc. Tech.,* 151**,** 70-79.

HUANG, Y. & YASUNOBU, S. (2000) A general practical design method for fuzzy PID control from conventional PID control. *The Ninth IEEE International Conference on Fuzzy Systems.* IEEE. San Antonio, Texas. 2, 969-972.

IVASKA, J. (2003) How important is roll forming lubrication compatibility. http*://www.thefabricator.com/RollForming/RollForming_Article.cfm?ID=727.*

JACQUES, N., ELIAS, A., POTIER-FERRY, M. & ZAHROUNI, H. (2007) Buckling and wrinkling during strip conveying in processing lines. *J. Mats. Proc. Tech.,* 190**,** 33-40.

JEONG, H.-W., HATA, S. & SHIMOKOHBE, A. (2003) Microforming of three-dimensional microstructures from thin-film metallic glass. *J. of Microelectromechanical Systems,* 12(1)**,** 42-52.

JILLSON, K. R. & YDSTIE, B. E. (2008) Process networks with decentralized inventory and flow control. *Journal of Process Control,* 17**,** 399-413.

JUNG, K. H., LEE, H. C., KANG, S. H. & IM, Y. T. (2008) Effect of surface roughness on friction in cold forging. *Journal of Achievements in Materials and Manufacturing Engineering*, 31, 2, 327-334.

KALPAKJIAN, S. & SCHMID, S. R. (2006) *Manufacturing Engineering and Technology*, Prentice Hall.

KIBE, Y., OKADA, Y. & MITSUI, K. (2007) Machining accuracy for shearing process of thin-sheet metals-Development of initial tool position adjustment system. *International Journal of Machine Tools & Manufacture,* 47**,** 1728-1737.

KIM, K., CHOI, Y.-M., GWEON, D.-G. & LEE, M. G. (2008) A novel laser micro/nano-machining system for FPD process. *J. Mats. Proc. Tech.,* 201, 1, 497-501.

KIM, M.-S. & CHUNG, S.-C. (2006) Integrated design methodology of ball-screw driven servomechanisms with discrete controllers. Part I: Modelling and performance analysis. *Mechatronics,* 16**,** 491-502.

KIMA, S. S., HANA, C. S. & LEE, Y.-S. (2005) Development of a new burr-free hydro-mechanical punching. *J. Mats. Proc. Tech.,* 162-163**,** 524-529.

KLOCKE, V. & GESANG, T. (2003) Nanorobotics for Micro Production Technology. *Klocke Nanotechnik, Pascalstr.* Proceedings of the SPIE, 4943, 132-141.

KLOCKE, V. (2002) Mikroproduktionsanlage zur automatisierbaren Mikromontage, Aufbau- und Verbindungstechnik. http://www.nanomotor.de/pdf/mps_components_d.pdf

KOLESAR, E. S., MONCRIEF, W. A., LEWIS, F. L. & MONCRIEF-O'DONNELL (2000) Introduction to Microeletromechanical Systems (MEMS). University of Texas at Arlington.

LAI, X., PENG, L., HUA, P., LAN, S. & NI, J. (2008) Material behavior modelling in micro/meso-scale forming process with considering size/scale effects. *Computational Materials Science,* 43**,** 1003-1009.

LANGE, K. (1985) *Handbook of Metal Forming,* Michigan, Society of Manufacturing Engineers.

LU, X. & TRUMPER, D. L. (2007) Spindle rotary position estimation for fast tool servo trajectory generation. *International Journal of Machine Tools and Manufacture,* 47**,** 1362-1367.

MAHABUNPHACHAI, S. & KOC, M. (2008) Investigation of size effect on material behaviour of thin sheet metals using hydraulic bulge testing at micro/meso-scales. *International Journal of Machine Tools & Manufacture*, 48, 1014-1029.

MANABE, K., SHIMIZUA, T., KOYAMAB, H., YANGA, M. & ITOC, K. (2007) Validation of FE simulation based on surface roughness model in micro-deep drawing. *J. Mats. Proc. Tech.,* 204**,** 89-93.

MANIN, L., MICHON, G., REMOND, D. & DUFOUR, R. (2008) From transmission error measurement to pully-belt slip determination in serpentine belt drives: influence of tensioner and belt characteristics. *Mechanism and Machine Theory,* 44**,** 813-821.

MATSUSHITA, N. (2003) Laser Micro-Bending for precise micro-fabrication of magnetic disk-drive components. *Int. Sympo. on Laser Precision Microfabrication.* No4, Munich.

MCCARTHY, K. (2006) The air bearing advantage in high-precision positioning. *NASA Tech Briefs.*
http://www.nasatech.com/motion/features/feat1_0406.html

MEI, X., TSUTSUMI, M., TAO, T. & SUN, N. (2003) Study on the load distribution of ball screws with errors. *Mechanism and Machine Theory,* 38**,** 1257-1269.

MEKID, S. & OLEJNICZAK, O. (2000) High precision linear slide. Part II: control and measurements. *International Journal of Machine Tools &Manufacture,* 40**,** 1051-1064.

MESSNER, A., ENGEL, U., KALS, R. & VOLLERTSEN, F. (1994) Size effect in the FE-simulation of micro-forming processes. *J. Mats. Proc. Tech.,* 45**,** 371-376.

MISHIMA, N., ASHIDA, K., TANIKAWA, T. & MAEKAWA, H. (2002) Design of a microfactory. *Proceedings of the ASME Design Engineering Technical Conference — 7th Design for Manufacturing Conference.* Montreal, Que., Canada.

Mitutoyo Surftest SV2000 catalogue no: E4222-178.

MITUTOYO, (2006) Vision Measuring Machine User's Manual.

MRACEK, M. & HEMSEL, T. (2006) Synergetic driving concepts for bundled miniature ultrasonic linear motors. *Ultrasonics,* 44**,** e597-e602.

MRAD, R. B. & TENZER, P. E. (2004) On amplification in inchworm(tm) precision positioners. *Mechatronics,* 14**,** 515-531.

OCAN˜A, J. L., MORALES, M., MOLPECERES, C., GARCı´A, O., PORRO, J. A. & GARCı´A-BALLESTEROS, J. J. (2007) Short pulse laser microforming of thin metal sheets for MEMS manufacturing. *Applied Surface Science,* 254**,** 997-1001.

OH, S. I., RHIM, S. H., JOO, B. Y., YOON, S. M., PARK, H. J. & CHOI, T. H. (2005) Forming of micro channels with ultra thin metal foil by cold isostatic pressing. *5th Japan-Korea Joint Symposium on Micro-Fabrication.*

OKAZAKI, Y., MISHIMA, N. & ASHIDA, K. (2002) Microfactory and micro machine tool. *The 1st Korea-Japan Conference on Positioning Technology.* Daejeon, Korea.

OKAZAKI, Y., MISHIMA, N. & ASHIDA, K. (2004) Microfactory – Concept, History, and Developments. *Journal of Manufacturing Science and Processing,* 126**,** 837-844.

PARK, C. H., OH, Y. J., SHAMOTO, E. & LEE, D. W. (2006) Compensation for five DOF motion errors of hydrostatics feed table by utilizing actively controlled capillaries. *Precision Engineering,* 30**,** 299-305.

PARK, J. H., YOSHIDA, K., NAKASU, Y. & YOKOTA, S. (2002) A resonantly-driven piezoelectric micropump for microfactory. *Proc. ICMT20002.* Kitakyushu.

PARK, J. S. (1996) Motion profile planning of repetitive point-to-point control for maximum energy conversion efficiency under acceleration conditions. *Mechatronics,* 6**,** 649-663.

PENG, L., HU, P., LAI, X., MEI, D. & NI, J. (2009) Investigation of Micro/meso Sheet Soft Punch Stamping Process simulation and experiments. *Materials and Design,* 30**,** 783-790.

PENG, L., LIU, F., NI, J. & LAI, X. (2007) Size effects in thin sheet metal forming and its elastic–plastic constitutive model. *Materials and Design,* 28**,** 1731-1736.

PENG, X. & QIN, Y. (2004) Analysis of the laser-heating methods for micro-parts stamping applications. *Journal of Materials Processing Technology,* 150**,** 84-91.

PETROV, M., GANCHEV, I. & TANEVA, A. (2002) Fuzzy PID control of non-linear plants. *2002 First International IEEE Symposium "Intelligent Systems".*

QIN, Y. & LEE, W. B. (2005) Advances in Materials Processing Technology (IFAMPT2005). *J. Mats. Proc. Tech.,* 167, 2-3.

QIN, Y. (2006a) MicroForming - Machine and tool development needs and perspectives. *J. Mats. Proc. Tech.,* 177**,** 8-18.

QIN, Y. (2006b) Forming-tool design innovation and intelligent tool-structure/system concepts. *International Journal of Machine Tool and Manufacture*. 46, 11, 1253-1260.

QIN, Y. (2006c) Micro-forming and miniature manufacturing systems - Development needs and perspectives. *11th International Conference on Micro-manufacturing.* Urbana-Champaign, USA.

QIN, Y. (2007) Advances in micro-manufacturing research and technological development and challenges/opportunities for micro-mechanical-machining. *Cutting Tools Congres.* Milano, Italy.

QIN, Y. (2009) Overview on Micro-Manufacturing. IN QIN, Y. (Ed.) *Micro-manufacturing Engineering and Technology.* Glasgow, Elsevier.

QIN, Y., MA, Y., HARRISON, C. S., BROCKETT, A., ZHOU, M., ZHAO, J., LAW, F., RAZALI, A. & SMITH, R. (2008) Development of a new machine

system for the forming of micro-sheet-products. *ESAFORM Conference Proceedings.* Lyon, France, Springer, Paris. 1-4.

ROBERTS, W. L. (1978) *Cold rolling of steel*, CRC Press.

ROGERS, J. R. & CRAIG, K. (2005) On-hardware optimization of stepper-motor system dynamics. *Mechatronics,* 15**,** 291-316.

ROLLOT, Y. & RÉGNIER, S. (2000) Micromanipulation par adhésion, Nano et micro technologies. 653-658.

ROTHBART, H. A., BROWN, T. H. & (JR.), T. H. B. (2006) *Mechanical design handbook: measurement, analysis, and control of dynamic systems*, McGraw-Hill Professional.

ROUGEOT, P., REGNIER, S. & CHAILLET, N. (2005) Forces analysis for micro-manipulation. *Computational Intelligence in Robotics and Automation, IEEE.* 105-110.

RUETER, A. (2002) Examining roll forming machinery, tooling, and lubrication. *http://www.thefabricator.com/RollForming/RollForming_Article.cfm?ID=90.*

RUSSELL, J. (2003) Handling appliance steel - Tips for processing surface-sensitive materials. *Stamping Journals(R).* http://www.thefabricator.com/MaterialsHandling/MaterialsHandling_Article.cfm?ID=781

SAHIN, M., CETINARSLAN, C. S. & AKATA, H. E. (2007) Effect of surface roughness on friction coefficients during upsetting processes for different materials. *Materials and Design*, 28, 633-640.

SAOTOME, Y. & OKAMOTO, T. (2001) An in-situ incremental microforming system for three-dimensional shell structures of foil materials. *J. Mats. Proc. Tech.,* 113**,** 636-640.

SATO, K. & MAEDA, G. J. (2008) Practical control method for ultra-precision positioning using a ballscrew mechanism. *Precision Engineering,* 30, 309-318.

SCHNEIDER, R. & GROCHE, P. (2004) Method for the optimization of forming presses for the manufacturing of micro-parts. *CIRP Annals.* 53, 1, 281-284.

SCHULER (1998) *Metal Forming Handbook*, Springer-Verlag Berlin Heidelberg New York.

SCHWARTZ, A. J., KUMAR, M. & ADAMS, B. L. (2000) *Electron Backscatter Diffraction in Materials Science*. Kluwer Academic/Plenum Publishers.

SHANAHAN, J. (2006) Trend in Micro Machining Technologies. http://www.makino.com/abaout/article/2-1-2008/Trends_in_Micro_machining_Technologies

SHIM, K. H., LEE, S. K., KANG, B. S. & HWANG, S. M. (2004) Investigation of blanking of thin sheet metal using the ductile fracture criterion and its experimental verification. *J. Mats. Proc. Tech.,* 155-156, 1935-1942.

SHINNO, H. & HASHIZUME, H. (1999) Nanometer positioning of a linear motor-driven ultraprecision aerostatic table system with electrorheological fluid dampers. *Annals of the CIRP,* 48, 1, 289-292.

SHINNO, H., YOSHIOKA, H. & TANIGUCHI, K. (2007) A newly developed linear motor-driven aerostatic X-Y planar motion table system for nano-machining. *Annals of the CIRP,* 56.

STAMPFLI, H. (2003) Linear motor applications: Ironcore versus ironless solutions. *HST-Etel Newsletter.*

SU, Y. X., SUN, D. & DUAN, B. Y. (2005) Design of an enhanced nonlinear PID controller. *Mechatronics,* 15**,** 1005-1024.

SUDA, M., FURATA, K., SAKUHARA, T. & ATAKA, T. (2000) The Microfactory System Using Electrochemical Machining. Chiba, Japan.

TANG, K. Z., HUANG, S. N., TAN, K. K. & LEE, T. H. (2004) Combined PID and adaptive nonlinear control for servo mechanical systems. *Mechatronics,* 14**,** 701-714.

THORNHILL, N. F., C., S., PATWARDHAN & SHAH, S. L. (2008) A continuous stirred tank heater simulation model with applications. *Journal of Process Control,* 18**,** 347-360.

TOMAS, J. (2007) Adhesion of ultrafine particles—A micromechanical approach. *Chemical Engineering Science,* 62**,** 1997-2010.

TREVELYAN, J. (2005) Industrial process communications and software timing issues. *Mechatronics Design*, 310.

URAOKA, A. & RAHN, C. D. (2009) Simulation of a sheet-handling machine. *Communications in Nonlinear Science and Numerical Simulation,* 14**,** 1617-1626.

VALLANCE, R. R., MORGAN, C. & SLOCUM, A. H. (2004) Precisely positioning pallets in multi-station assembly systems. *Precision Engineering,* 28**,** 218-231.

VOLLERTSEN, F., HU, Z., NIEHOFF, H. S. & THEILER, C. (2004) State of the art in micro forming and investigations into micro deep drawing. *J. Mats. Proc. Tech.,* 151, 1-3, 70-79.

VOLLERTSEN, F., NIEHOFF, H. S. & HU, Z. (2006) State of the art in micro forming. *International Journal of Machine Tools & Manufacture,* 46**,** 1172-1179.

WANG, G. & LIU, N. (2006) Design and implementation of a new approach based on the error feedforward compensation for motion controller. *25th Chinese Control Conference*. Harbin, Heilongjiang, IEEE.

WEST, E. V., YAMAMOTO, A. & HIGUCHI, T. (2009) Automatic object release in magnetic and electrostatic levitation systems. *Precision Engineering,* 33**,** 217-228.

WU, D., CHEN, K. & WANG, X. (2007) Tracking control and active disturbance rejection with application to noncircular machining. *International Journal of Machine Tools &Manufacture,* 47**,** 2207-2217.

YAMAZAKI, K., SRIYOTHA, P., NAKAMOTO, K. & SUGAI, M. (2006) Development of 5-axis linear motor driven super-precision machine. *Annals of the CIRP,* 55.

YAN, M.-T. & SHIU, Y.-J. (2008) Theory and application of a combined feedback-feedforward control and disturbance observer in linear motor drive wire-EDM machines. *International Journal of Machine Tools &Manufacture,* 48**,** 388-401.

YEN, J.-Y. & CHANG, H.-M. (2004) Performance robustness and stiffness analysis on a machine tool servo design. *International Journal of Machine Tools & Manufacture 44 (2004) 523–531,* 44**,** 9.

YEN, Y-T. & LIN, Y-C. (2007) Study of peeling strength of tape carrier packaging and chip scale packaging. *Sensors and Actuators A*, 139, 330-336.

ZHAO, S. & TAN, K. K. (2005) Adaptive feedforward compensation of force ripples in linear motors. *Control Engineering Practice,* 13**,** 1081-1092.

ZI-QIANG, Y. & SHENG-YI, L. (2006) High accuracy error separation technique for on-machine measuring straightness. *Precision Engineering,* 30**,** 192-200.

Webpage

Aerotech, http://www.aerotech.com visited in 2007

Airex, http://www.airex.com visited in 2007

Airturbine Tools, http://www.airturbinetools.com visited in 2007

Baldor, http://www.baldor.com visited in 2007

BOSE, http://www.bose.com visited in 2008

Bruderer, http://www.bruderer.com visited in 2007

CALinear, http://www.calinear.com visited in 2007

COE Press, http://www.cpec.com visited in 2007

Coilmate-Dickerman, http://www.coilmate-dickerman.com visited in 2007

Copley Controls, http://www.copleycontrols.com visited in 2007

Etel, http://www.etel.ch visited in 2007

EU MASMICRO Consortium, http://www.masmicro.net visited in 2007

Fanuc, http://www.fanuc.com visited in 2007

Hitachi, http://www.hitachi.co.jp visited in 2007

Intellidrives, http://www.intellidrives.com visited in 2007

Kollmorgen, http://www.kollmorgen.com visited in 2007

Kyocera, http://www.kyocera.com visited in 2007

Ledex, http://www.ledex.com visited in 2007

Linmot, http://www.linmot.com visited in 2007

Maxon Motor USA, http://www.maxon.com visited in 2008

Micos, http://www.micos.com visited in 2007

Minitools USA, http://www.minitools.com visited in 2007

Morgan Electro Ceramins, http://www.morganelectroceramics.com visited in 2007

Newport, http://www.newport.com visited in 2007

OAO Piezo, http://www.en.OAOpiezo.com visited in 2007

PA Industries, http://www.PA.com visited in 2007

Parker Motion, http://www.parkermotion.com visited in 2008

Physik Instrumente, http://www.pi.ws visited in 2007

POWair, http://www.powair.com visited in 2007

Renishaw, http://www.renishaw.com visited in 2008

Rockwell Automation, http://www.rockwellautomation.com visited in 2007

Sankyoseiki, http://www.sankyoseiki.co.jp/e/dtf/dtfI01.htm visited in 2007

SBC Slide, http://www.sbcslide.com visited in 2008

SMC Pneumatics, http://www.smcpneumatics.co.uk visited in 2008

Society for Amateur Scientists, http://www.sas.org visited in 2008

THK. http://www.thk.com visited in 2008

Yaskawa-Omron, http://www.yaskawa.com visited in 2007